# Deciphering immune signatures induced

# by viral vector vaccines against the Ebola virus

Dissertation with the aim of achieving a doctoral degree (Dr. rer. nat.)

at the Faculty of Mathematics, Informatics, and Natural Sciences

Department of Biology

University of Hamburg

submitted by

Etienne Bartels

Hamburg, May 2021

This dissertation was conducted between April 2018 and May 2021 in the research group Emerging Infections under the supervision of Prof. Dr. med. Marylyn Martina Addo at the Medical Center Hamburg-Eppendorf and Bernhard Nocht Institute for Tropical Medicine.

Reviewers of the dissertation:

1. Reviewer:

Prof. Dr. rer. nat. Tim-Wolf Gilberger

Bernhard Nocht Institute for Tropical Medicine

Cellular Parasitology Department

Bernhard-Nocht-Straße 74

D-20359 Hamburg

2. Reviewer:

Prof. Dr. med. Marylyn Martina Addo

Medical Center Hamburg-Eppendorf

Research group Emerging Infections

Martinistraße 52

D-20246 Hamburg

Day of oral defense: 20.08.2021

Chair of the examination commission: Prof. Dr. Esther Schnettler

Member of the examination commission:

Prof. Dr. rer. nat. Tim-Wolf Gilberger

Prof. Dr. med. Marylyn Martina Addo

Prof. Dr. Esther Schnettler

Prof. Dr. Minka Breloer

Prof. Dr. Julia Kehr

## Eidesstattliche Versicherung / Declaration on oath

Hiermit erkläre ich an Eides statt, dass ich die vorliegende Dissertationsschrift selbst verfasst und keine anderen als die angegebenen Quellen und Hilfsmittel benutzt habe.

*I hereby declare upon oath that I have written the present dissertation independently and have not used further resources and aids than those stated.*

Hamburg, 12.05.2021

Stadt, Datum | *City, date*

Unterschrift | *Signature*

## Language Certificate

My name is Madeleine Hamley and I am a native speaker.

I have read the present PhD thesis and hereby confirm that it complies with the rules of the English language.

Hamburg, 10.05.2021

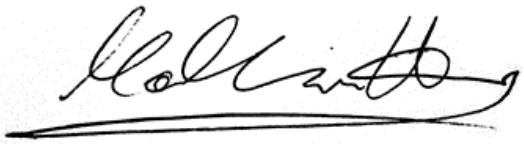

City, date | Signature

# Danksagung

Zuerst möchte ich der ganzen Arbeitsgruppe *Emerging infections* für die schöne Zeit und das wunderbare Arbeitsklima danken. Vielen Dank, dass ihr mich auf dem Weg meiner Promotion begleitet und unterstützt habt. Unsere legendären Kicker-Pausen werde ich stets in freudiger Erinnerung behalten. Mein besonderer Dank gilt Frau Prof. Dr. Marylyn M. Addo für das spannende Thema und Ihre herzliche Betreuung meiner Arbeit. Auch meinem Zweitprüfer Herrn Prof. Dr. Tim-Wolf Gilberger möchte ich für die Betreuung, lebhaften Diskussionen und seinen beispiellosen Einsatz herzlich danken. Zudem möchte ich mich auch bei Frau Dr. Christine Dahlke für Ihre nie endende Unterstützung und Bereitschaft ihr Wissen mit mir zu teilen bedanken. Auch Frau Dr. Susan Lassen-Hartje gehöhrt mein Dank für Ihre grenzenlose Hilfsbereitschaft. My Linh Ly und Monika Friedrich danke ich für die große Hilfe bei der Bewältigung des Laboralltags.

Des Weiteren möchte ich mich bei Frau Prof. Dr. Minka Breloer, Frau Prof. Dr. Julia Kehr und Frau Prof. Dr. Esther Schnettler für die Bereitschaft der Begutachtung meiner Disputation bedanken. Besonderer Dank gilt ebenfalls Herrn Prof. Dr. Gerd Sutter und seinem Team am Institut für Infektionsmedizin und Zoonosen an der Ludwig-Maximilians-Universität in München für die experimentelle Expertise. Außerdem danke ich herzlich Herrn Michael Spohn für sein Engagement und Unterstützung.

Mein besonderer Dank gilt außerdem allen Teilnehmern der Hamburger Gesundkohorte ohne deren Blutspenden diese Arbeit nicht möglich gewesen wäre. Den Mitarbeitern des Bernhard-Nocht-Institutes für Tropenmedizin und dem Heinrich-Pette-Institut für Experimentelle Virologie danke ich für die herzliche Atmosphäre und Unterstützung.

Ein besonderer Dank gilt ebenfalls meinen Freunden und meiner Famile. Vor allem meinen Eltern Dorina und Frank Bartels möchte ich für ihre langjährige Unterstützng danken. Ohne euch wäre dies alles nicht möglich gewesen. Vielen Dank! Besonders möchte ich auch meiner Partnerin Jessica Barton für ihre Unterstützung und nie endende Geduld danken. Vielen Dank, dass du immer an mich geglaubt hast und es auch in schwierigen Zeit schaffst mich zu motivieren. Danke für Alles!

# Abstract

The Ebola virus disease (EVD) is a severe, often fatal illness in humans. EVD is caused by the Ebola virus (EBOV) and is responsible for about 50–90 % deaths in diagnosed cases. The largest EVD outbreaks occurred in West Africa from 2013–2016 and in the Democratic Republic of the Congo (DRC) from 2018–2020. Vaccines are effective countermeasures against deadly diseases. The vector platforms vesicular stomatitis virus (VSV) and modified vaccinia virus Ankara (MVA) were used to develop viral vector vaccines against EBOV. While VSV can replicate in humans to some extent, MVA is replication-deficient. Both carry the immunogenic EBOV-glycoprotein (EBOV-GP). VSV-EBOV expresses the EBOV-GP on its surface instead of the VSV-GP, whereas MVA-EBOV only encodes for the EBOV-GP gene. Although VSV-EBOV was frequently used in the second largest outbreak in the DRC, exact mechanisms of induced immune signatures, especially innate immune responses, remain inadequately understood. However, innate immune responses can shape and influence adaptive immunogenicity and therefore contribute to vaccine efficacy. Since innate immunity is difficult to analyze comprehensively in clinical trials due to its early manifestation, it has not been well-investigated so far.

To elucidate specific innate immune mechanisms induced by MVA-EBOV and VSV-EBOV, *in vitro* stimulation assays of hPBMCs were implemented. Early immune responses were comprehensively monitored by longitudinal sampling and application of different methods. In the first 24 hours post-stimulation, the immune responses were investigated on mRNA level (RNA-Seq) and protein level (flow cytometry/cytokine secretion).

Flow cytometry approaches revealed a significantly secretion of IP-10 and a trend to altered expression of CD40, CD83, and CD86 on monocyte and DC subsets post VSV-EBOV stimulation. On the mRNA level VSV-EBOV stimulations resulted in an elevated expression of genes belonging to chemokine signaling. In contrast, MVA-EBOV showed mainly significantly decreased expression of CD86 on pDCs, $CD1c^{+}CD11c^{+}$ DCs, and $CD1c^{-}CD141^{+}$ DCs. Induced transcriptomic changes by MVA-EBOV included mainly interferon signaling and the defense response to viruses. Compared to VSV-EBOV, MVA-EBOV exhibited more differentially expressed genes with higher gene expression rates.

The decreased expression of CD86 on monocytes and DCs suggests an elevated immune response due to a lower suppressive effect of activated $CD86^{+}$ monocytes and DCs post MVA-EBOV stimulation. Both viral vector vaccines led to specific innate signatures, where MVA-EBOV seemed to induce a stronger anti-viral immune response than VSV-EBOV due to a higher number of DEG and the induction of anti-viral pathways. Thus, this dissertation deciphered distinct immune signatures of VSV-EBOV and MVA-EBOV emphasizing specific early transcriptomic changes which might contribute to different immunogenicity in vaccinees.

# Zusammenfassung

Die Ebolavirus Krankheit (*Ebola virus disease*: EVD) ist eine schwere, oftmals letale Erkrankung im Menschen. EVD wird durch das Ebolavirus (EBOV) hervorgerufen und ist für 50–90 % der Todesfälle bei diagnostizierten Patienten verantwortlich. Die größten EVD-Ausbrüche ereigneten sich in Westafrika von 2013–2016 und in der Demokratischen Republik Kongo (*Democratic Republic of the Congo*: DRC) von 2018–2020. Impfstoffe sind effektive Gegenmaßenahmen für tödliche Erkrankungen. Die Vektor-Plattformen Vesicular Stomatitis Virus (VSV) und der modifizierte Vaccinia Virus Ankara (MVA) wurden verwendet, um virale Vektorimpfstoffe gegen EBOV zu entwickeln. Während VSV im Menschen replizieren kann, ist MVA replikations-defizient. Beide Vektorimpfstoffe tragen das immunogene EBOV-Glykoprotein (EBOV-GP). VSV-EBOV trägt das EBOV-GP an seiner Oberfläche, wohingegen MVA-EBOV nur für das EBOV-GP Gen kodiert. Obwohl VSV-EBOV während des zweitgrößten Ausbruchs in der DRC häufig verwendet wurde, sind exakte Wirkmechanismen, insbesondere die der frühen angeborenen Immunantwort, bis heute unzureichend verstanden. Allerdings können angeborene Immunantworten die adaptive Immunantwort modellieren und beeinflussen und dadurch zu einer Impfstoffwirksamkeit beitragen. Da umfangreiche Analysen der frühen Immunantwort in klinischen Studien schwer zu realisieren sind, ist diese bis heute kaum untersucht.

Um frühe angeborene Immunmechanismen, welche durch MVA-EBOV und VSV-EBOV induziert werden, zu analysieren, wurden *in vitro* Stimulationsassays von menschlichen mononukleären Zellen des peripheren Blutes implementiert. Frühe Immunantworten wurden umfangreich durch eine longitudinale Probenentnahme und verschiedene Methoden untersucht. Die Immunantwort wurde in den ersten 24 Stunden nach einer Stimulation auf mRNA- (RNA-Seq) und Protein-Ebene (Durchflusszytometrie, Zytokinsekretion) analysiert.

Mittels Durchflusszytometrie wurden signifikant erhöhte Sekretionen von IP-10 und tendentiell veränderte Expressionen von CD40, CD83 und CD86 auf Untergruppen von Monozyten und Dendritischen Zellen (*dendritic cells*: DCs) nach einer VSV-EBOV Stimulation identifiziert. Auf mRNA-Ebene induzierte eine VSV-EBOV Stimulation vor allem eine erhöhte Expression von Genen, welche dem Zytokinsignalweg zugeorndet werden können. Dagegen induzierte MVA-EBOV vor allem eine signifkant reduzierte Expression von CD86 auf pDCs,

$CD1c^+CD11c^+$ DCs und $CD1c^-CD141^+$ DCs. Eine induzierte transkriptionelle Veränderungen durch MVA-EBOV beinhaltete hauptsächlich Interferon-vermittelte Signalwege und Verteidigungsmechanismen gegen Viren. MVA-EBOV wies verglichen mit VSV-EBOV mehr differentiell exprimierte Gene mit einer höheren Expressionsrate auf.

Durch die geringere Expression von CD86 auf Monozyten und DCs kann von einer erhöhten Immunantwort durch einen geringeren suppressiven Effekt von aktivierten $CD86^+$ Monozyten und DCs nach einer MVA-EBOV Stimulation ausgegangen werden. Beide viralen Vektorimpfstoffe führten zu einer spezifischen frühen Immunantwort, wobei MVA-EBOV aufgrund der erhöhten Anzahl an DEG und der Induktion antiviraler Signalwege eine stärkere antivirale Immunantwort hervorzurufen scheint. Somit zeigt die vorliegende Dissertation unterschiedliche Immunsignaturen von VSV-EBOV und MVA-EBOV auf, die sich vor allem auf verschiedenen transkriptionellen Auswirkungen in der frühen Phase der Immunantwort gründen und zu anderen Immunogenitäten in Impflingen führen könnten.

# Table of Contents

# Abbreviations

| | |
|---|---|
| µl | Microliter |
| ActB | Actin Beta |
| Ad | Adenovirus used as viral vaccine vector: e.g. Ad26 |
| AIDS | Acquired Immune Deficiency Syndrome |
| APCs | Antigen-Presenting Cells |
| APSV | Vaccina virus vaccine called Aventis-Pasteur WetVax® |
| B cells | B Lymphocytes |
| BDBV | Bundibugyo Ebola Virus |
| BHK | Cell line derived from Baby Hamster Kidney |
| bp | Base Pair |
| CD | Cluster of Differentiation |
| CDC | Centers for Disease Control and Prevention |
| cDNA | Complementary DNA |
| CEPI | Coalition for Epidemics and Preparedness Innovations |
| ChAd | Chimpanzee Adenovirus vector |
| CI | Confidence Interval |
| $CO_2$ | Carbon Dioxide |
| COVID-19 | Coronavirus Disease 2019 |
| Ct | Threshold Cycle in qPCR |
| CTL | Cytotoxic T Lymphocyte |
| CXCL9 | CXC-ligand 9 |
| CXCR3 | CXC Chemokine Receptor 3 |
| DAPI | 4’,6-Diamidino-2-Phenylindole |
| DCs | Dendritic Cells |
| DEG | Differentially Expressed Genes |
| DENV | Dengue Virus |
| DEPC | Diethyl Pyrocarbonate |
| DMSO | Dimethyl Sulfoxide |
| DNA | Deoxyribonucleic Acid |

| | |
|---|---|
| dNTPs | Deoxynucleotide Triphosphate |
| DRC | Democratic Republic of the Congo (DRC) |
| DTT | Dithiothreitol |
| EBOV | Ebola Virus |
| EBOV-GP | Ebola Virus Glycoprotein |
| EDTA | Ethylenediaminetetraacetic |
| EID | Emerging Infectious Diseases |
| ESR | Estrogen Receptors |
| ESR1 | Estrogen Receptor 1 |
| Et al. | lat. et alii; “and others” |
| EVD | Ebola Virus Disease |
| FCS | Fetal Calf Serum |
| FITC | Fluorescein Isothiocyanate |
| FMO | Fluorescence Minus One |
| FOXP3 | Forkhead-Box P3 |
| GAGE | Generally Applicable Gene-Set Enrichment |
| GAPDH | Glycerinaldehyd-3-Phosphat Dehydrogenase |
| GFP | Green Fluorescent Protein |
| GM-CSF | Granulocyte-Macrophage Colony-Stimulating Factor |
| GO | Gene Ontology |
| GP | Glycoprotein |
| HA | Hemagglutinin |
| HAI | Hemagglutination |
| HBV | Hepatitis-B Virus |
| HCC | Hepatocellular Carcinoma |
| HCV | Hepatitis-C Virus |
| HIV | Human Immunodeficiency Virus |
| HMBS | Hydroxymethylbilane Synthase |
| hPBMCs | Human Peripheral Blood Mononuclear Cells |
| HPIV | Human Parainfluenza Virus |
| HPRT | Hypoxanthine Phosphoribosyltransferase 1 |

| | |
|---|---|
| HSV | Herpes Simplex Virus |
| IFIT | Interferon-Induced proteins with Tetratricopeptide repeats |
| IFN | Interferon |
| IL | Interleukin |
| IP-10 | Interferon gamma-induced Protein 10 |
| IRF | IFN Regulatory Factor |
| KEGG | Kyoto Encyclopedia of Genes and Genomes |
| LAIV | Live Attenuated vaccine against Influenza Virus |
| LPS | Lipopolysaccharide |
| MARV | Marburg Virus |
| mCherry | Red Fluorescent Protein |
| MCP1 | Monocyte Chemoattractant Protein 1 |
| mDCs | Myeloid Dendritic Cells |
| MERS | Middle East Respiratory Syndrome |
| MERS-CoV | Middle East Respiratory Syndrome Coronavirus |
| MHC-I | Self-Major Histocompatibility Complex Class I |
| MHC-II | Self-Major Histocompatibility Complex Class II |
| MIG | Monokine-induced by Gamma Interferon |
| MIMIC™ | Modular IMmune *In vitro Construct* |
| miRNA | microRNA |
| MMR | Vaccine against Mumps, Measles and Rubella |
| moDCs | Monocyte-derived Dendritic Cells |
| MOI | Multiplicity of Infection |
| MVA | Modified Vaccinia Virus Ankara |
| MVA-EBOV | Viral vector vaccine based on the Modified Vaccinia Virus Ankara against the Ebola Virus |
| MVD | Marburg Virus Disease |
| NK cells | Natural Killer cells |
| NP | Nucleoprotein |
| ORA | Over-Representation Analysis |
| OVA | Ovalbumin |

| | |
|---|---|
| PAMPs | Pathogen Associated Molecular Patterns |
| PBMCs | Peripheral Blood Mononuclear Cells |
| PBS | Phosphate-Buffered Saline |
| PCA | Principal Component Analysis |
| PCR | Polymerase Chain Reaction |
| pDCs | Plasmacytoid Dendritic Cells |
| Pen | Penicillin |
| PFA | Paraformaldehyde |
| PFU | Plaque Forming Unit |
| PHEIC | Public Health Emergency of International Concern |
| PHIL | Public Health Image Library |
| qPCR | Quantitative PCR |
| RESTV | Reston Ebola Virus |
| rMVA | Recombinant Modified Vaccinia Virus Ankara |
| RNA | Ribonucleic Acid |
| RNase | Ribonuclease |
| RNA-Seq | RNA-Sequencing |
| RT | Room Temperature |
| RT-PCR | Reverse Transcriptase-Polymerase Chain Reaction |
| SARS-CoV-1 | Severe Acute Respiratory Syndrome Coronavirus 1 |
| SARS-CoV-2 | Severe Acute Respiratory Syndrome Coronavirus 2 |
| STAT1 | Signal Transducer and Activator of Transcription 1 |
| Strep | Streptomycin |
| SUDV | Sudan Ebola Virus |
| T cells | T Lymphocytes |
| TAFV | Taï Forest Ebola Virus |
| TBE | Tris Borate EDTA buffer solution |
| $T_H$ cell | T Helper cell |
| THP-1 | Monocyte cell line based on peripheral blood of an acute monocytic leukemia patient |
| TIV | Inactivated Trivalent Influenza Vaccine |

| | |
|---|---|
| TLR | Toll-Like Receptor |
| TNF | Tumor Necrosis Factor |
| $T_{reg}$ | Regulatory T cell |
| UDG | Uracil DNA Glycosylase |
| VACV | Vaccinia Virus |
| Vero81 | Epithelial cell line derived from *Cercopithecus aethiops* kidney (*verda reno*; green kidney) |
| VSV | Vesicular Stomatitis Virus |
| VSV-EBOV | Viral vector vaccine based on the Vesicular Stomatitis Virus against the Ebola Virus |
| VSVwt | Vesicular Stomatitis Virus wild type |
| WHO | World Health Organization |
| *x g* | Multiples of earth gravitational acceleration |
| XCI | X-Chromosome Inactivation |
| YF | Yellow Fever |
| YF-17D | Live attenuated Yellow Fever vaccine 17D |
| ZEBOV | Zaire Ebola Virus |

# List of figures

## Results

## Supplement

# List of tables

## Contribution to publications and manuscripts

### Deciphering transcriptomic changes elicited by viral vector vaccines against the Ebola virus disease

Authors: **Etienne Bartels**, Michael Spohn, Monika Friedrich, Asisa Volz, Gerd Sutter, Christine Dahlke, Marylyn M. Addo

Manuscript in preparation.
Parts of the dissertation are in the manuscript.

### Safety and immunogenicity of a modified vaccinia virus Ankara vector vaccine candidate for Middle East respiratory syndrome: an open-label, phase 1 trial

Authors: Till Koch, Christine Dahlke, Anahita Fathi, Alexandra Kupke, Verena Krähling, Nisreen M.A. Okba, Sandro Halwe, Cornelius Rohde, Markus Eickmann, Asisa Volz, Thomas Hesterkamp, Alen Jambrecina, Saskia Borregaard, My L. Ly, Madeleine E. Zinser, **Etienne Bartels**, Joseph S.H. Poetsch, Reza Neumann, Robert Fux, Stefan Schmiedel, Ansgar W. Lohse, Bart L. Haagmans, Gerd Sutter, Stephan Becker, Marylyn M. Addo

In: The Lancet Infectious Diseases
Published online 2020 April 21
DOI: 10.1016/S1473-3099(20)30248-6
PMCID: PMC7172913
PMID: 32325037

Etienne Bartels contributed to the processing of blood samples and assay implementation.

**Distinct early IgA profile may determine severity of COVID-19 symptoms: an immunological case series**

Authors: Christine Dahlke, Jasmin Heidepriem, Robin Kobbe, René Santer, Till Koch, Anahita Fathi, My L. Ly, Stefan Schmiedel, Peter H. Seeberger, **ID-UKE COVID-19 study group**, Marylyn M. Addo, Felix F. Loeffler

In: medRxiv
Posted online 2020 April 17
DOI: https://doi.org/10.1101/2020.04.14.20059733

Etienne Bartels contributed to the clinical monitoring and immunological analyses.

# Awards & presentations

## Awards

September 2019

Travel Grant – German Center for Infection Research DZIF
Attendance at 48th Annual Meeting of the German Society for Immunology

## Presentations

June 2019

**Deciphering the innate immune response elicited by viral vaccine vectors against emerging infectious diseases**
**Bartels E.**, Dahlke C., Zinser M.E., Fathi A., Lassen S., Ly M.L., Assagba G.F., Volz A., Sutter G., Addo M.M.
Novel Concepts in Innate Immunity, conference 2019 (poster presentation)

September 2019

**Deciphering the innate immune response elicited by viral vaccine vectors against emerging infectious diseases**
**Bartels E.**, Dahlke C., Assagba G.F., Zinser M.E., Fathi A., Lassen S., Ly M.L., Volz A., Sutter G., Addo M.M.
II. Joint Meeting of the German Society for Immunology and the Italian Society of Immunology, Clinical Immunology and Allergology (48th Annual Meeting of the German Society for Immunology) (poster presentation)

# 1. Introduction

## 1.1 Emerging infectious diseases

Emerging infectious diseases (EIDs) can result in public health challenges based on the lack of therapeutic countermeasures leading to a transmission from human to human. EIDs can be caused by several pathogens that "*have newly appeared in a population or have existed but are rapidly increasing in incidence or geographic range*" [1]. Infectious agents for potential EID outbreaks belong to categories of bacteria, viruses, fungi, protozoa, and helminths. Most EIDs that resulted in an outbreak have a viral origin. Emergence and transmission of EIDs are mainly influenced by host behavior, pathogen changes, spillover events between pathogen reservoirs to potential hosts, and environmental factors [2]. EIDs are correlated with environmental, socio-economic, and ecological factors, which create conditions for EIDs to thrive and spread in the human population [1,3–5]. Moreover, spreading of EIDs can be driven by war, loss of social cohesion, and natural disaster [4]. Since origin and pathogen leading to an EID outbreak are unpredictable, there is a lack of effective medical countermeasures. More than 60 % of all EIDs have a zoonotic origin, highlighting the complexity of potential pathogens and relevance of human-animal contacts for the incidence of EIDs [5]. One of the most prominent EIDs is the Ebola virus disease (EVD), which is caused by the Ebola virus (EBOV) and was linked to transmissions from wild animals to humans [6–11]. The most devastating EVD outbreak occurred in 2013–2016 resulting in more than 11,300 deaths [6–9,12]. In response to this public health emergency of international concern (PHEIC), the World Health Organization (WHO) published a R&D blueprint list of prioritizing diseases. Filovirus-associated diseases such as EVD and Marburg virus disease (MVD) as well as coronavirus-associated diseases including the Middle East respiratory syndrome (MERS) and the recently occurring coronavirus disease 2019 (COVID-19) are listed [13]. Despite this list and several aims to minimize the risk of EIDs were declared, the second largest EVD outbreak occurred between 2018-2020 in the Democratic Republic of the Congo (DRC) [14]. Until the end of June 2020, this outbreak took more than 2200 lives [14]. Although this outbreak ended in 2020, EBOV could reemerge in the DRC where on February 7$^{th}$ 2021 the Minister of Health of DRC declared an EBOV outbreak [15].

Furthermore, several cases with EBOV-specific symptoms occurred in Gouéké, Guinea starting in January 2021 [16,17]. The declaration of an EBOV outbreak followed by national authorities on February 14th. This reemergence of EBOV in one of the most affected areas emphasizes the potential threat of EBOV to public health. Therefore, effective countermeasures such as vaccines are mandatory to prevent public health crisis caused by EBOV.

### 1.1.1 Ebola virus: The causative agent for Ebola virus disease

EBOV is one of the 12 members of the *Filoviridae* family, which includes several human pathogenic members such as the genera *Ebolavirus* and *Marburgvirus* [9,18,19]. While the genus *Ebolavirus* includes the Bundibugyo Ebola virus (BDBV), Reston Ebola virus (RESTV), Sudan Ebola virus (SUDV), Taï Forest Ebola virus (TAFV), and Zaire Ebola virus (ZEBOV), the genus *Marburgvirus* includes the Ravn virus (RAVV) and Marburg virus (MARV) (figure 1) [9,19–21].

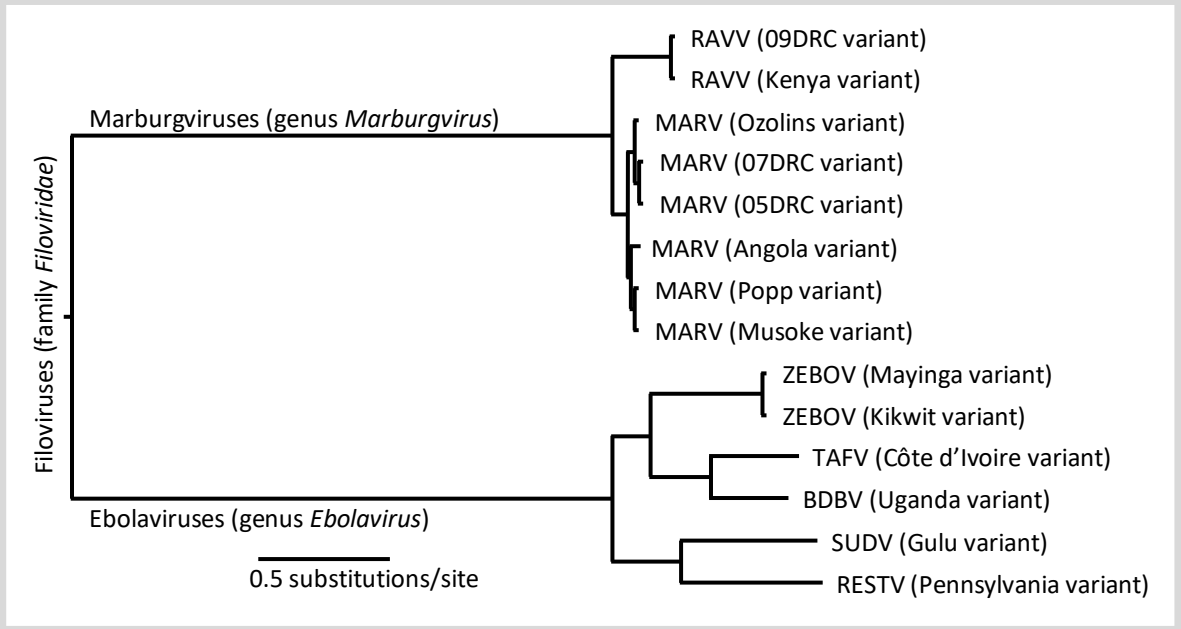


Figure 1: **Phylogenetic tree of EBOV and MARV.** The *Filoviridae* family includes the genus *Ebolavirus* and *Marburgvirus*. Both genera include different viruses: BDBV: Bundibugyo Ebola virus, RESTV: Reston Ebola virus, SUDV: Sudan Ebola virus, TAFV: Taï Forest Ebola virus, ZEBOV: Zaire Ebola virus, RAVV: Ravn virus, MARV: Marburg virus. Full-length genomes were investigated by Bayesian analysis. Figure modified from Conlan, S. et al., 2008 and International Committee on Taxonomy of Viruses et al., 2012 [20,21].

The first two confirmed EBOV outbreaks that occurred consecutive were detected in DRC and Sudan starting in 1976 [22,23]. In the following years, several outbreaks in different areas of Africa were determined (figure 2) [24].

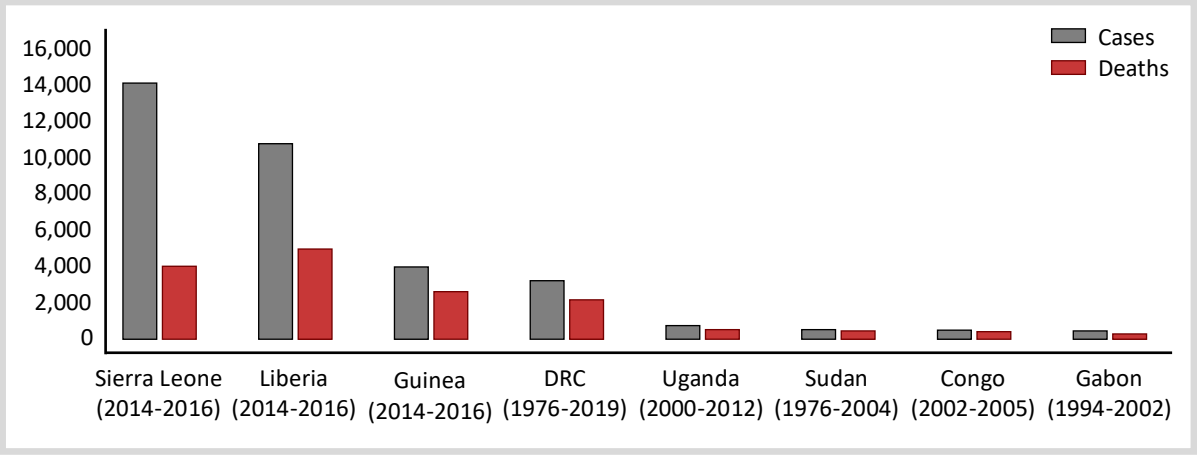


Figure 2: **EBOV outbreaks from 1976-2019.** Number of cases and deaths of EBOV infected individuals during different outbreaks in Africa are shown. Only outbreaks with more than 100 cases are depicted. Figure modified from Ezezika, O. & Keita, A. K., 2020 [24].

Due to past outbreaks and confirmed cases collected by the Centers for Disease Control and Prevention (CDC), Laura A. Skrip and Alison P. Galvani reported that countries for high risks of EBOV infections are predominantly located in Middle and West Africa around the equator (figure 3B) [25]. To date, the largest EVD outbreak started 2013 in West Africa (figure 3A) causing 28,616 cases and 11,325 deaths in Guinea, Liberia, and Sierra Leone (cf. figure 2) [6-9,12]. A comparison of areas prior to and after EBOV cases occurred showed trends for higher self-medication, decreased usage of health services, and reduced antenatal-care in 2014–2015 [26,27]. Meta-analysis of the whole West African EBOV outbreak revealed significant reductions in the utilization of health services in endemic areas [28]. Moreover, the implementation of vaccines such as MMR decreased in Liberia and Guinea resulting in a higher incidence over two years post EBOV outbreak [29,30]. This might also contribute to a higher mortality rate caused by coinfections in epidemic regions emphasizing the impact of EBOV on public health.

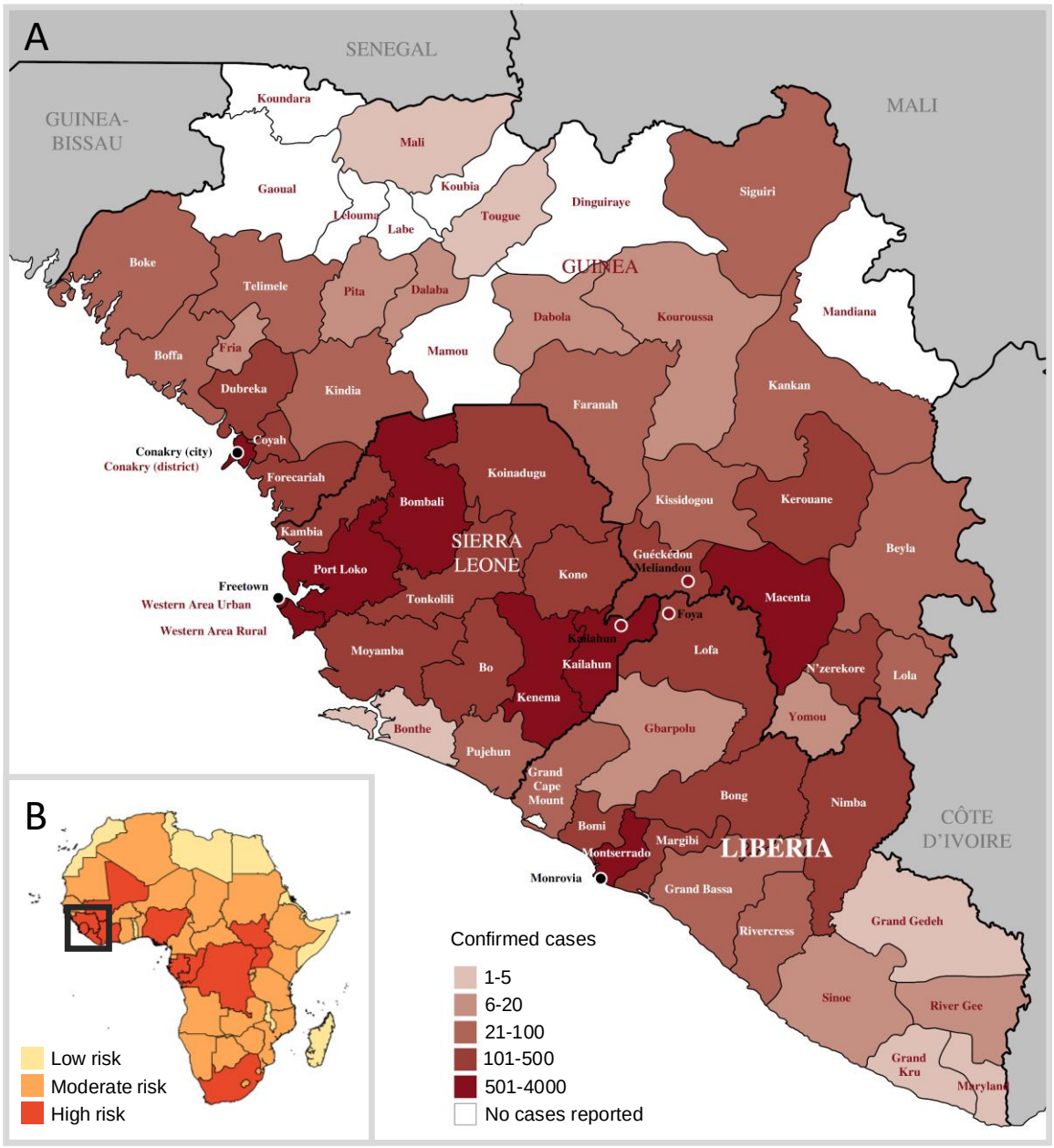


Figure 3: **Distribution of EBOV.** A) The most devastating EVD outbreak occurred in 2013-2016 resulting in more than 11,300 deaths in West Africa [6–9]. Red color indicates number of confirmed cases, where darker color represents countries with higher numbers of confirmed cases [8]. B) Due to historical outbreaks, confirmed cases collected by CDC, and the distance to countries with a high incidence different risk levels for EBOV infections in Africa were calculated [25]. Black square indicates areas of West Africa depicted in A. Red: high risk level; orange: moderate risk level; yellow: low risk level. A) Figure modified from Coltart, C. E. M. et al., 2017 [8]; B) Figure modified from Skrip, L. A. & Galvani, A. P., 2016 [25].

Viruses in the genus *Ebolavirus* and *Marburgvirus* are filamentous and consist of enveloped virions containing a single, linear, negative, non-segmented sense RNA genome

(figure 4A,B) [18,31,32]. The EBOV genome encodes mainly for seven different proteins including four viral proteins (VP), one nucleoprotein (NP), one glycoprotein (GP), and one RNA-dependent RNA polymerase L (figure 4B) [33]. While the host species for most filoviruses are still unknown, there is an increasing evidence that primates and bats are infected by EBOV as well as MARV and eventually transmit these pathogens to humans [7–10,18,31]. Filoviruses can cause hemorrhagic fever where ZEBOV from the genus *Ebolavirus* showed the highest case-fatality rate of up to 90 % [10,31,34,35]. After an incubation of five to seven days, in some cases up to two weeks, most patients develop fever, chills, muscle pain, headache, nausea, vomiting, abdominal pain, and diarrhea [35,36]. Patients who establish a severe illness with a fetal outcome exhibit a high viral load in their peripheral blood over the course of infection [37,38]. Since the EBOV-GP on the virus surface mediates the attachment, fusion, and cell entry [39], it is essential for the broad cell tropism. Due to this broad cell tropism EBOV leads to systemic cell and tissue damage explaining the high case-fatality rate of EBOV (cf. figure 2B) [40–43].

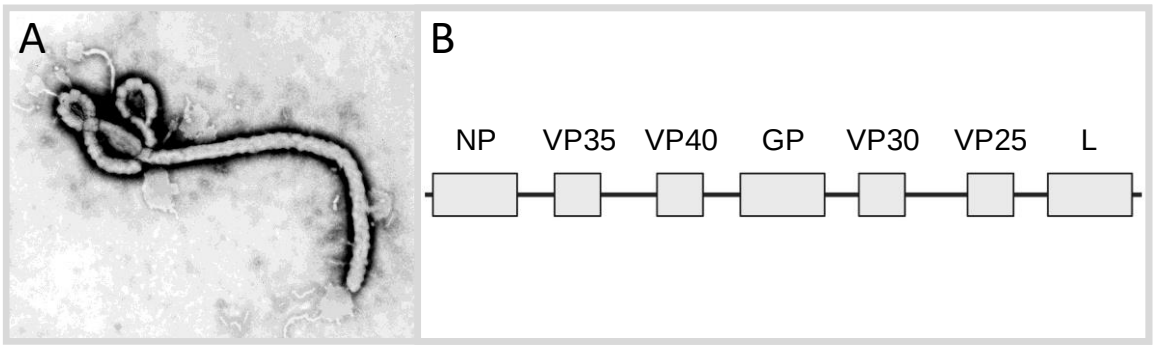


Figure 4: **EBOV electron microscopic image and genome structure.** A) Transmission electron microscopic image of an EBOV virion. Picture was created 1976 by Frederick A. Murphy and is provided by CDC in Public Health Image Library (PHIL) with the identification number #1181 [44]. B) Genome structure of EBOV. The EBOV genome encodes for seven major proteins as indicated: nucleoprotein (NP), viral proteins (VP), polymerase cofactor VP35, matrix protein VP40, glycoprotein (GP), hexameric zinc-finger protein VP30, membrane-associated protein VP24, and RNA-dependent RNA polymerase L (L). Figure created with BioRender.com, modified from Cantoni, D. & Rossman, J. S., 2018 [33].

Mucosal surfaces and the skin represent entry sites for EBOV [45]. At the entry site first immune cells, which get into contact with EBOV, are dendritic cells (DCs) and monocytes/macrophages. This results in an extensive secretion of cytokines and chemokines

which initiates the migration of other immune cells, enhances coagulopathy, and increases endothelial permeability [45–51]. Moreover, infected DCs and macrophages can transport the virus through lymph channels and the peripheral blood to lymph nodes and other tissues [35]. Although B- and T cells are not infected, most of them undergo apoptosis in later stages of infection [35]. Furthermore, dysregulation of T cell responses is associated with severe disease progression, which can lead to death [52]. Multilateral infections of cells and tissues like the liver and spleen result in disseminated intravascular coagulation and finally in systemic bleeding [35,51,53]. In the latest stage of an infection, necrosis of hepatocytes and tissue damage lead to organ failure, terminal shock, and death [51]. Several therapeutics to prevent lethal EVD outcomes were investigated during outbreaks in Africa focusing on antiviral drugs to reduce the mortality rate in humans [54]. To date, no licensed anti-viral therapeutics are available to treat the deadly EVD [54]. Therefore, vaccines that induce a broad immune response resulting in a life-long protection represent a great opportunity to combat EVD.

## 1.2 The immune system

The human body possesses many defense mechanisms to prevent infections with pathogens such as viruses, bacteria, helminths, and fungi. Once a pathogen has overcome anatomical barriers like the skin, first unspecific defense strategies including lysozyme, defensins and the complement system are activated. While lysozymes degrade the cell wall of bacteria, defensins destroy the cell membrane of bacteria. Moreover, the activation of the complement system can lead to the lysis and phagocytosis of the pathogen by innate immune cells [55].

Immune cells of the innate and adaptive immune response represent comprehensive defense mechanisms of the human body. Innate immune cells recognize pathogens by their specific characteristics summarized as pathogen-associated molecular patterns (PAMPs) via pattern recognition receptors (PRR) such as toll-like receptors (TLR). Also, endogenous molecules that indicate cellular stress and death named as damage-associated molecular patterns (DAMPs) are detected by receptors of innate immune cells. Macrophages, monocytes, DCs and granulocytes including neutrophiles, eosinophils, and basophils are innate immune cells which can phagocyte pathogens post detection by these receptors [56]. Upon phagocytosis

innate immune cells destroy the pathogen and secrete cytokines which are necessary for the activation and migration of other immune cells. For instance, type I interferons (IFN) are released by DCs resulting in an anti-viral milieu and enhanced expression of type I IFN stimulated genes of other immune cells. Besides their phagocytic activity, DCs are mainly professional antigen presenting cells that communicate between the innate and adaptive immune system. Their interface activity is realized by the uptake and processing of pathogens following antigen presentation which lead to an effective T cell activation. Furthermore, intracellular pathogens can predominantly eradicated by killing of infected cells. The antigen-independent recognition and killing of infected cells is realized by natural killer cells (NK cells) [56].

Immune responses mediated by the adaptive immune system require the presentation of antigens derived from the pathogen via self-major histocompatibility complex class I and II (MHC-I; MHC-II) which are located on other cells. Naïve $CD4^+$ T cells bind to antigen-MHC-II-complexes resulting in an activation and differentiation to effector cells that can activate (T helper cells: $T_H1$, $T_H2$, $T_H17$, and $T_{FH}$) or repress (regulatory T cell: $T_{reg}$) other immune cells. In contrast, naïve $CD8^+$ T cells interact with antigen-MHC-I-complexes leading to a differentiation to cytotoxic T lymphocytes (CTLs) which can kill infected cells [57]. After an activation of B cells, they proliferate and differentiate to plasma cells or memory cells. While T cells represent the cellular part of the adaptive immune response, antibodies secreted by plasma cells are described as humoral part. These antibodies are mandatory for neutralization and opsonization of pathogens as well as activation of the complement system [58]. While the innate immune response is unspecific and rapid, a specific long term protection is mainly mediated by memory B and T cells post infection and vaccination [59].

## 1.3 Vaccination

Vaccines are one of the most powerful countermeasures for infectious diseases. Only clean water as a public health measure has a bigger influence on mortality in the world vaccines [60,61]. In 1500 *variolation* was the first immunization approach of non-immune individuals using infectious material from smallpox patients [62,63]. In the following centuries, vaccines against different pathogens including mumps, measles, rubella (MMR) as well as

influenza, hepatitis A, B, C, and diphtheria were developed [64]. To date, vaccines against more than 20 different microorganisms are available and more than 20 additional vaccines against other microorganisms are under investigation [52-54]. Some vaccines like the MMR vaccine are considered for a long-lasting immunity resulting in lifelong protection [68]. Moreover, the impact of vaccines is emphasized by their protection of potentially deadly diseases such as poliomyelitis and smallpox [69,70]. Prior to vaccination strategies against smallpox, up to 30 % of infected people died [71]. Global vaccination campaigns against smallpox resulted in an eradication in 1980 [70,72]. While the WHO estimate that worldwide 2-3 million deaths are avoided each year by implementation of vaccines [67], other researcher calculated that even up to 6 million deaths are prevented [73]. Cases for measles, mumps, rubella, and *Haemophilus influenzae* type B were reduced by >99 % in 2012 in the United States compared to decades prior effective vaccination strategies [74–76]. To design effective vaccines against different diseases several vaccine platforms were developed.

### 1.3.1 Vaccine platforms & their induced immune responses

Since the first vaccination against smallpox (*variolation*) was implemented, several vaccines were developed based on inactivated and attenuated viruses (figure 5). While these strategies require an isolation of the pathogen, it also results in safety concerns or reduction of immunogenicity due to necessary pathogen inactivation. Prior to the development of other effective vaccines, the immunogenic structures of the pathogen have to be determined. Once these structures are identified, they can be used for several vaccine platforms (figure 5). For instance, recombinant subunits, proteins, or synthetic peptides are based on these structures. The goal of these vaccines is to induce an immune response specifically to the immunogenic structure. To improve immune responses to immunogenic antigens, different vaccine platforms were designed. For example, DNA vaccines consist of eukaryotic plasmids, which carry a heterologous, recombinant gene of interest and are replicated in bacteria cells [77]. Purified DNA-vectored plasmids are mainly injected intramuscularly by gene-gun or electroporation into vaccinees leading to gene production by transcription and translation [78]. Afterwards, plasmid-derived proteins can be processed and presented via MHC-I and MHC-II [77]. Also viral vector vaccines encode for heterologous, recombinant genes and are

presented based on their viral origin by MHC-I and MHC-II [79–82]. Therefore, both platforms result in an induced immune response to the specific gene of interest in vaccinees including humoral and cellular immune responses [77,83–86]. One of the most beneficial properties of both platforms is given by the fact that they can also result in an induced CTL-response. Furthermore, both platforms can encourage the magnitude of immune responses based on their intrinsic adjuvant property caused by PAMPs such as the immune modulatory genes in the gene-cassette of the DNA plasmids or the viral vector itself [78,87–89].

Depending on the vector platform, viral vectors have different advantages including high immunogenicity and safety profiles, long term gene expression, activation of adaptive and innate immune responses as well as drawbacks like pre-exiting immunity and risks for tumorigenesis [80–82,88,90]. Once a viral vector vaccine is administered to vaccinees, they will develop innate and adaptive immune responses including transcriptomic changes, immune cell activation, inductions of cytokines and antibodies [86,91–93].

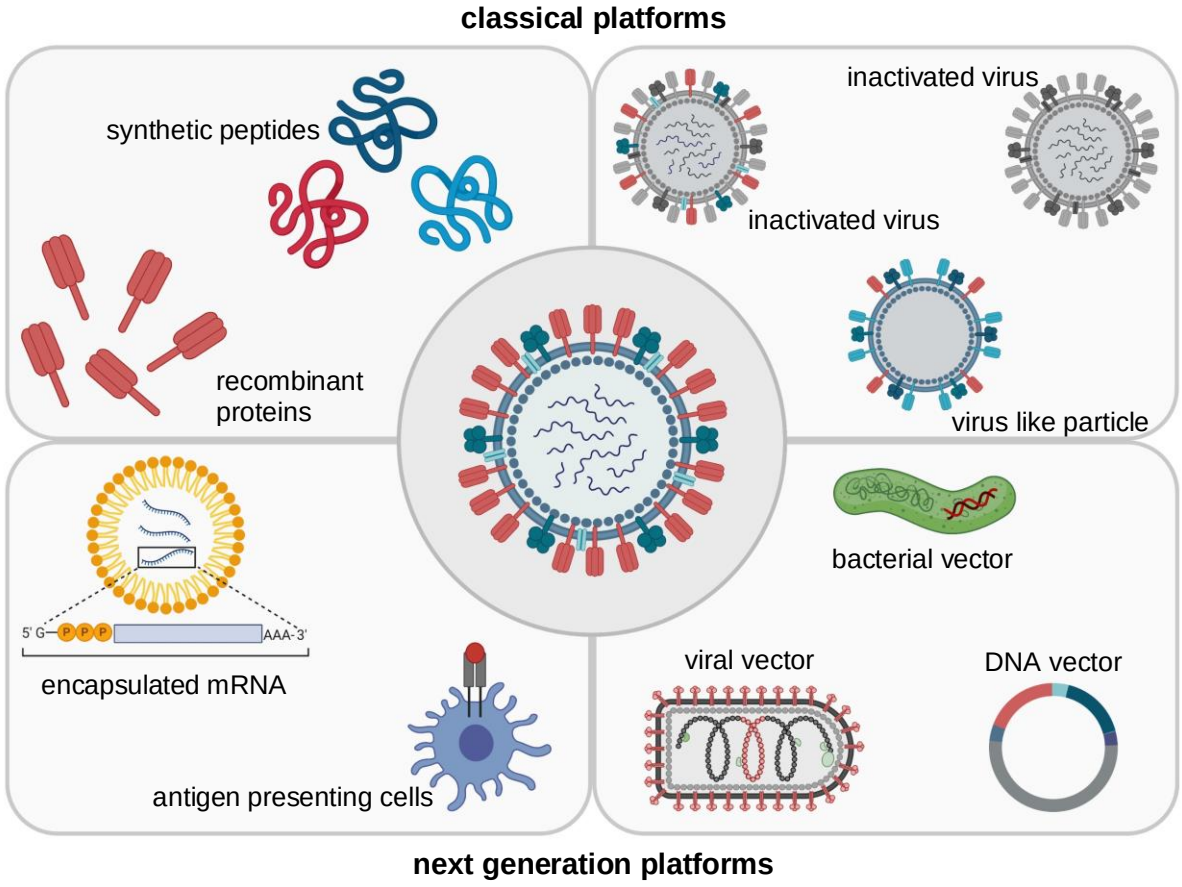


Figure 5: **Vaccine platforms.** Classical platforms and next generation platforms for vaccine development are depicted. Figure created with BioRender.com, modified from van Riel, D. & de Wit, E. 2020; Gray, R.,2020; Lambert, L. C. & Fauci, A. S., 2010 [94–96]

In the last decades, measurement of seroconversion was the gold standard to determine immune responses post vaccination. The protective role of antibodies was emphasized in studies with patients with immunological defects, the passive protection of antibody administration, and the success of vaccines that do not induced a T cell response [97]. Nevertheless, other immune cells are also mandatory for protective immune responses upon vaccination. In the last decade, T cells responses are getting more important as their activation is described to mediate protection via cellular effector functions, which is not limited to a successful B cell activation [98]. For instance, primed mice with non-lethal Dengue virus (DENV) strains showed protective $CD4^+$ and $CD8^+$ T cell responses which protected mice from lethal DENV infections [99].

Newly developed system vaccinology approaches lead to comprehensive investigations of induced immune responses by vaccines with respect to their specific mechanisms. In particular, modern technics including high-throughput technologies facilitated a broad investigation of global biology processes resulting in protection against diseases [100,101]. Innate immune responses such as activation of innate immune cells and cytokine profiles as well as T cell responses and transcriptomic changes are included in systems vaccinology approaches [101,102]. For instance, early gene expressions were correlated with later antibody responses post yellow fever (YF-17D) vaccination in humans [103]. Also, systems vaccinology approaches of influenza vaccination (Inactivated Trivalent Influenza Vaccine: TIV) in humans revealed a specific gene signature of B cells including immunoglobulin and chemokine receptors [104]. Moreover early transcriptomic signatures were correlated with hemagglutination (HAI) titers in vaccinated children emphasizing the power of systems vaccinology approaches to identify potentially biomarkers for vaccine-induced protection [105]. The above-described vaccine platforms (figure 5) were also used to design effective vaccines against EBOV.

### 1.3.2 Vaccines against the Ebola virus disease

Since the EBOV virion carries only the EBOV-GP on its surface, the immunogenic EBOV-GP was predominantly used in vaccine development [40–43,106] (table 1). However, some vaccines also included other EBOV proteins such as the EBOV-NP in vaccine formulation (table 1). While

one of the first vaccination strategies with inactivated viruses was abandoned due to safety concerns and low efficacy in non-human primates, DNA plasmids, virus like particles, and viral vector vaccines were used for the development of vaccine candidates [107–110]. Virus like particles encoding for EBOV-GP, -NP, and -VP40 revealed antibody-mediated protections in challenging models of nonhuman primates [110]. Clinical trials of DNA-vectored vaccines encoding for EBOV-GP of different EBOV strains and an EBOV-NP also determined EBOV-specific antibodies and T cell responses in humans [108]. Other vaccine strategies, which were also partially used for EVD vaccines, such as live-attenuated/inactivated vaccines, bacteria-vectored vaccines, antigen-presenting cells, protein-based vaccines, and RNA-vectored plasmids are discussed elsewhere [43,94,111–113].

Table 1: Selected vaccine candidates against EVD

| Vaccine candidate | Vaccine platform | Genome target | References |
|---|---|---|---|
| EBOV irradiated | Concentrated, gamma-irradiated whole-virion | Whole EBOV | 107 |
| EBOV irradiated | EBOVΔVP30, hydrogen peroxide inactivation | Whole EBOV | 114 |
| | | | |
| Liposomen-encapsulated EBOV | Encapsulated, gamma-irradiated EBOV particles in liposomes containing lipid A | Irradiated EBOV | 107,115 |
| | | | |
| DNA | DNA-vectored | EBOV-GP | 116 |
| DNA | DNA-vectored | EBOV-NP + two EBOV-GP from different EBOV strains | 108 |
| | | | |
| Virus like particle | Kunjin virus derived replicons | EBOV-GP | 117,118 |
| Virus like particle | EBOV like particles | EBOV-GP, -NP, -VP40 | 110 |
| | | | |
| Ad5-EBOV | Viral vector: Ad | EBOV-GP | 119 |
| ChAd3-EBO-Z | Viral vector: chimpanzee Ad | EBOV-GP | 120 |
| ChAd3-EBO-Z + MVA-BN Filo | Viral vector: chimpanzee Ad + MVA | EBOV-GP | 121 |
| ChAd3-EBO-Z + MVA-EBO-Z | Viral vector: chimpanzee Ad + MVA | EBOV-GP | 122 |
| ChAd3-EBO-Z + Ad26-ZEBOV | Viral vector: chimpanzee Ad + Ad | EBOV-GP | 123 |

| | | | |
|---|---|---|---|
| cAd5-EBO | Viral vector: chimpanzee Ad | EBOV-GP of two different EBOV strains | 124 |
| HPIV3-EBO-Z | Viral vector: human parainfluenza virus (HPIV) | EBOV-GP | 125 |
| MVA-EBOV (Mvabea) + Ad26.EBOV-GP (Zabdeno) | Viral vector: MVA and Ad in heterologous prime-boost regimen | Four *filoviridae* GP | 126,127 |
| VACV-EBOV | Viral vector: Vaccinia Virus | EBOV-GP | 107 |
| VEEV-EBOV | Viral vector: Venezuelan equine encephalitis virus | EBOV-GP and/or EBOV-NP | 107,128 |
| VSV-EBOV (Ervebo®) | Viral vector: VSV | EBOV-GP | 84,85,127, 129,130 |

Due to the broad immune response and beneficial safety profile of viral vector vaccines, different vectors were used for EBOV vaccine candidates (table 1). Since the first viral vector vaccine based on a modified vaccinia virus Ankara (MVA) strain was used to design a vaccine against the hepatitis B virus (HBV), several other vaccine candidates were developed based on the MVA platform [131–133]. In a recent study, our group demonstrated that the MVA-based viral vector vaccine MVA-MERS-S against MERS result in an induced immune signatures including humoral and cellular immune responses [134]. The immune response by MVA-MERS-S was efficient and still tolerable in humans highlighting the potential for MVA as viral vector against EIDs. The MVA platform was used to design different vaccine candidates encoding for the GP of ZEBOV or for four *filoviridae* proteins [126]. In addtion, the vesicular stomatitis virus (VSV), different adenovirus (Ad) strains, and the human parainfluenza virus were utilized for the development of vaccine candidates (table 1) [43,84,85]. Viral vector platforms for vaccine development, which were used for other diseases, are reviewed elsewhere [135,136]. Investigations of different viral vector vaccine candidates revealed VSV and MVA as the most promising platforms for EBOV vaccine designs.

### 1.3.3 Comparison of VSV-EBOV & MVA-EBOV

VSV-EBOV showed a rapid and protective immune response in humans and was the first licensed vaccine that is based on a viral vector (Ervebo®) [84,85,127,129,130]. While VSV-EBOV additionally expresses the heterologous EBOV-GP on its surface, MVA-EBOV only encodes for the respective EBOV-GP gene (figure 6) [137]. Another MVA platform called MVA-BN® by

Bavarian Nordic was used to design a viral vector vaccine against EBOV (MVA-BN-Filo: Mvabea®) [138,139]. Ervebo® was licensed in a single-dose immunization, whereas Mvabea® was licensed in a heterologous prime boost vaccination with the Ad26-based vaccine Zabdeno® (Ad26.EBOV-GP) [126,127,140]. While the licensed Mvabea® encodes for four *filoviridae* proteins including the GP of ZEBOV, SUDV, MARV and NP of TAFV [126], MVA-EBOV encodes only for the genetic information of the ZEBOV-GP. One important property of the viral vector MVA is that it cannot replicate in humans and therefore is a replication-deficient strain [133]. In contrast, VSV is a replication-competent strain, which replicates in human cells to some extent [137].

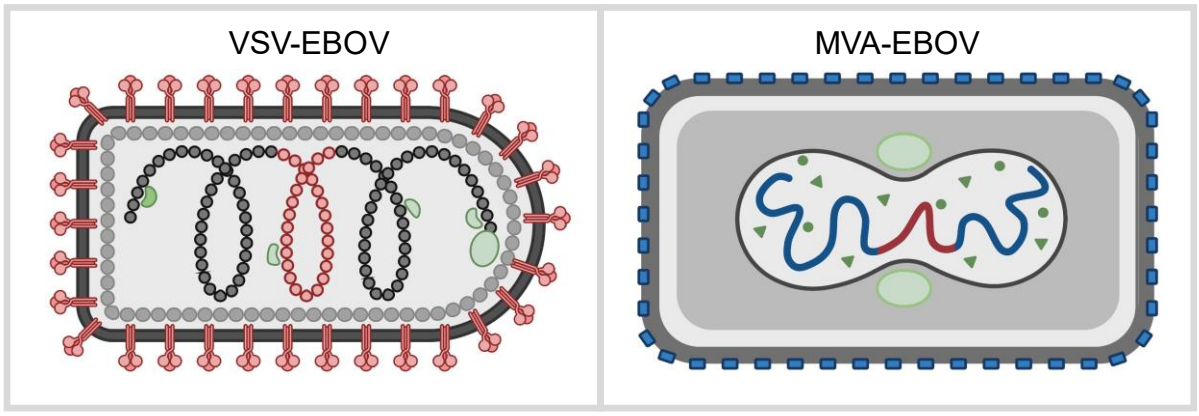


Figure 6: **Viral vector vaccines against EBOV.** Left: VSV-EBOV (Ervebo®) expressing the EBOV-GP on its surface instead of the VSV-GP. Right: MVA-EBOV encoding for the EBOV-GP gene. Figure created with BioRender.com; left side (VSV-EBOV) modified from Poetsch et al., 2019 [88]

Ervebo® revealed a 100 % protection in macaques and 97,5 % in human ring vaccination studies during the EVD outbreak in the DRC in 2018 [109,141,142]. However, the protection induced by MVA-EBOV encoding for the ZEBOV-GP has not been determined in humans, since no clinical trial was conducted to date. Transcriptomic changes including transcripts for innate and anti-viral immunity as well as B cell activation were observed in VSV-EBOV vaccinated cynomolgus macaques [93]. Moreover, VSV-EBOV vaccinated humans revealed an increased secretion of IP-10 which was linked to later antibody responses [92]. Interestingly, non–VSV-EBOV vaccinated cynomolgus macaques also showed an increased expression of *IP-10* post EBOV challenge emphasizing the relevance of induced IP-10 signatures [93]. Furthermore, the innate and adaptive immune signature can be modified by non-coding micro RNAs (miRNA). miRNAs exhibit a negative post-transcriptional regulation of

protein-coding mRNAs via not fully understood mechanisms [143–146]. Changes in the profile of several miRNAs were observed upon VSV-EBOV vaccination in humans and linked to adaptive immune responses [91].

Although several vaccines such as VSV-EBOV showed a high efficacy in men and women, there is an increasing evidence that men and women respond differently to outer stimuli including viral infections and their therapeutic countermeasure [147–151].

## 1.4 Sex differences in infectious diseases

The manifestation and magnitude of immune responses to infectious diseases can differ between men and women. In general, the incidence and severity of infectious diseases are enhanced in men compared to women including diseases caused by viruses, bacteria, fungi, and parasites [147,152,153]. Following sections will focus on sex-based differences in the immune responses to viral infections and vaccinations. Sex-based differences in bacterial, mycotic, and parasitic infections are summarized elsewhere [152,154,155].

### 1.4.1 Sex differences in the immune response

The frequency of immune cells can differ in the peripheral blood between men and women. While Kverneland *et al.* reported only tendencies for increased amounts of B- and T cells in women measured via a standardized flow cytometry protocol [156], other colleagues described partly significantly elevated frequencies of immune cells including B cells, T cells, myeloid DCs (mDCs), and monocytes in women and female non-human primates [157,158]. The immune response can be shaped and influenced by different aspects like (i) gender and socio-economic factors including behavior, environment, and constitution of each individual, (ii) biological factors including epigenetic modifications, imprinting of some genes, and sex chromosomes as well as (iii) molecular conditions such as microbiota and sex hormones (figure 7) [147,150,152,159–162].

Gender and socio-economic factors influence infections with pathogens by determining the individuals, which get into contact with infected reservoirs. Since many index patients of various EBOV outbreaks were infected in the forest by contaminated bushmeat, these

patients were suggested to be predominantly men who work more often in the forest compared to women. Moreover, it is postulated that women had a lower case-fatality rate compared to men, who stay longer in their community after the day of symptom onset [163]. Nevertheless, women are mainly infected during outbreak progression, since they generally take care of sick people, highlighting the relevance of socio-economic factors during EBOV outbreaks [164].

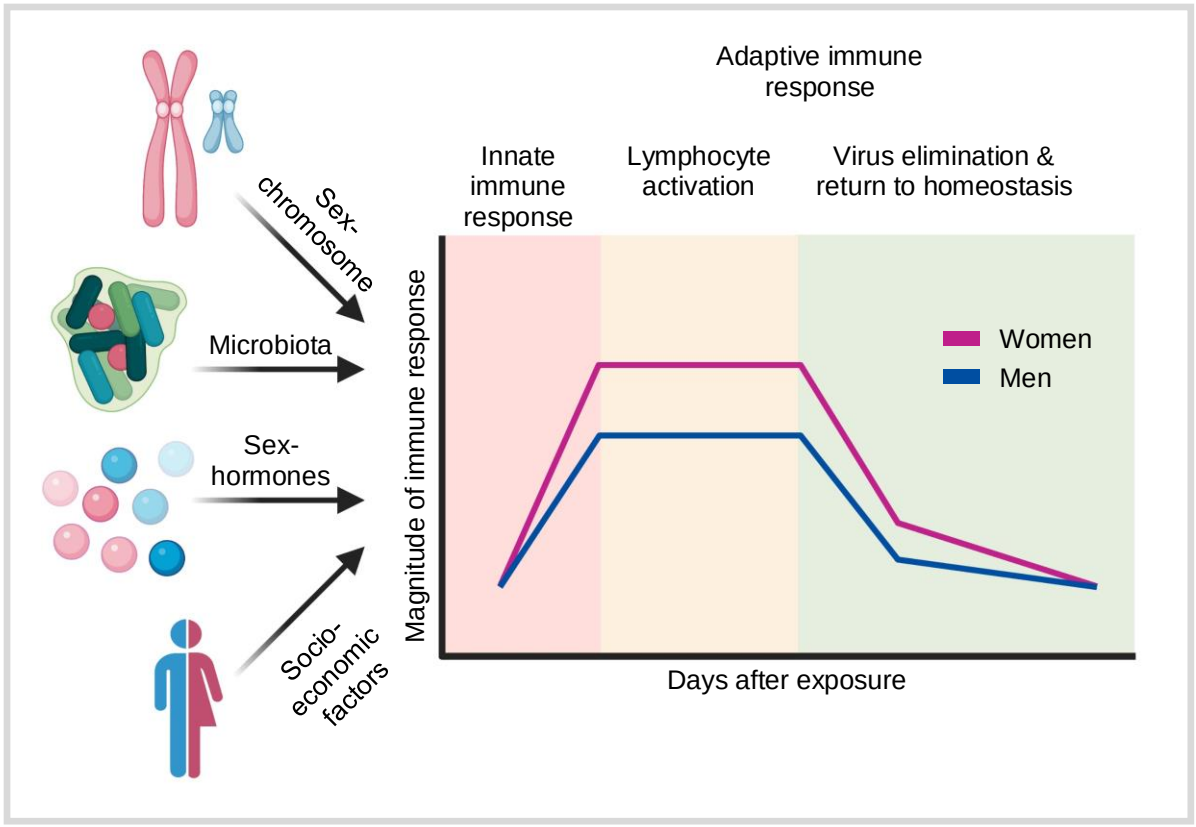


Figure 7: **Sex difference in immune responses to external stimuli.** Reasons for sex-based differences including sex chromosomes, sex hormones, microbiota, and socio-economic factors are depicted on the left side. These differences can result in different magnitudes of immune responses in men and women after exposure to outer stimuli like viral infections and the administration of vaccines. Above the diagram different phases of the immune response are depicted. Figure created with BioRender.com; modified from Klein, S. L., 2012 [147]; Markle, J. G. & Fish, E. N., 2014 [161]; Klein, S. L. et al., 2010 [165]

Furthermore, sex hormones such as estrogen, progesterone, and testosterone can influence immune cells [166]. These steroid hormones are present in men as well as women at different levels. While testosterone is defined as “male sex hormone”, estrogen and progesterone are typically “female sex hormones”. In terms of estrogen its immune-modulatory function is

mediated by binding estrogen-specific receptors (ESR), which exhibit a transcriptional activation or repression [160]. Genes which carry an ESR responsive-element are directly regulated by estrogen-ESR complexes, whereas the regulation of other genes is indirectly modified by the recruitment of other regulatory proteins [160,167]. Estrogen can shape the response of several immune cells, since B cells, T cells, macrophages, NK cells, neutrophils, and DCs express estrogen receptors [160]. This can lead to a higher cytokine secretion in women post infection and vaccination. For instance, IFNα is stronger enhanced in pDCs derived from women mediated by TLR7 post viral stimulation resulting in elevated immune responses on the one hand and in a higher risk for immunopathology on the other hand [168–170]. Besides IFNα secretion this included also increased mRNA levels of 13 *IFN*α subtypes and *IFN*β [171]. Moreover, higher basal mRNA levels of the *IFN regulatory factor 5 (IRF5)* correlate with increased *estrogen receptor 1 (ESR1)* mRNA levels elucidating enhanced IFNα levels in women [169]. Interestingly, immune cells like monocytes can also be higher activated in men indicating a testosterone-biased immune response [172]. Testosterone treated whole blood derived from women showed *in vitro* an increased secretion of IL-12 and IL-1β by monocytes compared to untreated monocytes [173]. In addition, reduced testosterone concentration in aged mice indicated a poor outcome of influenza A virus infection [174]. Therefore, sex hormones can have manifold effects on the immune response.

Moreover, specific transcription of genes that are located on the sex chromosome X (X-linked) can lead to sex-based differences in the immune response to external stimuli [175]. Several immune-related genes are located on the X-chromosome including TLR7/8, cytokine receptors including the CXC chemokine receptor 3 (CXCR3), and transcriptional factors like forkhead-box P3 (FOXP3) [160,176,177]. Genes such as *TLR7*, which can escape from X-chromosome inactivation (XCI), are elevated in women compared to men resulting in enhanced IFN type I immune cell response upon TLR7 activation [178–180]. A higher IFN type I response leads to a comprehensive activation of the immune system including several immune cells and an expression of IFN-stimulated genes that delimit viral spreading [181]. On the one hand this can result in faster clearance of the virus. On the other hand, this might also lead to enhanced immunopathology in women compared to men. All these different aspects influence the immunocompetence of men and women resulting in an altered immune signature also in response to viral infections.

### 1.4.2 Sex differences in viral infections

In general, men develop a lower innate and adaptive immune response to viruses, whereas women have to suffer from enhanced immunopathology effects resulting in a worse outcome compared to men (figure 7) [147]. According to this, a sex-based incidence for influenza A infection with an increased fatality rate in the female population was described [182]. Moreover, a sex-biased progression to the human immunodeficiency virus (HIV)-mediated acquired immunodeficiency syndrome (AIDS) was detected. Although women have commonly lower plasma RNA levels of HIV [183], the progression of AIDS is elevated in women compared to men [168]. In addition, women also exhibit an increased prevalence for the herpes simplex virus (HSV) and a higher risk for HSV anterior uveitis [184–186]. In contrast to HSV, the HBV serum prevalence and DNA titer are higher in men than in women [187,188]. Accordingly, the risk to develop HBV related hepatocellular carcinoma (HCC) is enhanced in men compared to women [189]. Furthermore, men are more prone to hepatitis C virus (HCV) infections. In accordance, a higher HCV incidence as well as progression to HCV-related HCC were determined in men [190].

In addition, emerging viruses indicated a sex-biased incidence and severity of illness related to socio-economic, gender, and sex related factors. While the severe acute respiratory syndrome coronavirus 1 (SARS-CoV-1), Middle East respiratory syndrome coronavirus (MERS-CoV), severe acute respiratory syndrome coronavirus 2 (SARS-CoV-2), Nipah virus, and hantavirus revealed an increased incidence in men, the dengue virus exhibited a higher incidence and more severe cases in girls and women [164,191–199]. Severe disease progression of COVID-19 occurred predominantly in SARS-CoV-2 infected men [197,198,200]. While men had an increased cytokine secretion mediated by innate immune cells and an enhanced activation of non-classical monocytes, women exhibited an elevated T cell response upon SARS-CoV-2 infection [201]. To date, sex-based differences in immune responses to EBOV are not properly investigated where differences in EBOV infection are mainly related to socio-economic and gender aspects rather than biological factors [202]. Epidemiological studies revealed a tendency that men are more frequently infected by EBOV than women [203]. Finally, all these examples highlight the complexity of sex-based immune responses to viral infections and lead to the question whether they should be considered in vaccination.

### 1.4.3 Sex differences in vaccination

Sex differences in infections lead to the assumption that vaccines, which are based on inactivated pathogens, components of the pathogen, or viral vectors, also result in different protective immune responses in men and women. In the last decade, sex-based differences in vaccination were described including influenza, measles-mumps-rubella, tetanus, and diphtheria vaccines [165,204–206]. In general, women develop a stronger immune response to vaccination than men [148,207,208]. They benefit from a higher magnitude of humoral and cellular immune responses but have to suffer from more adverse reactions than men, explicitly described for adults and children (figure 7) [148]. Moreover, different transcriptomic profiles were detected post vaccination and were associated with different outcomes in men and women [165,209].

Half-dose vaccination against influenza with TIV, licensed in different seasons 2000-2001 and 2004-2005, revealed sufficient immune response with significant higher antibody titers in women [205,210,211]. In addition, the live vaccinia virus (VACV) vaccine (Dryvax®) exhibited a sex-biased immune response post vaccination in humans. Besides higher neutralizing titers in women [212], different cellular immune responses between men and women were detected. While men had significantly higher antigen-specific total IFNγ ELISPOT responses and IL-1β secretion, women showed enhanced antigen-specific IL-2 and IL-10 secretion upon Dryvax® vaccination [213]. Moreover, a meta-analysis of a next generation replication-deficient smallpox vaccine based on MVA (MVA-BN: Imvamune®) showed higher specific antibody titer in men compared to women [214]. Also, the live attenuated yellow fever vaccine 17D (YF-17D) caused more adverse reactions in women [215]. Furthermore, transcriptome analysis indicated that innate immune responses including TLR-signaling are elevated in women post YF-17D [165]. However, no clear sex-based differences in the antibody titer were determined [216–219]. While in a double-blind clinical trial of the WHO-17D and Brazilian 17DD substrain against YF no sex-biased immune responses were observed [217], increased antibody titers were detected in men in a double-blind clinical trial of YF-17D manufactured in the USA and United Kingdom [216]. To date, sex-based differences in the immune response to viral vector vaccines are not well understood. No sex-based differences in the immune signature to VSV-EBOV or MVA-EBOV were observed until now [220,221]. Hence, further investigations are needed to

address sex-based differences in vaccination, reduce side effects in women and improve immune responses in men.

## 1.5 Aim of this study

Viral vectors can serve as excellent vaccine platforms to expeditiously develop and implement vaccines in response to EID outbreaks such as EBOV. In 2019, Ervebo® was the first licensed viral vector vaccine, which is based on the VSV platform (VSV-EBOV) [127,129,130]. In addition, the MVA platform was utilized to develop a vaccine against EBOV (MVA-EBOV). Most insights for vaccine-induced immune responses are linked to the induction of pathogen-specific antibodies and their neutralizing capacity.
Exact mechanisms of innate immune signatures by viral vector vaccines remain inadequately understood. Therefore, the overarching hypothesis of this study was that VSV-EBOV and MVA-EBOV induce distinct innate immune signatures which are influenced by the viral vector and sex of each individual.

This hypothesis was investigated in two specific aims:

1. **To decipher immune signatures induced by viral vector vaccines against EBOV.**

For this aim *in vitro* stimulation models of hPBMCs using VSV-EBOV and MVA-EBOV were implemented to investigate innate immune signatures longitudinally. System biology approaches such as analyses of cytokine profiles, activation of innate immune cells, and transcriptomic changes provided necessary information to dissect viral vector vaccine-induced immune signatures.

2. **To analyze vector- and sex-specific differences in the innate immune response to VSV-EBOV and MVA-EBOV.**

The understanding of vector-specific responses would elucidate the impact of viral vectors to immune signatures, while the identification of sex-based differences is necessary to reduce adverse reactions in women and increase immunity in men. This could lead to optimized

vaccine dosage and individualized immunization approaches, which ensure a maximal immune protection of both sexes.

In conclusion, insight into induced immune responses by VSV-EBOV and MVA-EBOV may help to accelerate and facilitate further developments and implementations also for future vaccine or immunotherapies based on VSV and MVA.

# 2. Materials

## 2.1 Consumable materials

All plastic consumable materials, which were used for methods described in section 3, were purchased at Bio-Rad Laboratories GmbH, eBioscience Inc., Eppendorf AG, Merck KGaA, Sarstedt AG & Co. KG, STEMCELL Technologies Inc., and Sigma-Aldrich Chemie GmbH.

## 2.2 Study cohort

Table 2: Blood donors for *in vitro* stimulations of hPBMCs using rMVA

| Sex | Subject ID# | Age |
|---|---|---|
| Female | 12 | 27 |
| | 14 | 30 |
| | 15 | 41 |
| | 17 | 29 |
| | 28 | 33 |
| | 31 | 35 |
| | 32 | 26 |
| | 167 | 42 |
| | 256 | 28 |
| | 260 | 29 |
| Male | 8 | 28 |
| | 27 | 28 |
| | 166 | 30 |
| | 226 | 28 |
| | 250 | 27 |
| | 262 | 32 |
| Female | Range (median) | 26-42 (30) |
| Male | Range (median) | 27-32 (28) |
| **All donors** | **Range (median)** | **26-42 (29)** |

Table 3: Blood donors for *in vitro* stimulations of hPBMCs using VSV-EBOV

| Sex | Subject ID# | Age |
|---|---|---|
| Female | 14 | 28 |
| | 17 | 29 |
| | 28 | 33 |
| | 29 | 38 |
| | 31 | 35 |
| | 34 | 28 |
| | 109 | 38 |
| | 167 | 42 |
| | 209 | 27 |
| | 260 | 29 |
| Male | 8 | 28 |
| | 27 | 28 |
| | 30 | 28 |
| | 32 | 43 |
| | 33 | 34 |
| | 117 | 39 |
| | 164 | 33 |
| | 228 | 32 |
| | 262 | 32 |
| | 268 | 27 |
| Female | Range (median) | 27-42 (31) |
| Male | Range (median) | 27-43 (32) |
| **All donors** | **Range (median)** | **27-43 (32)** |

Table 4: Blood donors for *in vitro* stimulations of hPBMCs using MVA-EBOV

| Sex | Subject ID# | Age |
|---|---|---|
| Female | 14 | 28 |
| | 28 | 33 |
| | 31 | 35 |
| | 36 | 27 |
| | 109 | 38 |
| | 209 | 27 |
| | 269 | 25 |
| Male | 27 | 28 |
| | 33 | 34 |
| | 37 | 28 |
| | 38 | 62 |
| | 43 | 31 |
| | 164 | 33 |
| | 228 | 32 |
| | 262 | 32 |
| | 270 | 29 |
| Female | Range (median) | 27-38 (28) |
| Male | Range (median) | 28-62 (32) |
| **All donors** | **Range (median)** | **27-62 (32)** |

Table 5: Blood donors used for analysis of transcriptomic changes upon stimulation. Transcriptomic changes were analyzed using the nanoString® technology (section 3.9) and RNA-Seq after VSV-EBOV *in vitro* stimulations.

| Sex | Subject ID# | Age |
|---|---|---|
| Female | 14 | 28 |
| | 29 | 38 |
| | 209 | 27 |
| | 260 | 29 |
| Male | 117 | 39 |
| | 164 | 33 |
| | 228 | 32 |
| | 262 | 32 |
| Female | Range (median) | 27-38 (29) |
| Male | Range (median) | 32-39 (33) |
| **All donors** | **Range (median)** | **27-39 (32)** |

Table 6: Blood donors used for analysis of transcriptomic changes upon stimulation. Transcriptomic changes were analyzed via RNA-Seq (section 3.9) after MVA-EBOV *in vitro* stimulations.

| Sex | Subject ID# | Age |
|---|---|---|
| Female | 14 | 28 |
| | 36 | 27 |
| | 109 | 38 |
| | 209 | 27 |
| Male | 33 | 34 |
| | 164 | 33 |
| | 228 | 32 |
| | 262 | 32 |
| Female | Range (median) | 27-38 (28) |
| Male | Range (median) | 32-34 (33) |
| **All donors** | **Range (median)** | **27-38 (32)** |

## 2.3 Eukaryotic cell lines

Table 7: Eukaryotic cell lines for *in vitro* stimulation models of eukaryotic cells

| Cell line | Origin - organism | Tissue | Cell type | Company | Catalog # |
|---|---|---|---|---|---|
| Vero81 cells | African green monkey (*Cercopithecus aethiops*) | Kidney | Epithelial cells | ATCC®, Manassas, USA | ATCC® CCL-81™ |
| THP-1 | Human (*Homo sapiens*) | Peripheral blood | Monocytes | DSMZ | ACC16 |

## 2.4 Chemicals, media, and buffer

Table 8: Chemicals

| Name | Additional information | Catalog # | Company |
|---|---|---|---|
| 10x TBE-buffer | Agarose gel electrophoresis | 574795 | Sigma-Aldrich Chemie GmbH, Taufkirchen, Germany |
| 50 bp DNA ladder | Agarose gel electrophoresis | 10416014 | ThermoFisher Scientific Inc., Waltham, USA |
| Agarose | Agarose gel electrophoresis | A9539-250G | Sigma-Aldrich Chemie GmbH, Taufkirchen, Germany |

| | | | |
|---|---|---|---|
| Chloroform | With 0.75% ethanol; for RNA isolation | 7386 | Fisher Scientific GmbH, Schwerte, Germany |
| Counting chamber | Used with cell counter T20 | 145-0011 | Bio-Rad Laboratories GmbH, Feldkrichen, Germany |
| Crystal violet | Plaque assay | C6158 | Sigma-Aldrich Chemie GmbH, Taufkirchen, Germany |
| DAPI | Immunofluorescence | D1036 | ThermoFisher Scientific Inc., Waltham, USA |
| dd $H_2O$ | Milli-q | | Merck Millipore KGaA, Darmstadt, Germany |
| DEPC-treated $H_2O$ | RNA elution | T143.2 | Carl Roth GmbH + Co. KG, Karlsruhe, Germany |
| DMSO | In combination with cell media for long term storage of cells (10 %) | 34869 | Sigma-Aldrich Chemie GmbH, Taufkirchen, Germany |
| dNTPs | cDNA synthesis | 18427-013 | ThermoFisher Scientific Inc., Waltham, USA |
| DTT | 0.1 M supplied with SuperScript™ III | 18080044 | ThermoFisher Scientific Inc., Waltham, USA |
| EDTA | 0.5 M, pH 8.0, RNase-free | AM9260G | ThermoFisher Scientific Inc., Waltham, USA |
| Ethanol | Surface disinfection (70 %) | 22805000 | Th Geyer GmbH & Co. KG, Renningen, Germany |
| Ethanol | RNA isolation | 64-17-5 | Merck KGaA, Darmstadt, Germany |
| Ethidium bromide | Agarose gel electrophoresis | 100027642 | ThermoFisher Scientific Inc., Waltham, USA |
| FCS | Fetal calf serum, inactivation at 56°C | 0817D | Merck KGaA, Darmstadt, Germany |
| Glycine | Immunofluorescence | 50046-250g | Sigma-Aldrich Chemie GmbH, Taufkirchen, Germany |
| GlycolBlue™ | Coprecipitant during RNA isolation | AM9515 | ThermoFisher Scientific Inc., Waltham, USA |
| Hank's balanced salt solution | Buffer for density gradient centrifugation (Ficoll) | H6648 | Sigma-Aldrich Chemie GmbH, Taufkirchen, Germany |
| Histopaque®-1077 | Medium for density gradient centrifugation (Ficoll), with Pen/Strep (1 %) | H8889 | Sigma-Aldrich Chemie GmbH, Taufkirchen, Germany |
| Intracellular fixation buffer | Staining and fixation buffer flow cytometry | 00-8222-49 | eBioscience Inc., San Diego, USA |

| | | | |
|---|---|---|---|
| Isopropanol | RNA isolation | 348638.5L | Sigma-Aldrich Chemie GmbH, Taufkirchen, Germany |
| Lymphoprep™ | Medium for density gradient centrifugation (SepMate™) | 07811 | STEMCELL Technologies Inc., Grenoble, France |
| Random primer | cDNA synthesis | S13309 | ThermoFisher Scientific Inc., Waltham, USA |
| RNase OUT | Reverse transcription | 10777019 | ThermoFisher Scientific Inc., Waltham, USA |
| Sekusept™ plus | inactivation of cell culture waste (4 %) | 3030910 | Ecolab Deutschland GmbH, Monheim am Rhein, Germany |
| TBE | Agarose gel electrophoresis | 574795 | Sigma-Aldrich Chemie GmbH, Taufkirchen, Germany |
| TriReagent® | RNA isolation | 93289 | Sigma-Aldrich Chemie GmbH, Taufkirchen, Germany |
| Triton X-100 | Immunofluorescence | T9284-100ml | Sigma-Aldrich Chemie GmbH, Taufkirchen, Germany |
| Trizol | RNA storage + isolation | 93289 | Sigma-Aldrich Chemie GmbH, Taufkirchen, Germany |
| Trypan blue | Cell counting | T8154 | Sigma-Aldrich Chemie GmbH, Taufkirchen, Germany |
| Ultra pure™ destilled water | DNase-, RNase-free | 10977-035 | ThermoFisher Scientific Inc., Waltham, USA |
| UltraComp eBeads™ | Compensation flow cytometry | 4287713 | eBioscience Inc., San Diego, USA |
| Zombie NIR™ | Live dead staining in flow cytometry, APC-Cy7 channel, dilution: 1:500 | 423106 | BioLegend Inc., San Diego, USA |

Table 9: Media and buffer

| Name | Aditional information | Catalog # | Company |
|---|---|---|---|
| 1 % methylcellulose solution | Solution for plaque assay containing 5 ml 10x MEM, 2.93 ml sodium bicarbonate, 1.25 ml Hepes (1 M), 15.82 ml distilled water, and 25 ml sterile methylcellulose (2 % in distilled water) | | |
| Fixation buffer | PBS with 4 % PFA (flow cytometry staining) or 2 % (Plaque assay) | | |
| Hepes | 1 M in water | 83264 | Sigma-Aldrich Chemie GmbH, Taufkirchen, Germany |
| hPBMCs medium | Cell culture medium for hPBMCs, RPMI-1640 with L-glutamine (1 %) Pen/Strep (1 %) | | |
| L-Glutamine | Cell culture | G7513 | Sigma-Aldrich Chemie GmbH, Taufkirchen, Germany |
| MEM-eagle | Medium | M2279 | Sigma-Aldrich Chemie GmbH, Taufkirchen, Germany |
| Methylcellulose | Plaque assay, autoclaved prior usage | M0512-100G | Sigma-Aldrich Chemie GmbH, Taufkirchen, Germany |
| Paraformaldehyde | Flow cytometry staining (4 %) | P6148 | Sigma-Aldrich Chemie GmbH, Taufkirchen, Germany |
| PBS | Phosphate buffered saline | S0615 | Merck KGaA, Darmstadt, Germany |
| Penicillin (Pen), Streptomycin (Strep) | Cell culture | P433-100ML | Sigma-Aldrich Chemie GmbH, Taufkirchen, Germany |
| RPMI-1640 | Cell medium | R8758-500ML | Sigma-Aldrich Chemie GmbH, Taufkirchen, Germany |
| Sodium bicarbonat | Plaque assay | S6014 | Sigma-Aldrich Chemie GmbH, Taufkirchen, Germany |
| Staining medium | PBS + 2 % FCS | D8862 | Sigma-Aldrich Chemie GmbH, Taufkirchen, Germany |

| | | | |
|---|---|---|---|
| Vero81 medium | Cell culture medium for Vero81 cells, MEM-earl with<br>Pen/Strep (1 %)<br>Glutamine (1 %) | | |

## 2.5 Laboratory equipment

Table 10: Laboratory equipment

| Name | Additional information | Company |
|---|---|---|
| BD LSRFortessa™ | Flow cytometry | Becton Dickinson GmbH, Heidelberg, Germany |
| Centrifuge | 5810R<br>X3R | Eppendorf AG, Hamburg, Germany<br>ThermoFisher Scientific Inc., Waltham, USA |
| ChemiDoc Touch Imaging System | Agarose gel documentation | Bio-Rad Laboratories GmbH, Feldkrichen, Germany |
| Counting slide | Used with TC20 cell counter | Bio-Rad Laboratories GmbH, Feldkrichen, Germany |
| Freezer | U101 Inova, -80°C | New Brunswick Scientific, Eppendorf AG, Hamburg, Germany |
| Fridge | 4°C, -20°C | Liebherr-International Deutschland GmbH, Biberach an der Riß, Germany |
| Gel chamber and comb | Agarose gel electrophoresis | Bio-Rad Laboratories GmbH, Feldkrichen, Germany |
| Heating plate | | IKAMAG® RCT, Fisher Scientific GmbH, Schwerte, Germany |
| Incubator | Model CB, cell culture: 37°C; 5 % $CO_2$ | Fa. BINDER GmbH, Tuttlingen, Germany |
| Laminar flow cabinet | Maxisafe 2020<br>KS12 hera safe | ThermoFisher Scientific Inc., Waltham, USA |
| Light microscope | Inverted microscope, cell culture | KERN & SOHN GmbH, Balingen, Germany |
| Lightcycler 96 | qPCR cyler | Eppendorf AG, Hamburg, Germany |
| Liquid nitrogen tank | MVE HEco 800-190,<br>Long term storage of hPBMCs and eucaryotic cell lines (-190°C) | MVE Biological Solutions, Georgia, USA |

| | | |
|---|---|---|
| Locker for hazardous substances | With ventilation | asecos GmbH, Gründau, Germany |
| Mastercycler | Vapo.protect; PCR cycler | Eppendorf AG, Hamburg, Germany |
| Microwave | | Sharp Electronics GmbH, Hamburg, Germany |
| Milli-Q purification system | Distilled water | Merck Millipore KGaA, Darmstadt, Germany |
| Nanodrop | Measurement of DNA and RNA concentration | DeNovix Inc., Wilmington, USA |
| nCounter® SPRINT Profiler | Expression analysis | NanoString Technologies® Inc., Seattle, USA |
| Olympus IX-81 | Confocal laser scanning microscope | Olympus Europa SE & Co. KG, Hamburg, Germany |
| Pipetboy | Pipetboy 2 | Integra Biosciences GmbH, Biebertal, Germany |
| Pipett | 2 µl | Gilson Inc., Middleton, USA |
| Pipetts | 10, 100, 200, 1000 µl | Eppendorf AG, Hamburg, Germany |
| RNA/DNA bench | UVC/T-M-AR | Grant-bio, Fisher Scientific GmbH, Schwerte, Germany |
| Shaker | | Eppendorf AG, Hamburg, Germany |
| Stratacooler | Slow freezing of hPBMCs and eucaryotic cell lines | Agilent Technologies Inc., Santa Clara, USA |
| Table centrifuge | 200 µl, 1.5 ml, and 2 ml tubes | Biozym Scientific GmbH, Hessisch Oldendorf, Germany |
| TC20™ automatic cell counter | Cell counting of hPBMCs, Vero81, and THP-1 | Bio-Rad Laboratories GmbH, Feldkrichen, Germany |
| Thermomix | ThermoMixer® Comfort | Eppendorf AG, Hamburg, Germany |
| UV-light irradiation | Visualization of agarose gel electrophoresis | Bio-Rad Laboratories GmbH, Feldkrichen, Germany |
| Vortexer | Vortexe-Genie 2 | Scientific Industries Inc., Bohemia, USA |
| Water bath | 37°C/56°C | GFL GmbH, Burgwedel, Germany |

## 2.6 DNA oligonucleotides

Table 11: DNA oligonucleotides

| Primer | Direction | Sequenz (5'-3') | Additional information |
|---|---|---|---|
| ActB | Forward | CTGGAACGGTGAAGGTGACA | Housekeeping gene |
| | Reverse | AAGGGACTTCCTGTAACAATGCA | |
| CLEC5A | Forward | GTTTCACCACCACCAGGAGC | Obtained from Cheng, Y. et al., 2016 [222] |
| | Reverse | GGCATTCTTCTCACAGATCC | |
| GAPDH | Forward | GTCGGTGTGAACGGATTTGG | Housekeeping gene |
| | Reverse | TTCCCATTCTCGGCCTTGAC | |
| HMBS | Forward | GGCAATGCGGCTGCAA | Housekeeping gene |
| | Reverse | GGGTACCCACGCGAATCAC | |
| HPRT | Forward | TGACACTGGCAAAACAATGCA | Housekeeping gene |
| | Reverse | GGTCCTTTTCACCAGCAAGCT | |
| IP-10 | Forward | TGAAATTATTCCTGCAAGCCAATT | Provided by HPI, Hamburg (Virus Immunology, Marcus Altfeld) |
| | Reverse | CAGACATCTCTTCTCACCCTTCTTT | |
| MVA-UDG | Forward | GGTAGAGTTTTATAACGAAGTAGCCAGTT | Detection of MVA-EBOV or rMVA-stimulated cells obtained from Chahroudi, A. et al., 2006 [223] |
| | Reverse | CTCGTTTATTTCTAAGCGGTTGTTT | |
| VSV-NP | Forward | GAC CTT GTA TCC TTG AAA GCC | Detection of VSV-EBOV−stimulated cells |
| | Reverse | CAT TTG TGT TCT GCC CAC TC | |
| | Probe | FAM-TGCT TCC AGA ACC AGC GCA GAT GAC AAA-BBQ | |

## 2.7 Kits

Table 12: Kits

| Name | Additional information | Catalog # | Company |
|---|---|---|---|
| AgPath-ID™ | One-step qPCR (viral load of RNA virus) | AM1005 | Applied Biosystem, Waltham, USA |
| Human immunology panel v2 | Expression analysis | XT-CSO-HIM2-12 | nanoString Technologies® Inc., Seattle, USA |
| KAPA RNA HyperPrep kit | Library preparation for RNA-Seq | KK8541 | Roche Molecular Systems Inc., Basel, Swiss |
| LEGENDplex™ | Customized panel analytes: IL-1, IL-2, IL-4, IL-6, IL-8, IL-10, IL-12, IP-10, IFNα, IFNγ, MCP-1, MIG, and TNFα | | BioLegend Inc., San Diego, USA |
| LEGENDplex™ | Pre-defined anti-virus response panel analytes: IL-1β, IL-6, IL-8, IL-10, IL-12p70, IP-10, TNFα, IFNλ1, IFNλ2/3, IFNα2, IFNβ, IFNγ, and GM-CSF | 740390 | BioLegend Inc., San Diego, USA |
| NEBNext Ultra II RNA library kit | Library preparation for RNA-Seq | E7770L | New England Biolabs GmbH, Frankfurt am Main, Germany |
| QiAamp® DNA Mini kit | DNA isolation | 51304 | Qiagen N.V., Venlo, Netherlands |
| SensiMix™ SYBR® No-ROX kit | One-step qPCR (viral load of DNA virus)<br>two-step qPCR (gene expression) | QT650-05 | Meridian Bioscience Inc., Cincinnati, USA |
| SP reagent kit | NovaSeq 6000 reagent kit | 20040326 | Illumina Inc., Berlin, Germany |

## 2.8 Enzymes

Table 13: Enzymes

| Name | Additional information | Catalog # | Company |
|---|---|---|---|
| DNase I | Degrades DNA | 18068-015 | ThermoFisher Scientific Inc., Waltham, USA |
| Red HS Taq Master Mix | PCR | 331126 | Biozym Scientific GmbH, Hessisch Oldendorf, Germany |
| RNase H | Degrades RNA | M0297S | New England Biolabs GmbH, Frankfurt am Main, Germany |
| SuperScript™ III | cDNA Synthesis | 18080044 | ThermoFisher Scientific Inc., Waltham, USA |
| Trypsin-EDTA | 1 M + 0.02 % EDTA | T3924 | Sigma-Aldrich Chemie GmbH, Taufkirchen, Germany |

## 2.9 Antibodies

Table 14: Fluorochrome-conjugated antibodies used for section 4.1.2 and 6

| Epitope | Fluorochrome | Dilution | Clone | Company |
|---|---|---|---|---|
| CD1c | FITC | 1:50 | L161 | BioLegend Inc., San Diego, USA |
| CD3 | APC-Cy7 | 1:100 | SK7 | BioLegend Inc., San Diego, USA |
| CD11b | BUV395 | 1:100 | D12 | Becton Dickinson GmbH, Heidelberg, Germany |
| CD11c | APC | 1:100 | S-HCL-3 | BioLegend Inc., San Diego, USA |
| CD14 | BV711 | 1:33.3 | M5E2 | BioLegend Inc., San Diego, USA |
| CD16 | BV510 | 1:33.3 | 3G8 | BioLegend Inc., San Diego, USA |

| | | | | |
|---|---|---|---|---|
| CD19 | APC-Cy7 | 1:100 | SJ25C1 | BioLegend Inc., San Diego, USA |
| CD40 | PE | 1:100 | 5C3 | BioLegend Inc., San Diego, USA |
| CD83 | BV421 | 1:100 | HB15e | BioLegend Inc., San Diego, USA |
| CD86 | PE-CF5948 | 1:50 | IT2.2 | BioLegend Inc., San Diego, USA |
| CD141 | PE-Cy7 | 1:33.3 | M80 | BioLegend Inc., San Diego, USA |
| CD303 | PerCP-Cy5.5 | 1:33.3 | 201A | BioLegend Inc., San Diego, USA |
| HLA-DR | BV785 | 1:33.3 | L243 | BioLegend Inc., San Diego, USA |
| Anti EBOV-GP | FITC | 1:100 | | Kindly provided by the Bernhard Nocht Institute (Virus Immunology, César Muñoz-Fontela) |

Table 15: Fluorochrome-conjugated antibodies used for section 6.1.5

| Epitope | Fluorochrome | Dilution | Clone | Company |
|---|---|---|---|---|
| CD3 | BUV395 | 1:50 | SK7 | Becton Dickinson GmbH, Heidelberg, Germany |
| CD11c | APC | 1:100 | S-HCL-3 | BioLegend Inc., San Diego, USA |
| CD14 | BV711 | 1:33.3 | M5E2 | BioLegend Inc., San Diego, USA |
| CD16 | BV510 | 1:33.3 | 3G8 | BioLegend Inc., San Diego, USA |
| CD19 | PerCP-Cy5.5 | 1:50 | HIB19 | BioLegend Inc., San Diego, USA |
| CD56 | Pacific Blue | 1:50 | HCD56 | BioLegend Inc., San Diego, USA |
| HLA-DR | BV785 | 1:33.3 | L243 | BioLegend Inc., San Diego, USA |

## 2.10 Viruses

Table 16: Viruses

| Name | Properties | Additional information |
|---|---|---|
| rMVA | Recombinant MVA encodes for GFP and mCherry | Kindly provided by the Ludwig Maximilian University of Munich (Virology, Gerd Sutter), generated by homologous recombination of MVA, promoter for GFP: Pvgf, promoter for mCherry: P11 [224–226] |
| MVA-EBOV | Recombinant MVA encodes for EBOV-GP | Kindly provided by the Ludwig Maximilian University of Munich (Virology, Gerd Sutter) |
| VSV-EBOV (Ervebo®) | Recombinant VSV encodes for EBOV-GP | The licensed VSV-EBOV vaccine (Ervebo®) was passaged by the infection of BHK cells |

## 2.11 Software and database

Table 17: Software and database

| Name | Additional information | Company |
|---|---|---|
| BD FACSDiva™ | v8.0.1 | Becton Dickinson GmbH, Heidelberg, Germany |
| BioRender | BioRender.com | ©bioRender, Toronto, Canada |
| BioVenn | Https://www.biovenn.nl/vendiagram.tk/create.php | Hulsen, T., de Vlieg, J. & Alkema, W., 2008 [227] |
| FlowJo | v10 | FlowJo LLC, Becton Dickinson GmbH, Heidelberg, Germany |
| FV10-ASW | v4.2, for confocal laser scanning microscope XI-81 | Olympus Europa SE & Co. KG, Hamburg, Germany |
| GraphPad Prism | v7 + v8 | GraphPad Software, Californian, USA |
| ImageJ | with Fiji plugin | NIH, Maryland, USA |
| LEGENDplex data analysis software | v7 + v8 | VigeneTech Inc., Massachusetts, USA |
| Mendeley | Citation of references | Elsevier B.V., Amsterdam, Netherlands |
| Microsoft Office | Word, Excel, Power Point | Microsoft Corporation, Washington, USA |
| nCounter® advanced analysis software v2.0.115 | with R3.3.2 and Xquartz | NanoString Technologies® Inc., Seattle, USA |

| | | |
|---|---|---|
| nSolver™ | v4 | NanoString Technologies® Inc., Seattle, USA |
| PubMed | Https://pubmed.ncbi.nlm.nih.gov/ | National Center for Biotechnology Information |
| Webgestalt | http://webgestalt.org/ | WEB-based GEne SeT AnaLysis Toolkit by Zhang et al., 2005; Wang et al., 2013; Wang et al., 2017; Liao et al., 2019 [228–231] |

# 3. Methods

## 3.1 Cell culture

To investigate the immune response to viral vector vaccines upon *in vitro* stimulation of eukaryotic cells, primary human peripheral blood mononuclear cells (hPBMCs), the eukaryotic cell line THP-1 derived from peripheral blood of an acute monocytic leukemia patient, and Vero81 cells derived from *Cercopithecus aethiops* kidney (*verda reno*; green kidney) were used. hPBMCs were freshly isolated from whole blood donations of different healthy individuals (section 3.2). The monocyte cell line THP-1 was obtained from DSMZ and the epithelial cell line Vero81 was purchased from ATCC®.

### 3.1.1 Maintenance

Cell culture experiments were performed under sterile conditions in a biosafety two laboratory. To this end, cells were cultured in a humidified growth chamber at 37°C and 5 % $CO_2$. Long term storage conditions included -190°C, cell type specific media and 10 % dimethyl sulfoxide (DMSO). For cultivation, adherent Vero81 cells were detached with trypsin-ethylenediaminetetraacetic (EDTA, 0.02 %) after reaching a confluence higher than 80 %. Prior to detaching, media were decanted and cells were washed with phosphate buffered saline (PBS). Afterwards, the cells were incubated 3 min with trypsin at 37°C. The trypsin reaction was stopped by adding fresh media including MEM-earl with 5 % fetal calf serum (FCS), 1 % penicillin, and streptomycin (pen/strep) as well as 1 % L-glutamine.

### 3.1.2 Counting

To calculate the amount of hPBMCs, THP-1 cells, and Vero81 cells, an automated cell counter TC20™ by Bio-Rad Laboratories GmbH was used. To this end, 10 µl of a Trypan Blue and cell suspension mixture (1:1) were measured. While hPBMCs range in size between 6–17 nm, THP-1 cells and Vero81 cells were analyzed in a range of 11–21 nm.

## 3.2 Blood samples

Blood donations from participants of the Hamburg healthy cohort were approved by the ethics committee of the Medical Association Hamburg (PV4780) and conducted at the University of Hamburg Eppendorf, Germany, and its associated institutes (Bernhard-Nocht institute for Tropical Medicine and Heinrich Pette Institute for Experimental Virology, Hamburg, Germany). The study group included only individuals who were able to consent to all necessary terms and did not have an anemia or positive serology for HCV, HIV, or HBV. Comprehensive tables of all anonymized individuals are shown in table 2-6. The collection of whole blood samples was done by trained staff using 9 ml EDTA-tubes.

## 3.3 Isolation of hPBMCs density gradient centrifugation

To isolate hPBMCs from whole blood samples of healthy individuals (section 3.2) a gradient density centrifugation was performed. An in-house gradient density centrifugation protocol called Ficoll (section 3.3.1) and a modified protocol by STEMCELL Technologies Inc. called SepMate™ (section 3.3.2) were utilized. In both protocols all reagents were heated up to 37°C prior to hPBMCs isolation. All centrifugation steps were performed at room temperature (RT).

### 3.3.1 Using Ficoll

The in-house Ficoll protocol was performed with a Histopaque®-1077 density gradient medium by Sigma-Aldrich Chemie GmbH. A maximum of 27 ml whole blood was transferred to one 50 ml tube and centrifuged for 10 min at 200 *x g*. Afterwards, the upper 8 ml of each tube were transferred into a new tube and handled like described in section 3.3.3 to collect plasma. Remaining blood was filled up to 30 ml with Hanks balanced salt solution (Hanks) and layered on top of 14 ml Histopaque®-1077. Following centrifugation with no breaks (accelerate: 1; break: 0) and 500 *x g* for 30 min, the hPBMC layer was harvested and transferred into a new 50 ml tube. Enriched hPBMCs were washed twice with 40 ml Hanks and a centrifugation at 600 *x g* for 10 min with breaks on (accelerate: 9; break: 9). Afterwards, the hPBMCs were resuspended in cell media and counted (section 3.1.2). Cells were either

directly used for *in vitro* stimulation assays (section 3.5) or frozen at -190°C for long-term storage (section 3.1.1).

### 3.3.2 Using SepMate™

For hPBMCs separation 50 ml SepMate™ tubes with 15 ml Lymphoprep™ density gradient medium by STEMCELL Technologies Inc. were used. Whole blood samples were diluted 1:1 in PBS containing 2 % FCS and pipetted on top of the Lymphoprep™. The centrifugation was performed with 1200 *x g* for 10 min at RT and breaks on (accelerate: 9; break: 9). Following centrifugation, the first 8 ml of each tube were added to a new tube and handled like described in section 3.3.3 to collect plasma. Enriched hPBMCs were pipetted into a new tube, washed two times with 40 ml PBS containing 2 % FCS and centrifugated at 500 *x g* for 8 min in. Upon washing, hPBMCs were counted (section 3.1.2) in cell media and used for *in vitro* stimulation assays (section 3.5) or stored for long term at -190°C (section 3.1.1).

### 3.3.3 Plasma separation

In order to collect cell-free plasma from whole blood samples, the liquid phase collected during the hPBMCs separation in section 3.3.1 and 3.3.2 was centrifuged at 1000 *x g* for 15 min at RT. After centrifugation, plasma samples were aliquoted and stored at -80°C.

## 3.4 Plaque assay

Plaque assays were performed to determine the infectivity of viruses. The viral vector vaccine VSV-EBOV (Ervebo®) was passaged by the infection of baby hamster kidney cells (BHK). Multiplied 2$^{nd}$ line VSV-EBOV were used in plaque assays. One day prior to the infection, $6 \cdot 10^5$ Vero81 cells were seeded per well of a six well cell culture plate and incubated overnight at 37°C and 5 % $CO_2$ to obtain a confluent monolayer. Next day, the media were removed and Vero81 cells were infected with 1 ml of a 10-fold serial dilution of VSV-EBOV ($10^{-3}$–$10^{-6}$). After 1 h at 37°C and 5 % $CO_2$, 2 ml of a 2 % methylcellulose solution were added to each well. After 24 h incubation at 37°C and 5 % $CO_2$, cells were fixed with 2 % paraformaldehyde (PFA) for 15 min.

For visualization, plaques were stained with 1 ml crystal violet for 10 min at RT. Afterwards, crystal violet was decanted and removed by several washing steps with distilled water. The virus titer was described as plaque forming unit per ml (PFU/ml) and calculated with the formula [1].

[1] $$\frac{PFU}{ml} = \frac{(\sum plaques \cdot dilution\ factor\ a) + (\sum plaques \cdot dilution\ factor\ b)}{\frac{ml\ virus\ soultion}{well} \cdot number\ of\ wells\ counted}$$

$\sum Plaques$ = sum of counted plaques of one dilution in x wells

$number\ of\ wells\ counted$= all counted wells for all dilutions

$ml\ virus\ soultion$= 1 ml were used for viral infection

## 3.5 *In vitro* stimulation assay

To reveal induced immune signatures by viral vector vaccines, *in vitro* stimulation assays were performed. To this end, hPBMCs were stimulated *in vitro* using two different viral vector vaccines MVA-EBOV and VSV-EBOV. Besides these viral vector vaccines, a recombinant MVA (rMVA) strain, which encodes for GFP and mCherry, was used to establish the *in vitro* stimulation protocol and related methods (section 6.1).

To perform *in vitro* stimulation assays, freshly isolated hPBMCs were used (section 3.3.2). Since serum can contain sex hormones like estrogens, the whole *in vitro* stimulation assay was performed in RPMI-1640 (containing L-glutamine) without any sera. After isolation, hPBMCs were rested at $10 \cdot 10^6$ cells/ml in 50 ml tubes for 1 h at 37°C and 5 % $CO_2$. Upon 1 h resting, hPBMCs were stimulated with a multiplicity of infection (MOI) of 1 using rMVA, MVA-EBOV or VSV-EBOV respectively, and incubated for 1 h (mixed every 15 min). To calculate the amount of viral stock, which is necessary to stimulate a specific cell count with a MOI of 1, the formula in [2] was used.

[2] $$volume\ virus\ stock\ [\mu l] = \frac{PFU_{needed}}{PFU_{virus\ stock}/\mu l} \qquad | PFU_{needed} = MOI \cdot cell\ count$$

Upon 1 h of stimulation, hPBMCs were centrifuged at 600 *x g* for 5 min at RT. Afterwards, the supernatant was decanted and hPBMCs were resuspended in $2 \cdot 10^6$ cells/ml of fresh RPMI-1640. Afterwards, hPBMCs were incubated at 37°C, 5 % $CO_2$ up to 47 h.

Besides cell-culture supernatants, cells for isolation of nucleic acids (section 3.6, 3.7) and cells for cell stainings were collected at different time points. For each condition stimulated and unstimulated controls were analyzed. Cell-culture supernatants and samples for RNA or DNA isolation were harvested immediately after hPBMCs isolation and 1 h, 3 h, and 6 h upon stimulation. To this end, stimulated and their unstimulated counterparts were centrifuged for 3 min at 6,000 *x g* and 4°C. While supernatants were stored at -20°C for further analysis (section 3.12.1), cell-pellets were washed once with PBS and stored dry at -20°C in terms of DNA or at -80°C resuspend in TRI Reagent® Sigma-Aldrich Chemie GmbH in terms of RNA-isolation. Furthermore, hPBMCs were harvested immediately after isolation as well as 6 h, 12 h, and 24 h upon stimulation to analyze the expression of surface markers. Both, stimulated and unstimulated samples were stained (section 3.12) with the antibody panel of choice immediately after harvesting (section 2.9, table 14–15). Additionally, cell-culture supernatants from 12 h and 24 h were collected and stored at -20°C for further analysis.

## 3.6 DNA isolation

To analyze the viral load of DNA viruses like rMVA and MVA-EBOV, whole DNA was isolated from *in vitro* stimulated hPBMCs. One DNA isolation-mixture consisted of $10^6$ cells in 200 µl PBS, 20 µl proteinase K, and 200 µl AL lysis buffer. DNA was extracted by the usage of the QiAamp® DNA Mini Kit by Qiagen and corresponding spin protocol for blood and body fluids by the manufacturer.

## 3.7 RNA isolation

After *in vitro* stimulation of hPBMCs, the total RNA was isolated by phenol-chloroform-extraction and an in-house protocol. One RNA isolation-mixture consisted of $5 \cdot 10^6$ cells, 1 ml TRI Reagent® (Sigma-Aldrich Chemie GmbH), and 200 µl chloroform. The RNA isolation-mixture was inverted for 30 s and incubated on ice for 5 min. After a centrifugation at

12000 *x g* for 15 min, the upper aqueous phase was harvested and mixed with 500 µl isopropanol as well as 1 µl of a co-precipitant GlycolBlue™ (ThermoFisher Scientific Inc.). This solution was incubated at RT for 10 min following a second centrifugation at 12000 *x g* for 5 min at 4°C. Next, supernatant was decanted and total RNA was washed twice with 75 % ethanol (diluted in ultra pure™ distilled water). Subsequent to the last centrifugation step, RNA pellet was air dried for 10 min at RT, resuspended in 30 µl diethyl pyrocarbonate (DEPC) treated water and incubated for 10 min on ice. Upon determination of RNA concentration with a Nanodrop, RNA was aliquoted and stored at -80°C.

## 3.8 Polymerase Chain Reaction (PCR)

The amplification of DNA or RNA by a polymerase chain reaction (PCR) can be used to determine the viral load of stimulated hPBMCs and/or the expression level of a gene of interest. Different PCR methods were performed after DNA or RNA isolation (section 3.6, 3.7). All forward and reverse primers, which were used for PCR, are shown in table 11 section 2.6.

### 3.8.1 Gradient PCR

Prior to gene expression analysis or viral load determination, a gradient PCR was performed to optimize the annealing temperature of each primer pair. One 20 µl PCR reaction consisted of 10 µl Red HS Taq Master Mix (Biozym Scientific GmbH), 0.8 µl forward and reverse primer (400 nM), 2 µl cDNA (section 3.8.4) and 6.4 µl nuclease free water. A gradient PCR was performed with 12 consistent temperature steps between 55–65°C and the underneath depicted PCR program (table 18).

Table 18: Gradient PCR program

| Cycles | Temperature | Duration | Notes |
|---|---|---|---|
| 1x | 95°C | 1-2 min | Initial denaturation |
| 40x | 95°C | 15 s | Denaturation |
| | 55-65°C | 15 s | Annealing |
| | 72°C | 60 s | Extension |

**Agarose Gel Electrophoresis**

For the visualization of all PCR-amplificons upon gradient PCR an agarose gel electrophoresis was used. One agarose gel consisted of 3 g agarose (2 % (w/v)), 145 ml nuclease free, distilled water, and 5 ml 10x TBE-buffer. The gel solution was heated up until a homogenous solution has formed. Afterwards, 7.5 µl ethidium bromide (10 mg/ml) were added to the gel solution and cooled down in a gel chamber with a comb. 10 µl of PCR product were added to each camber of the comb. The ladder consisted of 4 µl nuclease free, distilled water, 1 µl 6x TriTrak DNA Loading Dye, and 1 µl GeneRuler 50 bp DNA ladder (0.5 µg/µl, ThermoFisher Scientific Inc.). An agarose gel electrophoresis run was performed in 0.5 % TBE buffer and 85 V for 90 min. Finally, DNA bands were visualized by UV light irradiation and evaluated with the software ImageJ.

### 3.8.2 Quantitative PCR

To analyze the viral load a quantitative PCR (qPCR) was used with a one-step protocol. First, total RNA or DNA were isolated from *in vitro* stimulated hPBMCs and their unstimulated counterparts (section 3.5). The qPCR was performed with at least duplicates of each sample. After qPCR, the viral load was calculated as described in section 3.8.3.

**One-step qPCR**

The viral load of rMVA and MVA-EBOV were determined by the usage of the SensiMix™ SYBR® No-ROX kit by Meridian Bioscience Incorporated. One 25 µl one-step qPCR reaction consisted of 12.5 µl SensiMix™ SYBR® No-ROX, 0.625 µl forward and reverse primer for an MVA-specific uracil-DNA-glycosylase (UDG) (10 µM), 9.25 µl DEPC treated water and 2 µl DNA (60 ng, diluted in DEPC treated water). The one-step qPCR program is depicted below in table 19.

Table 19: qPCR program: viral load of DNA viruses and gene expression

| Cycles | Temperature | Duration | Notes |
|---|---|---|---|
| 1x | 95°C | 10 min | Polymerase activation |
| 40x | 95°C | 15 s | Denaturation |
| | 58°C | 15 s | Annealing |
| | 72°C | 15 s | Extension |

To investigate the viral load of VSV-EBOV the AgPath-ID™ one-step RT-PCR by ThermoFisher Scientific Inc. and VSV nucleoprotein (NP)-specific primer were used. One 12.5 µl one-step qPCR reaction consisted of 6.25 µl 2x RT-PCR Buffer (ThermoFisher Scientific Inc.), 0.5 µl 25x RT-PCR Enzyme MIX, 0.75 µl forward and reverse primer (10 µM), 0.25 µl probe (0.2 µM), and 4 µl RNA (50 ng, diluted in DEPC treated water). The one-step qPCR program is depicted underneath in table 20.

Table 20: One-step qPCR program: viral load of RNA viruses

| Cycles | Temperature | Duration | Notes |
|---|---|---|---|
| 1x | 50°C | 15 min | Preincubation |
| | 95°C | 10 min | Polymerase activation |
| 45x | 95°C | 10 s | Denaturation |
| | 60°C | 40 s | Annealing |

### 3.8.3 Quantification of qPCR results

In order to define the viral load of *in vitro* stimulated hPBMCs, qPCR results were absolutely quantified by a standard curve method. Each qPCR run included 6-8 standard curve samples of a 10-fold serial dilution. DNA/RNA with known concentrations of the viral stock solution, which were also used for the *in vitro* stimulation assays, were utilized in duplicates. The mean of each dilution replicate was visualized in a Ct-dilution plot (Ct: cycle threshold). Only standard curves with $R^2$>0,99 were used for quantification.

The general formula of a straight line [3] in standard curve methods can be applied to a Ct-dilution plot [4]. To quantify the unknown amount of viral nucleic acids in samples of interest, the transformed formula in [5] were used.

[3] $f(x) = m \cdot x + b$

[4] $Ct\ value = m \cdot amount_{nucleic\ acid} + b$

[5] $amount_{nucleic\ acid} = \frac{Ct\ value - b}{m}$

By using the calculated DNA/RNA amount in each sample [5], the copy number of the specific virus (rMVA/MVA-EBOV or VSV-EBOV) can be determined [6] [232–234].

[6] $copy\ number = \frac{amount_{nucleic\ acid} \cdot (avogadro\ constant)}{lenght \cdot (1 \cdot 10^9) \cdot average\ molecular\ weight\ nucleic\ acid}$

$avogadro\ constant = 6{,}022 \cdot 10^{23}$
$average\ molecular\ weight\ dsDNA = 660$
$average\ molecular\ weight\ ssRNA\ = 340$
$lenght\ of\ amplificate\ (MVA\text{-}UDG) = 54$
$lenght\ of\ amplificate\ (VSV\text{-}NP) = 131$

### 3.8.4 Reverse transcription (RT-PCR)

To investigate the expression level of a gene of interest a reverse transcription is mandatory to generate complementary DNA (cDNA), which can be analyzed in a semi-quantitative PCR (semi-qPCR) (section 3.8.5). To this end, the SuperScript™ III reverse transcriptase by ThermoFisher Scientific Inc. was used. Prior to amplification 500 ng of RNA were mixed with 1 µl random primer (6 µM) as well as 1 µl dNTPs (10 mM) and filled up to 13 µl with DEPC treated water. Following 5 min at 65°C and 1 min on ice, 5 µl first strand buffer (ThermoFisher Scientific Inc.), 1 µl dithiothreitol (DTT), 1 µl RNase out (ThermoFisher Scientific Inc.) as well as 1 µl SuperScript™ III (200 units/µl) were added. Afterwards, the cDNA synthesis was

performed at 25°C for 5 min, following 50°C for 50 min and a final incubation at 70°C for 15 min. To remove the initial RNA, all samples were incubated at 37°C for 20 min with RNase H.

### 3.8.5 Semi-quantitative PCR (semi-qPCR)

To analyze the expression of genes of interest a semi-qPCR was used with a two-step protocol. First, total RNA was isolated from *in vitro* stimulated hPBMCs and their unstimulated counterparts (section 3.5). Afterwards, a RT-PCR was performed to generate cDNA (section 3.8.4). The semi-qPCR was performed with at least duplicates of each sample. After semi-qPCR the gene expression was calculated as described in section 3.8.6.

**Two-step semi-qPCR**

Upon cDNA synthesis (section 3.8.4), the expression of a gene of interest was investigated by a two-step semi-qPCR. To this end, the SensiMix™ SYBR® No-ROX kit by Meridian Bioscience Inc. and specific primers (table 11 section 2.6) were used. A semi-qPCR reaction consisted of 12.5 µl SensiMix™ SYBR® No-ROX, 0.625 µl forward and reverse primer (10 µM), 2 µl cDNA (section 3.8.4), and 9.25 µl nuclease free water. The semi-qPCR program is depicted above in table 19.

### 3.8.6 Quantification of semi-qPCR results

To determine the relative expression of a gene of interest, the ΔΔCt method ($2^{-\Delta\Delta Ct}$) was used. First, the mean of all duplicates including housekeeping genes (in this case HPRT, cf. section 6.2) and genes of interest were calculated. Second, the mean Ct value of the gene of interest from one sample was subtracted by the mean Ct value of HPRT from the same sample leading to ΔCt [7]. To normalize all expression values to the unstimulated 0 h control, the mean of all ΔCt values of unstimulated 0 h control was calculated and subtracted from ΔCt resulting in ΔΔCt [8]. Afterwards, the ΔΔCt were used to calculate the relative mRNA expression of a gene of interest [9].

[7] $mean\ Ct_{target\ gene} - mean\ Ct_{reference\ gene} = \Delta\mathrm{Ct}$

[8] $\Delta\mathrm{Ct} - \mathrm{mean}\ \Delta\mathrm{Ct}_{unstimulated\ 0\ \mathrm{h}} = \Delta\Delta\mathrm{Ct}$

[9] $relative\ mRNA\ expression = 2^{-\Delta\Delta Ct}$

To calculate the fold change of a gene of interest, the relative mRNA expression [9] of stimulated samples can be divided by unstimulated samples of the same time point [10].

[10] $$\frac{relative\ mRNA\ expression\ of\ gene\ x_{stimulated\ sample}}{reletive\ mRNA\ expression\ of\ gene\ x_{unstimulated\ sample}}$$

## 3.9 NanoString®

Transcriptome changes upon *in vitro* stimulation were analyzed using a human immunology panel v2 (XT-CSO-HIM2-12) by nanoString®. This enzyme-free gene expression analysis is based on the hybridization of target RNA and the target-specific capture probe as well as reporter probe, which carry a target-specific color-coded barcode. The molecular counting of each color-coded barcode allows a simultaneous multiplex measurement for all targets. The human immunology panel v2 includes 594 immune related genes and 15 reference genes. All included genes, their annotation and pathway affinity can be found on the nanoString® homepage (https://www.nanostring.com).

For transcriptome analyses of VSV-EBOV, stimulated hPBMCs derived from 8 donors (4 men and 4 women; section 2.2, table 5) of three time points were used. To this end, unstimulated hPBMCs after hPBMCs separation (0 h) and 1 and 6 h after stimulation were analyzed. 75 ng RNA were used and handled according to the manufacturer recommendations (nanoString® expression-panel manual, 2020). All samples were analyzed at the UKE with a nCounter® SPRINT Profiler by nanoString®. The performance quality check, normalization, evaluation, and visualization of the results were done with the nSolver™ Software v4, the nCounter® advanced analysis software v2.0.115 with R3.3.2 and XQuartz as well as GraphPad Prism v7 and v8. Only runs and samples with no serious performance or quality warnings were included in further analysis and normalized to 15 reference genes. Further information of the nSolver™

Software v4 and related tools can be found on the nanoString® website (www.nanostring.com).

## 3.10 RNA-Sequencing

To investigate transcriptomic changes after *in vitro* stimulations comprehensively, a sequencing of total RNA (RNA-Seq) was performed at the Quantitative Biology Center (QBiC) and c.ATG in cooperation with the NGS Competence Center Tübingen (NCCT) (section 3.5 + 3.7). The library preparation for all VSV-EBOV–stimulated samples was conducted with the NEBNext Ultra II RNA library kit by New England Biolabs®. For all MVA-EBOV–stimulated samples the KAPA RNA HyperPrep kit by Roche was used. The RNA-Seq was based on the Illumina technology and performed with the Illumina NovaSeq6000 including a depth of more than 21 million clusters in mean and more than 60,000 genes. Besides 6 h *in vitro* stimulated hPBMCs, unstimulated hPBMCs (0 h and 6 h) were also analyzed. All in DEPC treated water diluted RNA samples were stored and shipped at -80°C. VSV-EBOV− and MVA-EBOV−stimulated hPBMCs derived from 8 donors (4 men and 4 women; section 2.2, table 5−6) of three time points were investigated via RNA-Seq. To this end, unstimulated hPBMCs after hPBMCs separation (0 h), post 6 h *in vitro* cultivation, and 6 h after stimulation were analyzed.

## 3.11 Immunofluorescence

For immunofluorescence studies, stimulated and unstimulated counterparts were stained in imaging dishes by IBIDI®. For the immunofluorescence staining of adherent Vero81 cells the cells were seeded first in imaging dishes and finally stimulated after 12 h. In contrast, hPBMCs were seeded in imaging dishes after an *in vitro* stimulation. Upon stimulation the cells were fixed with 200 µl 4 % PFA for 15 min at RT, following three times washing with PBS. To permeabilize Vero81 cells and hPBMCs, Triton X-100 (0.1 % in PBS) was used. After an incubation at RT for 5 min, cells were washed three times with PBS. Following an incubation with 200 µl glycine (0.1 M in PBS) at RT for 15 min, cells were washed two times with PBS and blocked by 200 µl FCS (1.5 % in PBS) for 15 min at RT. Afterwards, the blocking solution was

removed and 200 µl DAPI (1:1,000 in PBS) was added for 2 h at RT. Following three times washing with PBS for 5 min, 1 ml PBS was added to each imaging dish. Stained cells were analyzed immediately after staining with a confocal laser scanning microscope XI-81 by Olympus.

## 3.12 Flow cytometry

Flow cytometry stainings and analyses of hPBMCs were performed to analyze the expression of selected surface markers on several immune cell subsets. Besides the detection of the cell size and granularity via forward- and sideward-scatters, the method also allows the determination of surface markers by fluorochrome-conjugated antibodies.

Prior to staining of surface markers from hPBMCs, cells were washed twice with staining-buffer consisting of PBS, 1 % FCS, and 1 mM EDTA. Afterwards, hPBMCs were stained in 96-well plates with 100 µl staining buffer and different panels related to the objective of choice. All used antibodies are shown in section 2.9, table 14–15. Following an incubation at 37°C for 15 min, the cells were washed three times with staining buffer and incubated at 37°C for 15 min with 4 % PFA. After three washing steps with staining buffer cells were resuspended in 100 µl and stored in the dark at 4°C until measurement. All samples of one experiment were analyzed on the same day with a BD LSRFortessa™ and a FACSDiva software version 8.0.1. The results were evaluated with the software FlowJo v10 and visualized with GraphPad Prism v8.

### 3.12.1 Bead-based immunoassay

For the investigation of secreted cytokines by immune cells after an *in vitro* stimulation the supernatants of stimulated and unstimulated hPBMCs were analyzed by a bead-based immunoassay. Here, a pre-defined human anti-virus response LEGENDplex™ panel by BioLegend with the analytes: IL-1β, IL-6, IL-8, IL-10, IL-12p70, IP-10, TNFα, IFNλ1, IFNλ2/3, IFNα2, IFNβ, IFNγ, and GM-CSF or a customized panel with the analytes: IL-1β, IL-2, IL-4, IL-6, IL-8, IL-10, IL-12, IP-10, IFNα, IFNγ, MCP-1, MIG, and TNFα was used. The analysis of all supernatants was performed according to the manufacturer (LEGENDplex™ Multi-Analyte

Flow Assay Kit Manual, 2020). All samples were recorded on the same day of assay implementation with a BD LSRFortessa™ and a FACSDiva software version 8.0.1. The results were evaluated with LEGENDplex Data Analysis software by VigeneTech Inc. and visualized with GraphPad Prism v7 and v8.

## 3.13 Statistical analysis

For statistical tests of a given hypothesis, the software GraphPad Prism v7 and v8 were used. Prior to analysis, every data set was tested for Gaussian distribution. A D'Agostino-Pearson omnibus test in case of eight or more values and a Shapiro-Wil test in case of three to seven values was performed. Since all data sets were nonparametric, the depicted figures in section 4 and section 6 represent the median of the specific data set. Furthermore, only the t-test-based, unpaired, nonparametric Mann-Whitney test was utilized to proof a given hypothesis for significance. The p-values are indicated as follows: $p \leq 0.05$ *; $p \leq 0.01$ **; $p \leq 0.001$ ***; $p \leq 0.0001$ ****.

To identify differentially expressed gens (DEG) in nanoString® and RNA-Seq analysis different cutoffs were used. Since the nanoString® immunology panel contains only 594 genes, a cutoff with a log2fold change ≤ -1 or ≥ 1 and a p-value < 0.001 was used. To reduce noise of slightly up- or downregulated genes in RNA-Seq analysis, a log2fold change ≤ -1.5 or ≥ 1.5 and a p-value < 0.01 were chosen. The analysis of RNA-Seq raw fastq-files was performed by Michael Spohn from the University Medical Center Hamburg-Eppendorf, Bioinformatics Core, Hamburg, Germany. To this end, he calculated the log2 fold changes.

# 4. Results

*In vitro* stimulations of freshly isolated hPBMCs using VSV-EBOV and MVA-EBOV were implemented and analyzed longitudinally to elucidate induced immune signatures by both viral vector vaccines (figure 8). Using these *in vitro* stimulation assays, a comprehensive revelation of immune responses including cytokine secretion, activation of innate immune cells, and transcriptomic changes were investigated (figure 8). Furthermore, differences in the immune signature due to the different vectors VSV or MVA as well as sex-based differences to viral vector vaccines were evaluated.

Infectious 2nd line VSV-EBOV (cf. section 6.1.1, S.1) of the licensed Ervebo® as well as a not licensed MVA-EBOV were used for *in vitro* stimulations of hPBMCs. All *in vitro* stimulations of freshly isolated hPBMCs derived from healthy donors (cf. section 2.2, table 2–6 and section 3.3) were performed in RPMI-1640 medium (no further supplements; cf. section 6.1.2, S.2–3) and at a multiplicity of infection (MOI) of 1 (cf. section 6.1.3, S.4). Effective *in vitro* stimulations of Vero81 cells and hPBMCs were confirmed by flow cytometry, immunofluorescence, and semi-qPCR (cf. section 6.1.4–6.1.6, S.5-8). In addition, information of established analytic methods including qPCR and flow cytometry to monitor induced immune responses by VSV-EBOV and MVA-EBOV are summarized in section 6.2 (cf. S.9–10).

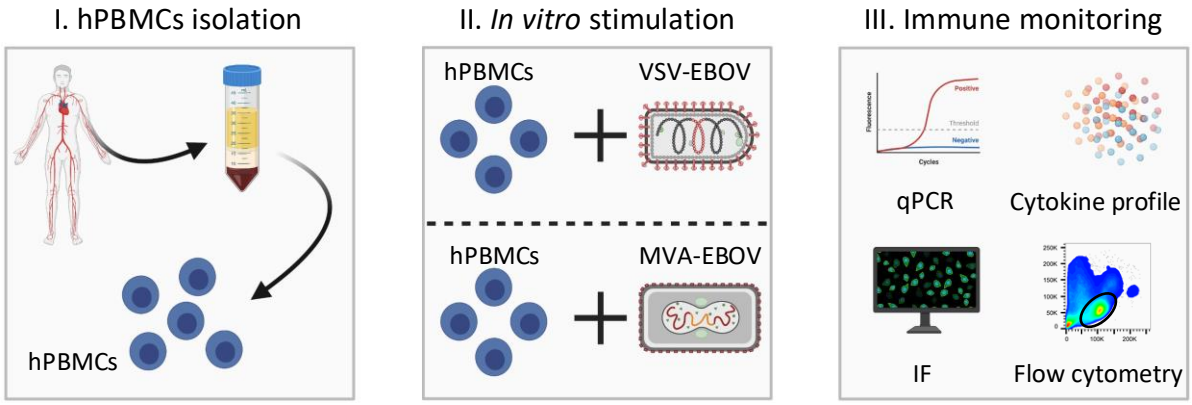


Figure 8: **Experimental setup for immune monitoring upon stimulation.** Freshly isolated hPBMCs were stimulated using VSV-EBOV or MVA-EBOV, respectively. To this end, whole hPBMCs derived from 20 different donors were *in vitro* stimulated with VSV-EBOV (section 2.2, table 3) and 16 with MVA-EBOV (section 2.2, table 4) (MOI 1). Induced immune responses were investigated via several methods including qPCR, bead-based immunoassays, immunofluorescence (IF), and flow cytometry to monitor the immune signature over time (section 3.8-3.12). Samples were collected longitudinally at different time points as indicated in the following sections. Figure created with BioRender.com; VSV-EBOV modified from Poetsch et al., 2019 [88]

## 4.1 Induced immune signature by VSV-EBOV and MVA-EBOV

Since innate immune cells can initiate and shape adaptive immune responses to infection as well as vaccination [235–241], very early immune responses upon stimulation were the center of investigation. Moreover, a trained innate immunity of monocytes and antigen presentation via DCs represents important mechanisms in vaccine-induced immunity [55,59,242]. Therefore, the *in vitro* induced cytokine profile of hPBMCs by the viral vector vaccine VSV-EBOV was investigated via bead-based immunoassays (section 4.1.1). Moreover, the activation status of monocytes and DCs was assessed via flow cytometry upon *in vitro* stimulations using VSV-EBOV and MVA-EBOV, respectively (section 4.1.2).

### 4.1.1 Cytokine profile upon stimulation

One of the first responses to external stimuli like the administration of vaccines is the release of cytokines, which can lead to immune cell activation and migration to the entry site [92,243,244]. The secretion of IL-1β, IL-2, IL-4, IL-6, IL-8, IL-10, IL-12, interferon gamma-induced protein 10 (IP-10), interferon alpha (IFNα), IFNγ, monocyte chemoattractant protein 1 (MCP-1), tumor

necrosis factor alpha (TNFα) as well as CXC-ligand 9 (CXCL9) were analyzed based on their antiviral function and capacity to modulate the immune response upon stimulation [47,92,251,141,243,245–250]. To this end, a customized bead-based immunoassay by BioLegend (LEGENDplex™, section 3.12.1) was utilized to investigate *in vitro* stimulated hPBMCs using VSV-EBOV.

While the secretion of IL-2, IL-4, IL-6, IL-12, IFNα, and IFNγ was low or not detectable over time (data not shown), IL-1β, IL-8, IL-10, IP-10, MCP-1, TNFα, and CXCL9 revealed a higher dynamic over time (figure 9). In general, the secretion of cytokines peaked at later time points between 12 h and 24 h post-stimulation (figure 9). Whereas for the majority of analyzed cytokines VSV-EBOV−stimulated samples showed a low induction compared to unstimulated samples, IP-10 was significantly induced 24 h after stimulation. While the secretion of IP-10 increased from 11.6 pg/ml to 24.0 pg/ml in median (N=20) for stimulated hPBMCs, corresponding unstimulated samples revealed 2.1 pg/ml in median after 12 h of stimulation and 10.7 pg/ml 24 h post-stimulation. Additionally, 24 h post-stimulation MCP-1 ($p=0.08$) showed the highest secretion in median (N=20) with 18.3 pg/ml compared to unstimulated samples with 13.6 pg/ml.

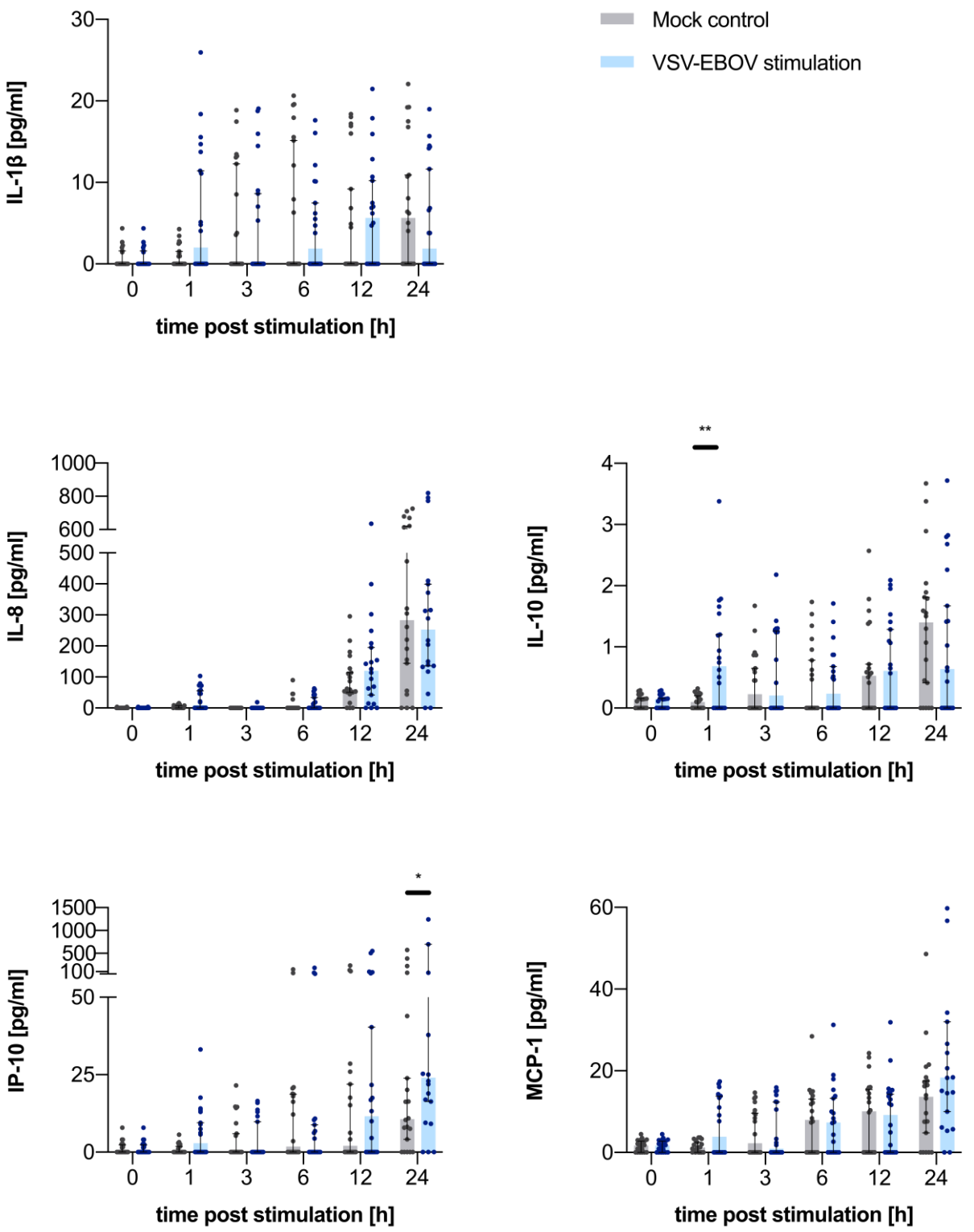


Figure legend is depicted on page 54.

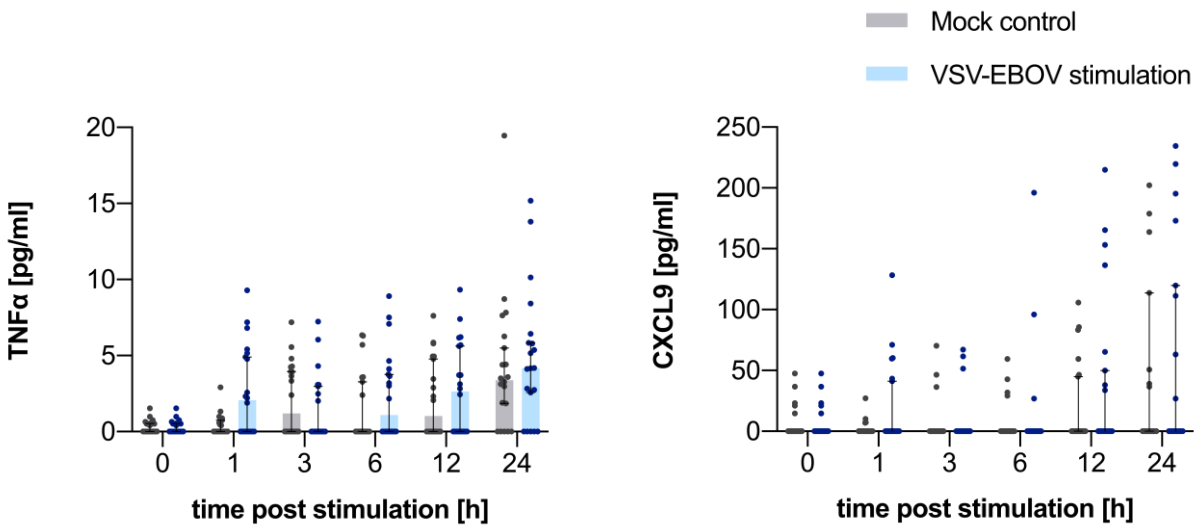


Figure 9: **Cytokine secretion of stimulated hPBMCs using VSV-EBOV.** Freshly isolated hPBMCs were *in vitro* stimulated with a MOI of 1. The cytokine profile was analyzed via a customized LEGENDplex™ by BioLegend (section 3.12.1) including the analytes: IL-1β, IL-8, IL-10, IP-10, MCP-1, TNF-α, and CXCL9, data not shown for: IL-2, IL-4, IL-6, IL-12, IFNα, and IFNγ. Each graph represents the cytokine secretion [pg/ml] of $2 \cdot 10^6$ hPBMCs over time in unstimulated (black) and stimulated (blue) samples. Each dot indicates a different donor (N=20), the top of each bar represents the median, and black error bars the 95 % confidence interval (CI) of the median. For significance determination the t-test based unpaired, nonparametric Mann-Whitney test was performed. The p-values are indicated as follows: $p \leq 0.05$ * and $p \leq 0.01$ **; p-value for MCP-1 0.08 after 24 h, for TNF-α 0.08 after 1 h.

In contrast, IL-1β, IL-8, and TNFα exhibited in median the highest induction compared to unstimulated samples already after 12 h, whereas stimulated to unstimulated amounts were 0 pg/ml to 5.6 pg/ml, 61.2 pg/ml to 120.0 pg/ml, and 1.0 pg/ml to 2.6 pg/ml in median (N=20), respectively. IL-10 and CXCL9 showed only a minor induction for nine or six different donors, respectively, whereas the other donors exhibited no induction. Six cytokines out of 13 analytes were chosen for an overall analysis based on their high dynamic over time. In median the total cytokine response including IL-1β, IL-8, IL-10, IP-10, MCP-1, and TNFα increased from 149.6 pg/ml to 302.4 pg/ml, highlighting an overall cytokine induction of 102.1 % (figure 10). While the amount of MCP-1, IL-8, and IP-10 was twice as high after 24 h compared to 12 h, TNFα revealed an induction of 58.1 % and IL-10 of 4.5 %. In contrast, the secretion of IL-1β was 66.1 % lower after 24 h compared to 12 h. Both time points revealed comparable composition of cytokines where IL-8, IP-10, and MCP-1 were the most prominent cytokines (figure 11). However, the proportion of IL-1β and IL-10 peaked 12 h upon stimulation and decreased to later time points. Finally, a VSV-EBOV *in vitro* stimulation of hPBMCs showed a

distinct cytokine signature where 24 h showed twice as high cytokine amounts compared to 12 h.

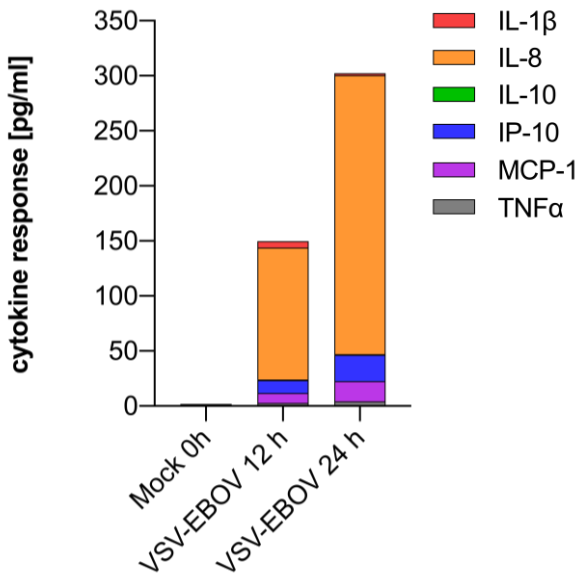


Figure 10: **Cytokine profile of stimulated hPBMCs using VSV-EBOV.** Freshly isolated hPBMCs were *in vitro* stimulated with a MOI of 1 following cytokine measurements via a customized LEGENDplex™ by BioLegend (section 3.12.1). This bead-based immunoassay included the analytes: IL-1β, IL-8, IL-10, IP-10, MCP-1, TNFα, data not shown for: IL-2, IL-4, IL-6, IL-12, IFNα, IFNγ, and CXCL9. Each bar represents the cytokine secretion [pg/ml] in median (N=20) per $2 \cdot 10^6$ hPBMCs including IL-1β (red), IL-8 (orange), IL-10 (green), IP-10 (blue), MCP-1 (purple), and TNFα (grey) 0 h, 12 h or 24 h post-stimulation.

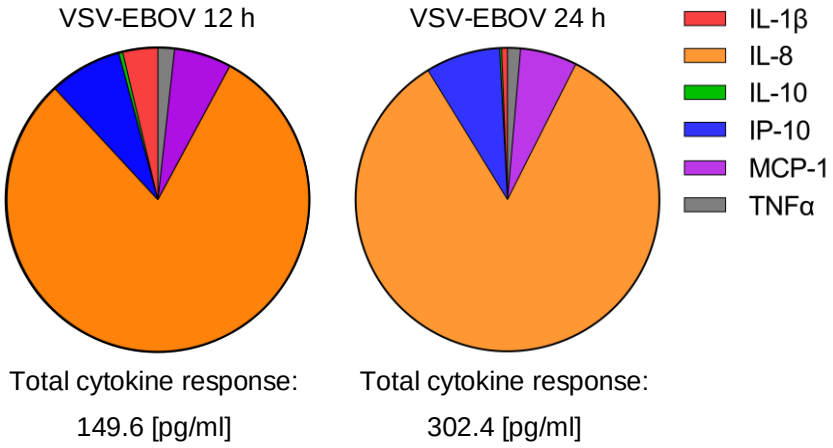


Figure legend is depicted on page 56.

Figure 11: **Total cytokine profile of stimulated hPBMCs using VSV-EBOV.** Freshly isolated hPBMCs were *in vitro* stimulated with a MOI of 1, following cytokine measurements via a customized LEGENDplex™ by BioLegend (section 3.12.1). This bead-based immunoassay included the analytes: IL-1β, IL-8, IL-10, IP-10, MCP-1, TNFα, data not shown for: IL-2, IL-4, IL-6, IL-12, IFNα, IFNγ, and CXCL9. Each pie chart represents the cytokine secretion [pg/ml] per $2 \cdot 10^6$ hPBMCs in median (N=20). The cytokines IL-1β (red), IL-8 (orange), IL-10 (green), IP-10 (blue), MCP-1 (purple), and TNFα (grey) are shown post 12 h or 24 h VSV-EBOV stimulation. Under each pie chart the whole cytokine secretion [pg/ml] for all depicted cytokines per $2 \cdot 10^6$ hPBMCs is shown.

### 4.1.2 Activation of DC & monocyte subsets

Besides the amount of secreted cytokines, the activation of immune cell subsets represents an indication for induced immune responses upon stimulation. Innate immune cells such as monocytes and DCs initiate the first responses against infections where DCs also represent an interface between innate and adaptive immunity. To this end, these immune cells were analyzed upon *in vitro* stimulation of hPBMCs with VSV-EBOV or MVA-EBOV, respectively. After separation hPBMCs were harvested at different time points (0 h, 6 h, 12 h, and 24 h post-stimulation) and stained with fluorochrome-conjugated antibodies (section 3.5 & 3.12). To investigate the activation status of different DC and monocyte subsets the expression of CD40, CD83, and CD86 were analyzed by flow cytometry. For this approach hPBMCs derived from 20 different donors for VSV-EBOV and 16 different donors for MVA-EBOV *in vitro* stimulations (section 2.2, table 3-4) were investigated. All single, live $CD3^-CD19^-$, $HLADR^+$ cells were analyzed based on their expression of CD11b (figure 12A). While DC subsets including pDCs, $CD16^+$ DCs, $CD141^+$ DCs, and $CD1c^+CD11c^+$ DCs exhibit no expression of CD11b (figure 12B), monocyte cell subsets including classical ($CD14^+CD16^-$), intermediate ($CD14^+CD16^+$), and non-classical ($CD14^{dim}CD16^+$) monocytes are $CD11b^+$ (figure 12C). The expression of activation markers on these immune cell subsets were analyzed in stimulated and unstimulated samples (figure 12D). The function of each surface marker and the rationale for investigation are summarized in table 21.

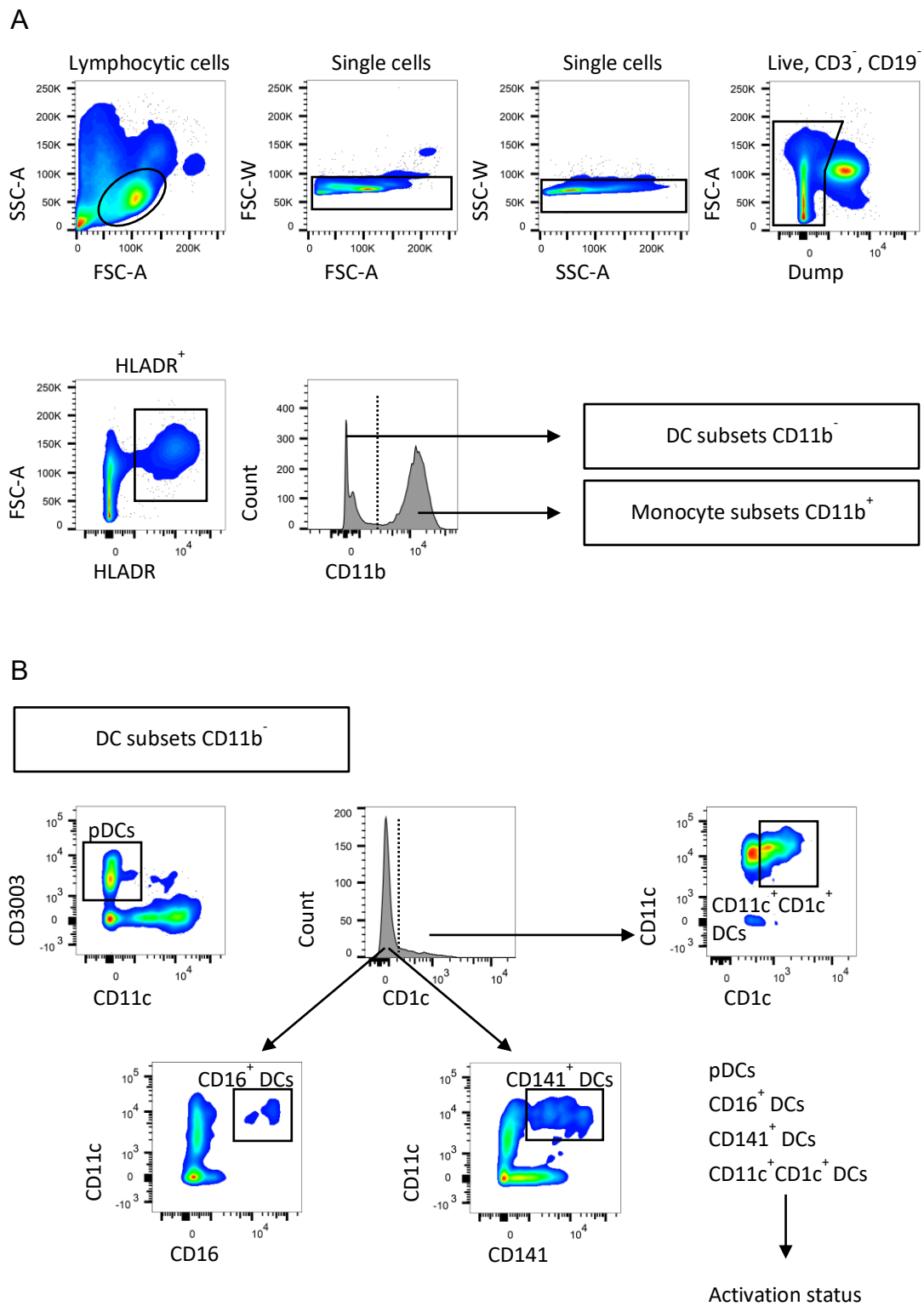


Figure legend is depicted on page 58.

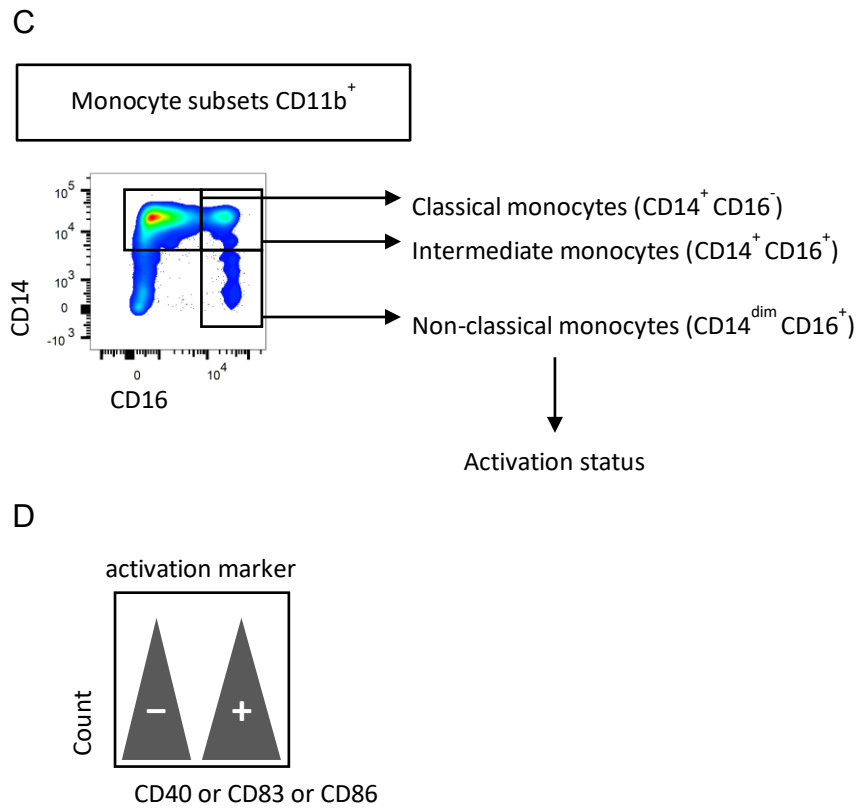


Figure 12: **Gating strategy to investigate innate immune cells.** In order to investigate the expression of the activation markers CD40, CD83, and CD86 on monocyte and DC subsets the cells were stained with fluorochrome-conjugated antibodies (section 3.12) and analyzed using the LSRFortessa™ by BD. (A) All single, live & Dump$^-$, HLADR$^+$ cells were analyzed in FlowJo based on their expression of CD11b. (B) DC subsets (CD11b$^-$) were divided in pDCs (CD303$^+$CD11c$^+$), CD1c$^-$ CD16$^+$ DCs, CD1c$^-$ CD141$^+$ DCs, and CD1c$^+$ CD11c$^+$ DCs. (C) Monocyte subsets (CD11b$^+$) were distinguished based on their expression of CD14 and CD16, where CD14$^+$CD16$^-$ are classical monocytes, CD14$^+$CD16$^+$ are intermediate monocytes, and CD14$^{dim}$CD16$^+$ are non-classical monocytes. (D) All DC and monocyte subsets were analyzed based on their expression of CD40, CD83, and CD86.

Table 21: Function and rationale for used cell surface markers

| Epitope | General function | Rationale |
|---|---|---|
| CD1c | Antigen presentation | Identification of different DC subsets |
| CD3 | TCR-component, activation of T cells | Exclude T cells |
| CD11b | Cell adhesion, phagocytosis | Differentiate between monocyte and DC subsets |
| CD11c | Cell adhesion, chemotaxis | Identification of different DC subsets |
| CD14 | Receptor function, bind LPS | Monocyte cell subsets |
| CD16 | Fc receptor, phagocytosis, antibody-dependent cellular cytotoxicity | |
| CD19 | BCR co-receptor, activation, proliferation, differentiation of B cells | Exclude B cells |
| CD40 | Receptor for CD40L, cell activation | Activation marker |
| CD83 | Expressed by activated cells, can have an immune suppressive function | |
| CD86 | Expressed on antigen presenting cells (APCs) costimulatory signal for T cell activation | |
| CD141 | Thrombomodulin cofactor for thrombin | Identification of $CD141^+$ DCs |
| CD303 | C-type lectin with several functions | Identification of pDCs |
| HLA-DR | MHC-II receptor, antigen presentation | Focus on antigen-presenting cells |

**Activation of monocyte cell subsets upon VSV-EBOV and MVA-EBOV stimulation**

Upon VSV-EBOV *in vitro* stimulations of hPBMCs no statistically significant differences compared to unstimulated counterparts were detected. However, non-classical monocytes exhibited a tendency for an increased expression of CD83 and CD86 (figure 13A–C) compared to unstimulated counterparts. The expression of CD83 peaked 12 h after stimulation where the median MFI was 2.6 times higher upon stimulation compared to unstimulated samples. In addition, the CD86 expression on non-classical monocytes showed the highest difference

between stimulated and unstimulated samples with a fold change of 1.32 12 h post-stimulation. Intermediate monocytes showed 1.21 times higher median CD83 MFI upon 12 h VSV-EBOV stimulation. Moreover, CD86 expression on intermediate monocytes exhibited a fold change of 1.15 compared to unstimulated counterparts 24 h post-stimulation.

While no tendency for an altered expression of CD40 on monocyte cell subsets was detected post VSV-EBOV stimulation, all monocyte cell subsets had an elevated expression 24 h after MVA-EBOV stimulations (figure 14A). Compared to unstimulated samples the median CD40 MFI increased slightly for classical monocytes with a fold change of 1.05, for intermediate monocytes 1.12, and for non-classical monocytes 1.15 post MVA-EBOV stimulation. In addition, the expression of CD83 on classical and intermediate monocytes peaked 12 h or 24 h, respectively, upon MVA-EBOV stimulation (figure 14B). In contrast to VSV-EBOV, MVA-EBOV stimulation resulted in significant altered expressions of CD83 and CD86 (figure 14B, C). Here, the median MFI expression of CD83 was 1.2 and 3.0 times higher upon stimulation for classical and intermediate monocytes, respectively, post 24 h stimulation (figure 14B). Moreover, MVA-EBOV stimulation also led to a significantly decreased expression of CD86 on classical, intermediate, and non-classical monocyte cell subsets over time compared to unstimulated counterparts (figure 14C). All monocyte cell subsets showed the highest significant decrease with a 0.2 to 0.3 fold change 12 h post MVA-EBOV stimulation.

Finally, this approach revealed differences in the activation of monocyte cell subsets upon *in vitro* stimulation of hPBMCs using VSV-EBOV and MVA-EBOV, respectively. While upon VSV-EBOV stimulation mainly intermediate and non-classical monocytes showed a tendency for an enhanced activation based on their expression of CD83 and CD86, MVA-EBOV stimulation led primarily to a higher expression of CD40. Here, only MVA-EBOV resulted in a significant upregulation of CD83 on intermediate monocytes and downregulation of CD86 on all monocyte cell subsets.

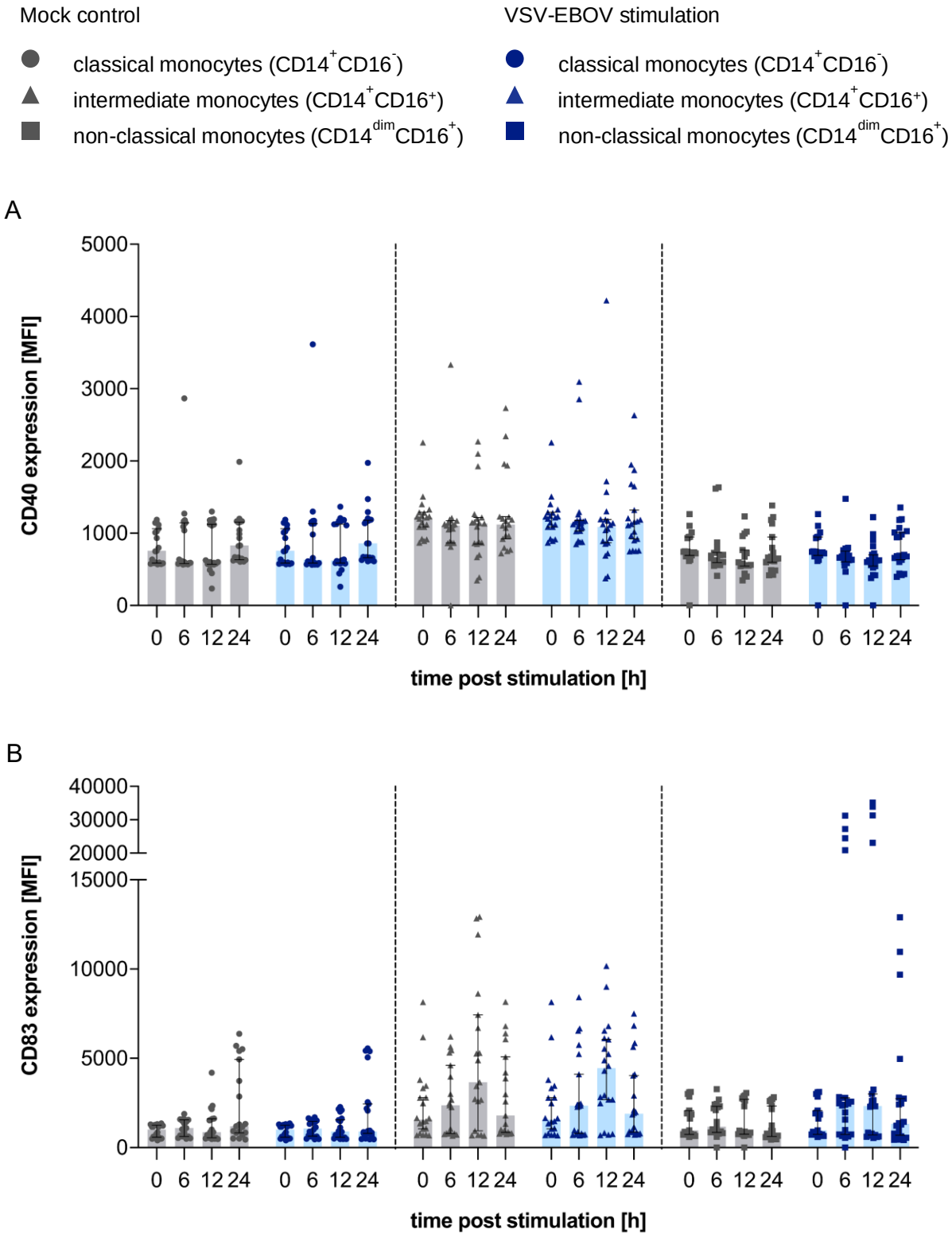


Figure legend is depicted on page 62.

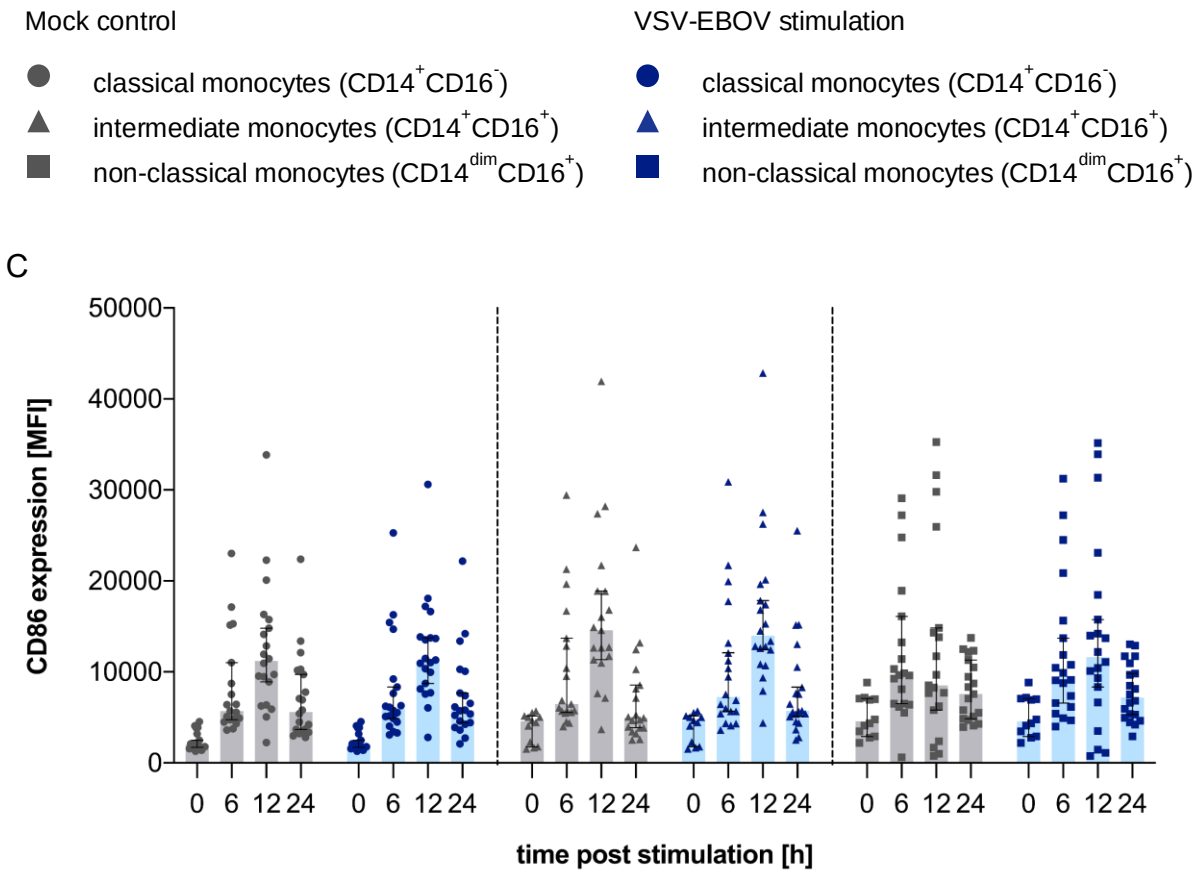


Figure 13: **Expression of activation markers on monocytes upon VSV-EBOV stimulation.** The expression of A) CD40, B) CD83, and C) CD86 on classical ($CD14^+CD16^-$, dots), intermediate ($CD14^+CD16^+$, triangle), and non-classical monocytes ($CD14^{dim}CD16^+$, square) were analyzed via flow cytometry (section 3.12, antibodies table 14) upon *in vitro* stimulation of whole hPBMCs using VSV-EBOV (MOI 1). All samples were gated as described in figure 12. Besides unstimulated (grey) also stimulated samples (blue) were investigated based on the MFI of all three activation marker. The maximum of each bar represents the median including error bars indicating the 95 % CI. No statistically significant differences in the expression of CD40, CD83, and CD86 were detected using the t-test based unpaired, nonparametric Mann-Whitney test. The p-values are indicated as follows: $p \leq 0.05$ *; $p \leq 0.01$ **; $p \leq 0.001$ ***; $p \leq 0.0001$ ****. Analyzed samples N=20 (section 2.2, table 3).

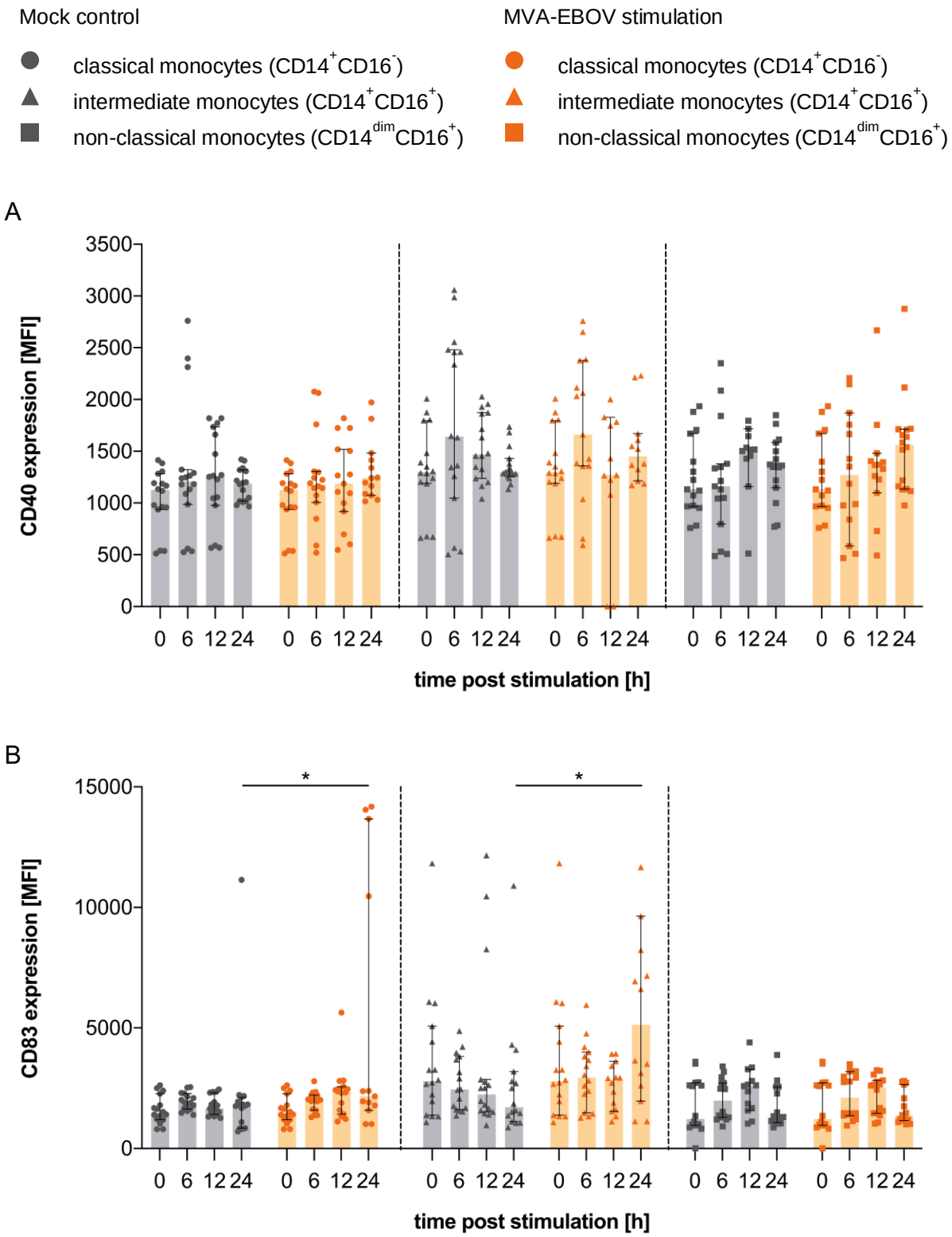


Figure legend is depicted on page 64.

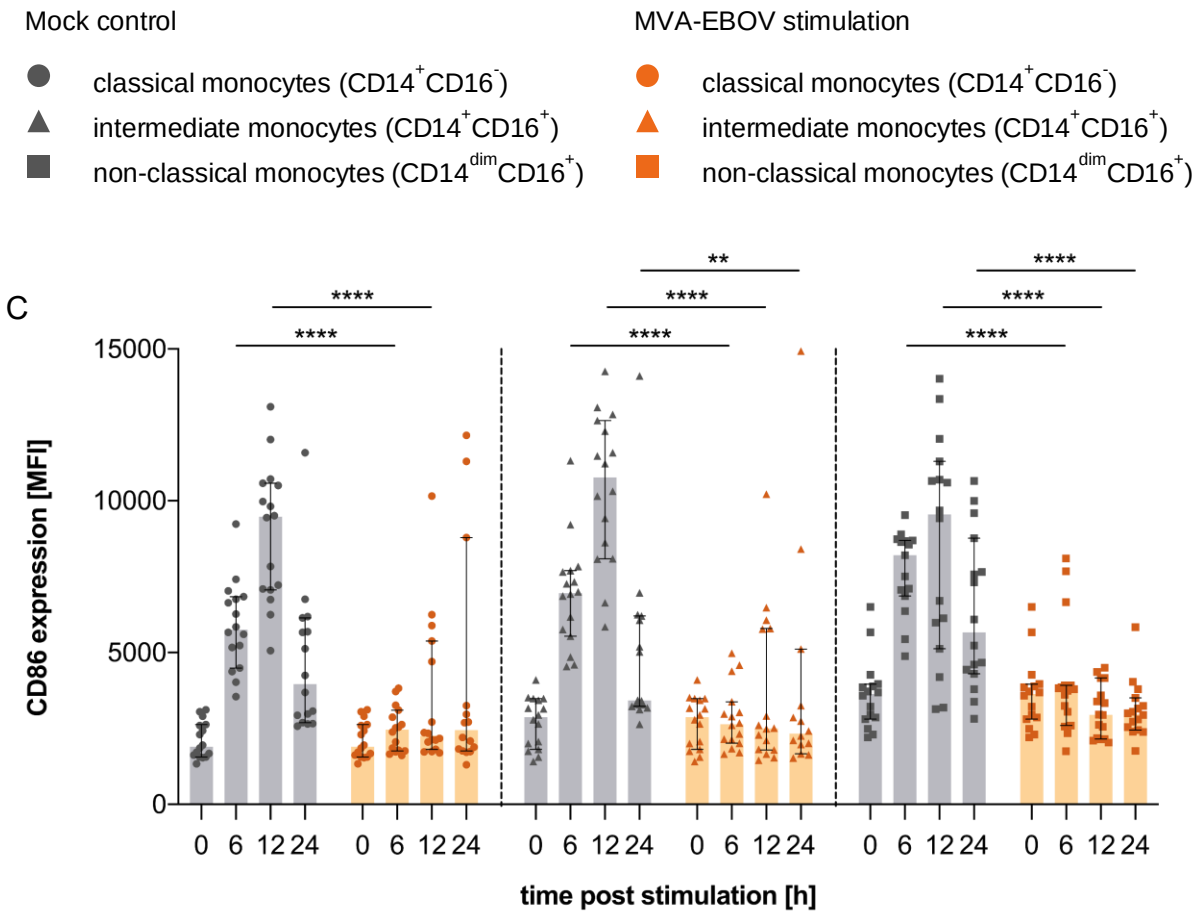


Figure 14: **Expression of activation markers on monocytes upon MVA-EBOV stimulation.** The expression of A) CD40, B) CD83, and C) CD86 on classical ($CD14^+CD16^-$, dots), intermediate ($CD14^+CD16^+$, triangle), and non-classical monocytes ($CD14^{dim}CD16^+$, square) were analyzed via flow cytometry (section 3.12, antibodies table 14) upon *in vitro* stimulation of whole hPBMCs using MVA-EBOV (MOI 1). All samples were gated as described in figure 12. Besides unstimulated (grey) also stimulated samples (orange) were investigated based on the MFI of all three activation marker. The maximum of each bar represents the median including error bars indicating the 95 % CI. For significance determination the t-test based unpaired, nonparametric Mann-Whitney test was performed. The p-values are indicated as follows: $p \leq 0.05$ *; $p \leq 0.01$ **; $p \leq 0.001$ ***; $p \leq 0.0001$ ****. Analyzed samples N=16 (section 2.2, table 4).

### Activation of pDCs and $CD1c^+CD11c^+$ DCs upon VSV-EBOV or MVA-EBOV stimulation

DCs are one of the first immune cells to come in contact with a viral infection or administration of vaccines and are important in the communication of innate and adaptive immunity [45,47,48].

Different DC subsets exhibited a distinct expression profile of the activation marker CD40, CD83, and CD86. In accordance with the monocyte cell subset findings, a VSV-EBOV *in vitro* stimulation revealed no statistically significant modification in the expression of these activation markers on pDCs and CD1c$^+$CD11c$^+$ DCs. After an *in vitro* stimulation, CD1c$^+$CD11c$^+$ DCs exhibited a higher dynamic of CD40, CD83, and CD86 on its surface compared to pDCs (cf. section 6.3 S.11A,B). Moreover, CD1c$^+$CD11c$^+$ showed a slightly increased expression of CD86 compared to unstimulated samples peaking at 12 h post-stimulation. Here, the median MFI was 1.1 times higher post-stimulation (figure 15).

While pDCs and CD1c$^+$CD11c$^+$ DCs had a significantly reduced expression of CD86 post MVA-EBOV stimulations, CD40 and CD83 exhibited no statistically changes over time (cf. section 6.3 S.12A,B). CD86 on pDCs showed a significantly decreased expression 24 h post-stimulation with a fold change of 0.6. In contrast, CD1c$^+$CD11c$^+$ DCs revealed a decreased expression compared to unstimulated counterparts for all time points (figure 16).

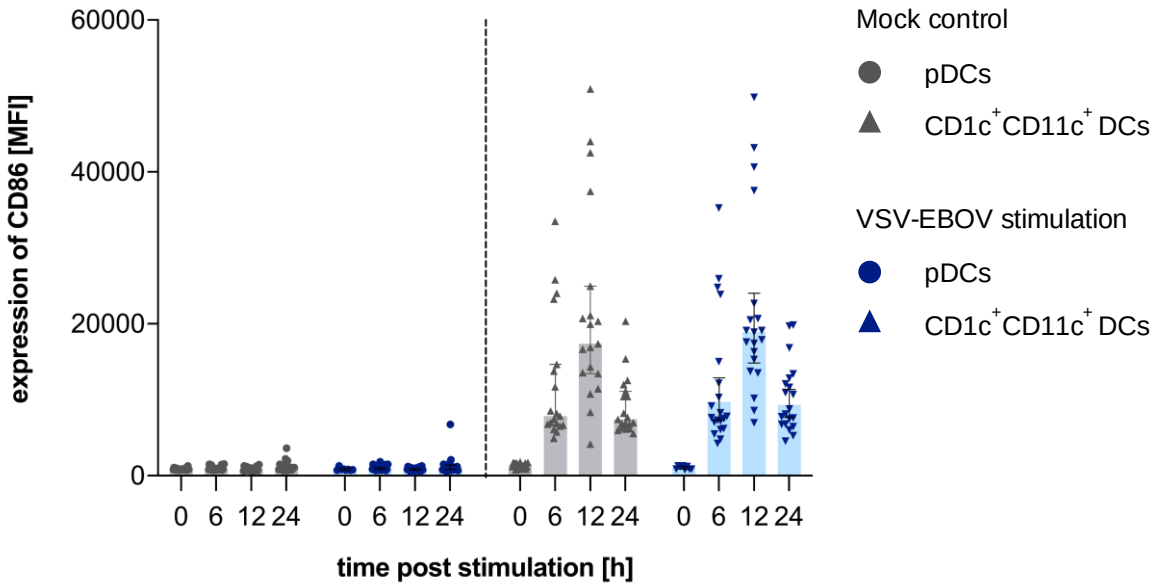


Figure 15: **Expression of CD86 on pDCs and CD1c$^+$CD11c$^+$ DCs upon VSV-EBOV stimulation.** The expression of CD86 was analyzed via flow cytometry (section 3.12, antibodies table 14) upon *in vitro* stimulation of whole hPBMCs using VSV-EBOV (MOI 1). All samples were gated like described in figure 12. Besides stimulated (blue) also unstimulated samples (grey) were investigated based on the MFI of CD86. Dots indicate pDCs and triangle CD1c$^+$CD11c$^+$ DCs. The maximum of each bar represents the median including error bars indicating the 95 % CI. No statistically significant differences in the expression of CD40, CD83, and CD86 were detected using the t-test based unpaired, nonparametric Mann-Whitney test. The p-values are indicated as follows: $p \leq 0.05$ *; $p \leq 0.01$ **; $p \leq 0.001$ ***; $p \leq 0.0001$ ****. Analyzed samples N=20 (section 2.2, table 3).

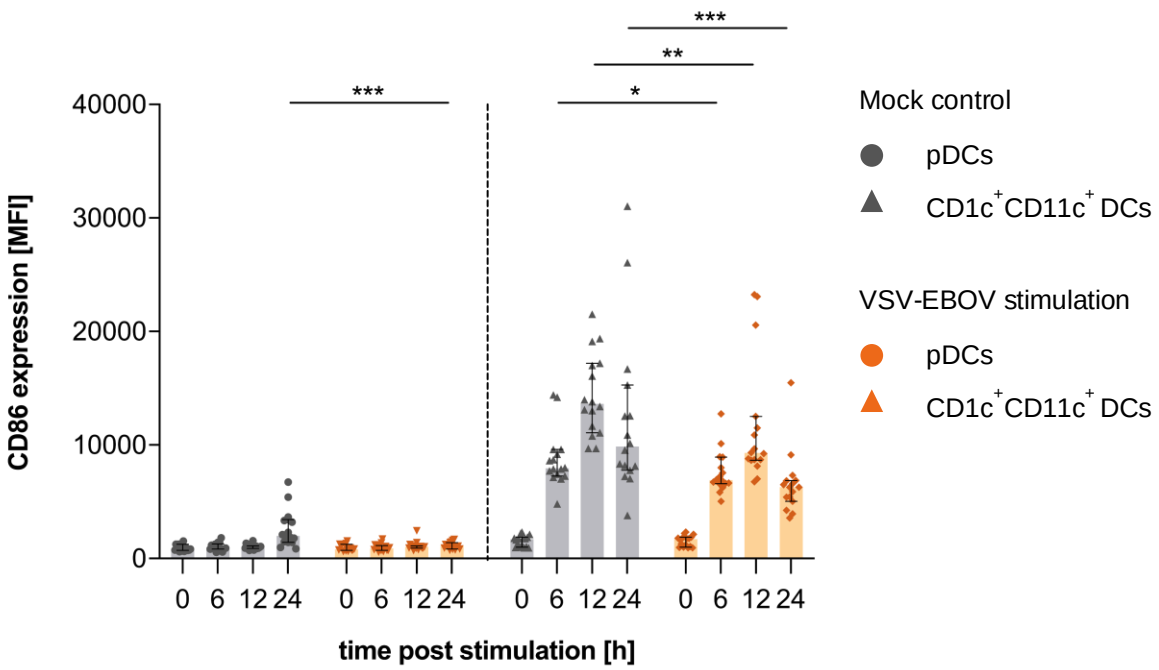


Figure 16: **Expression of CD86 on pDCs and CD1c$^+$CD11c$^+$ DCs upon MVA-EBOV stimulation.** The expression of CD86 was analyzed via flow cytometry (section 3.12, antibodies table 14) upon *in vitro* stimulation of whole hPBMCs using MVA-EBOV (MOI 1). All samples were gated like described in figure 12. Besides stimulated (blue) also unstimulated samples (orange) were investigated based on the MFI of CD86. Dots indicate pDCs and triangle CD1c$^+$CD11c$^+$ DCs. The maximum of each bar represents the median including error bars indicating the 95 % CI. For significance determination the t-test based unpaired, nonparametric Mann-Whitney test was performed. The p-values are indicated as follows: $p \leq 0.05$ *; $p \leq 0.01$ **; $p \leq 0.001$ ***; $p \leq 0.0001$ ****. Analyzed samples N=16 (section 2.2, table 4).

### Activation of CD141$^+$ and CD16$^+$ DCs upon VSV-EBOV or MVA-EBOV stimulation

CD1c$^-$ DC subsets revealed mandatory functions in the response to viruses due to their ability to cross-present antigens for CTL differentiation/activation [252]. These CD1c$^-$ DCs including CD16$^+$ and CD141$^+$ DCs exhibited only tendencies for an altered expression of CD40, CD83, and CD86 upon VSV-EBOV stimulation (cf. section 6.3, S.13A,B). Specifically, CD141$^+$ DCs showed an elevated expression of CD86 24 h post-stimulation (median MFI 6807 vs. 8235) (figure 17). While upon VSV-EBOV stimulation mainly CD86 showed an enhanced expression, an MVA-EBOV stimulation resulted in an elevated expression of CD40 on CD141$^+$ DCs 24 h post-stimulation (cf. section 6.3, S.14). Here, the median MFI exhibited a fold change of 1.45 post-stimulation. Moreover, CD83 and CD86 showed significantly altered expression upon

stimulation using MVA-EBOV (figure 18). The CD83 expression was significantly decreased on CD141$^+$ DCs with a fold change of 0.5 and 0.2 12 h and 24 h post MVA-EBOV *in vitro* stimulation (figure 18A), whereas CD86 was significantly reduced on CD16$^+$ DCs with a fold change of 0.8 6 h after stimulation (figure 18B).

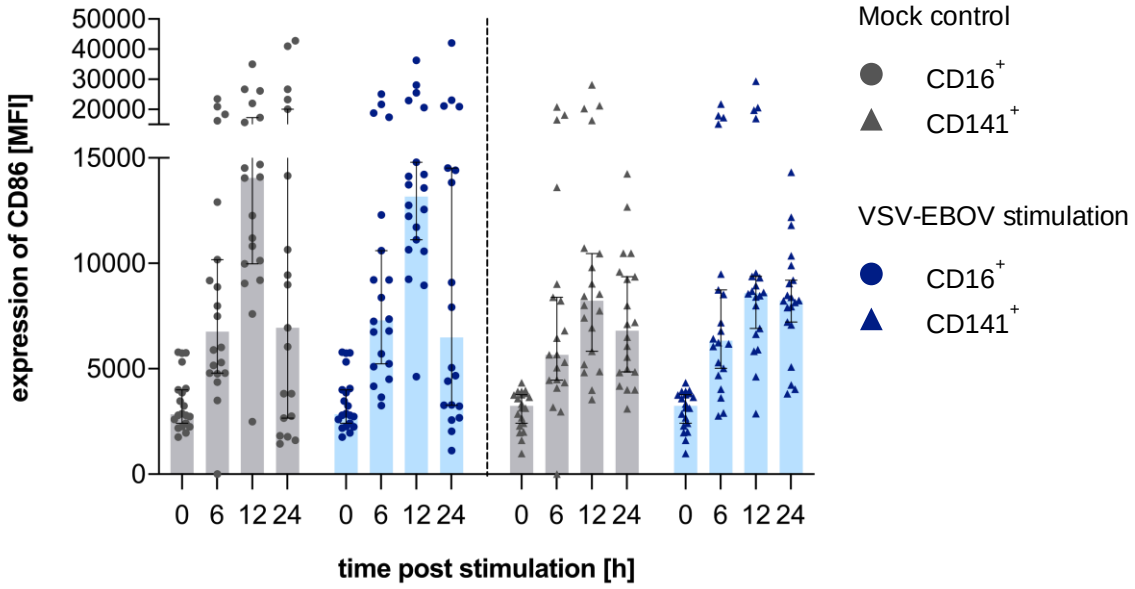


Figure 17: **Expression of CD86 on CD16$^+$ and CD141$^+$ DCs upon VSV-EBOV stimulation.** The expression of CD86 was analyzed by flow cytometry (section 3.12, antibodies table 14) upon *in vitro* stimulation of whole hPBMCs using VSV-EBOV (MOI 1). All samples were gated as described in figure 12. Besides stimulated (blue) also unstimulated samples (grey) were investigated based on the MFI of CD86. Dots indicate CD16$^+$ and triangle CD141$^+$ DCs. The maximum of each bar represents the median including error bars indicating the 95 % CI. No statistically significant differences in the expression of CD86 was detected using the t-test based unpaired, nonparametric Mann-Whitney test. The p-values are indicated as follows: $p \leq 0.05$ *; $p \leq 0.01$ **; $p \leq 0.001$ ***; $p \leq 0.0001$ ****. Analyzed samples N=20 (section 2.2, table 3).

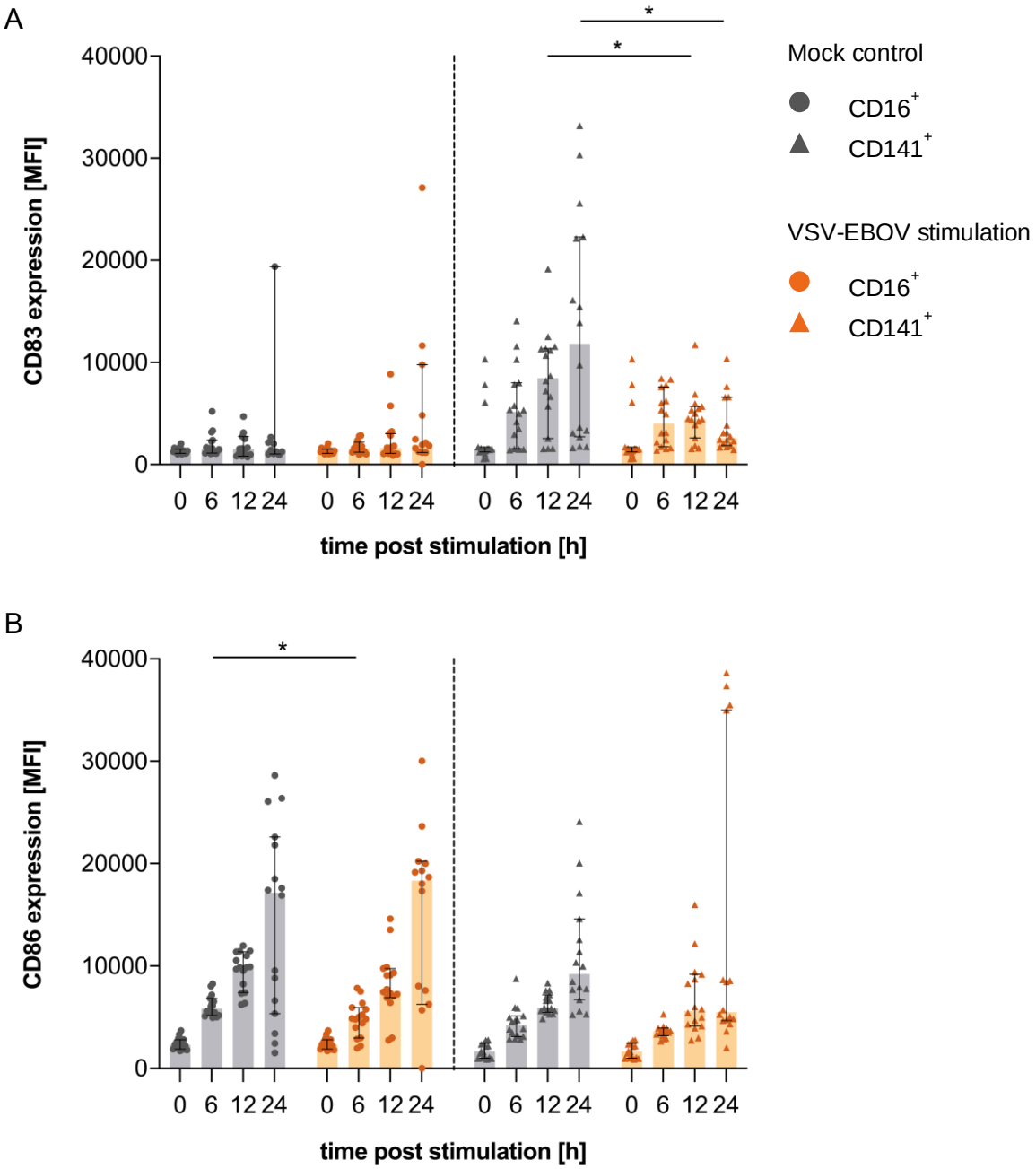


Figure 18: **Expression of CD83 and CD86 on CD16⁺ and CD141⁺ DCs upon MVA-EBOV stimulation.** The expression of A) CD83 and B) CD86 were analyzed by flow cytometry (section 3.12, antibodies table 14) upon *in vitro* stimulation of whole hPBMCs using MVA-EBOV (MOI 1). All samples were gated as described in figure 12. Besides stimulated (orange) also unstimulated samples (grey) were investigated based on the MFI of CD83 and CD86. Dots indicate CD16⁺ and triangle CD141⁺ DCs. The maximum of each bar represents the median including error bars indicating the 95 % CI. For significance determination the t-test based unpaired, nonparametric Mann-Whitney test was performed. The p-values are indicated as follows: $p \leq 0.05$ *; $p \leq 0.01$ **; $p \leq 0.001$ ***; $p \leq 0.0001$ ****. Analyzed samples N=16 (section 2.2, table 4).

In brief, an *in vitro* stimulation of hPBMCs using VSV-EBOV mainly revealed tendencies for an enhanced expression of CD86 on $CD1c^+CD11c^+$ and $CD141^+$ DCs. In contrast, an MVA-EBOV stimulation led to a higher expression of CD40 on $CD141^+$. Furthermore, only MVA-EBOV stimulations revealed significant reductions of mainly CD86 expressions on monocyte cell subsets as well as DC subsets compared to unstimulated samples. Therefore, VSV-EBOV and MVA-EBOV may induce different immune responses upon stimulation. Whether these differences are also determined by an altered transcriptomic profile needs to be investigated.

## 4.2 Transcriptomic changes upon *in vitro* stimulation

To investigate the immune signature upon *in vitro* stimulation in more detail, comprehensive transcriptomic analyses were performed. A combination of different approaches was used to gain more knowledge on differentially expressed genes (DEG) upon VSV-EBOV or MVA-EBOV *in vitro* stimulation of hPBMCs (section 3.5) (figure 19). First, the nanoString® technology was used to receive more insights for induced transcriptomic changes upon *in vitro* stimulations using VSV-EBOV. These findings were validated by qPCR and expanded by RNA-Sequencing (RNA-Seq) to gain more knowledge on transcriptomic changes upon VSV-EBOV or MVA-EBOV *in vitro* stimulations (figure 19). Using different gene sets and pathway analyses the functionality of all DEG were investigated post-stimulation.

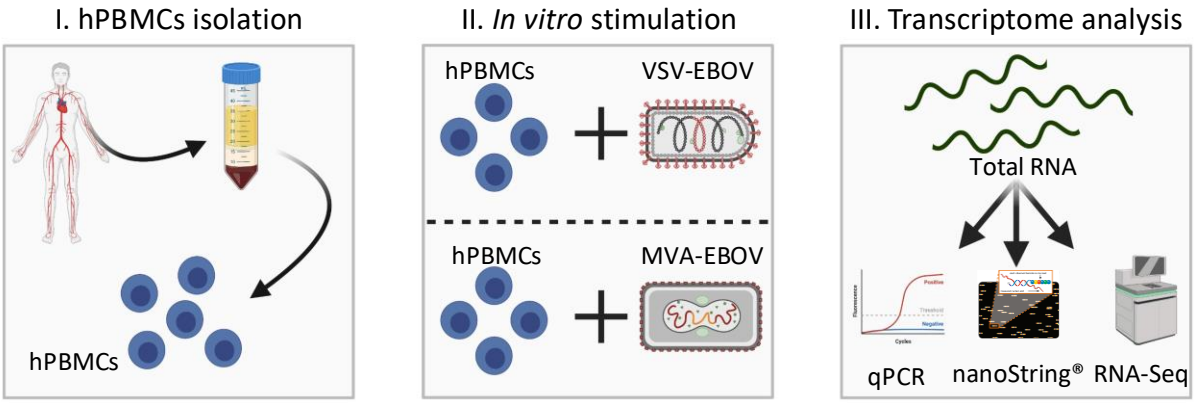


Figure 19: **Experimental setup to decipher transcriptomic changes.** Freshly isolated hPBMCs were *in vitro* stimulated using VSV-EBOV or MVA-EBOV, respectively. hPBMCs derived from 20 different donors were stimulated with VSV-EBOV (section 2.2, table 3) and 16 with MVA-EBOV (section 2.2, table 4) (MOI 1). The transcriptomic profile of whole hPBMCs was investigated via qPCR, the nanoString® technology and RNA-Seq to monitor immune signatures over time. Figure created with BioRender.com, nanoString® symbol obtained from Cesano, A. 2015 [253].

### 4.2.1 Revealing transcriptomic changes using the nanoString® technology

Transcriptome changes upon *in vitro* stimulation were analyzed using a human immunology panel v2 by nanoString® (section 3.9). This panel is an enzyme-free gene expression analysis based on the hybridization of target-RNA and a specific capture probe as well as target-specific color-coded barcode reporter probes. Molecular counting of each color-coded barcode allows a simultaneous multiplex measurement for all targets. The human immunology panel v2 includes 594 immune-related genes and 15 reference genes. For transcriptome analyses of *in vitro* stimulated hPBMCs using VSV-EBOV, total RNA from hPBMCs derived from 8 donors (sex ratio 50:50, section 2.2, table 5) at three different time points was investigated. To this end, unstimulated hPBMCs after isolation (0 h) and early after stimulation (1 h and 6 h) were analyzed. By comparing unstimulated and stimulated samples, the influence of VSV-EBOV on transcriptomic changes was addressed. All genes which exhibited a log2 fold change ≤ -1 or ≥ 1 and a p-value < 0.001 were counted as DEG.

While after 1 h of VSV-EBOV *in vitro* stimulation 66 DEG including 33 up- and 33 downregulated genes were detected, 135 DEG including 51 up- and 84 downregulated genes were observed 6 h post-stimulation (figure 20A). Therefore, VSV-EBOV seems to influence the

transcriptomic profile of stimulated samples. Furthermore, longer stimulations had a stronger effect on transcriptomic changes compared to short term stimulations. Both time points shared only 29 DEG (figure 20B) indicating that the gene expression is influenced and changed by VSV-EBOV over time.

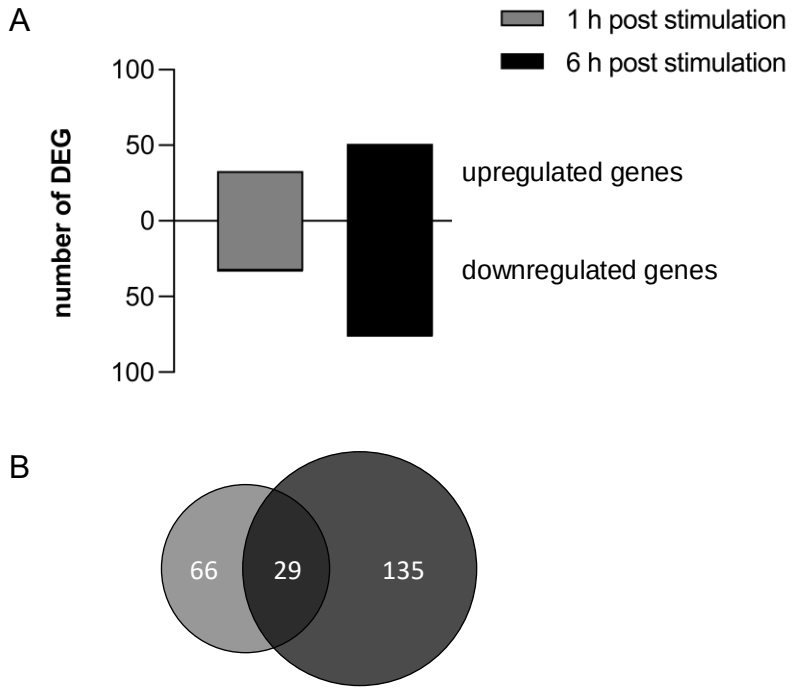


Figure 20: **Number of DEG upon VSV-EBOV stimulation of hPBMCs.** Total RNA of 1 h and 6 h *in vitro* stimulated and unstimulated samples (N=8, section 2.2, table 5) was analyzed via a human immunology panel microarray by nanoString® (section 3.9). Genes, which exhibited a log2 fold change ≤ -1 or ≥ 1 and a p-value < 0.001 compared to unstimulated samples (0 h), were counted as DEG. DEG of 1 h stimulated samples are depicted in grey and those of 6 h stimulation are depicted in black. A) Number of DEG post 1 h and 6 h are shown. B) DEG in 1 h, 6 h or in both stimulations are depicted. Venn diagram designed with BioVenn a web-based application [227].

Additionally, a principal component analysis (PCA) revealed distinct differences between stimulated and unstimulated samples (figure 21). In particular, PC1 and PC2 showed differences between 0 h unstimulated and 1 h or 6 h stimulated samples indicating an influence of VSV-EBOV to transcriptomic changes. The PCA revealed a bigger difference between unstimulated and 6 h stimulated samples compared to shorter stimulations indicating a higher impact for long term stimulations to transcriptomic changes.

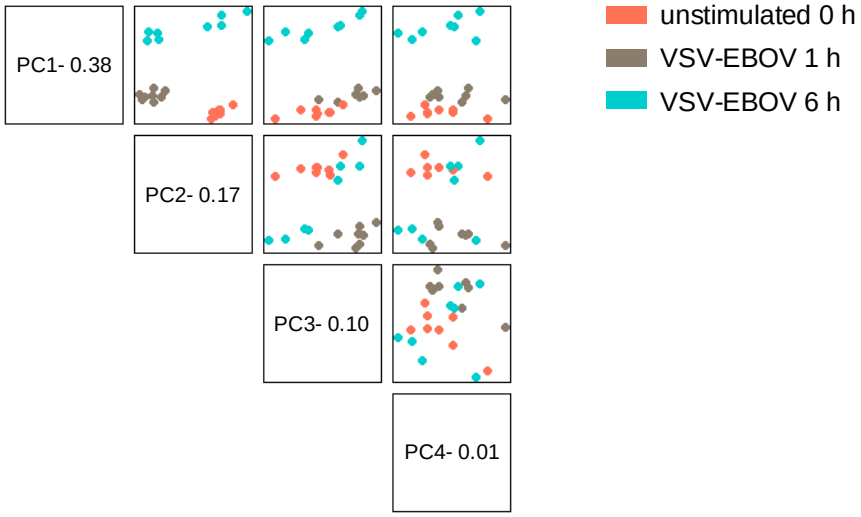


Figure 21: **Principal component analysis of stimulated hPBMCs using VSV-EBOV.** Total RNA of 1 h and 6 h VSV-EBOV–stimulated (MOI 1) and 0 h unstimulated samples (N=8, section 2.2, table 5) was analyzed via a human immunology panel microarray by nanoString® (section 3.9). Here, the first four principal components of genes and selected covariates are shown. Unstimulated 0 h (orange), 1 h stimulated (brown) and 6 h stimulated (blue) hPBMCs are depicted. PCA were performed with the nSolver™ Software v4, the nCounter® advanced analysis software v2.0.115 including R3.3.2 and XQuartz.

To gain insight into the functionality of DEG upon stimulation, an over-representation analysis (ORA) was performed based on the reactome database of the top five regulated pathways. ORA of differently up- or downregulated genes showed distinct signatures for pathway enrichment (figure 22). While three pathways are associated to differently up- and downregulated genes post 1 h stimulation (figure 22A), only one pathway included differently up- and downregulated genes after 6 h stimulation (figure 22B). Moreover, an induction of pathways with an anti-viral function was detected 6 h post-stimulation compared to 1 h. After 6 h stimulation upregulated genes belonged to interleukin, cytokine, and chemokine signaling. Furthermore, the anti-inflammatory IL-10 signaling was also elevated 6 h upon stimulation. Nevertheless, immunoregulatory interactions between lymphoid and non-lymphoid cells belonged to downregulated pathways indicating a well-regulated but not overwhelming anti-inflammatory response.

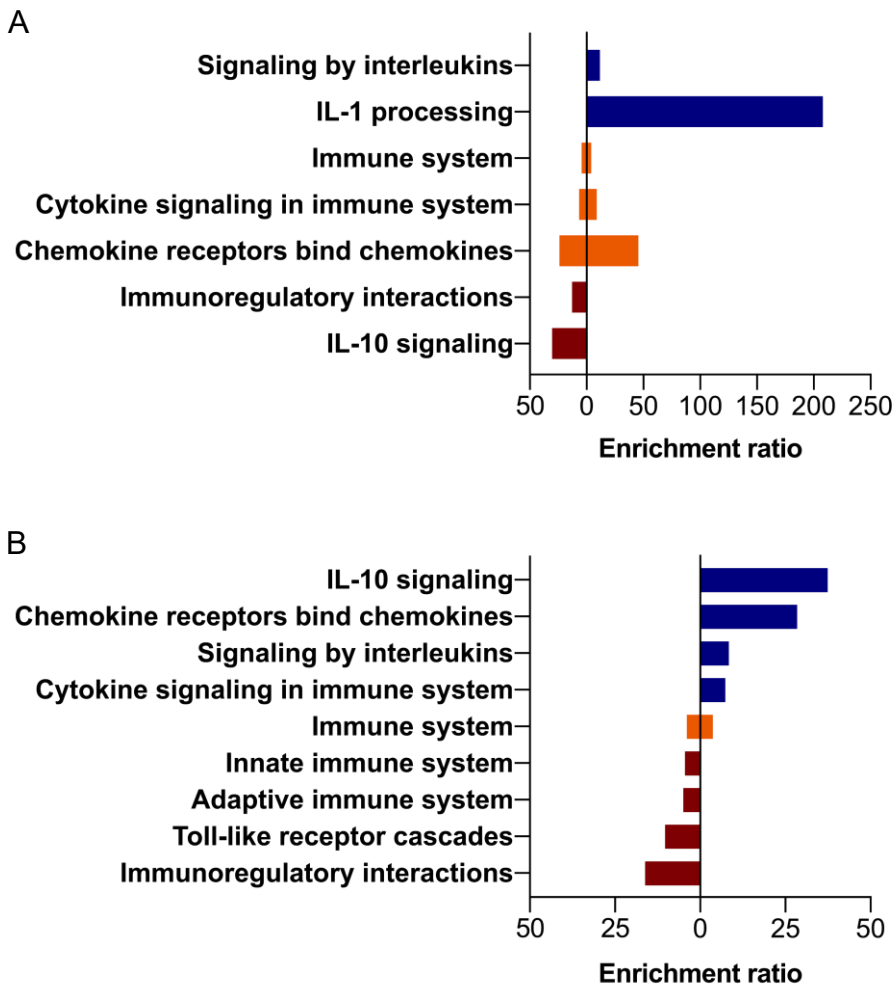


Figure 22: **ORA of DEG after VSV-EBOV stimulation.** Total RNA of A) 1 h and B) 6 h VSV-EBOV *in vitro* stimulated (MOI 1) and 0 h unstimulated samples (N=8, section 2.2, table 5) was analyzed via a human immunology panel microarray by nanoString® (section 3.9). Genes, which exhibited a log2 fold change ≤ -1 or ≥ 1 and a p-value < 0.001 compared to unstimulated samples 0 h upon hPBMC isolation, were counted as DEG. Enrichment ratios were calculated with the web tool: webgestalt.org [228–231] using only the top 5 pathways of up- or downregulated genes with a false discovery rate (FDR) ≤ 0.05. Pathways which contain only differently upregulate gens (blue), downregulated genes (red), and up- as well as downregulated genes (orange), are depicted.

To verify genes that are associated with the determined pathways, all genes of 1 h and 6 h were depicted in a volcano plot (figure 23). The volcano plots highlighted that 6 h of stimulation induced a stronger dynamic of transcriptomic changes, since more genes showed a higher fold change upon 6 h of stimulation (figure 23B) compared to 1 h (figure 23A). In particular, two genes called *IP-10* and *C-type lectine 5A* (*CLEC5A*) exhibited a stronger induction post 6 h with a log2 fold change of 6.9 and 5.5, respectively. Both have pro-inflammatory functions resulting in potentially diminished infections. However, IP-10 and

CLEC5A can also facilitate or promote infections and their pathogenicity [254,255]. IP-10 can mediate chemotaxis of CXCR3$^{+}$ cells, proliferation, apoptosis, regulation of cell growth, and angiogenesis in infections [255–260]. CLEC5A can act as a ligand for several viruses like dengue, influenza, and the Japanese encephalitis virus resulting in enhanced viral pathology based on induced pro-inflammatory cytokine secretion [261–263]. Moreover, several genes with a pro-inflammatory/anti-viral function were enhanced post-stimulation. While the expression of *IL-1α* increased over time emphasized by an elevated log2 fold change from 4.25 to 5.2, *GBP1*, *IDO1*, and *MCP-1* were first upregulated upon 6 h of stimulation with log2 fold changes of 3.2, 3.5, and 3.7, respectively.

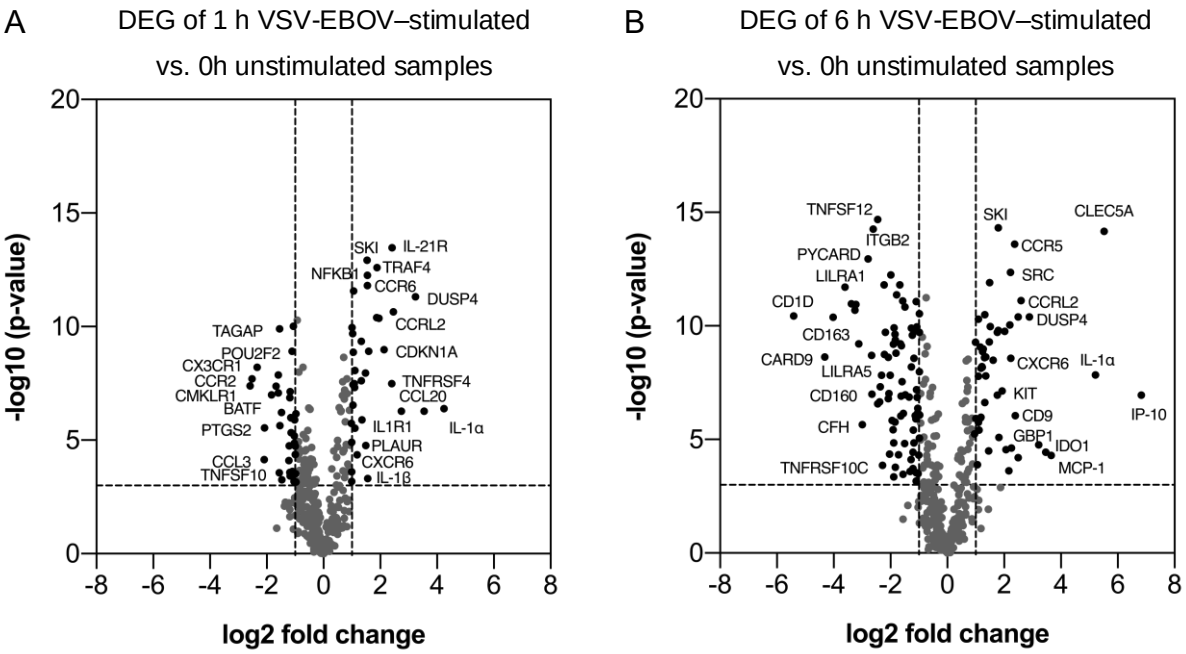


Figure 23: **Volcano plots of stimulated hPBMCs using VSV-EBOV.** Total RNA of A) 1 h and B) 6 h VSV-EBOV *in vitro* stimulated (MOI 1) and 0 h unstimulated samples (N=8, section 2.2, table 5) was analyzed via a human immunology panel microarray by nanoString® (section 3.9). Genes, which exhibited a log2 fold change ≤ -1 or ≥ 1 and a p-value < 0.001 compared to unstimulated 0 h controls, were counted as DEG. A) While in the left volcano plot all analyzed genes 1 h after stimulation are shown, B) all genes 6 h post-stimulation are depicted in the right volcano plot. Black dots indicate DEG and grey dots represents not DEG separated by dotted lines.

To validate the expression of *IP-10* and *CLEC5A* a semi-qPCR was performed (section 3.8.5). First, the relative expression of both genes to unstimulated samples (0 h) was calculated with the ΔΔCt method ($2^{-\Delta\Delta Ct}$). This analysis revealed an expression of *IP-10* and *CLEC5A* over time

(cf. section 6.4.1, S.15). While 12 out of 20 samples showed a higher expression of *IP-10* 6 h post-stimulation, *CLEC5A* was elevated in 10 samples compared to unstimulated samples (figure 24).

Using the relative expression of *IP-10* and *CLEC5A*, the fold change of VSV-EBOV-stimulated samples was calculated. Thereby, stimulated and unstimulated samples of the same time point were compared to determine the fold change over time (section 3.8.6). This analysis revealed an elevated expression of *IP-10* and *CLEC5A* peaking at 6 h post VSV-EBOV stimulation with a fold change of 1.6 and 1.4, respectively (figure 25).

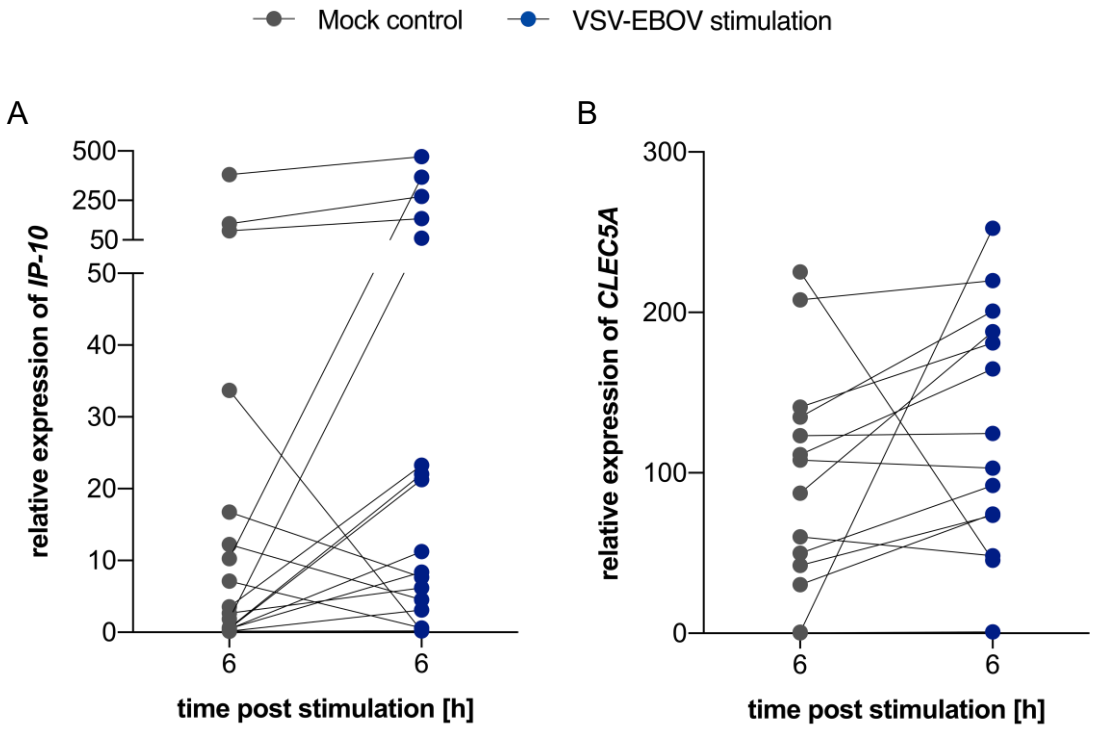


Figure 24: **Relative expression of *IP-10* and *CLEC5A* after VSV-EBOV stimulation.** Total RNA of 6 h was analyzed via semi-qPCR (section 3.8.5; section 2.6, primer sequence table 11). Besides VSV-EBOV *in vitro* stimulated (MOI 1; blue) also unstimulated samples (grey) were investigated. Each dot indicates a different blood donor (N=20, section 2.2, table 3). Stimulated and unstimulated samples of the same donor are connected via black lines. A) The relative expression of *IP-10* is depicted. B) The relative expression of *CLEC5A* is shown. Relative expressions were calculated with the ΔΔCt method (section 3.8.6). While 12 samples showed a higher expression of *IP-10*, *CLEC5A* was elevated in 10 samples compared to unstimulated samples.

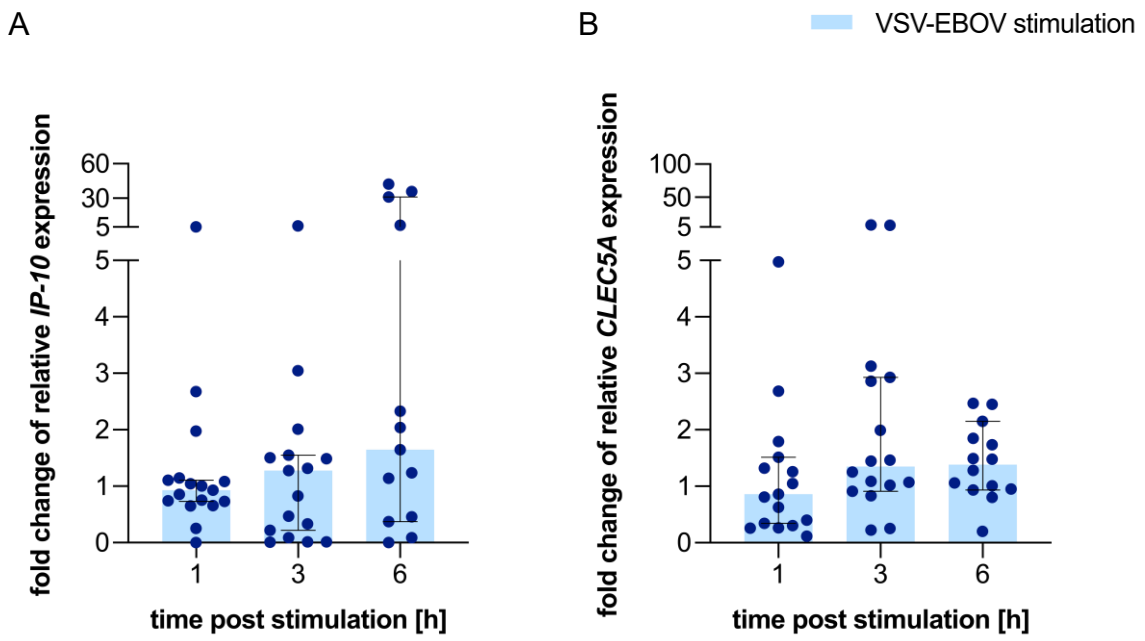


Figure 25: **Fold change of *IP-10* and *CLEC5A* after VSV-EBOV stimulation.** Total RNA of 0 h, 1 h, 3 h, and 6 h was analyzed via semi-qPCR (section 3.8.5; section 2.6, primer sequence table 11). Besides VSV-EBOV *in vitro* stimulated (MOI 1; blue) also unstimulated samples (grey) were investigated. Each dot indicates a different blood donor (N=20, section 2.2, table 3). The maximum of each bar represents the median including the 95 % CI. A) The fold change of *IP-10* is depicted. B) The fold change of *CLEC5A* is shown. Relative expressions were calculated with the ΔΔCt method and used to calculate the fold change (section 3.8.6).

Finally, a distinct transcription profile of *in vitro* stimulated hPBMCs using VSV-EBOV could be observed. Especially, genes with an anti-viral function including *IP-10*, *CLEC5A*, *GBP1*, *IL-1α*, *IDO1*, *and MCP-1* were elevated 6 h post-stimulation.

### 4.2.2 Comprehensive analysis of transcriptomic changes using RNA-Seq

To investigate transcriptomic changes upon *in vitro* stimulation in more depth, RNA-Seq analysis of VSV-EBOV as well as MVA-EBOV–stimulated samples were performed (section 3.10). Total RNA of unstimulated (0 h and 6 h) and 6 h stimulated samples was analyzed. The RNA-Seq was based on the Illumina technology and included more than 60,000 genes with a depth of approximately 21 million clusters in average. By comparison of unstimulated and stimulated samples, the influence of VSV-EBOV or MVA-EBOV on transcriptomic changes should be addressed. To this end, all genes which exhibited a log2 fold change ≤ -1.5 or ≥ 1.5 and a false discovery rate (FDR) < 0.01 were counted as DEG.

Using unstimulated hPBMCs after isolation (0 h) (section 3.3) a validation of induced transcriptomic changes due to VSV-EBOV or MVA-EBOV 6 h post-stimulation as well as 6 h of *in vitro* cultivation was performed. While a 6 h *in vitro* stimulation using VSV-EBOV showed 643 DEG including 420 up- and 223 downregulated genes compared to 0 h, 6 h unstimulated samples exhibited 299 DEG containing 284 up- and 15 downregulated genes (figure 26A). Moreover, an MVA-EBOV stimulation resulted in a higher number of DEG compared to unstimulated counterparts. In this case, an MVA-EBOV stimulation resulted in 3,599 DEG containing 1,749 up- and 1,850 downregulated genes, whereas unstimulated samples exhibited 2,262 DEG including 1,013 up- and 1,249 downregulated genes (figure 26A). In addition, both stimulations shared up to 68.0 % of their differently up- or downregulated genes with fractions of unstimulated counterparts (figure 26B,C). After 6 h of VSV-EBOV stimulation, 242 of all differently up- and 13 of all downregulated genes were also differently expressed in unstimulated 6 h samples (figure 26B). In contrast, upon MVA-EBOV stimulation 484 genes were differently up and 792 were differently downregulated in stimulated and unstimulated samples post 6 h (figure 26C). While a VSV-EBOV stimulation led to 643 DEG, MVA-EBOV resulted in 3,599 DEG (figure 26D). Both stimulations shared 170 significantly upregulated and 110 downregulated genes. Therefore, MVA-EBOV induced 5.6 times more DEG compared to VSV-EBOV.

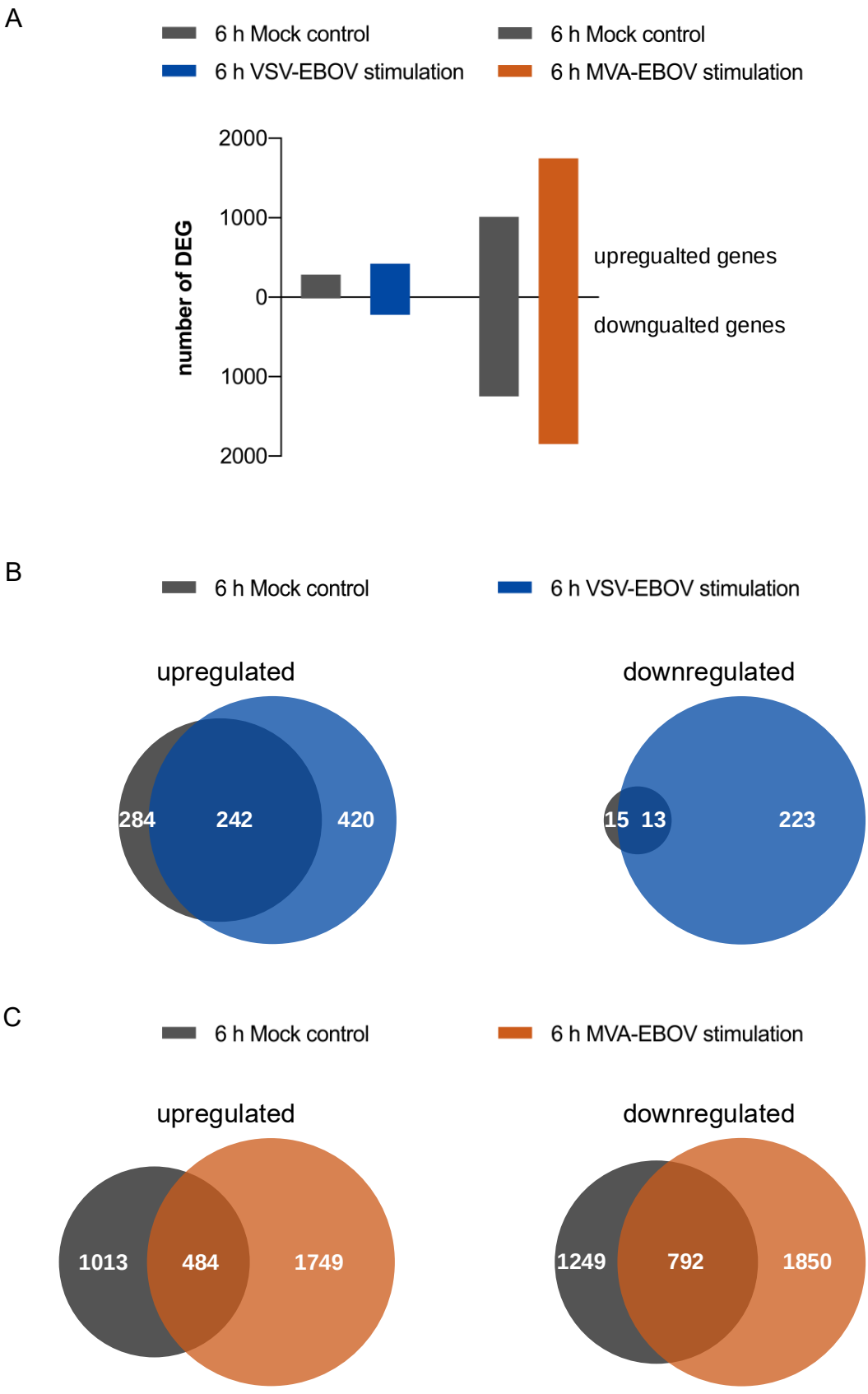


Figure legend depicted on page 79.

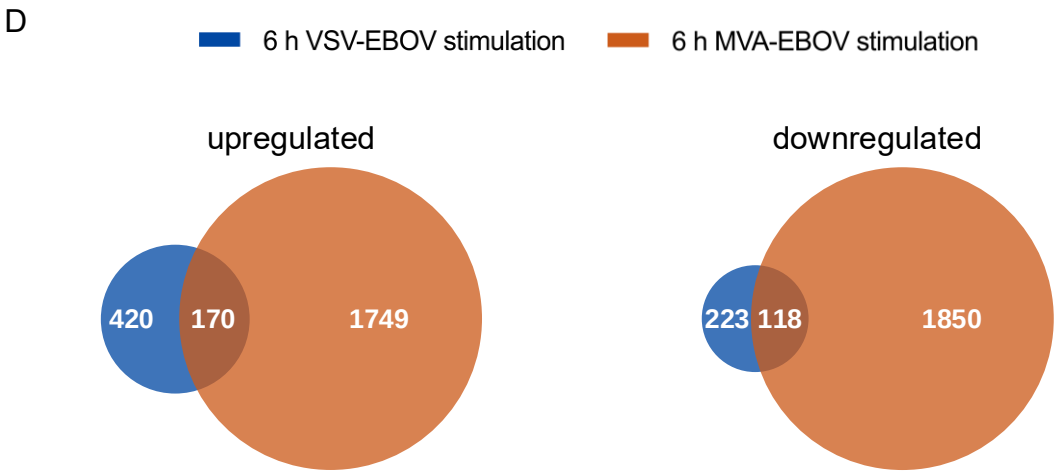


Figure 26: **Number of DEG upon VSV-EBOV or MVA-EBOV stimulation.** Total RNA of 6 h *in vitro* stimulated (MOI 1) as well as 0 h and 6 h unstimulated samples (N=8 section 2.2, table 5-6) was analyzed via RNA-Seq (section 3.10). Genes which exhibited a log2 fold change ≤ -1.5 or ≥ 1.5 and an FDR < 0.01 compared to unstimulated 0 h controls were counted as DEG. A) While the number of DEG upon VSV-EBOV *in vitro* stimulation are depicted in blue, all DEG after MVA-EBOV stimulation are shown in orange. Grey bars indicate the specific unstimulated counterparts. B, C) Number of up- and downregulated genes which are differently expressed in stimulated, unstimulated or in both fractions, are depicted in Venn diagrams. Besides stimulated samples (VSV-EBOV: blue; MVA-EBOV: orange) also unstimulated samples (grey) are shown. D) Venn diagram of MVA-EBOV and VSV-EBOV 6 h post-stimulation represents genes, which are differently expressed in VSV-EBOV−stimulated (blue), MVA-EBOV−stimulated (orange) or in both. Venn diagram designed with BioVenn a web-based application [227].

To investigate the impact of both stimulations on the expression profile of hPBMCs a PCA was performed. Both stimulations exhibited differences between stimulated and unstimulated samples (figure 27–28). While VSV-EBOV *in vitro* stimulations showed no distinct cluster for stimulation conditions, MVA-EBOV exhibited three separated clusters. Nevertheless, stimulated and unstimulated samples from different donors clustered together post VSV-EBOV stimulation indicating that VSV-EBOV also induced transcriptomic changes over time.

After an MVA-EBOV stimulation a high variance in PC1 was observed indicating a bigger difference in the expression profile of stimulated (6 h) compared to unstimulated (0 h or 6 h) samples. Thereby, an MVA-EBOV stimulation revealed a variance of 52 % between stimulated and both unstimulated samples (figure 28).

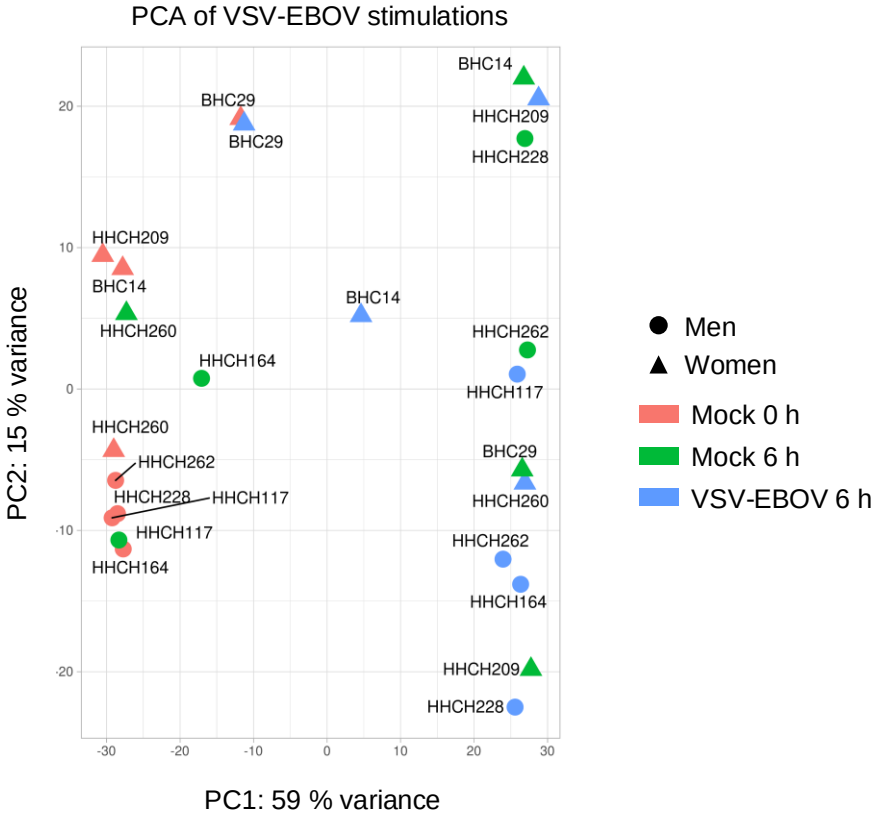


Figure 27: **PCA of stimulated hPBMCs using VSV-EBOV.** Total RNA of 6 h *in vitro* stimulated (MOI 1) as well as 0 h and 6 h unstimulated samples (N=8 section 2.2, table 5) was analyzed via RNA-Seq (section 3.10). Here, the first two principal components of analyzed genes are shown. 0 h unstimulated (red), 6 h unstimulated (green), and 6 h stimulated (blue) hPBMCs are depicted.

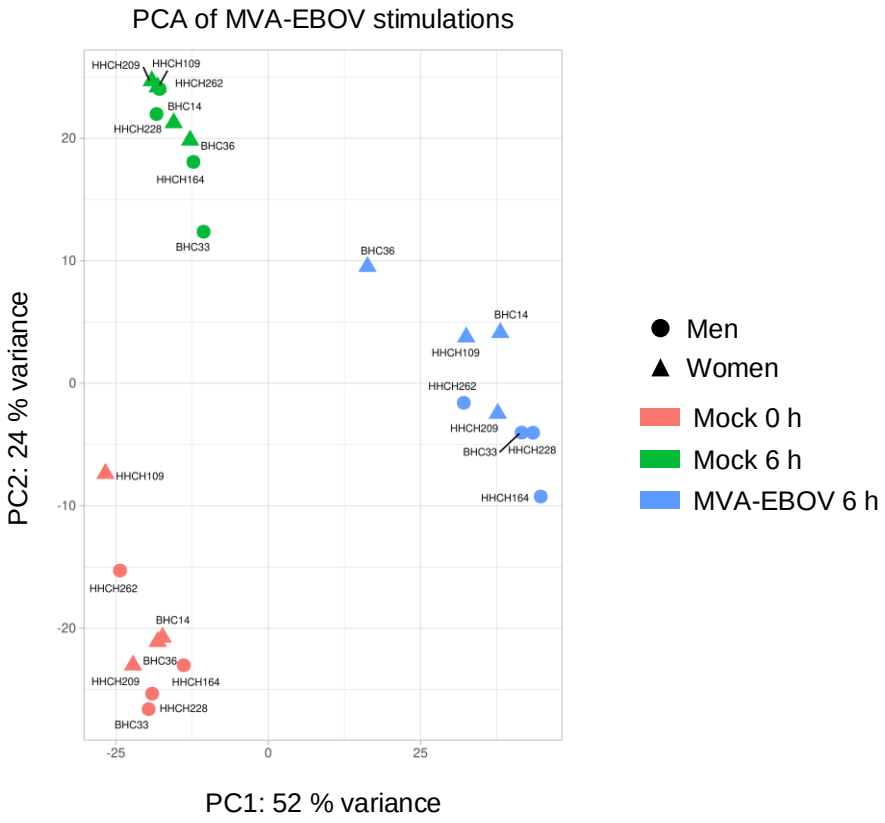


Figure 28: **PCA of stimulated hPBMCs using MVA-EBOV.** Total RNA of 6 h *in vitro* stimulated (MOI 1) as well as 0 h and 6 h unstimulated samples (N=8 section 2.2, table 6) was analyzed via RNA-Seq (section 3.10). Here, the first two principal components of analyzed genes are shown. 0 h unstimulated (red), 6 h unstimulated (green), and 6 h stimulated (blue) hPBMCs are depicted.

Whole gene expression profiles upon stimulation using VSV-EBOV or MVA-EBOV depicted in hierarchical clustering heat maps were distinct between stimulations of both viral vector vaccines (cf. section 6.4.2, S.16–17). Furthermore, 6 h VSV-EBOV− or MVA-EBOV−stimulated and unstimulated samples showed different transcriptomic signatures (cf. section 6.4.2, S.16−17). To elucidate the functionality of all these DEG, pathway analysis including ORA and generally applicable gene-set enrichment (GAGE) were performed. An ORA of all DEG revealed the pathway chemokine receptors bind chemokines among the top 5 most regulated pathways upon 6 h VSV-EBOV stimulation compared to 0 h unstimulated controls (figure 29). In contrast, DEG induced by MVA-EBOV belonged to pathways including interferon signaling, cytokine signaling, and immunoregulatory interactions between lymphoid and non-lymphoid cells. Although unstimulated counterparts of VSV-EBOV and MVA-EBOV stimulations also exhibited several DEG (cf. figure 26) after 6 h, no specific

antiviral or pro-inflammatory pathway was detected in unstimulated 6 h samples of both stimulations (cf. section 6.4.3, S.18).

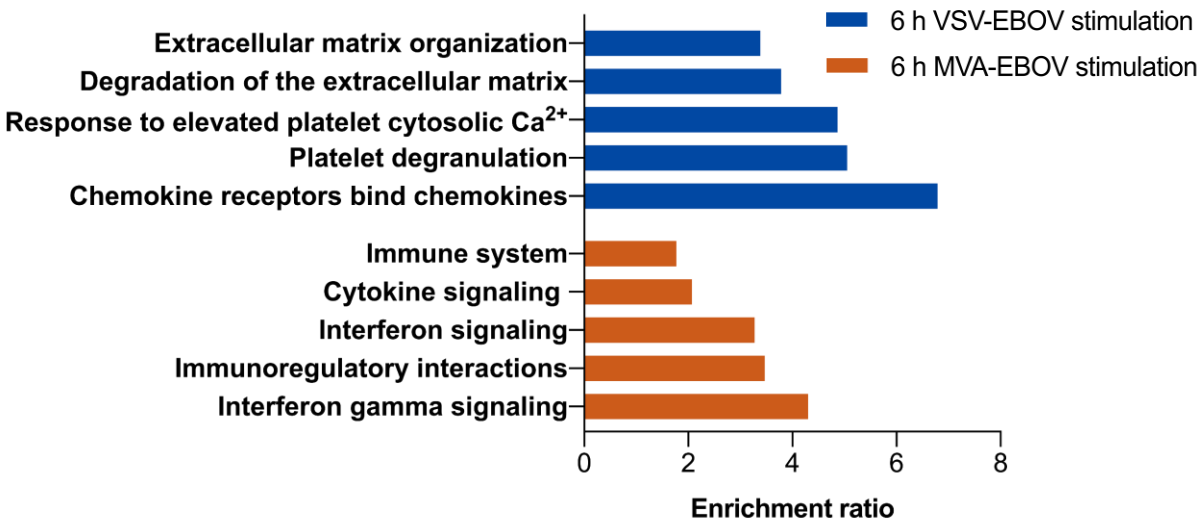


Figure 29: **ORA of DEG after stimulations using VSV-EBOV or MVA-EBOV.** Total RNA of 6 h *in vitro* stimulated (MOI 1) and 0 h unstimulated samples (N=8, section 2.2, table 5-6) was analyzed via RNA-Seq (section 3.10). Genes, which exhibited a log2 fold change ≤ -1.5 or ≥ 1.5 and an FDR < 0.01 compared to unstimulated 0 h controls, were counted as DEG. Enrichment ratios were calculated with the web tool: webgestalt.org [228–231] using only the top 5 of pathways with an FDR ≤ 0.05. VSV-EBOV (blue) and MVA-EBOV (orange) 6 h *in vitro* stimulations are depicted.

Moreover, a GAGE based on the Kyoto encyclopedia of genes and genomes (KEGG) revealed different induced pathways in VSV-EBOV and MVA-EBOV−stimulated hPBMCs. Compared to unstimulated 0 h controls, VSV-EBOV−stimulated samples had mainly upregulated cytokine-cytokine receptor interactions and chemokine signaling pathways (cf. section 6.4.4, S.19). However, no significant gene ontology (GO) terms could be detected for VSV-EBOV−stimulated samples. A GAGE based on KEGG revealed for MVA-EBOV−stimulated samples primarily upregulated pathways for NOD-like receptor signaling and Influenza A response (cf. section 6.4.4, S.20). Additionally, significantly GO terms for upregulated genes including defense response to virus (GO:0051607) and response to virus (GO:0009615) were detected in MVA-EBOV−stimulated samples. In addition to ORA, neither a GAGE based on KEGG nor GO terms indicated significant regulated pathways in unstimulated 6 h samples compared to unstimulated 0 h controls.

All genes of VSV-EBOV and MVA-EBOV−stimulated as well as unstimulated 6 h counterparts were normalized to unstimulated 0 h and depicted in volcano plots indicating their log2 fold changes and corresponding FDR (figure 30–31, cf. section 6.4.5, S.21–22). In addition to the number of DEG (cf. figure 26), an MVA-EBOV stimulation revealed more genes with a higher log2 fold change and FDR compared to stimulations with VSV-EBOV (figure 30–31). Therefore, both viral vector vaccines generated transcriptomic changes, whereas MVA-EBOV had a higher impact on the expression than VSV-EBOV.

The finding that the activation marker CD40, CD83, CD86 were differently expressed on immune cells upon *in vitro* stimulation (cf. section 4.1.2) was encouraged by RNA-Seq. While VSV-EBOV showed tendencies for an altered expression of these activation markers on monocyte and DC subsets compared to unstimulated counterparts, an MVA-EBOV stimulation revealed significant reductions especially for CD86. For CD40 and CD83 no differential expression was detected via RNA-Seq post VSV-EBOV or MVA-EBOV stimulation. However, VSV-EBOV led to a slightly upregulation of *CD86* with a log2 fold change of 1.3, whereas an MVA-EBOV stimulation resulted in a reduction with a log2 fold change of -2.0. The upregulation of *CD80*, a closely related factor of CD86, upon VSV-EBOV stimulation strengthen the hypothesis that VSV-EBOV led to an upregulation of CD86.

In addition to the transcriptomic signature deciphered by the nanoString® technology (cf. section 4.2.1), *CLEC5A* was among the most induced genes upon 6 h VSV-EBOV stimulation with a log2 fold change of 2.7 (figure 30). Also, *IP-10*, *IL-1α*, *GBP1*, *MCP-1*, and *IDO1* showed in RNA-Seq analysis an elevated expression with a log2 fold change of 1.3, 1.8, 1.7, 1.6, and 1.7, respectively, emphasizing an anti-viral response upon VSV-EBOV stimulation. MVA-EBOV stimulations also led to an elevated expression of *IP-10*, *IL-1α*, *GBP1*, *MCP-1*, and *IDO1*, where corresponding log2 fold changes were 4.9, 2.7, 3.8, 2.1, and 3.2, respectively (figure 31). In contrast to VSV-EBOV, *CLEC5A* was not differently expressed after an MVA-EBOV stimulation. One of the most induced expressions by MVA-EBOV was *IFNβ1* with a log2 fold change of 8.3. Moreover, other IFNs like *IFNα1* and *IFNγ* showed enhanced log2 fold changes of 2.2 and 2.6, respectively. In contrast, none of these three IFNs were differently expressed after a VSV-EBOV stimulation. These findings indicate further differences in induced immune responses to both viral vector vaccines and are consistent with findings that both viral vector vaccines exhibited different anti-viral immune signatures.

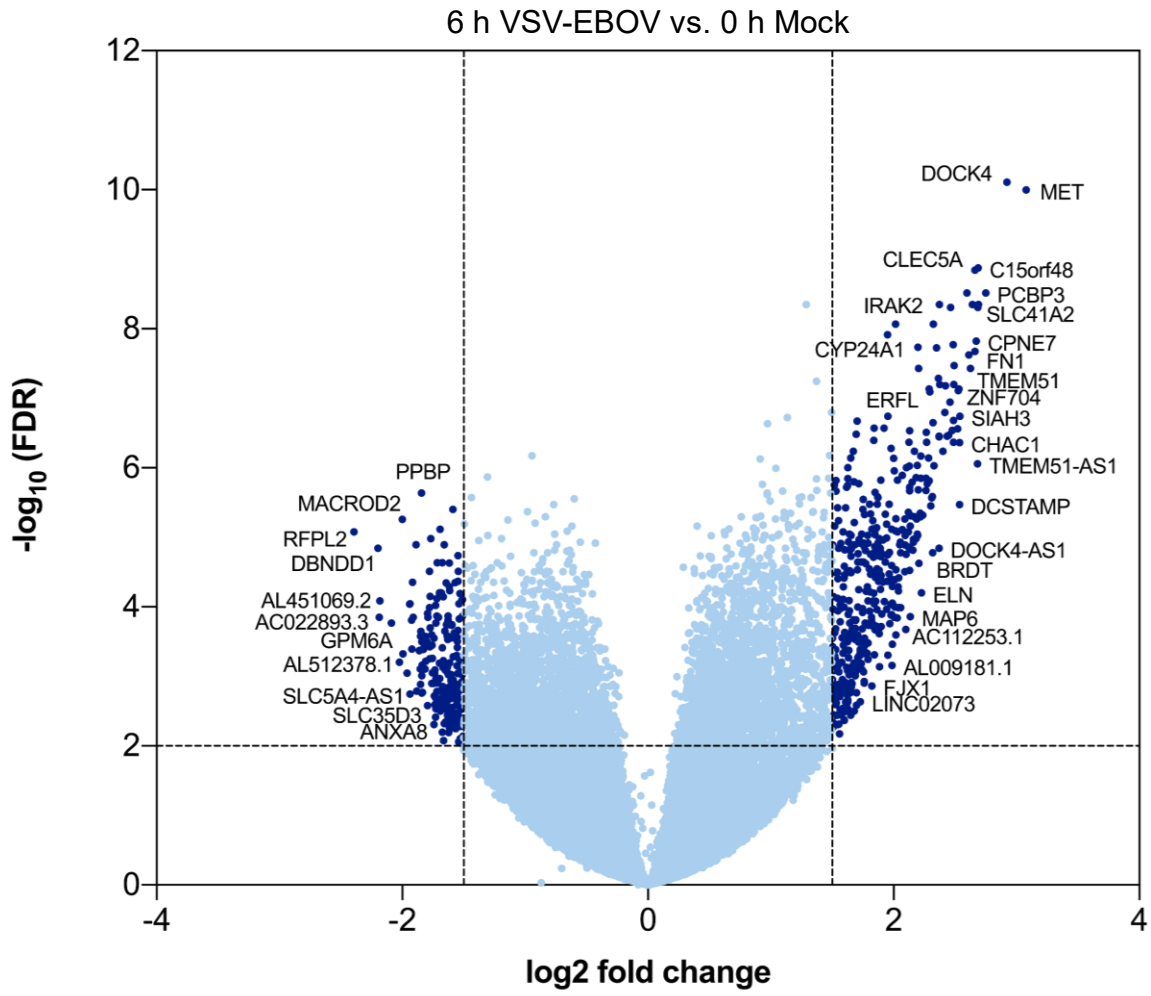


Figure 30: **Volcano plot of stimulated hPBMCs using VSV-EBOV.** Total RNA of 6 h *in vitro* stimulated (MOI 1) and 0 h unstimulated samples (N=8, section 2.2, table 5) was analyzed via RNA-Seq (section 3.10). Genes, which exhibited a log2 fold change ≤ -1.5 or ≥ 1.5 and an FDR < 0.01 compared to unstimulated 0 h controls, were counted as DEG. All detected genes upon VSV-EBOV stimulation are shown. Each dot indicates a different gene and darker color represents DEG and lighter color not DEG separated by dotted lines.

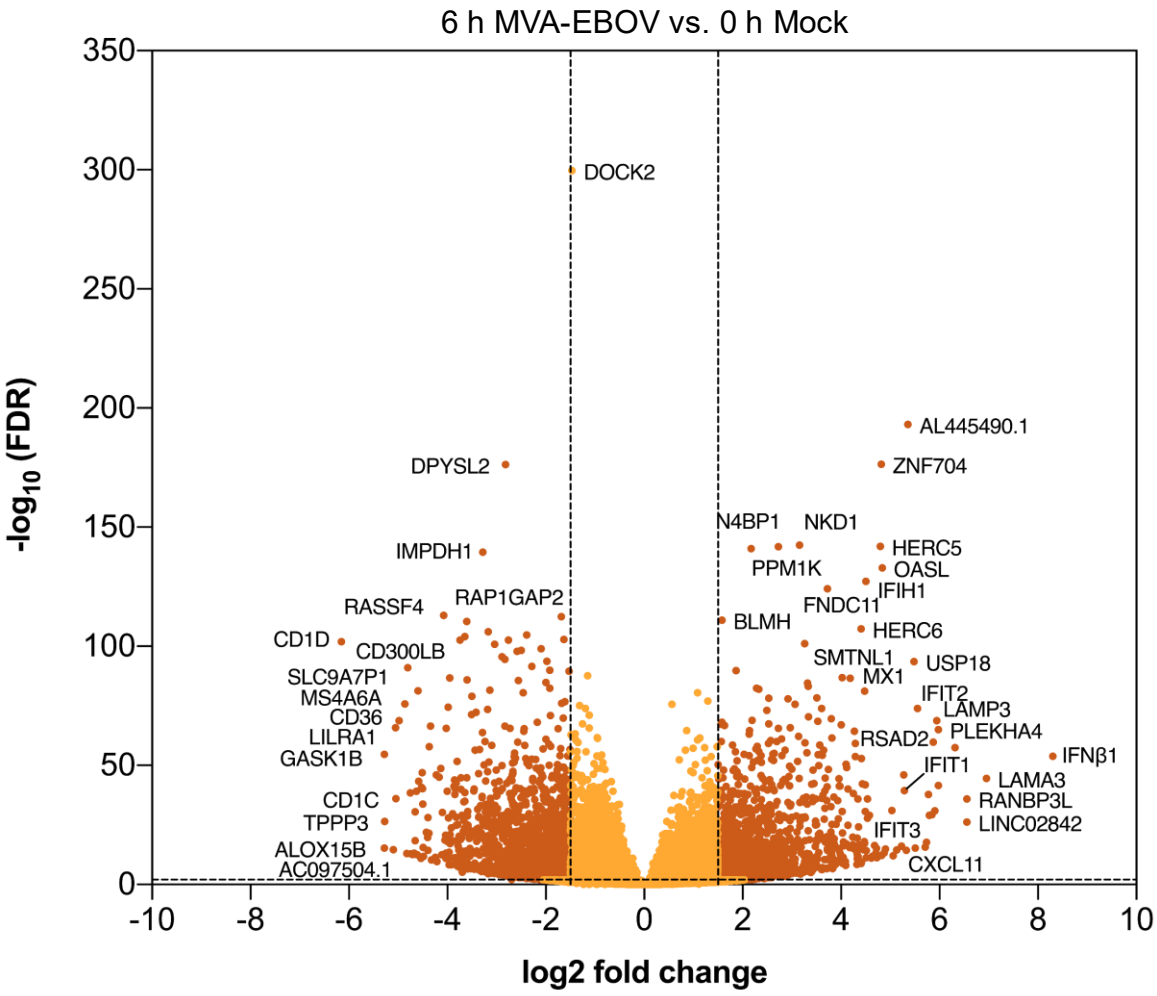


Figure 31: **Volcano plot of stimulated hPBMCs using MVA-EBOV.** Total RNA of 6 h *in vitro* stimulated (MOI 1) and 0 h unstimulated samples (N=8, section 2.2, table 6) was analyzed via RNA-Seq (section 3.10). Genes, which exhibited a log2 fold change ≤ -1.5 or ≥ 1.5 and an FDR < 0.01 compared to unstimulated 0 h controls, were counted as DEG. All detected genes upon MVA-EBOV stimulation are shown. Each dot indicates a different gene and darker color represents DEG and lighter color not DEG separated by dotted lines.

Furthermore, a hierarchical clustering heat map of IFN signaling was generated due to its important role in viral infections and vaccination, a strong enrichment in ORA as well as high induction for single genes in stimulated samples. This analysis was based on the reactome database where the gene set IFN signaling included 228 genes in total. Out of these 228 genes, 5 were differently expressed in stimulated and/or unstimulated samples of VSV-EBOV (figure 32). Here, hPBMCs derived from two different blood donors showed a higher induction in unstimulated samples compared to VSV-EBOV–stimulated once indicating that VSV-EBOV induced not in all hPBMCs the same induction. In contrast, an MVA-EBOV stimulation

revealed 73 DEG in stimulated and/or unstimulated samples (figure 33). While 53 genes showed an elevated expression in MVA-EBOV–stimulated samples, 19 genes had a decreased expression compared to 0 h unstimulated controls. Only few genes in the lower third of the heat map exhibited a slightly higher expression in unstimulated 6 h compared to stimulated samples. This emphasizes the differences in the induced transcriptomic changes of VSV-EBOV and MVA-EBOV–stimulated samples. Moreover, most unstimulated samples revealed no stimulus-specific transcriptomic changes especially in MVA-EBOV–stimulated samples.

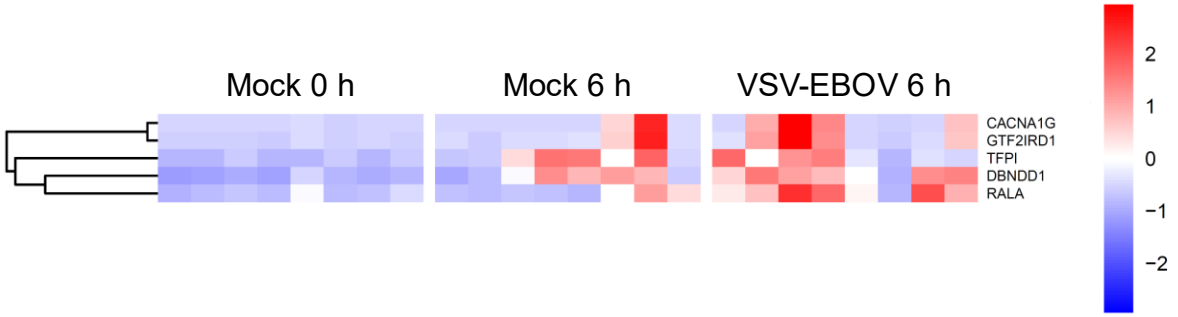


Figure 32: **Hierarchical clustering heat map of VSV-EBOV stimulations.** Total RNA of 6 h VSV-EBOV *in vitro* stimulated (MOI 1) and unstimulated samples (N=8, section 2.2, table 5) was analyzed via RNA-Seq (section 3.10). Genes which exhibited a log2 fold change ≤ -1.5 or ≥ 1.5 and an FDR < 0.01 were counted as DEG. Selected genes belong to IFN signaling based on the reactome database, where the gene set IFN signaling included 228 genes in total (only DEG are shown). Besides unstimulated 0 h and 6 h controls, also 6 h stimulated samples are depicted. Each condition is separated in further columns indicating different blood donors.

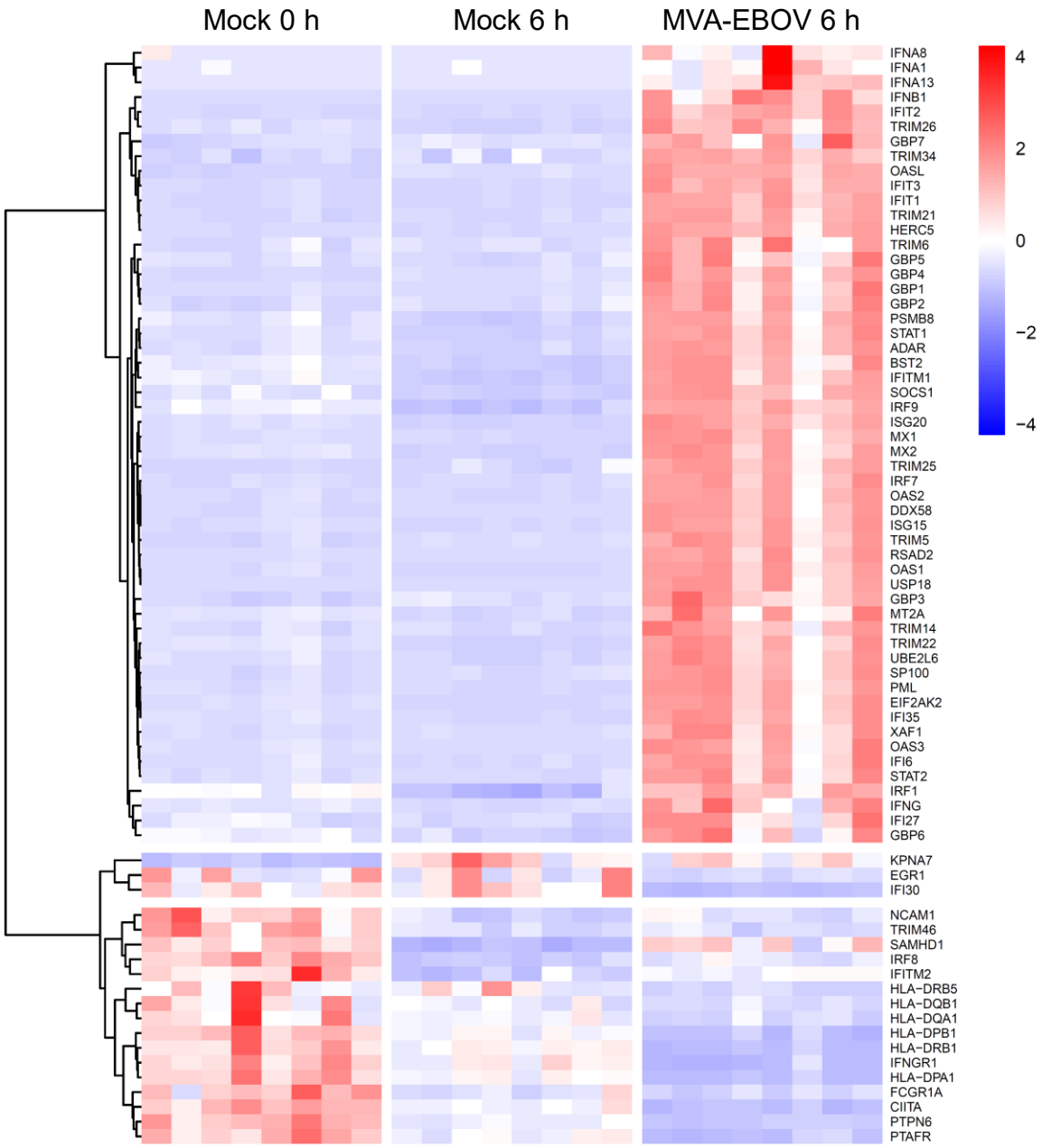


Figure 33: **Hierarchical clustering heat map of MVA-EBOV stimulations.** Total RNA of 6 h MVA-EBOV *in vitro* stimulated (MOI 1) and unstimulated samples (N=8, section 2.2, table 6) was analyzed via RNA-Seq (section 3.10). Genes which exhibited a log2 fold change ≤ -1.5 or ≥ 1.5 and an FDR < 0.01 were counted as DEG. Selected genes belong to IFN signaling based on the reactome database, where the gene set IFN signaling included 228 genes in total (only DEG are shown). Besides unstimulated 0 h and 6 h controls, also 6 h stimulated samples are depicted. Each condition is separated in further columns indicating different blood donors.

## 4.3 Sex differences upon *in vitro* stimulation

Over the course of a lifetime immune responses to viral infections as well as vaccination differs between men and women. In general, women develop a greater immune response after vaccination than men [147,148]. They benefit from a higher magnitude of humoral and cellular immune responses but have to suffer from more adverse reactions compared to men. To decipher sex-specific differences in the immune response to VSV-EBOV or MVA-EBOV *in vitro* stimulations, all data of section 4.1 and 4.2 were stratified by sex.

### 4.3.1 Immune signature of men and women upon stimulation

**Immune status**

First, technical issues which can influence the immune response post-stimulation were investigated. The amount of stimulation reagent is relevant to ensure the same stimulation condition. Here, no differences in the copy number of VSV-specific NP or MVA-specific UDG were determined via qPCR in stimulated hPBMCs derived from men and women (data not shown). Moreover, no correlation between the copy number of virus-specific genes and the cytokine secretion measured by LEGENDplex™ (cf. section 4.1.1) was detected. To this end, potential sex differences in the immune response are suggested to be not related to technical issues of the *in vitro* stimulation assay.

Furthermore, the pre-stimulation statuses of innate immune cells in hPBMCs derived from men and women were investigated. Accordingly, the frequency of monocytes including classical, intermediate, and non-classical monocytes as well as DCs including $CD1c^+CD11c^+$, $CD16^+$, $CD141^+$ DCs, and pDCs were analyzed prior *in vitro* stimulation (0 h) (figure 34–35). Although minor differences between both sexes were detected in the composition of these immune cell subsets used for VSV-EBOV (figure 34) and MVA-EBOV (figure 35) stimulations, these differences were not statistically significant. This suggests that potential sex-based differences are not related to different immune statuses of men and women.

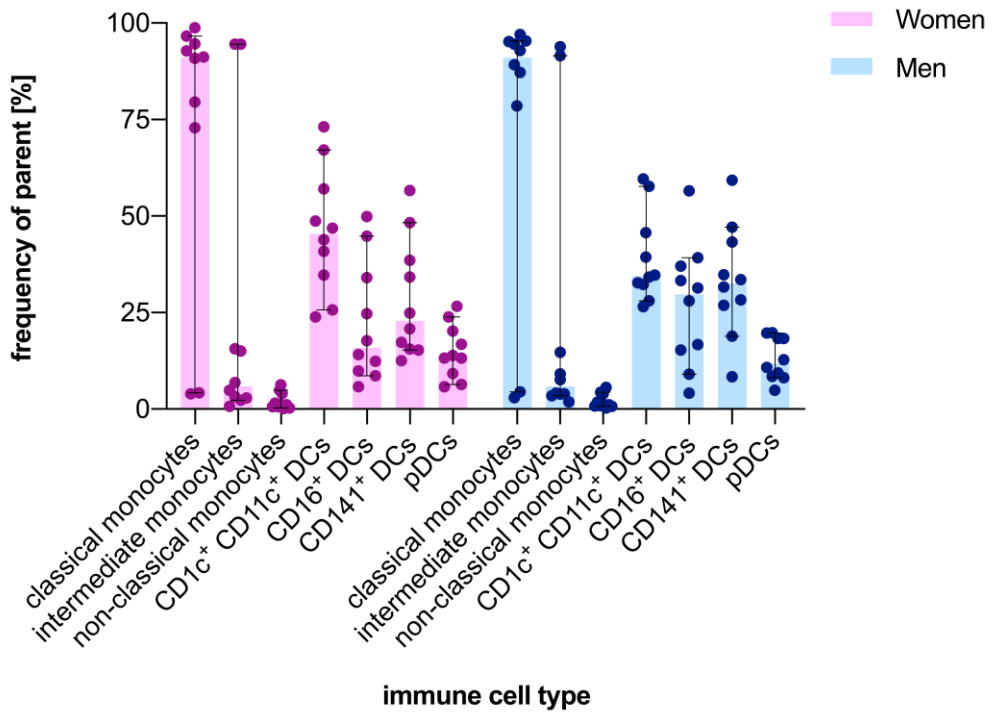


Figure 34: **Frequency of innate immune cells in samples used for VSV-EBOV stimulation.** The amount of different innate immune cell subsets measured via flow cytometry and corresponding cell staining (section 3.12, antibodies table 14) was stratified by sex. Frequencies of unstimulated 0 h samples are shown. Here, a purple color indicates samples derived from women (N=10) and blue from men (N=10). Each dot represents a different blood donor (N=20; section 2.2, table 3). All analyzed immune cell types are depicted on the x-axis. Specific gating strategies for each subset are shown in figure 12 (section 4.1.2). The maximum of each bar represents the median including error bars indicating the 95 % CI. No statistically significant differences in the frequency of innate immune cells were detected using the t-test based unpaired, nonparametric Mann-Whitney test. The p-values are indicated as follows: $p \leq 0.05$ *; $p \leq 0.01$ **; $p \leq 0.001$ ***; $p \leq 0.0001$ ****.

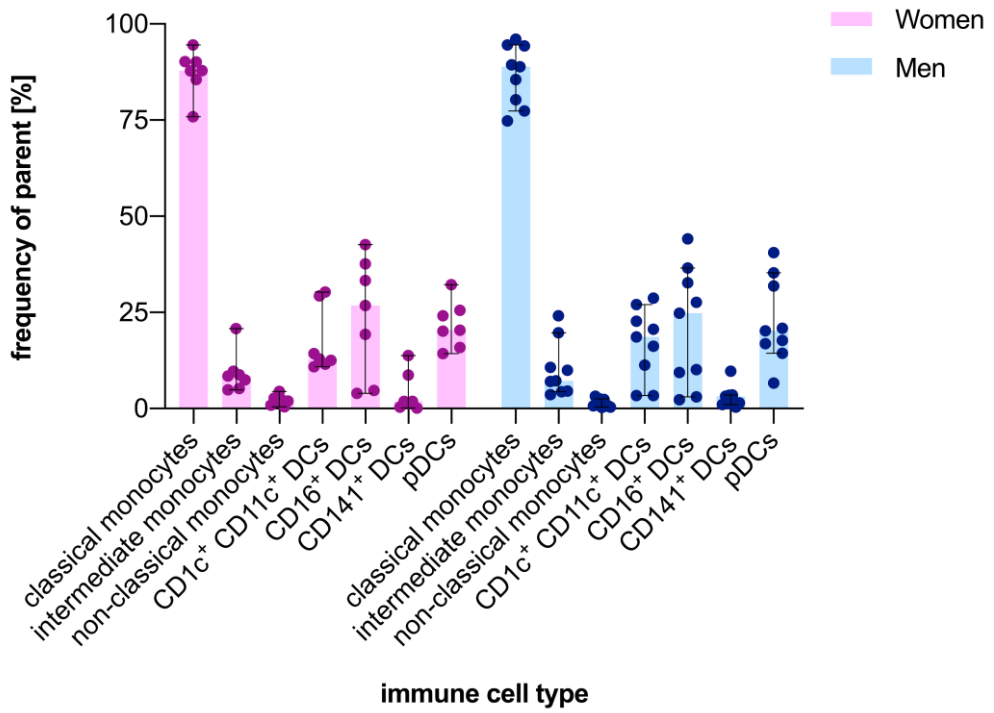


Figure 35: **Frequency of innate immune cells in samples used for MVA-EBOV stimulation.** The amount of different innate immune cell subsets measured via flow cytometry and corresponding cell staining (section 3.12, antibodies table 14) was stratified by sex. Frequencies of unstimulated 0 h samples are shown. Here, a purple color indicates samples derived from women (N=7) and blue from men (N=9). Each dot represents a different blood donor (N=16; section 2.2, table 4). All analyzed immune cell types are depicted on the x-axis. Specific gating strategies for each subset are shown in figure 12 (section 4.1.2). The maximum of each bar represents the median including error bars indicating the 95 % CI. No statistically significant differences in the frequency of innate immune cells were detected using the t-test based unpaired, nonparametric Mann-Whitney test. The p-values are indicated as follows: $p \leq 0.05$ *; $p \leq 0.01$ **; $p \leq 0.001$ ***; $p \leq 0.0001$ ****.

### Cytokine profiles

Since cytokine profiles can differ between men and women upon stimulation, resulting in altered immune responses, the cytokine secretion measured via a customized LEGENDplex™ (section 3.12.1) was stratified by sex. Overall, the cytokine induction upon *in vitro* stimulation using VSV-EBOV peaked at 12 h or 24 h post-stimulation (cf. section 4.1.1 figure 9). For the analytes IL-1β, IL-2, IL-4, IL-6, IL-10, IL-12, CXCL9, MCP-1, IFNα, IFNγ, and TNFα no statistically significant sex-based difference in the secretion was detected (data not shown). When normalized to specific unstimulated counterparts, IL-8 and IP-10 exhibited tendencies for different secretions in men and women. In this case, women showed an increased secretion for IL-8 and men exhibited a higher secretion of IP-10 (figure 36). Despite these differences

on the protein level not being statistically significant, transcriptomic changes including *IP-10* revealed more insight into sex-based differences (section 4.3.2).

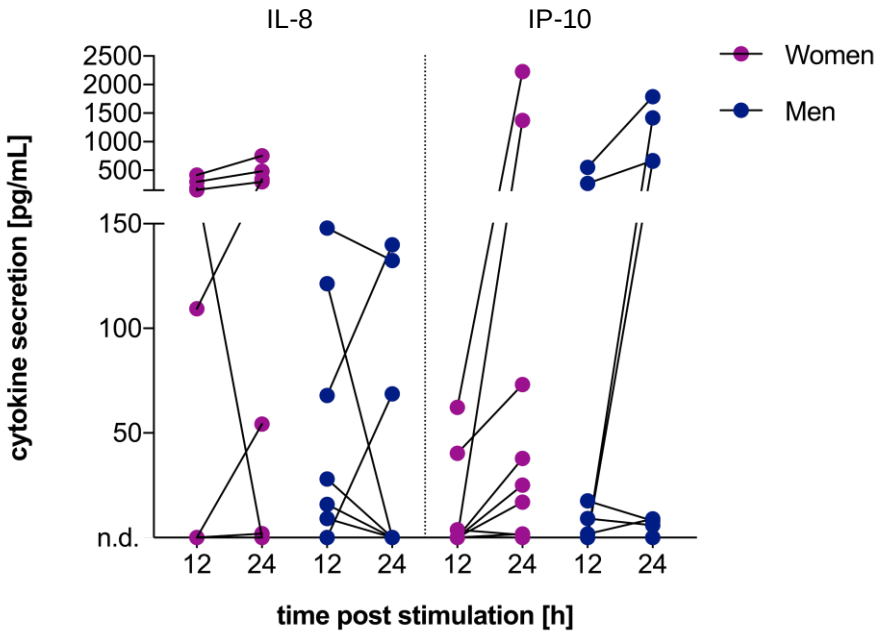


Figure 36: **Secretion of IL-8 and IP-10 upon VSV-EBOV stimulations stratified by sex.** Freshly isolated hPBMCs were *in vitro* stimulated with a MOI of 1 using VSV-EBOV. The cytokine secretion of IL-8 and IP-10 was analyzed via a customized LEGENDplex™ by BioLegend (section 3.12.1). The graph represents the cytokine secretion [pg/ml] of $2 \cdot 10^6$ hPBMCs over time in 12 h and 24 h stimulated samples, which were normalized to their specific unstimulated samples. Each dot indicates a different donor (N=20, section 2.2, table 3). While the secretion of IL-8 (left side) and IP-10 (right side) by hPBMCs derived from women are depicted in purple (N=10), samples derived from men are shown in blue (N=10).

**Immune cell activation**

Although significant or at least strong tendencies for sex-based differences in the expression of CD40, CD83 or CD86 on monocyte and DC subsets were detected, these differences were not reliable due to the lack of significant differences between stimulated and unstimulated counterparts (data not shown). Therefore, MVA-EBOV and VSV-EBOV may induce a similar activation of monocytes and DCs derived from men and women. Whether this will also lead to similar overall immune signatures of innate immune cells needs to be determined.

### 4.3.2 Changes in the transcriptomic profile differ between men and women

**Using the nanoString® technology**

First insight into sex-based differences upon *in vitro* stimulation measured via cytokine secretion assays (cf. section 4.3.1) was extended by transcriptomic changes. Here, the nanoString® technology revealed different signatures 6 h post VSV-EBOV stimulation. Genes which exhibited a log2 fold change of ≤-1 or ≥1 and p-value < 0.001 were counted as DEG. Both sexes showed comparable numbers of DEG 1 h post-stimulation (figure 37A). After 6 h of stimulation 142 DEG including 40 up- and 102 downregulated genes were detected in samples derived from women, whereas in samples derived from men 86 DEG including 31 up and 55 downregulated genes were identified. Hence, women exhibited 46 % more differently downregulated genes than men. Out of all DEG women and men shared 77 genes upon 6 h of stimulation indicating that nearly the half of all DEG in women were also differently expressed in men (figure 37B).

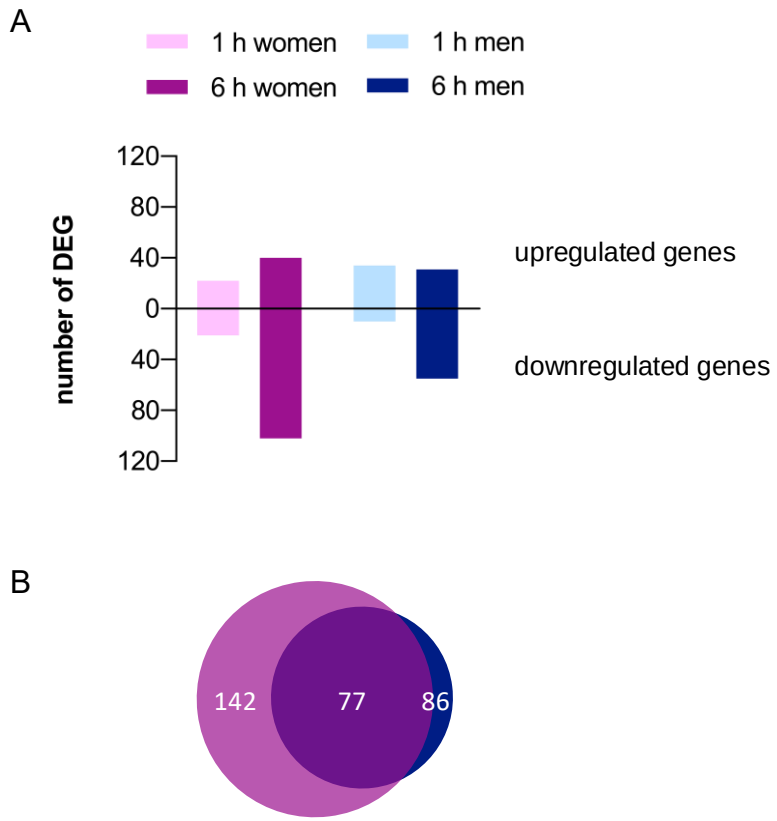


Figure legend depicted on page 93.

Figure 37: **Number of DEG stratified by sex after VSV-EBOV stimulation.** Total RNA was isolated 0 h, 1 h, and 6 h after VSV-EBOV *in vitro* stimulations (MOI 1) of hPBMCs and analyzed using a microarray by nanoString® (section 3.9, N=8 sex ratio 50:50, section 2.2, table 5). Genes, which exhibited a log2 fold change ≤ -1 or ≥ 1 and a p-value < 0.001 compared to unstimulated samples 0 h, were counted as DEG. DEG of women are depicted in purple and those of men are depicted in blue. Lighter color indicates 1 h post-stimulation, whereas darker color represents 6 h upon stimulation. A) Number of DEG post 1 h and 6 h stratified by sex are shown. B) DEG of women, men or both are depicted post 6 h stimulations. Venn diagram designed with BioVenn a web-based application [227].

Although different numbers of DEG were detected indicating different immune responses, DEG in men and women belonged to similar pathways (figure 38). An ORA of the top 3 most induced pathways revealed mainly an induction of cytokine signaling in immune system and immune system. Nevertheless, women showed a higher enrichment ratio for these pathways as well as an induction of DEG for innate immune system, whereas men exhibited an induction for signaling by interleukins.

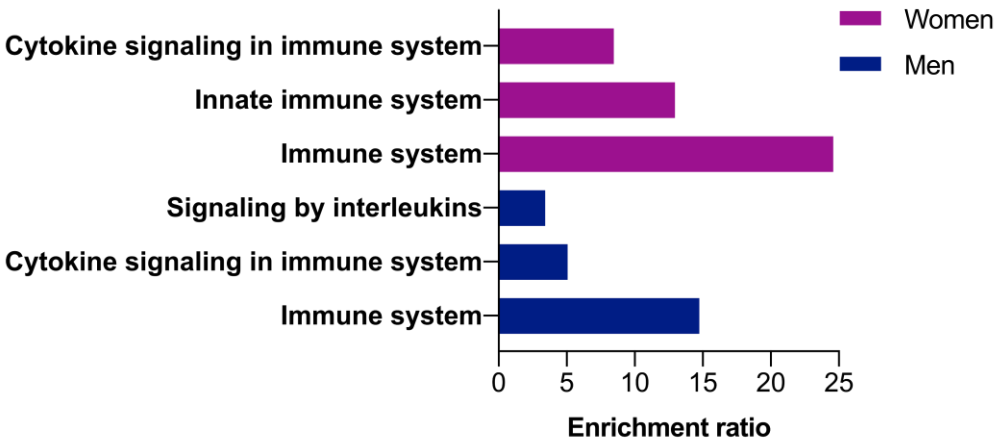


Figure 38: **ORA of DEG after stimulation stratified by sex.** Total RNA of 6 h VSV-EBOV *in vitro* stimulated (MOI 1) and 0 h unstimulated hPBMCs (N=8 sex ratio 50:50, section 2.2, table 5) was analyzed via a human immunology panel microarray by nanoString® (section 3.9). Genes, which exhibited a log2 fold change ≤ -1 or ≥ 1 and a p-value < 0.001 compared to unstimulated samples 0 h, were counted as DEG. Enrichment ratios of DEG were calculated with the web tool: webgestalt.org [228–231] using only the top 3 of pathways with an FDR ≤ 0.05. Pathways elevated in women (purple) and in men (blue) 6 h post-stimulation are shown.

Moreover, women revealed a higher dynamic of selected pre-defined gene sets including response to virus, response to external stimulus, and response to stress (figure 39). The global significance score, which summarizes differential expression in each gene set with respect to

up and down regulation, showed a high induction of the gene sets response to virus and response to stress for women 6 h post VSV-EBOV stimulation. In contrast, these gene sets were slightly decreased in men or on a similar level over time. In addition to differences in the number of DEG, this may be another hint for sex-based differences in transcriptomic changes post-stimulation using VSV-EBOV.

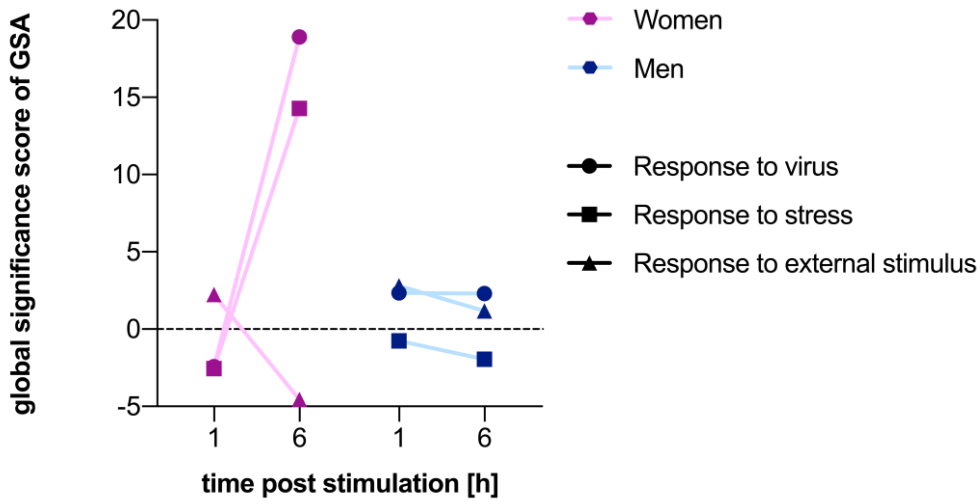


Figure 39: **Direct global significance scores of selected gene sets stratified by sex.** Total RNA of 6 h VSV-EBOV *in vitro* stimulated (MOI 1) and 0 h unstimulated hPBMCs (N=8 sex ratio 50:50, section 2.2, table 5) was analyzed via a human immunology panel microarray by nanoString® (section 3.9). The analysis was done with the nSolver™ Software v4, the nCounter® advanced analysis software v2.0.115 with R3.3.2 and Xquartz. Direct global significance scores, which summarize differential expression in each gene set, for 3 different "response to" gene sets are depicted. The algorithm to calculate the global significance score is described by nanoString® as follows: *"The directed global significance score is calculated as the square root of the mean signed squared t-statistic for the genes in a gene set, with t-statistics coming from the linear regression underlying our differential expression analysis"* (described in the nCounter® advanced analysis software v2.0.115 part of the nSolver™ Software v4). While purple symbols represent samples derived from women, blue symbols indicate samples derived from men. Dots: *response to virus*; Triangle: *response to external stimulus*; Square: *response to stress.*

Additionally, analyses of samples derived from one sex revealed differences in the expression of previously described genes. Women had a log2 fold change of 4.2 for *IP-10* post-stimulation, whereas men exhibited an elevated log2 fold change of 7.1. Also, *MCP-1* and *IDO1* were increased in men with a log2 fold change of 5.4 and 2.2 compared to women with 1.8 and 0.4, respectively. However, the previously described induction of anti-viral genes including *CLECA*, *GBP1*, and *IL-1α* was comparable in men and women [5.2 vs. 5.7, 2.8 vs. 1.5, 5.3 vs. 4.6]. *IP-10*, *MCP-1*, and *IDO1* showed no significant sex-based differences in whole

analyses comparing samples derived from men and women directly. However, this could be a hint for sex-based differences in the expression of vital genes for induced transcriptomic changes by viral vector vaccines. Due to the sample size a validation with more blood donors should be performed to strengthen these findings for sex-based differences.

**Using RNA-Seq**

Also, RNA-Seq data were satisfied by sex resulting in first insight into sex-specific differences upon stimulation with VSV-EBOV or MVA-EBOV. Although differences in the whole gene expression profile were induced due to different conditions rather than sex (cf. section 4.2.2, figure 27–28), variations in the expression of single genes were detected (figure 40). According to the PCA of VSV-EBOV–stimulated samples (cf. section 4.2.2, figure 27), no significant changes in DEG were detected between men and women. In contrast, MVA-EBOV *in vitro* stimulations induced slightly different signatures of DEG in both sexes (figure 40). While hPBMCs derived from men led to 6 DEG (figure 40; upper third), women exhibited 11 DEG (figure 40; lower third). However, most genes which were differently expressed in men and women were also elevated in unstimulated 6 h samples to a lower extent. This emphasizes that an MVA-EBOV stimulation increase the expression of these genes but only to a low magnitude. To this end, both sexes revealed comparable transcriptomic changes.

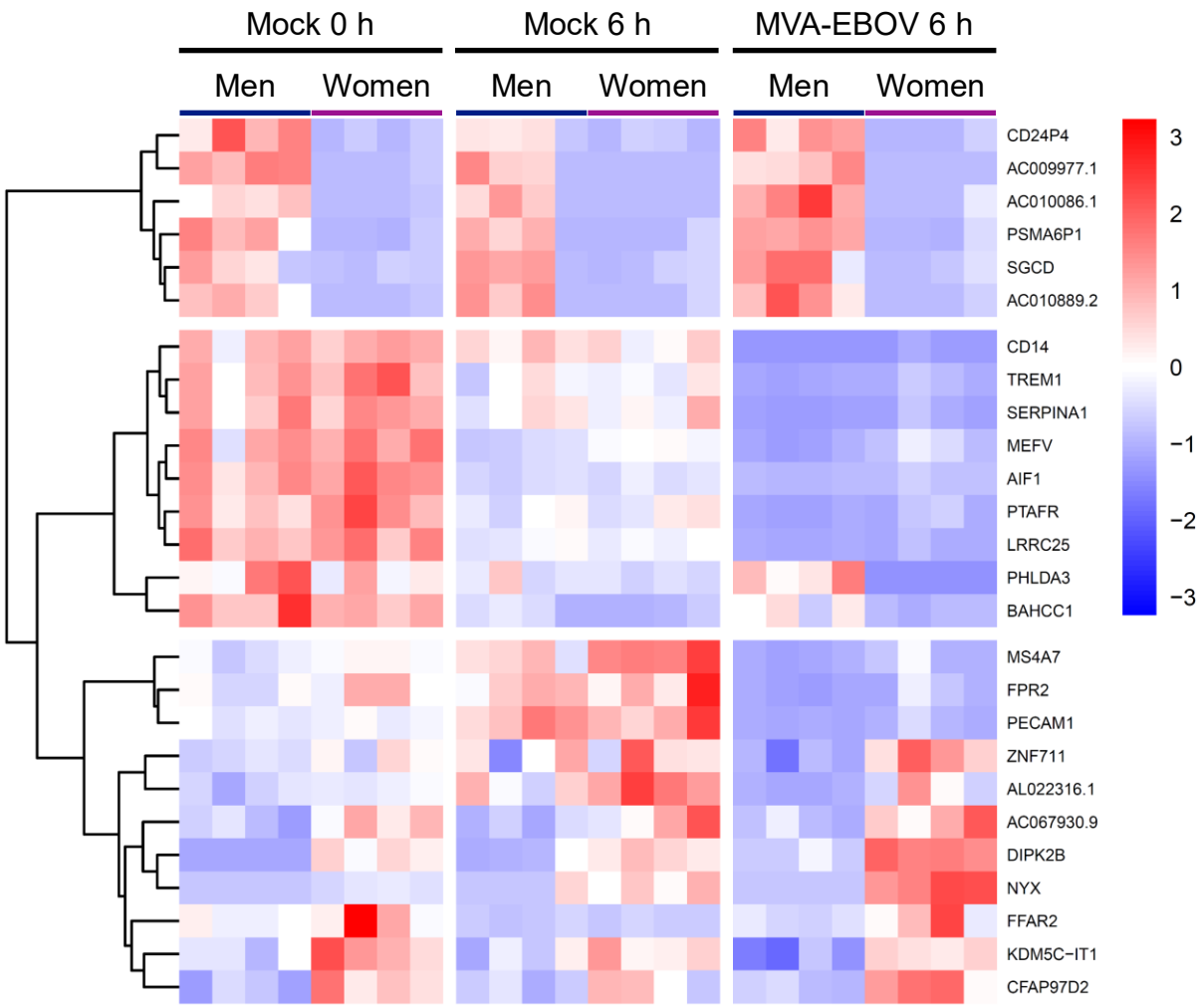


Figure 40: **Sex differences in transcriptomic changes after MVA-EBOV stimulation.** Total RNA of 6 h MVA-EBOV *in vitro* stimulated (MOI 1) and unstimulated samples (N=8, section 2.2, table 6) was analyzed via RNA-Seq (section 3.10). Genes which exhibited a log2 fold change ≤ -1.0 or ≥ 1.0 and an FDR < 0.1 were counted as DEG. Besides unstimulated 0 h and 6 h controls, also 6 h stimulated samples are depicted. Each condition is separated in samples derived from men (blue) and women (purple) where single columns indicating different blood donors.

# 5. Discussion

The Ebola virus disease (EVD) is a life-threatening illness in humans that can result in a severe diseases progression with 50−90 % deaths in diagnosed cases. EVD, one of the most severe viral hemorrhagic fever, is caused by the Filovirus Ebola virus (EBOV). This virus caused several outbreaks in the past, leading to many deaths due to the lack of efficient medical countermeasures. The most affected areas are countries in West and Middle Africa where the two biggest outbreaks occurred in Guinea, Liberia, and Sierra Leone from 2013−2016 and in the Democratic Republic of the Congo (DRC) from 2018−2020. A high case-fatality rate, the existence of other endemic infectious diseases, and reduced access to medical maintenance due to the proceeding of EBOV epidemics are reasons for the high number of deaths. Several vaccine candidates were investigated to prevent further outbreaks of these fatal illness and provide protective, cost-effective therapeutics to low-income countries.

In the last decades, several new vaccine platforms were developed (section 1.3.1, figure 5). One of these platforms are viral vector vaccines which showed beneficial safety and immunogenicity profiles in clinical trials against EIDs [84,134]. Thus, different viral vector vaccines based on the platforms VSV and MVA were licensed to prevent the emerging EVD [126,127,130]. While the replication-competent VSV-EBOV (Ervebo®) was licensed in a single-dose immunization, the replication-deficient MVA-BN-Filo® (Mvabea®) was liciensed in a heterologous prime-boost regimen with Ad26.ZEBOV-GP (Zabdeno®) [126,127,129,130,140]. To date, most insights into vaccine-induced immunogenicity are based on the induction of specific antibodies. During the second largest EBOV outbreak in the DRC, VSV-EBOV was frequently used. Nevertheless, exact mechanisms of induced immune signatures, especially innate immune responses, remain inadequately understood. Innate immune responses can shape and influence the adaptive immunogenicity and therefore contribute to vaccine efficacy. Due to its early manifestation innate immunity is difficult to analyze in clinical trials and therefore is not well investigated until now. Also, the impact of different vectors on the immune response remain inadequately elucidated.

Hence, this study aimed to decipher induced immune responses by two viral vector vaccines against EBOV, the licensed Ervebo® (VSV-EBOV) and MVA-EBOV, which was not tested in clinical trials until now (cf. section 1.3.3). Although immune sigantures in humans

including humoral and cellular immune responses were described post VSV-EBOV vaccination [86,92,109,141,142], no correlates of protection were determined for VSV-EBOV so far. Furthermore, VSV-EBOV revealed a 100 % protection in macaques and 97.5 % in human ring vaccination studies during the EVD outbreak in the DRC [109,141,142]. In contrast, the potentially protective immune response of MVA-EBOV needs be determined. While the licensed VSV-EBOV additionally expresses the heterologous EBOV-GP on its surface, MVA-EBOV encodes only for the genetic information of the EBOV-GP [137]. Moreover, responses to vaccines can differ between men and women, including humoral and cellular immunity [148,165,204–206]. In order to investigate immune signatures induced by VSV-EBOV and MVA-EBOV in men and women comprehensively, *in vitro* stimulation assays were performed in the present study.

## 5.1 *In vitro* stimulation models

*In vitro* stimulation models represent a powerful tool to gain insights into immune responses elicited by viruses and vaccines. The understanding of underlying mechanisms in viral infections such as the EBOV-GP binding to specific cell surface GPs could be enhanced by *in vitro* models [264,265]. They also contributed to the understanding of mechanisms that may result in vaccine-induced immunogenicity leading to optimization approaches in vaccine design [266]. The investigation of *in vitro* MVA-stimulated monocyte-derived DCs (moDCs) revealed an activation of moDCs which could explain the immunogenicity of MVA in absence of an effective replication in hPBMCs of this attenuated vaccine vector [267]. Subsequently, *in vivo* mice models verified that DCs are main targets for MVA and are required for MVA-induced immunogenicity [268]. Models such as the modular immune *in vitro construct* (MIMIC™) were developed to ensure standardized testing systems that reflect the human immune system *in vitro* [269–271]. Similar to the *in vivo* situation the MIMIC™ system showed an age-dependent antibody production as well as T cell response post-stimulation with a trivalent influenza vaccine (TIV) [271]. Furthermore, network analysis of transcriptional changes post YF-17D vaccination in humans and *in vitro* stimulations using the MIMIC™ system exhibited similar transcriptional nodes indicating a comparable transcriptional profile upon

YF-17D *in vivo* and *in vitro* immunizations [272]. Moreover, *in vitro* vaccine quality checks of different batches help to avoid animal experiments and consequently contribute to the 3Rs principle (replace, reduce, and refine animal models) [273–275]. They can also be used to screen for efficient medications. For instance, several agents with a potentially anti-viral function against EBOV such as ion channel inhibitors and anti-microbial substances were identified by *in vitro* models [276].

On the other hand, *in vitro* models generally represent the immune system at a distinct phase of its development [277]. Moreover, they exhibit different conditions like cell density, cell-cell interaction and surrounding milieus compared to *in vivo* characteristics [277]. Although for example MIMIC™ responds similar to TIV administration in humans, it is limited in the variety of immune cell types and representation of lymphoid organs. In addition, adaptive immune responses and underlying mechanisms are difficult to investigate with *in vitro* models until now. Many important discoveries in immunology and vaccinology were made with *in vivo* models using inbred animals and their genetic modification [278]. However, animal models like mice do not reflect the human immune system in every detail [278]. Some pathogens induce a comparable disease progression in animals compared to humans, whereas others such as EBOV induces different pathologies and do not result in lethal outcome in wild type mice [279,280].

Finally, *in vitro* models are meaningful tools if more information is needed prior *in vivo* studies or other testing systems reach their limitations. For instance, the innate immune response cannot be well addressed comprehensively in clinical trials due to its early manifestation.

Here, *in vitro* stimulation assays of freshly isolated hPBMCs were implemented and monitored longitudinally to decipher induced immune signatures by VSV-EBOV and MVA-EBOV on mRNA and protein level. Analytical techniques included transcriptomic changes, cytokine secretion, and activation of innate immune cells. Furthermore, differences in the immune signature due to different viral vectors and sex-based differences in response to both viral vector vaccines VSV-EBOV and MVA-EBOV were evaluated.

Prior stimulations of hPBMCs, *in vitro* stimulation assays and corresponding analytic methods were established (cf. section 6.1−6.2, S.1–10). Based on cytokine secretions, amount of live cells upon stimulation, and the literature a MOI of 1 was used (cf. section 6.1) [267,281–283].

Freshly isolated hPBMCs were exposed for 1 h to the viral vector vaccines and harvested longitudinally at several time points post-stimulation for different analytic methods such as flow cytometry, bead-based immunoassays, and gene expression analysis (figure 8–40). Post 1 h exposure, the inoculum was substituted with fresh media according to the literature [268,281,284,285]. Moreover, an efficient *in vitro* stimulation using VSV-EBOV or MVA-EBOV was determined by transcriptomic changes over time in stimulated hPBMCs, the identification of viral antigens, an induced cytokine secretion, and an altered expression of activation markers on monocytes and DCs (cf. section 4.1, 6.1 and 6.3). In contrast to the present study, *in vitro* investigations of the live attenuated viral vaccine YF-17D against the yellow fever virus (YF) were performed in serum supplemented media for 24 h [281]. Also, *in vitro* stimulations of freshly isolated hPBMCs using the MVA and VSV vaccine vector were performed in serum supplemented media [285,286]. As investigations of sex differences were also of interest, hPBMCs were cultured in serum-free media to hamper the contact to sex hormones like estrogen, which is contained in the commonly used FCS [287]. A reduction of estrogen by charcoal-stripped FCS was not used, since estrogen and other steroids cannot be completely eradicated by charcoal dextran [287–289]. Moreover, comparable live cell counts and activation statuses of *in vitro* models using THP-1 cells cultured in serum-containing and serum-free media strengthen a usage of serum-free media for human cells (cf. section 6.1, S.2–3). Thus, a hormone-biased investigation of sex differences after *in vitro* stimulation was reduced.

Single cell suspensions can potentially be used to investigate the immune response upon stimulation on specific cell types in detail [281,290–292]. However, commonly used murine and human models of monocyte-derived DCs and macrophages are reported to consist of different subsets and do not exhibit the same properties and functional capacities as *in vivo* DCs and macrophages [293–295]. Furthermore, single cell suspensions do not reflect the comprehensive immune system, since not all immune cell subsets are present. Hence, whole hPBMCs represent the *in vivo* characteristic better than mono cell cultures.

Besides altered cytokine responses and activation of innate immune cells, different transcriptomic profiles were also detected using the nanoString® technology and RNA-Seq. These transcriptomic analyses revealed induced anti-viral responses after *in vitro* stimulations that were mainly consistent with the literature (cf. section 4.2–4.3 and 6.4) [93,296,297].

Finally, *in vitro* stimulations using VSV-EBOV and MVA-EBOV induced distinct immune signatures, highlighting that *in vitro* stimulation assays were effective and therefore can be used to investigate immune responses upon stimulation with viral vector vaccines.

## 5.2 VSV-EBOV induces a distinct cytokine profile

One of the first immune responses to vaccines is the release of cytokines, which can lead to activation and migration of immune cells to the entry site [92,243]. Furthermore, the activation of different innate immune cells by a natural infection, vaccination or released cytokines can modulate the innate-adaptive interface. Induced cytokine secretions of hPBMCs by *in vitro* stimulations using VSV-EBOV were investigated in the present study via bead-based immunoassays (cf. section 4.1.1). Out of 13 tested cytokines, interleukins (IL) including IL-1β, IL-8, IL-10, interferon gamma-induced protein 10 (IP-10), monocyte chemoattractant protein 1 (MCP-1), and tumor necrosis factor alpha (TNFα) revealed an induction over time compared to unstimulated samples (cf. section 4.1.1, figure 9−11). In general, a higher amount was detected 24 h after stimulation compared to 12 h. While the composition of these six elevated cytokines in *in vitro* stimulations did not change at later time points, IP-10, MCP-1, and IL-8 revealed a twice as high amount after 24 h compared to 12 h stimulation. In particular, IP-10 exhibited a significant induction 24 h post-stimulation compared to unstimulated counterparts. Sources of enhanced IP-10 and MCP-1 secretion could be monocytes and DCs, which are described to produce high amounts of these cytokines upon activation [281,298,299]. Moreover, non-structural and truncated surface EBOV-GP molecules are released by EBOV-infected cells and activate non-infected macrophages and DCs, resulting in a massive cytokine secretion of pro- and anti-inflammatory cytokines such as IL-1, IL-6, IL-8, TNFα, and IL-10 [300–302]. Likewise monocytes revealed an activation by EBOV infections mediated via TLR4 and EBOV-GP release by infected immune cells [50,302–304]. In this manner activated monocytes contribute for example to NK cell activation by IL-18 and IL-12 secretion and therefore are mandatory for a comprehensive immune cell activation [305].

An early induction of IP-10 was correlated to an increased antibody response post VSV-EBOV vaccination [92]. Hence, an IP-10 response upon VSV-EBOV stimulations might contribute to a

beneficial vaccine-induced immunogenicity. The IP-10 secretion of hPBMCs derived from vaccinees was also increased post EBOV-specific *ex vivo* stimulation [86]. Besides VSV-EBOV, immunizations with YF-17D, another live attenuated viral vaccine that replicates only to some extent in humans, resulted in an altered cytokine profile [266]. EBOV and YF both carry a single stranded RNA genome and are mainly endemic in Africa [18,25,306,307]. *In vitro* stimulations using YF-17D exhibited similar cytokine profiles compared to present VSV-EBOV *in vitro* stimulations. For instance, YF-17D primarily revealed an increased secretion of IP-10 and MCP-1 [103,281]. The role of IP-10 to vaccine-induced immunogenicity was emphasized by YF-17D and TIV, since IP-10 also showed significantly elevated amounts one or three days post YF-17D and TIV administration [103,308]. IP-10 has diverse functions including chemotaxis of $CXCR3^+$ cells, proliferation, apoptosis, regulation of cell growth, and angiogenesis in infections [255–260]. Based on the immune status of the host and the pathogen IP-10 can facilitate or diminish viral infections [255]. However, in VSV-EBOV vaccination IP-10 is rather beneficial than harmful due to its link to increased EBOV-specific antibodies [92]. In the present study, the IP-10 effect is encouraged by a slightly increased expression of IL-8 and MCP-1, which also act in a pro-inflammatory and chemoattractant fashion [309,310]. Furthermore, MCP-1 and six additional cytokines/chemokines that have a monocyte-related function were detected in VSV-EBOV vaccinees one day after vaccination [311]. The described *in vitro* signatures and *in vivo* studies strengthen the contribution of monocytes to effective vaccine-induced immunogenicity.

EBOV and VSV-EBOV carry both the EBOV-GP on their surface which mediates cell attachment and entry [39]. Furthermore, both are enveloped and contain a non-segmented RNA genome that encodes for a RNA-dependent RNA polymerase and several viral proteins [18,33,312]. The RNA genome, the exposed immunogenic EBOV-GP, and other viral structures such as matrix proteins and nucleoproteins can act as PAMPs resulting in a PRR-mediated activation of the innate immune system post EBOV infection or VSV-EBOV vaccination. A natural EBOV infection and vaccination induce similar cytokine profiles. Both, EBOV infections and VSV-EBOV vaccination in humans induced IL-1, IL-6, IL-8, IP-10, TNFα, and MCP-1 [46,51,311,313,314]. In contrast to vaccination, a natural EBOV infection can lead to a massive cytokine storm leading to immunopathology. IP-10 and MCP-1 were also elevated in VSV-EBOV *in vitro*-simulated samples emphasizing the impact of these cytokines upon infection and vaccination. These responses might be EBOV-GP–specific, since EBOV infections

as well as *in vivo* and *in vitro* VSV-EBOV studies revealed an induction. However, unspecific innate immune responses mediated by TLR stimulation based on viral structures could also explain comparable signatures upon infection and *in vivo* as well as *in vitro* studies of EBOV and VSV-EBOV. For instance, viral RNA will be unspecifically detected by diverse TLRs including TLR3, TLR7, and TLR8 resulting in a pro-inflammatory and anti-viral response [315]. Nevertheless, EBOV-GP alone induced a pro-inflammatory immune response suggesting that observed cytokine inductions *in vitro* could be EBOV-specific [304]. *In vitro* investigations using mouse derived macrophages and human derived monocytes revealed an increased expression of *TNFα*, *IL-1*β, and *IL-6* [304]. Additionally, *in vivo* immunizations using EBOV-GP revealed an induction of innate cytokines including IL-1β, IL-6, TNFα, and MCP-1 [304]. Although these data indicate that specific immune responses to EBOV-GP are also detectable in *in vitro* studies, they could not verify an EBOV-GP–specific response measured by an IP-10 and MCP-1 secretion. To confirm EBOV-specific responses and determine correlates of protection more investigations are needed.

Furthermore, the vector itself can lead to an induced innate and adaptive immune response post-stimulation or vaccination [90]. The *in vitro* stimulation of hPBMCs using VSV led mainly to increased secretion of IP-10, TNFα, and IFNα [286]. Moreover, antigen-specific adaptive signatures were linked to the vector VSV post VSV-EBOV vaccination in humans. The investigation of hPBMCs from vaccinees revealed VSV-specific CTLs with an elevated secretion of IFNγ, IL-2, and TNFα upon stimulation using inactivated VSV wild type (VSVwt) [88]. Additionally, CTL responses were detected in VSV-EBOV vaccinees [86]. Besides increased specific antibodies, CTL responses are also elevated in EBOV survivors compared to non-survivors indicating that CTL responses contribute to survival [316,317]. Moreover, MVA infected moDCs and whole hPBMCs revealed an enhanced secretion of IP-10 and MCP-1 emphasizing the impact of viral vectors to vaccine-induced immunogenicity [290,318]. Whether CTL signatures are also present in MVA-EBOV vaccinees need to be determined. Since adaptive signatures such as CTL responses cannot be determined via *in vitro* stimulations, the present study could not predict adaptive immunogenicity induced by VSV-EBOV and MVA-EBOV.

While VSV-EBOV immunizations led to inductions of monocyte related cytokines [86,311,314,316,317], EBOV infections induce a stronger and more comprehensive

secretion of cytokine profiles [46,51,313]. Finally, *in vitro* stimulations and vaccinations using VSV-EBOV as well as natural EBOV infections revealed due to its virus characteristics a comparable anti-viral cytokine signature.

## 5.3 VSV-EBOV and MVA-EBOV modify the expression of activation markers on monocyte and DC subsets

Since DCs and monocytes can determine later immune responses to infections as well as vaccination, the activation status of these immune cells was assessed via flow cytometry upon *in vitro* stimulation using VSV-EBOV and MVA-EBOV, respectively (cf. section 4.1.2, figure 12–18) [235–241].

### 5.3.1 Activation of monocyte cell subsets

After *in vitro* stimulation using VSV-EBOV mainly intermediate and non-classical monocytes revealed a tendency for an enhanced activation based on their expression of CD83 and CD86. Interestingly, a higher frequency of $CD86^+$ monocytes was determined three days post vaccination in VSV-EBOV vaccinees [92]. Additionally, the YF-17D vaccine resulted in an elevated frequency of $CD86^+$ monocytes peaking seven days post vaccination, indicating a vaccine-dependent expression of activation markers on innate immune cells [103]. In contrast to trends for an increased expression of CD83 and CD86 post VSV-EBOV *in vitro* stimulation, MVA-EBOV led to a significant upregulation of CD83 on intermediate monocytes and downregulation of CD86 on classical, intermediate, and non-classical monocytes. After TIV vaccination an elevated frequency of intermediate monocytes with an increased amount of cytokine-positive cells was detected, indicating an activation of monocytes upon vaccination [319]. The elevated frequency of $CD86^+$ monocytes in VSV-EBOV vaccinees showed a negative correlation with antibody responses [92]. Although the co-stimulatory signal mediated by CD86 is required for T cell proliferation, activation, and finally efficient antibody production, a suppressive function of activated inflammatory monocytes has been described in ovalbumin (OVA) or hemagglutinin (HA) vaccinated mice [299]. Moreover, an activation of

human monocytes mediated by several TLRs led to a reduced expression of CD86 in a partially IL-10 dependent manner [320,321]. A decreased expression of CD80 and CD86 on monocytes prior to TIV vaccination was also correlated with seroconversion upon vaccination [321]. This further indicates that a reduced expression of CD86 might be a prediction marker for vaccine-induced immunogenicity. Hence, in the present study the significantly decreased expression of CD86 on monocytes after MVA-EBOV *in vitro* stimulations might indicate an increased anti-viral response with a stronger potential to initiate seroconversion, which might be more effective compared to VSV-EBOV.

### 5.3.2 Activation of DC subsets

In accordance with a natural EBOV infection [268,285], the vector MVA infects antigen presenting cells (APCs) and predominantly DCs as shown in the present study. To this end, different DC subsets were investigated based on their ability to express the activation marker CD40, CD83 or CD86. In addition to the monocyte cell subset findings, a VSV-EBOV *in vitro* stimulation revealed no statistically significant altered expression of CD40, CD83, and CD86 on pDCs, $CD1c^{+}CD11c^{+}$ DCs, $CD1c^{-}CD16^{+}$ DCs, and $CD1c^{-}CD141^{+}$ DCs. Interestingly, a higher frequency of $CD86^{+}$ DCs was determined three days post VSV-EBOV vaccination in humans, where the elevated frequency of $CD86^{+}$ DCs showed a negative correlation with antibody responses [92].
In contrast, pDCs, $CD1c^{+}CD11c^{+}$ DCs, and $CD1c^{-}CD141^{+}$ DCs exhibited a significantly lower expression of CD86 in MVA-EBOV *in vitro* stimulated samples compared to unstimulated counterparts. In addition to activated monocytes, an increased DC activation mediated via CD86 might also lead to a vaccine-induced counter-regulatory response [92,299]. Accordingly, reduced expression of CD86 on DCs post MVA-EBOV *in vitro* stimulation might increase later immune responses. This hypothesis is emphasized by the decreased expression of CD86 on monocytes that share several markers and cellular characteristics with DCs. Furthermore, CD83 showed a significantly decreased expression on $CD1c^{-}CD141^{+}$ DCs post MVA-EBOV *in vitro* stimulation.
However, whole DCs derived from lymph nodes of DNA-vaccinated mice showed an induction of CD40 and CD86 [322]. Moreover, immature and mature DCs are described to express CD40 and CD86 to a higher extent upon bacterial DNA stimulation [323]. Furthermore, viral stimuli

including the YF-17D vaccine led to an induction of the activation marker CD83 and CD86 on human moDCs and CD86 on myeloid DCs and pDCs [103,281]. These discrepancies may be explained by the usage of *in vivo* studies or by different immune responses due to different stimulation mechanisms. While vaccines like YF-17D and VSV-EBOV contain a RNA genome, DNA-vectored vaccines as well as MVA-based vaccines consists of DNA resulting in different TLR recognition of innate immune cells [78,307,312]. The site of antigen expression could potentially contribute to these differences. Different sites of transcription and replication such as the cytoplasm in case of YF-17D, VSV- and MVA-based vaccines or the nucleus in case of DNA plasmid-vaccines result in different mechanisms of immune cell activation [78,324–327]. Accordingly, different pathways will be activated leading to different responses. An *in vitro* stimulation of human moDCs using MVA resulted in a slightly upregulated expression of CD83 and CD86 [267]. However, they used a 5 times higher MOI of MVA compared to the present study and observed only a low, not significant MFI of 17 for CD83 and 55 for CD86 compared to isotype controls. Higher MFIs were only detected in populations of $MVA^+$ murine bone marrow-derived DCs (BMDC) post-stimulation where ten times higher MOIs were used [268]. While these studies performed stimulations with single cell suspensions, *in vitro* stimulations using VSV-EBOV and MVA-EBOV were performed with whole hPBMCs. Hence, VSV-EBOV and MVA-EBOV stimulation assays represent immune responses elicited by different immune cell types and therefore reflect the *in vivo* situation better than single cell suspensions. Nevertheless, single cell stimulation indicated that MVA and MVA-based vaccines might not induce the expression of activation markers on DCs. Furthermore, some viral infections of DCs result in an increased immune response and fast clearance of the virus, whereas others including CMV, measles, and HIV dampen the immune response [328–331]. This strengthens the findings of VSV-EBOV and MVA-EBOV *in vitro* stimulations, which showed different tendencies for DC activation.

In the present study, a significant reduction of CD86 on pDCs, $CD1c^+CD11c^+$ DCs, and $CD1c^-CD141^+$ DCs as well as of CD83 on $CD1c^-CD141^+$ DCs was detected post MVA-EBOV stimulation, whereas VSV-EBOV indicated no significant altered expression of these markers. Whether this is mediated by MVA and results in an increased immune response due to a lower cross-regulatory effect or a decreased immune response based on less DC activation needs to be determined.

## 5.4 VSV-EBOV and MVA-EBOV alter the transcriptomic profile of stimulated hPBMCs

Since transcriptomic changes were detected and correlated to antibody titers post vaccination, they represent insights into mechanisms that may result in protection of vaccinees [93,296,297,332]. To decipher transcriptomic changes by *in vitro* stimulations using VSV-EBOV and MVA-EBOV comprehensively the nanoString® technology and RNA-Seq were utilized (cf. section 4.2, figure 19–33).

### 5.4.1 VSV-EBOV and MVA-EBOV induced different anti-viral signatures in hPBMCs

A screening for altered gene expressions in VSV-EBOV–stimulated hPBMCs using the nanoString® technology revealed several differentially expressed genes (DEG) over time with bigger differences in PCA after 6 h of stimulation than 1 h. Moreover, the number of DEG was two times higher after 6 h compared to 1 h in VSV-EBOV *in vitro* stimulated hPBMCs. In addition, transcriptomic changes peaked 1 day post VSV-EBOV vaccination in humans where later time points returned to baseline [297]. In contrast, a VSV-EBOV vaccination of cynomolgus macaques led to delayed transcriptomic changes. A higher number of DEG was detected seven days post vaccination compared to three days post vaccination in cynomolgus macaques [93,296]. Vaccinated cynomolgus macaques showed a similar number of DEG post vaccination compared to *in vitro* VSV-EBOV stimulations [296]. However, stricter cutoffs with a log2 fold change of ≥ 2 may explain this low transcriptional induction *in vivo*. After VSV-EBOV *in vitro* and *in vivo* stimulation, an anti-viral signature were detected. While the top upregulated pathways of DEG included cytokine, interleukin, and chemokine signaling post VSV-EBOV *in vitro* stimulation, induced GO terms of vaccinated cynomolgus macaques included but are not limited to immune system process, receptor signaling pathways, response to cytokines, and defense response [93,296]. Accordingly, VSV-EBOV resulted *in vivo* to a comprehensive systemic anti-viral response, whereas *in vitro* stimulations mainly induced cytokine responses [93,296].

Also, RNA-Seq analysis of VSV-EBOV *in vitro* stimulations revealed distinct transcriptomic signatures. These signatures were comparable to the findings with the nanoString®

technology and could be expanded by RNA-Seq due to the higher number of analyzed genes. After 6 h of a VSV-EBOV *in vitro* stimulation 643 DEG were detected in the present study. In contrast, MVA-EBOV induced 5.6 times more DEG 6 h post *in vitro* stimulation compared to VSV-EBOV. In addition, VSV-EBOV vaccinees showed more than 5,000 differently expressed genes peaking one day post vaccination and returning to baseline in the following 20 days [297]. Furthermore, unstimulated samples also exhibited DEG after 6 h of *in vitro* cultivation. The number of DEG were higher in stimulated compared to unstimulated samples. Additionally, ORA, KEGG, and GO term analysis revealed no significantly responses in unstimulated samples and therefore DEG in unstimulated samples were interpreted as background noise. Moreover, both *in vitro* stimulations using VSV-EBOV and MVA-EBOV exhibited differences in a PCA of stimulated and unstimulated samples emphasizing a specific altered transcriptomic profile upon stimulation. Since some VSV-EBOV–stimulated and unstimulated samples clustered together post 6 h, the transcriptomic changes by VSV-EBOV might be not so strong compared to MVA-EBOV–stimulated samples which did not cluster together with unstimulated samples.

While a VSV-EBOV *in vitro* stimulation resulted mainly in a pathway induction of chemokine receptors bind chemokines in ORA, MVA-EBOV primarily induced pathways for interferon signaling and cytokine signaling. This highlights distinct transcriptomic profiles by VSV-EBOV and MVA-EBOV stimulations. Despite one study that indicated an induced IFN signaling upon natural EBOV infections of cynomolgus macaques, no enhanced IFN signaling in EBOV infections was determined [333]. Since the difference between VSV-EBOV, MVA-EBOV and EBOV are manifold, several reasons could explain different pathway inductions such as different viral origins and different kinetics of *in vitro* and *in vivo* stimulations. Also, suppressive mechanisms mediated by EBOV-VP24 and -VP35 might explain a lower induction of IFN signaling in natural EBOV infections [334–339]. VSV-EBOV vaccinated cynomolgus macaques showed a slight induction for IFN signaling after EBOV challenge emphasizing a vaccine-specific induction, since IFN signaling was not elevated post EBOV infections [93,340]. By using murine BMDC, MVA stimulations also revealed an induction of type I IFN-specific genes and an increased secretion of type I IFNs in a TLR-independent manner [341,342]. The vaccina virus vaccine called Aventis-Pasteur WetVax® (APSV) revealed IFN-induced and TNFα-induced genes five to seven days post vaccination in humans [343]. In addition, YF-17D vaccination in

humans revealed an increased gene expression especially seven days post vaccination. Predominantly genes that mediate interferon and anti-viral responses were elevated [103,272]. Also, investigations of different seasonal TIV vaccinations highlighted the impact of IFN signaling. Using previously defined human blood transcriptional modules showed a mainly innate immune signature one and three days post TIV vaccination [332,344]. In particular, DC activation and expression of IFN were associated with antibody responses post TIV vaccination [332]. This vaccine-specific pathway inductions *in vivo* were better reflected by MVA-EBOV *in vitro* stimulations than VSV-EBOV *in vitro* stimulations.

Moreover, GO term analysis revealed different signatures in MVA-EBOV and VSV-EBOV-stimulated hPBMCs. Significant GO terms for upregulated genes included defense response to virus (GO:0051607) and response to virus (GO:0009615) post MVA-EBOV *in vitro* stimulation. In contrast, VSV-EBOV exhibited no significant GO terms post *in vitro* stimulation. Therefore, MVA-EBOV *in vitro* stimulated samples may induce a stronger anti-viral response than VSV-EBOV–stimulated samples. Also, YF-17D vaccinees mainly exhibited an upregulation of immune response and response to virus in GO term analysis [103]. Additionally, independent component analysis (ICA) followed by gene set enrichment analysis mainly revealed for YF-17D vaccination in humans and *in vitro* stimulations of the MIMIC™ system an expression of genes that were induced by IFNs and viruses [272]. Similar GO signatures were detected post APSV vaccination in humans including immune cell activation, cellular defense response and inflammatory response [343]. Besides MVA-EBOV *in vitro* stimulations, VSV-EBOV vaccinated cynomolgus macaques revealed an elevated defense response to virus and type I IFN signaling [93]. Furthermore, strong upregulation of mainly responses to virus and IFN signaling were detected in VSV-EBOV-vaccinated humans [297]. Hence, *in vitro* stimulation using MVA-EBOV seem to be more comprehensive and reflect the VSV-EBOV *in vivo* transcriptomic profiles in cynomolgus macaques and humans better than VSV-EBOV *in vitro* stimulation [93,297,340].

One explanation for lower transcriptomic changes upon VSV-EBOV *in vitro* stimulation might be that VSV-EBOV is an attenuated vaccine that can replicate in human cells to some extent [220,345]. Accordingly, the VSV-EBOV *in vitro* stimulation might be stronger compared to the replication-deficient MVA-EBOV resulting in highly infected cells that undergo apoptosis. On the other hand, no significant drop in live cell counts of VSV-EBOV *in vitro* stimulated

hPBMCs was detected. To investigate whether hPBMCs of both stimulations exhibit the same condition, apoptotic markers should be used in further experiments. Moreover, *in vivo* a replication-competent vaccine might be beneficial due to a stronger induction of the immune response. Since, viral loads of VSV-EBOV and MVA-EBOV were comparable in hPBMCs as indicated by virus-specific gene detection, other effects must be the reason for the discrepancy of induced transcriptomic changes. VSV leads to lower amounts of phosphorylated eukaryotic translation initiation factor 4E (eIF4E) and eIF4E-binding protein 1 (4EBP1), resulting in reduced host cell translation [346–348]. The dephosphorylation of 4EBP1 is mainly mediated by the viral M-protein resulting in more than 60 % of cytoplasmatic and polysome-associated viral mRNA [349]. This was described to occur already 6 h post infection. Moreover, unassociated mRNAs were reported to have a shorter half-life which might also affect *in vitro* transcriptome analysis explaining lower transcriptomic changes in VSV-EBOV–stimulated hPBMCs [349]. Furthermore, different viral vector vaccines might have different kinetics in *in vitro* stimulations of hPBMCs. To address whether VSV-EBOV could lead to delayed transcriptomic changes, later time points of *in vitro* stimulations should be investigated in further studies. Moreover, a second line VSV-EBOV which was passaged by the infection of BHK cells was used in the present study. Hence, the replication of VSV-EBOV prior *in vitro* stimulations of hPBMCs might also affect the outcome of immune signatures.
Here, different transcriptomic profiles after VSV-EBOV and MVA-EBOV *in vitro* stimulation were identified. While VSV-EBOV mainly induced cytokine signaling including interleukins and chemokines, MVA-EBOV stimulations led to IFN signaling, cytokine signaling, and defense responses to virus.

### 5.4.2 VSV-EBOV and MVA-EBOV led to different gene expressions in stimulated hPBMCs

The induced pathways by VSV-EBOV and MVA-EBOV were associated with different gene expressions post *in vitro* stimulation. An anti-viral signature induced by VSV-EBOV was determined using the nanoString® technology. For instance, the anti-viral signature was indicated by an increased expression of *IP-10*, *CLEC5A*, *GBP1*, *IL-1α*, *IDO1*, and *MCP-1*. Since IP-10 and MCP-1 were also elevated on the protein level, the relevance of these cytokines was intensified post VSV-EBOV *in vitro* stimulation. Moreover, a natural EBOV infection

showed an enhanced expression of *IP-10* and *MCP-1* measured by transcriptomic changes in PBMCs derived from infected cynomolgus macaques [333]. Accordingly, VSV-EBOV vaccinated humans revealed an elevated expression of *MCP-1* after vaccination [297]. An increased expression of *IP-10* was also determined in hPBMCs of vaccinia virus vaccinated humans using APSV [343]. In addition, the viral vaccina YF-17D showed an elevated *IP-10* expression in vaccinated humans peaking seven days post vaccination [103,332]. A beneficial vaccine-induced profile of IP-10 was emphasized due to its link to increased EBOV-specific antibodies post VSV-EBOV vaccination [92]. Accordingly, a substantial vaccine-specific signature was determined post VSV-EBOV *in vitro* stimulation using the nanoString® technology.

RNA-Seq analysis revealed comparable gene expression signatures and led to more insights into induced transcriptomic changes. An increased expression of several genes was linked to a reduced replication of EBOV in infected human embryonic kidney cells (HEK) [350]. Some of the top 20 upregulated genes were also elevated in the present study post *in vitro* stimulation. While VSV-EBOV *in vitro* stimulation led to significantly elevated expression of *CD9*, MVA-EBOV resulted in an increased expression of *GBP2*, *IFI6*, *BTN3A3*, *IRF7*, and *IFIH1* [350]. In addition to previously described findings of MVA-EBOV, this increased number of genes that were correlated with reduced EBOV replication emphasize the beneficial immune signature induced by MVA-EBOV that might contribute to protection in vaccinees.

The viral vaccine YF-17D led to a comparable gene signature *in vivo* and *in vitro* [103,272]. More than half of the *in vivo* DEG were also elevated in *in vitro* stimulations of hPBMCs three and seven days post YF-17D vaccination indicating conserved responses [103]. ICA followed be gene enrichment analysis revealed a distinct regulation of transcription factors which were responsible for downstream gene expressions post YF-17D vaccination in humans [272]. Three major transcription factors the interferon regulatory factor 7 (IRF7), signal transducer and activator of transcription 1 (STAT1), and ETS proto-oncogene 2 (ETS2) were identified in hPBMCs of YF-17D vaccinees and in *in vitro* stimulations of the MIMIC™ system using YF-17D [272]. In addition, another live attenuated viral vaccine against the influenza virus (LAIV) exhibited an increased expression of genes with innate immune related functions such as *STAT1* and IRF7 [308,344]. While VSV-EBOV showed no elevated expression of these transcription factors in the present study, MVA-EBOV stimulations resulted in a significantly increased expression of *IRF7* and *STAT1*. These two genes were also elevated in the first seven days post

VSV-EBOV vaccination in human and cynomolgus macaques as well as following EBOV challenge of vaccinated cynomolgus macaques [93,297]. Therefore, IRF7 and STAT1 might have conserved functions in vaccine-induced immune responses which could also contribute to MVA-EBOV immunogenicity.

Moreover, single-gene analysis revealed further insights into immune signatures post VSV-EBOV stimulation. A natural EBOV infection is mediated by the interaction of the EBOV-GP and host cell receptors. Besides phosphatidylserine receptors, C-type lectins (CLECs) are one of the major binding receptors in natural EBOV infections [351]. CLECs are located on DCs, monocytes, and macrophages. Here, *CLEC5A* was among the top 10 upregulated genes post VSV-EBOV *in vitro* stimulation. The interaction of EBOV and CLECs may result in immunosuppressive effects as described for the measles virus (MV) [352]. However, a long-lasting immunity was correlated to genotypes, *IFNγ*, and *CLEC5A* expression post YF-17D vaccination emphasizing a manifold response of CLECs depending on the infection or vaccination [353]. Accordingly, an enhanced expression of general *CLECs* might contribute to a reduced host cell immune response upon VSV-EBOV *in vitro* stimulations, whereas an enhanced expression of *CLEC5A* could lead to long-lasting immunity. In contrast to VSV-EBOV, MVA-EBOV mainly induced an elevated expression of *IFNs* and IFN-related genes. Additionally, compared to YF-17D vaccination, MVA-EBOV led to an enhanced expression of *IFNγ* [353]. Also, interferon-induced proteins with tetratricopeptide repeats (IFIT) such as *IFIT1*, *IFIT3*, *IFI27*, and *IFI44* had an increased expression post MVA-EBOV stimulation. These genes were also elevated in VSV-EBOV vaccinees over the first two weeks post vaccination, emphasizing their contribution to a vaccine-induced immune signature [297]. Furthermore, 65 genes which were elevated in VSV-EBOV vaccinees and linked to enhanced innate antiviral and IFN signaling were also enhanced in YF-17D vaccinated humans [103,297]. Since this induction was detected over seven days post VSV-EBOV and YF-17D vaccination, the authors hypothesized a long-lasting innate immune response [297]. Out of these 65 genes only *GBP1*, *IFIT2*, and *OASL* were significantly upregulated post VSV-EBOV *in vitro* stimulation in the present study, whereas MVA-EBOV resulted in 44 significantly upregulated genes, which mainly belongs to cytokine and IFN signaling. Therefore, MVA-EBOV might result in a long-lasting innate immune response which could contribute to an elevated adaptive immune response.

Moreover, data of altered expression of CD86 upon *in vitro* stimulations on innate immune cells (section 5.3.2) could be intensified by RNA-Seq. VSV-EBOV led to an upregulation of *CD86*, whereas an MVA-EBOV stimulation resulted in a significant reduction. The upregulation of *CD80*, a closely related factor of CD86, strengthens the hypothesis that VSV-EBOV led to an upregulation of CD86, indicating an increased anti-viral response. However, MVA-EBOV might have a stronger potential to initiate seroconversion as described for other vaccines due to lower cross-regulation mediated via CD86 [92,299,321]. This seroconversion might be more effective upon MVA-EBOV immunization compared to VSV-EBOV which induced a higher expression post *in vitro* stimulation. Since first insights into different activation statuses of innate immune cells were determined using flow cytometry and RNA-Seq, this might be an additional reason for different transcriptomic changes post VSV-EBOV and MVA-EBOV stimulation. These findings emphasize that both viral vector vaccines may stimulate different subsets of immune cells due to their different surface receptors. Hence, the expression of EBOV-GP on the surface of VSV-EBOV could lead to a different cell tropism compared to MVA-EBOV which only encodes for the EBOV-GP sequence without any surface expression.
The nanoString® technology and RNA-Seq exhibited transcriptomic changes of distinct genes after VSV-EBOV or MVA-EBOV *in vitro* stimulation. Both showed inductions of *IP-10*, *IL-1α*, *GBP1*, *MCP-1*, and *IDO1* post-stimulations. While VSV-EBOV induced mainly *IP-10* and *CLEC5A*, MVA-EBOV exhibited especially for *IFN*β1 and IFN related genes an increased expression. In conclusion, these findings indicate further differences in immune responses to both viral vector vaccines and are consistent with the findings of different anti-viral signatures.

## 5.5 VSV-EBOV and MVA-EBOV induce slightly different immune responses in men and women

The immune response to vaccines can differ between men and women, where women generally develop a stronger immune response than men [147,148]. They benefit from a higher magnitude of humoral and cellular immune responses but have to suffer from more adverse reactions. To decipher sex-based differences in VSV-EBOV- and MVA-EBOV-induced immunogenicity, all data of VSV-EBOV and MVA-EBOV *in vitro* stimulations were stratified by sex (cf. section 4.3, figure 34–40).

Despite some hints for different amounts of T cells, B cells, monocytes, and mDCs in both sexes exists [157,158], no different frequencies in hPBMCs of monocyte and DC subsets were detected in the present study. Out of 13 analyzed cytokines only IL-8 and IP-10 revealed slightly tendencies for an elevated secretion of IL-8 in women and IP-10 in men. These tendencies were strengthened using the nanoString® technology. Here, slightly increased numbers of DEG were detected in women 6 h post-stimulation. In addition to an increased level of IP-10, men exhibited an elevated log2 fold change of *IP-10* 6 h post-stimulation. Furthermore, women had an enhanced global significance score for pre-defined gene sets including response to virus and response to stress post VSV-EBOV *in vitro* stimulation. To date, no sex-based differences in the immune signature to VSV-EBOV have been described [220,221]. After VSV-EBOV vaccination an early induction of IP-10 was correlated to an increased antibody response in vaccinees [92]. Hence, the IP-10 induction observed in VSV-EBOV *in vitro* stimulated hPBMCs on protein and mRNA level might result in an elevated vaccine-induced immunogenicity in men. Immune-relevant genes that escape from X-chromosome inactivation (XCI) might affect the immunocompetence due to an enhanced expression in immune cells of women. The IP-10 receptor CXCR3 can also be more highly expressed in women due to XCI [160,176,177], which may lead to an enhanced signaling and therefore potentially compensate for lower amounts of IP-10 in women. Whether this might affect vaccine-induced protection has to be determined, since XCI occurs at different intensities in various immune cells [354]. In contrast to VSV, vaccinia virus (VACV)-derived vaccines showed first hints for sex-based differences. The VACV vaccine (Dryvax®) exhibited higher neutralizing titer in women than in men [212]. While men had significantly higher IFNγ and increased IL-1β levels, women showed enhanced IL-2 and IL-10 secretion upon Dryvax® vaccination [213]. Out of these enhanced cytokines by Dryvax®, only *IFNγ* was significantly upregulated in the present study post MVA-EBOV *in vitro* stimulations indicating a characteristically female response. Furthermore, a meta-analysis of a next generation smallpox vaccine based on MVA (MVA-BN: Imvamune®) showed higher specific antibody titer in men compared to women [214]. These different cytokine and antibody responses emphasize a complex sex-biased immunity upon vaccination.

Here, RNA-Seq analysis revealed no sex-biased transcriptomic changes in hPBMCs post VSV-EBOV *in vitro* stimulation, whereas MVA-EBOV induced slightly different expressions in

men and women. While hPBMCs derived from men showed a significant induction of 6 genes, women exhibited 11 genes. Whether these different transcriptomic changes might contribute to sex-biased immune response in MVA-based vaccines such as Imvamune® needs to be determined in larger studies. Finally, first insights into sex-biased cytokine and transcriptomic signatures was elucidated post *in vitro* stimulations using VSV-EBOV and MVA-EBOV.

## 5.6 Conclusion

This dissertation contributed to the understanding of induced immune signatures by VSV-EBOV and MVA-EBOV, which revealed cytokine inductions and different expression of activation markers on monocytes and DCs as well as transcriptomic changes over time. In contrast to VSV-EBOV, MVA-EBOV might leads to an increased immune response due to a lower cross-regulatory effect of $CD86^+$ monocytes and DCs. While VSV-EBOV *in vitro* stimulations of hPBMCs mainly showed elevated cytokine signaling, MVA-EBOV stimulations primarily elucidated induced IFN signaling. In addition, VSV-EBOV showed an increased expression of *IP-10* and *CLEC5A*, whereas MVA-EBOV stimulation led to an enhanced expression of *IFN*β1 and IFITs.

Findings like these are important since they can foster further vaccine development. During the largest EBOV outbreak in West Africa many vaccine candidates based on different platforms were investigated (section 1.3.2, table 1). Increased understanding of vaccine-induced immunogenicity by different platforms facilitated the development and implementation in the following decades as emphasized by the ongoing SARS-CoV-2 pandemic. Existing vaccine platforms, production pipelines, and know-how led to an accelerated development and finally resulted in licensed vaccines one year after SARS-CoV-2 emerged. Besides mRNA vaccines, viral vector vaccines are promising candidates where an Ad.26- and ChAdOx1-based vaccine were already licensed against SARS-CoV-2 in Europe, highlighting the relevance of viral vector vaccine in the combat of EIDs [355,356]. In contrast to Ad.26 and ChAdOx1, an MVA-based vaccine called MVA-SARS-2-S showed lower immune responses in a clinical phase I trial [357]. However, due to this knowledge a modified viral vector vaccine candidate based on MVA was designed and will be tested in clinical trials. To improve the tolerability and immune response in humans a heterologous prime-boost regimen using

different vaccine platforms might be efficient. Here, a priming by a mRNA vaccine and a boost by a viral vector vaccine could be powerful to reduce side effects during the boost in heterologous mRNA immunizations and improve overall immune responses.

Furthermore, insights into sex-specific responses were observed post *in vitro* stimulations using VSV-EBOV and MVA-EBOV, indicating slightly increased transcriptomic changes with an anti-viral function in women. To determine whether this sex-bias may lead to different outcomes of vaccination and finally to distinct protection in men and women, further investigations are needed. The identification of sex-based differences is mandatory to protect both sexes equally, reduce side effects in women, improve immune responses in men and prevent a drop of promising vaccine candidates due to a bad overall efficacy [358]. In conclusion, different immune signatures of *in vitro* stimulated hPBMCs using VSV-EBOV and MVA-EBOV were determined indicating distinct correlates of protection, which were mainly dependent on the viral vector vaccine rather than sex.

## 5.7 Future perspectives

To determine the impact of different immune signatures by VSV-EBOV and MVA-EBOV, a modulation of gene expressions in human cell lines or animal models could be utilized. Using RNA interference (RNAi), a knock-down with a decreased expression rate of a specific gene of interest could be achieved. By comparing these knock-down approaches to knock-out experiments realized by homologous recombination would allow a comprehensive investigation of gene-specific contributions to induced immune responses. Interesting candidates for further gene expression analysis are *IP-10* and *CLEC5A* due to their elevated expression in VSV-EBOV *in vitro* stimulated hPBMCs as well as *IFNs* and *IFITs* as they were only higher expressed post MVA-EBOV stimulation. Furthermore, an investigation of immune responses prior to and post infection might reveal potential biomarkers that correlate with protection. The identification of correlates of protection such as specific gene expressions, cytokines or miRNAs [91,92], which are linked to adaptive immune responses, might increase the understanding of vaccine-induced immunogenicity. Moreover, this could accelerate further vaccine development. Improved *in vitro* stimulations combined with an increased knowledge of correlates of protection might lead to better testing systems for vaccine quality checks of

different batches. This would reduce the need for animal models in accordance with the 3Rs principle first described by W.M.S. Russel and R.L. Burch to replace, reduce, and refine animal models [273]. Furthermore, a reduction in costs and time could be obtained by using *in vitro* stimulations for vaccine testing [274].

First insights into sex-specific differences in induced immune responses by viral vector vaccines such as VSV-EBOV and MVA-EBOV were detected using *in vitro* stimulation assays. To validate and gain more knowledge further investigations are needed. Hence, experiments with more donors are required to detect significant differences and investigate smaller differences in detail, which might have a strong impact on later immune responses. In addition, the modification of the hormone milieu by adding or substituting sex hormones in *in vitro* stimulation assays could elucidate the impact of sex hormones on the immunocompetence. Gelded animals and/or sex hormone replacement could further lead to deciphered sex-specific differences and their specific reason. Insight into disease progression of COVID-19 revealed a worse outcome for men with a testosterone disorder combined with manifold metabolic malfunction emphasizing a high versatility of reasons for sex-biased immunogenicity [359]. In addition, the age can also have an effect on the immunocompetence of men and women [360,361]. In particular, *in utero*, pre- and post-puberty, and old ages influence T cell ratios, T cell activity, NK cell activity, and antibody titer [206]. Accordingly, sex- and age-specific modifications of transcriptomic changes, epigenetic modifications, metabolomics, and microbiota should also be further addressed to validate differences in vaccination. Findings of vaccine-induced immunogenicity, correlates of protection, sex- and age-specific differences would contribute to faster vaccine design and ensure a personalized medication.

# 6. Supplement

## 6.1 Establishment of *in vitro* stimulation assays

To investigate induced immune signatures by the viral vector vaccines VSV-EBOV (Ervebo®) and MVA-EBOV *in vitro* stimulation assays were utilized. Initially, the infectivity of a 2nd line VSV-EBOV was tested following MOI titration and the determination of cell culture conditions. To confirm an effective viral stimulation flow cytometry and immunofluorescence analysis of *in vitro* stimulated hPBMCs were performed. In addition, viral RNA or DNA of *in vitro* stimulated samples were analyzed by qPCR.

### 6.1.1 Infectivity of 2nd line VSV-EBOV

The infectivity of a 2nd line VSV-EBOV, which was passaged by the infection of BHK cells, was measured by plaque assay (section 3.4). In S.1 representative sections of the infected wells of one replicate are shown for different dilutions.

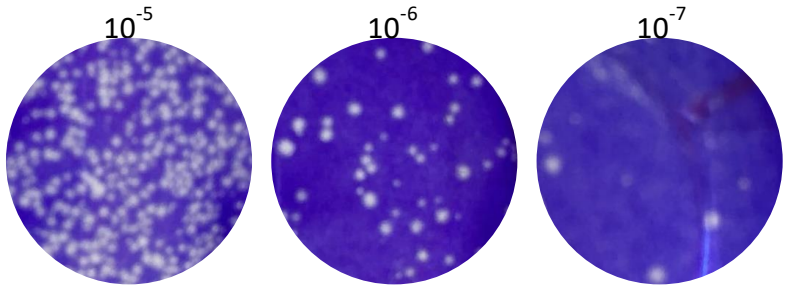


S.1: **Plaque assay of VSV-EBOV–infected Vero81 cells.** Vero81 cells were infected after reaching a confluent monolayer using a 2nd line VSV-EBOV (MOI 1) and stained with crystal violet 24 h post infection. The number of plaques were used to calculate the PFU/ml with formula [1]. Representative wells of three different 10-fold dilutions ($10^{-5}$, $10^{-6}$, and $10^{-7}$) of 2nd line VSV-EBOV stock are shown.

To analyze the number of infectious particles of the 2nd line VSV-EBOV stock solution the plaque forming units per ml (PFU/ml) were calculated using the formula [1].

[1] $$\frac{PFU}{ml} = \frac{(\sum plaques \cdot dilution\ factor\ a) + (\sum plaques \cdot dilution\ factor\ b)}{\frac{ml\ virus\ soultion}{well} \cdot number\ of\ wells\ counted}$$

In the case of a VSV-EBOV plaque assay two wells were infected with the same dilution resulting in the following values for formula [1]:

$$dilution\ factor\ a = 10^6$$
$$dilution\ factor\ b = 10^7$$
$$\sum plaques\ for\ dilution\ factor\ a = 160 + 161 = 321$$
$$\sum plaques\ for\ dilution\ factor\ b = 14 + 16 = 30$$
$$number\ of\ wells\ counted = 4$$
$$ml\ virus\ solution = 1$$

Values used in formula [1]:

$$\frac{PFU}{ml} = \frac{(321 \cdot 10^6) + (30 \cdot 10^7)}{1\,\frac{ml}{well} \cdot 4} = \frac{6.21 \cdot 10^8}{4\ ml} \approx 1.6 \cdot 10^8$$

The PFU/mL of $1.6 \cdot 10^8$ were utilized to calculate the amount of 2nd line VSV-EBOV stock solution for an MOI of 1, which was used for *in vitro* stimulations (section 3.5).

### 6.1.2 Cell culture conditions for *in vitro* stimulation assays

In this study sex-based differences of induced immune signatures by VSV-EBOV and MVA-EBOV were to be investigated (section 4.3). Since media supplements like FCS can contain variable concentrations of hormones including estrogen, serum-free media were tested prior to *in vitro* stimulations. To this end, a human monocytic cell line called THP-1 was used as a model for *in vitro* stimulations of hPBMCs. To induce a comprehensive cell response a lipopolysaccharide (LPS) stimulation was performed using 100 ng LPS. THP-1 were cultured during LPS stimulation in serum-free X-VIVO™ 15, RPMI-1640 or serum-containing RPMI-1640 + 10 % FCS. Afterwards, the amount of live cells and the activation status were measured by flow cytometry. Both serum-free and serum-supplemented media showed no

difference in the amount of live cells over time (S.2). Moreover, stimulated cells had the same amount of live cells compared to unstimulated cells over time (S.2).

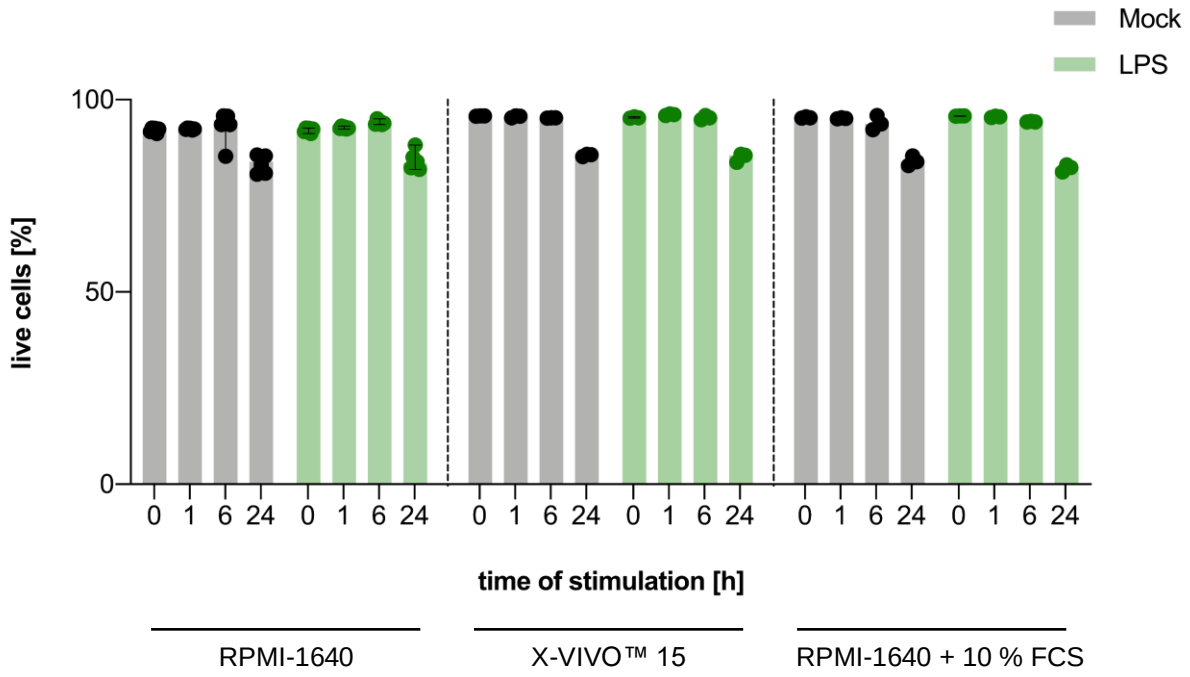


S.2: **Frequency of live THP-1 cells upon *in vitro* stimulation using LPS.** Serum-free (RPMI-1640 and X-VIVO™ 15) and serum-containing (RPMI-1640 + 10 % FCS) media were used for THP-1 stimulation assays. The cells were stimulated with 100 ng LPS. Afterwards, cells were stained (section 3.12) with the Zombie NIR™ viability dye and analyzed via flow cytometry. Besides, stimulated samples depicted in green also unstimulated samples depicted in black were investigated based on their frequency of live cells (negative for Zombie NIR™). Black error bars represent the 95 % CI of the median. RPMI-1640 N=6; X-VIVO™ 15 N=3; RPMI-1640 + 10 % FCS N=3.

The activation of THP-1 cells based on the expression of the activation marker CD40, CD83, and CD86 showed the same pattern over time on cells cultured in serum-free and serum-containing media (S.3). While the fold change of CD83 MFIs showed the highest differences between serum-free and serum-containing media, fold changes in the MFI of CD40 and CD86 showed only minor differences between the different culture conditions ranging from 0.95 to 1.1. Therefore, RPMI-1640 without any serum was used for *in vitro* stimulations of hPBMCs (section 4 and 6).

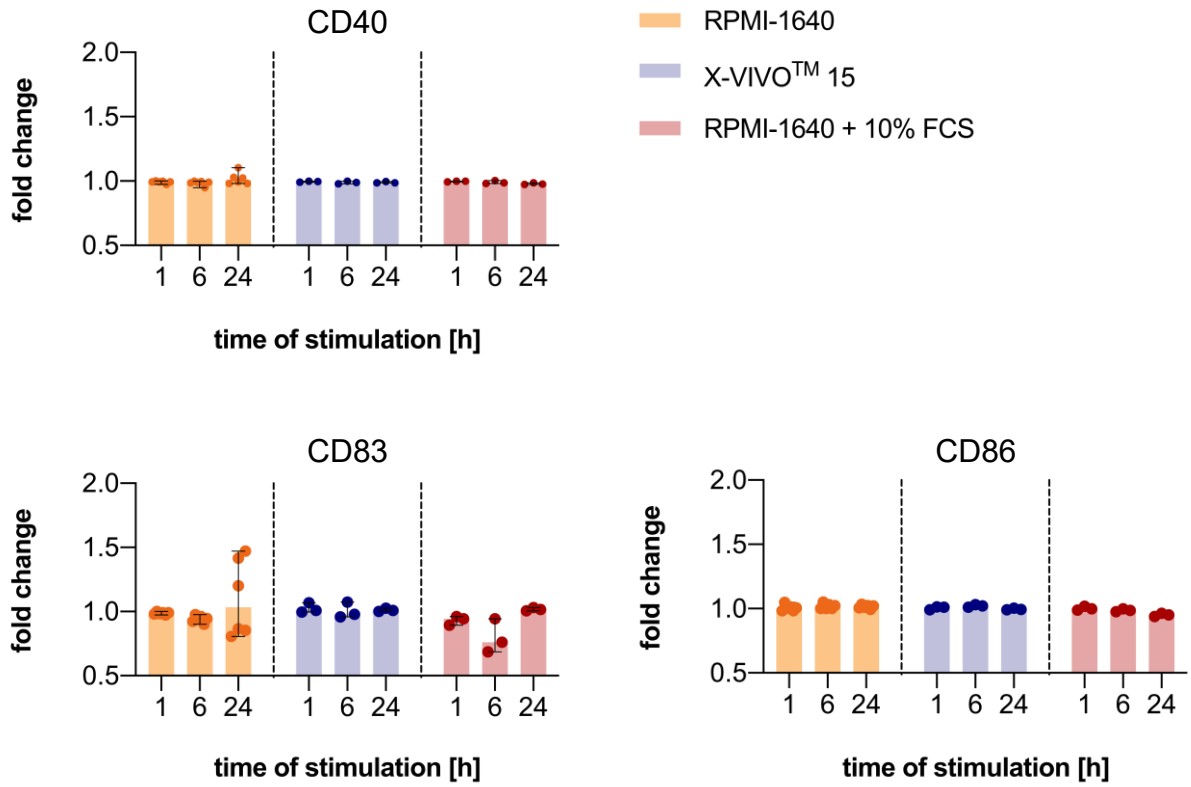


S.3: **Expression of activation markers on THP-1 cells upon *in vitro* stimulation using LPS.** Besides serum-free media (RPMI-1640 (orange) and X-VIVO™ 15 (blue)) also serum-containing medium (RPMI-1640 + 10 % FCS (red)) were used for *in vitro* stimulations. Cells were stimulated with 100 ng LPS. Afterwards, the expression of CD40, CD83, and CD86 of live cells were analyzed via flow cytometry (section 3.12, antibodies table 14). Fold changes to the specific unstimulated counterpart of stimulated samples are depicted. Black error bars represent the 95 % CI of the median. RPMI-1640 N=6; X-VIVO™15 N=3; RPMI-1640 + 10 % FCS N=3.

### 6.1.3 MOI titration

For further experiments the MOI was determined based on the literature [267,281–283] and cytokine secretion of whole hPBMCs upon *in vitro* stimulations using VSV-EBOV. Following hPBMC isolation (section 3.3.1) *in vitro* stimulations were performed with different MOIs of VSV-EBOV ranging from 0.001 to 1. Different TLR agonists like the TLR4 agonist LPS, TLR7 agonist imiquimod, and TLR9 agonist CpG were used as positive controls to validate the functionality of the *in vitro* stimulation assay. While for a LPS stimulation 100 ng/ml were used, imiquimod and CpG stimulations were performed with 5 µg/ml or 10 µg/ml, respectively. After 20 h of *in vitro* stimulation, the cell suspension was centrifuged for 3 min at 600 *x g* and 4°C. To investigate the cytokine secretion the supernatant was analyzed by a

pre-defined LEGENDplex™ by BioLegend (section 3.12.1). Since viral infections are of interest, a human anti-virus response panel including the analytes: IL-1β, IL-6, IL-8, IL-10, IL-12p70, IP-10, TNFα, IFNλ1, IFNλ2/3, IFNα2, IFNβ, IFNγ, and granulocyte-macrophage colony-stimulating factor (GM-CSF), was used. While the majority of analyzed cytokines showed an increasing cytokine secretion with enhanced MOIs, some cytokines like IFN-λ showed a decreased secretion upon a stimulation with MOI 0.01 (S.4).

Furthermore, a MOI of 1 showed a cytokine induction of IFNα, IFNβ, IL-6, and IP-10 indicating an anti-viral response of *in vitro* stimulated hPBMCs. In comparison to VSV-EBOV stimulations, imiquimod exhibited a higher IL-6 and IP-10 response but a lower secretion of IFNα and IFNβ. Only LPS led to a strong cell activation with high cytokine secretion of IL-6. Overall, the highest cytokine secretion of *in vitro* stimulated hPBMCs using VSV-EBOV was observed for a MOI of 1.

Since a stimulation with a MOI of 1 showed the highest cytokine induction and revealed no difference in the live count of THP-1 cells (cf. section 6.1.2, S.2), this MOI was used for further investigations (section 4 and 6).

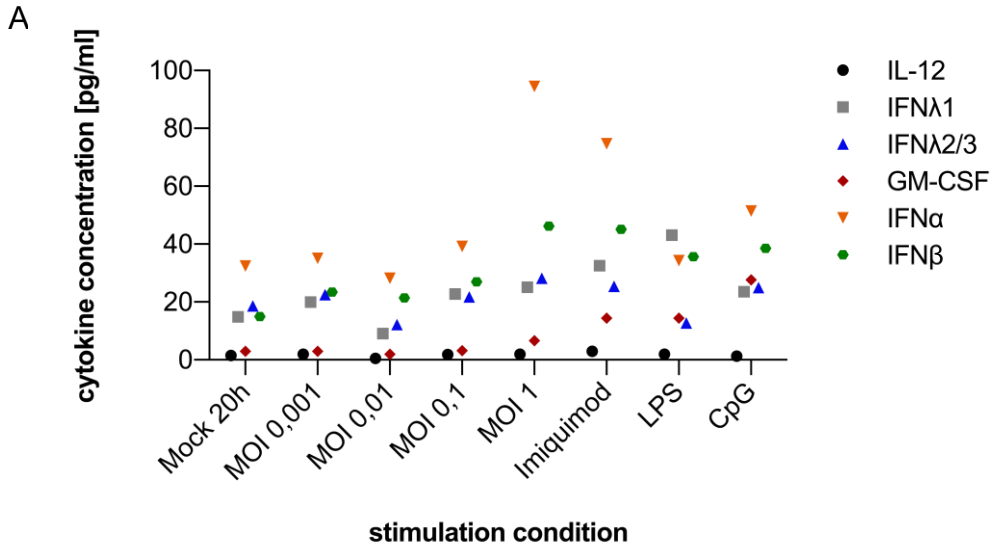


Figure legend depicted on page 123.

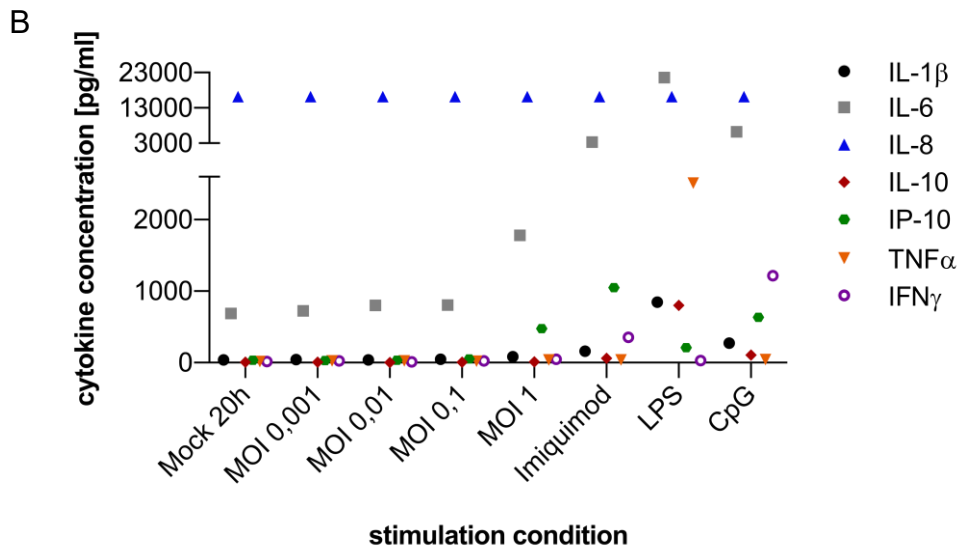


S.4: **Cytokine secretion of *in vitro* stimulated hPBMCs using VSV-EBOV and TLR agonists.** The cytokine profile of *in vitro* stimulated hPBMCs using different MIOs of VSV-EBOV (0.01-1), 100 ng/ml LPS, 5 µg/ml imiquimod or 10 µg/ml CpG, respectively, were analyzed by a pre-defined LEGENDplex™ (section 3.12.1 N=1). The human anti-virus response panel by BioLegend included the analytes: IL-1β, IL-6, IL-8, IL-10, IL-12p70, IP-10, TNFα, IFNλ1, IFNλ2/3, IFNα2, IFNβ, IFNγ, and GM-CSF. Each graph (A-B) represents different cytokines like depicted in the specific legend.

### 6.1.4 Flow cytometry analysis of *in vitro* stimulated hPBMCs using VSV-EBOV

Since primary hPBMCs were cultured in serum-free medium (cf. section 6.1.2), the stimulation assays of hPBMCs were used up to 24–48 h to investigate the immune signature upon stimulation. Moreover, hPBMCs do not proliferate in serum- and cytokine-free medium. Vero81 cells were used as a model for *in vitro* stimulations of human cells, since EBOV-infected cells could not be determined post 48 h via surface expression of EBOV proteins based on their absent expression. Also, other research groups could not detect EBOV proteins on the cell surface of infected cells prior 48 h. Vero81 cells were stimulated up to 48 h in serum-free medium using VSV-EBOV with a MOI of 1. Afterwards, the cells were stained with the Zombie Aqua™ viability dye by BioLegend and an anti-EBOV-GP FITC-conjugated antibody. All live cells which expressed the EBOV-GP on its surface were successfully stimulated by VSV-EBOV (S.5). While 6 h upon stimulation 2 % of all live Vero81 cells were positive for EBOV-GP (data not shown), 24 h after simulation 57 % of all live Vero81 cells were EBOV-GP$^+$ (S.5). In contrast, unstimulated samples revealed a background signal of up to 0.2 %.

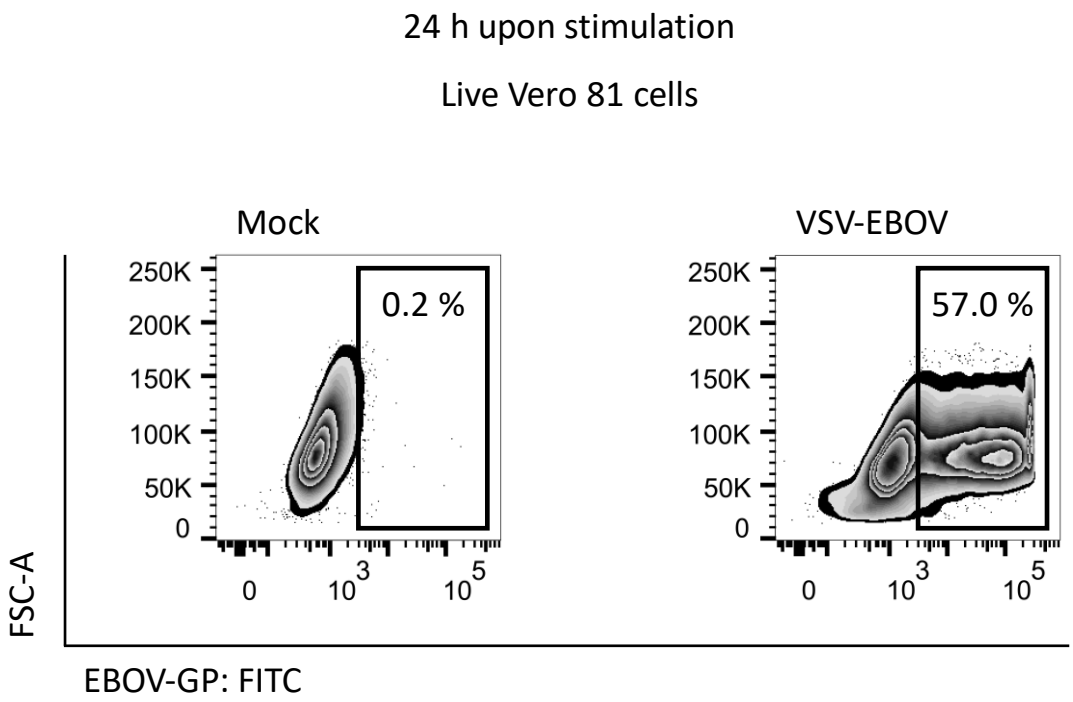


S.5: **Flow cytometry analysis of stimulated Vero81 cells using VSV-EBOV.** Stimulated (MOI 1) and unstimulated cells were stained with the Zombie Aqua™ viability dye by BioLegend and an anti-EBOV-GP FITC-conjugated antibody. Only live cells upon 24 h *in vitro* stimulations are shown. For a stimulated and unstimulated sample, the 5 % counter plot with outliers are depicted. Percentages indicate the frequency of EBOV-GP$^+$ live Vero81 cells (black rectangle).

### 6.1.5 Immunofluorescence & flow cytometry of *in vitro* stimulated hPBMCs using rMVA

To confirm an effective *in vitro* stimulation by MVA-EBOV a reporter-strain of the vector MVA was used. The reporter strain called recombinant MVA (rMVA) encodes for the green fluorescent protein (GFP) and a red fluorescent protein mCherry. Therefore, rMVA can directly be used to investigate stimulated cells via immunofluorescence. Vero81 cells and freshly isolated hPBMCs (section 3.3.1) were stimulated with rMVA (MOI 1) and analyzed after several time points. Following fixation, permeabilization, and blocking of unspecific binding sites, stimulated and unstimulated Vero81 cells as well as hPBMCs were stained with DAPI to visualize the nucleus of all cells (section 3.11). Afterwards, all samples were measured by a confocal laser scanning microscope XI-81 by Olympus. While Vero81 cells and hPBMCs express GFP 24 h upon stimulation at high level, not all Vero81 cells and no hPBMCs showed a signal for mCherry (S.6). Since GFP is under the control of an early promotor and mCherry

under the control of a late promotor, stimulated cells express GFP earlier than mCherry. However, some Vero81 cells expressed mCherry faster than hPBMCs confirming the results of an absent EBOV-GP expression in VSV-EBOV–stimulated hPBMCs, which would take more time (cf. section 6.1.4). Nevertheless, this high amount of GFP-expressing cells indicates a successful *in vitro* stimulation by rMVA.

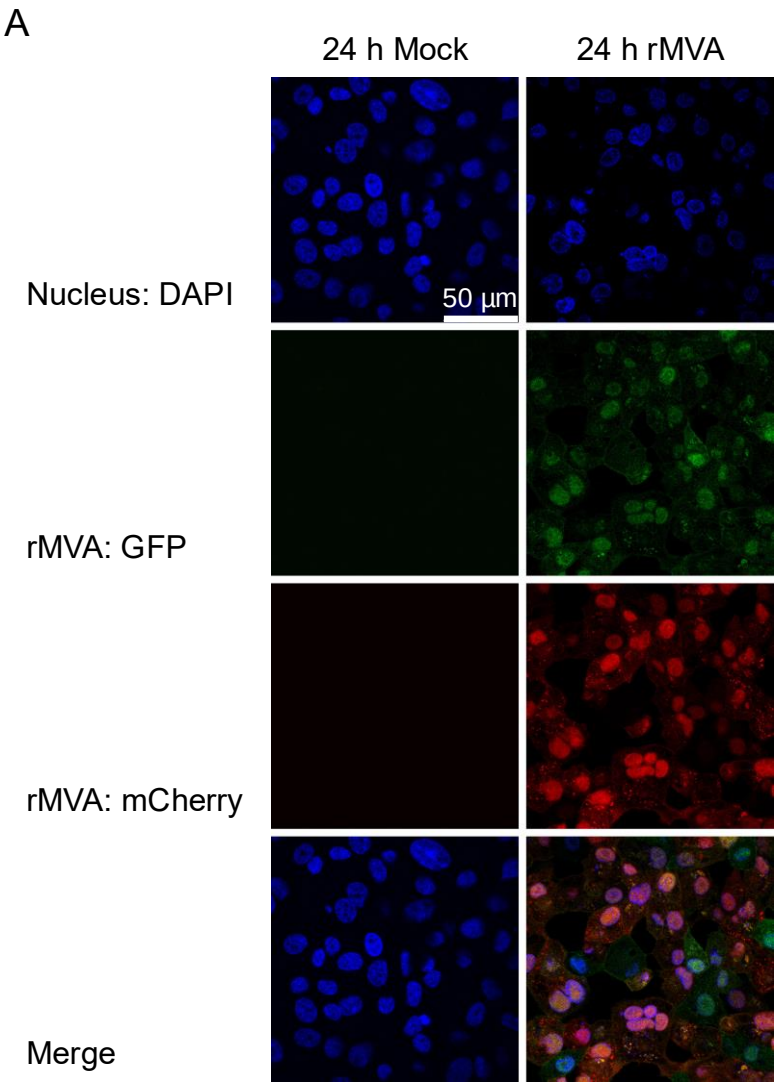


Figure legend depicted on page 126.

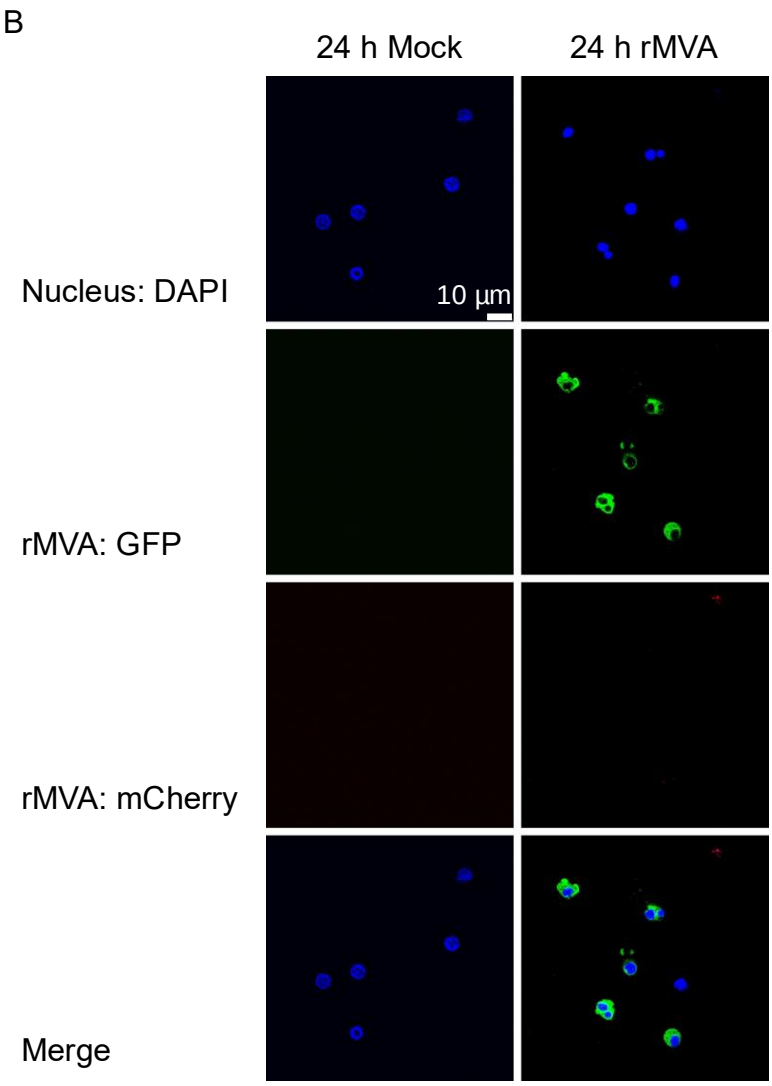


S.6: **Immunofluorescence of stimulated Vero81 cells and hPBMCs using rMVA.** A) Vero81 cells were cultured and *in vitro* stimulated (MOI=1) on polymer coverslips by ibidi®, whereas B) hPBMCs were *in vitro* stimulated in falcons and stained for immunofluorescence on coverslips. Stimulated and unstimulated cells were stained with DAPI to visualize the nucleus (blue signal). Green and red signals represent the expression of GFP and mCherry, respectively, which are encoded by rMVA. Besides single fluorescence measurements also the merge of all fluorescence signals is depicted. All samples were analyzed at 100x magnification with a confocal laser scanning microscope XI-81 by Olympus.

Moreover, the *in vitro* stimulation of hPBMCs using rMVA could be confirmed via flow cytometry. After stimulation, the cells were stained by a Zombie NIR™ viability dye (BioLegend) and various fluorescent conjugated antibodies (section 3.12, table 15) to distinguish between different immune cell subsets like B cells, T cells, NK cells, DCs, and monocytes. Although a MOI titration revealed that a MOI of 10 increased the amount of

rMVA$^+$ hPBMCs compared to a MOI of 1 (S.7 A), the following experiments were performed with a MOI of 1, due to a decreased amount of live cells (data not shown).

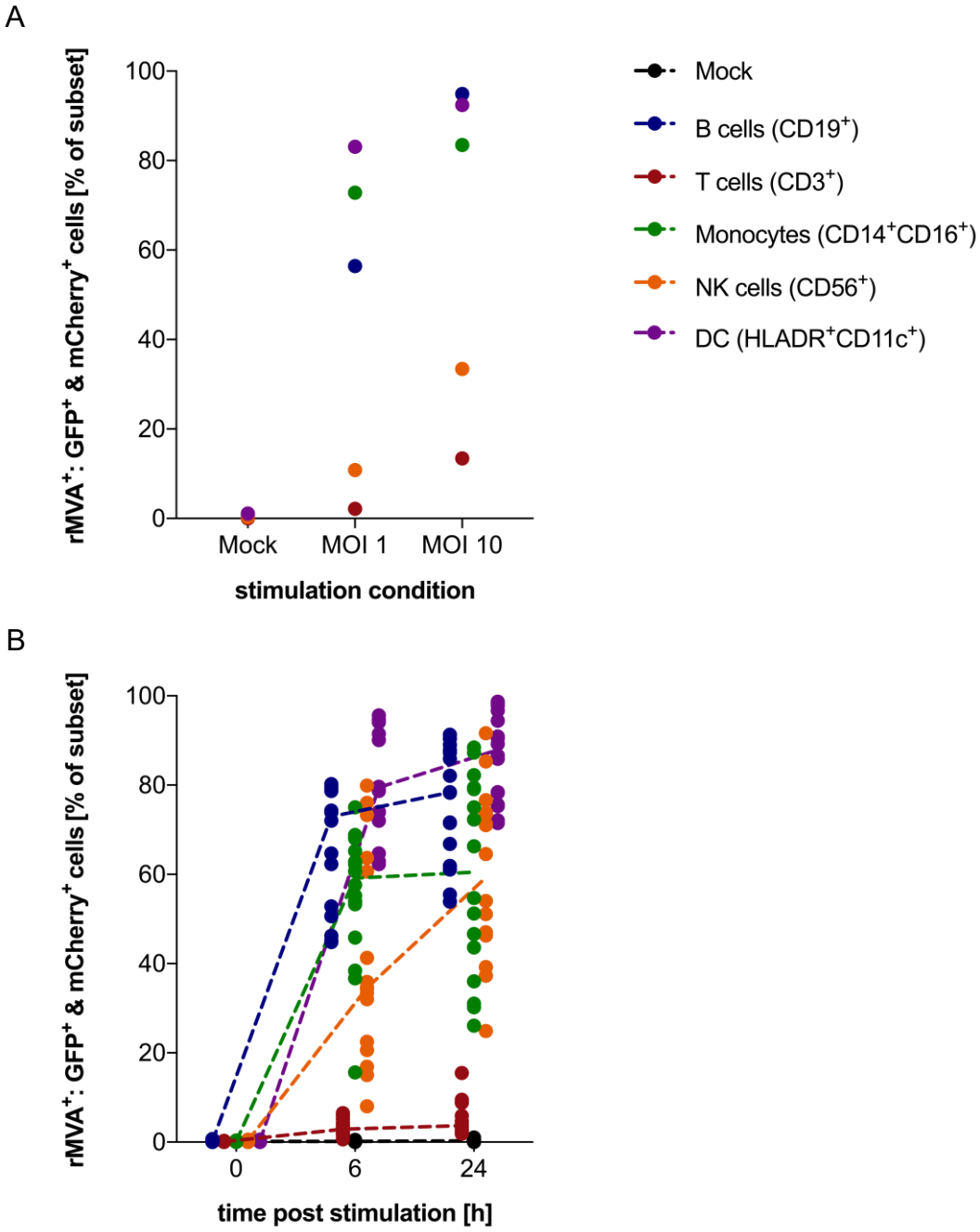


S.7: **Flow cytometry analysis of stimulated hPBMCs using rMVA.** The *in vitro* stimulation of hPBMCs were performed with a MOI of 1. After stimulation, the cells were stained with a Zombie NIR™ viability dye (BioLegend) and various fluorescent conjugated antibodies to distinguish between different immune cell subsets like B cells (CD19$^+$, blue), T cells (CD3$^+$, red), monocytes (CD14$^+$CD16$^+$, green), NK cells (CD56$^+$, orange), and DCs (HLADR$^+$CD11c$^+$, purple) (section 3.12, antibodies table 15). A) MOI titration (A; 24 h post-stimulation; N=1) and B) *in vitro* stimulations of several hPBMCs derived by different healthy donors (N=16, table 2) were performed. While each dot represents a different donor, the dotted lines indicate the median over time.

Furthermore, a MOI of 1 also exhibited a high amount of rMVA$^+$ immune cells 24 h upon stimulation.

The *in vitro* stimulation of hPBMCs derived from 16 healthy donors revealed a distinct amount of rMVA$^+$ immune cell subsets based on the immune cell type (S.7B). While the highest amount of rMVA$^+$ cells was observed for live B cells (CD19$^+$) and DCs (HLADR$^+$ CD11$^+$) 24 h after stimulation with a median of 78.4 % and 87.9 %, respectively, T cells (CD3$^+$) exhibited in median 3.7 % rMVA$^+$ cells. In conclusion, the *in vitro* stimulation using rMVA with a MOI of 1 could be confirmed via immunofluorescence and flow cytometry. Therefore, also MVA-EBOV *in vitro* stimulations were performed with a MOI of 1.

### 6.1.6 Detection of viral RNA/DNA

To validate an *in vitro* stimulation of hPBMCs using VSV-EBOV or MVA-EBOV, respectively, a qPCR was performed. Following stimulation (section 3.5) the total RNA and DNA of stimulated and unstimulated samples was isolated (section 3.6 & 3.7) and analyzed by qPCR (section 3.8.2) using NP-specific primer for VSV and UDG-specific primer for MVA. Both stimulations exhibited high copy numbers of NP and UDG, respectively, over time, whereas unstimulated samples showed no copy number at all (S.8). Hence, *in vitro* stimulations using VSV-EBOV and MVA-EBOV were also confirmed on the RNA/DNA-level.

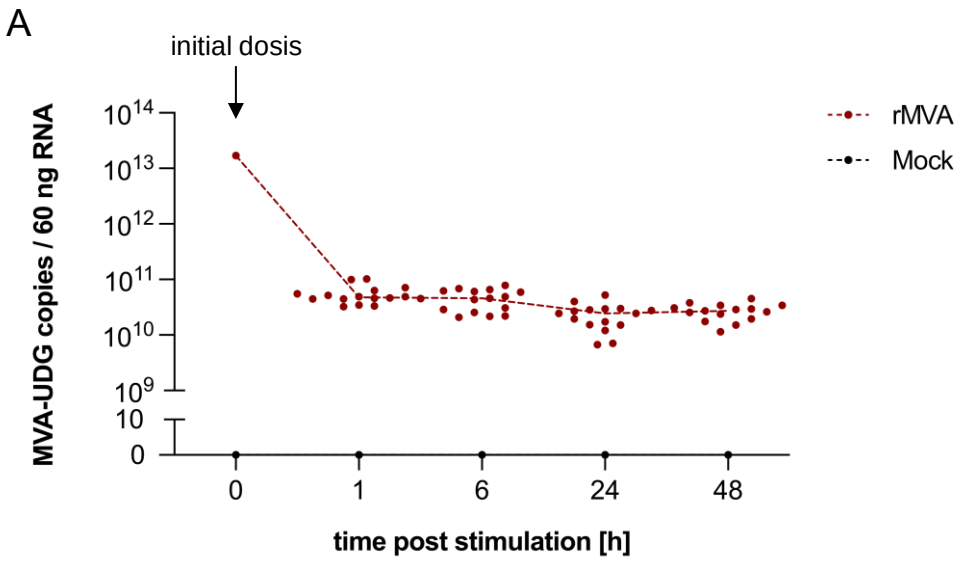


Figure legend depicted on page 129.

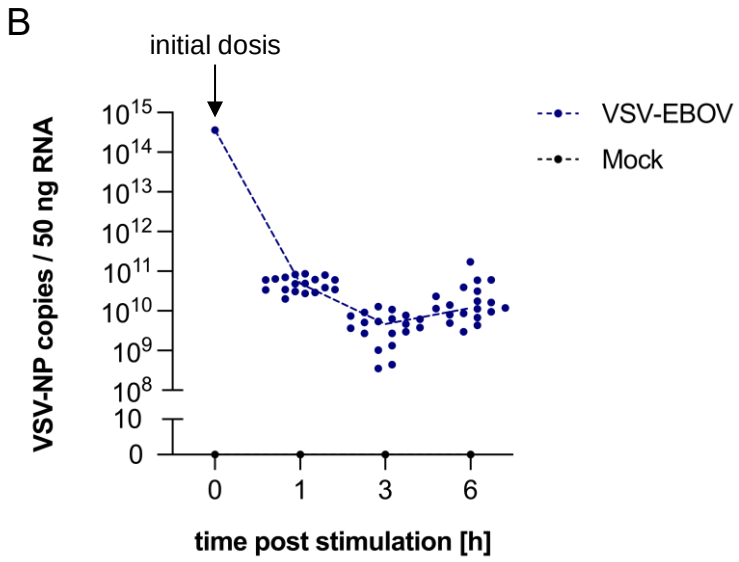


S.8: **Detection of viral DNA/RNA of rMVA and VSV-EBOV.** *In vitro* stimulations with A) rMVA or B) VSV-EBOV (MOI=1) were confirmed by qPCR using VSV-NP or MVA-UDG−specific primer (section 3.8.3, primer sequence table 11). Each dot represents a different donor (rMVA N=16, table 2; VSV-EBOV N=20, table 3). The dotted line indicates the median over time. Initial dose for rMVA represents the copy number that was used for one experiment to stimulate $20 \cdot 10^6$ cells of one donor. Initial dose for VSV-EBOV indicates the copy number that was used for one experiment to stimulate $35 \cdot 10^6$ cells of one donor.

## 6.2 Establishment of analytic methods for *in vitro* stimulation assays

### 6.2.1 Stability of housekeeping genes in stimulated samples

The expression of four housekeeping genes of *in vitro* stimulated hPBMCs using VSV-EBOV derived from ten donors was investigated to determine the most stable expressed housekeeping gene over time. Total RNA of VSV-EBOV−stimulated and unstimulated samples was isolated (section 3.7) and analyzed with a semi-qPCR using primers for hydroxymethylbilane synthase (HMBS), hypoxanthine phosphoribosyltransferase 1 (HPRT), glycerinaldehyd-3-phosphat dehydrogenase (GAPDH), and actin beta (ActB) (section 3.8.5, table 11). Since HPRT was the most stable housekeeping gene over time in stimulated and unstimulated samples (S.9), this housekeeping gene was used as a reference gene in relative expression analysis using the ΔΔCt method ($2^{-\Delta\Delta Ct}$) (section 3.8.6).

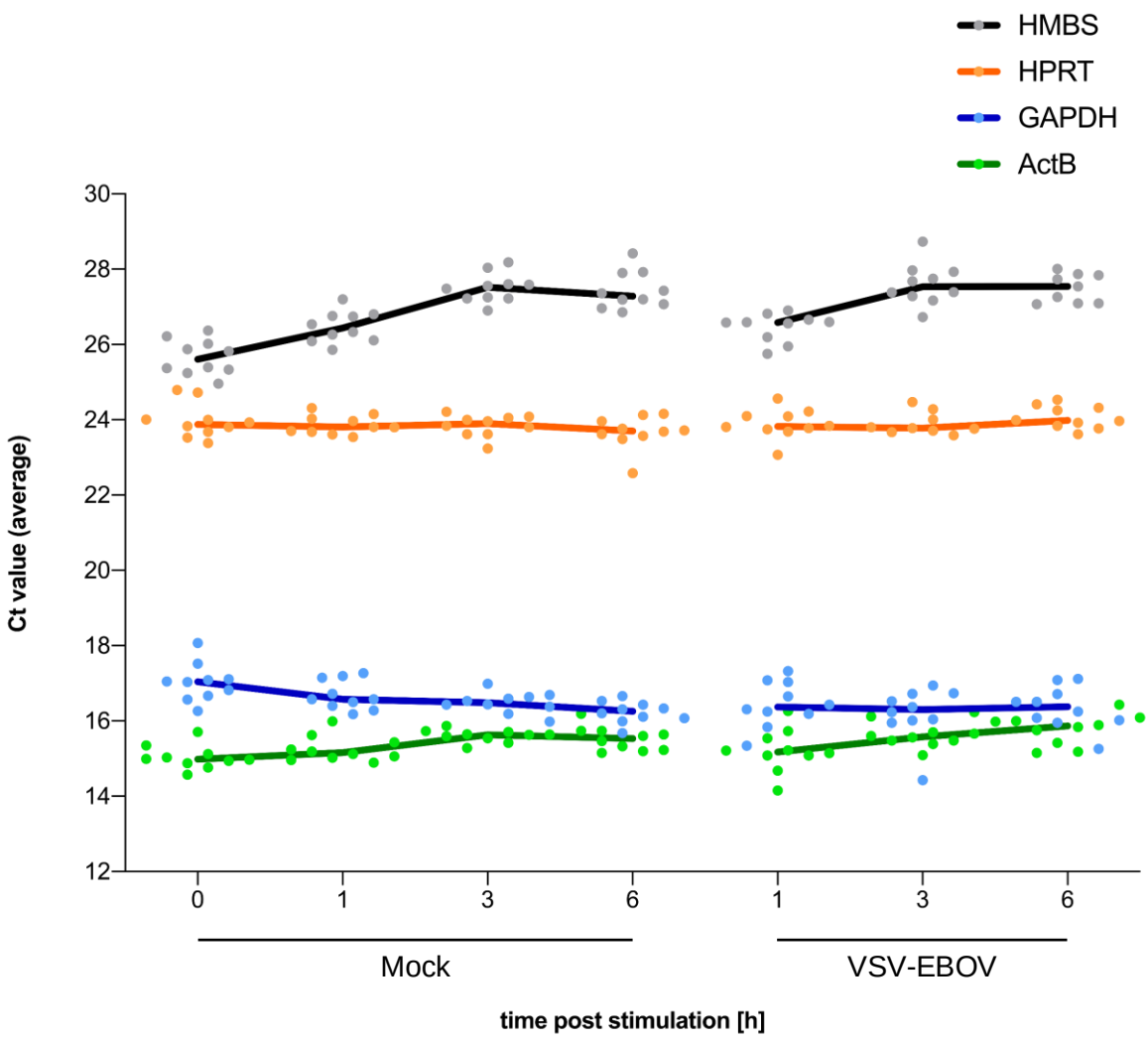


S.9: **Expression of housekeeping genes upon stimulation using VSV-EBOV.** The expression of four housekeeping genes upon *in vitro* stimulations of hPBMCs derived from 10 donors were investigated over time (section 2.2, table 3). Stimulations were utilized using VSV-EBOV with a MOI of 1. Total RNA of VSV-EBOV–stimulated and unstimulated samples was isolated (section 3.7) and analyzed with a semi-qPCR using specific primers for hydroxymethylbilane synthase (HMBS, black), hypoxanthine phosphoribosyltransferase 1 (HPRT, orange), glycerinaldehyd-3-phosphat dehydrogenase (GAPDH, blue), and actin beta (ActB, green) (section 3.8.5, primer sequence table 11). Values for threshold cycles (Ct values) of duplicates are shown. Each dot indicates a different donor, whereas the line represents the median over time.

### 6.2.2 Titration of fluorochrome-conjugated antibodies

Prior to analyses of *in vitro* stimulated hPBMCs using flow cytometry, fluorochrome-conjugated antibodies were titrated to use an optimal amount for cell staining. To this end, $1 \cdot 10^6$ hPBMCs were stained in 100 µl FACS-buffer with indicated amounts of fluorochrome-conjugated antibodies (section 3.12) and analyzed using the BD LSRFortessa™ (S.10).

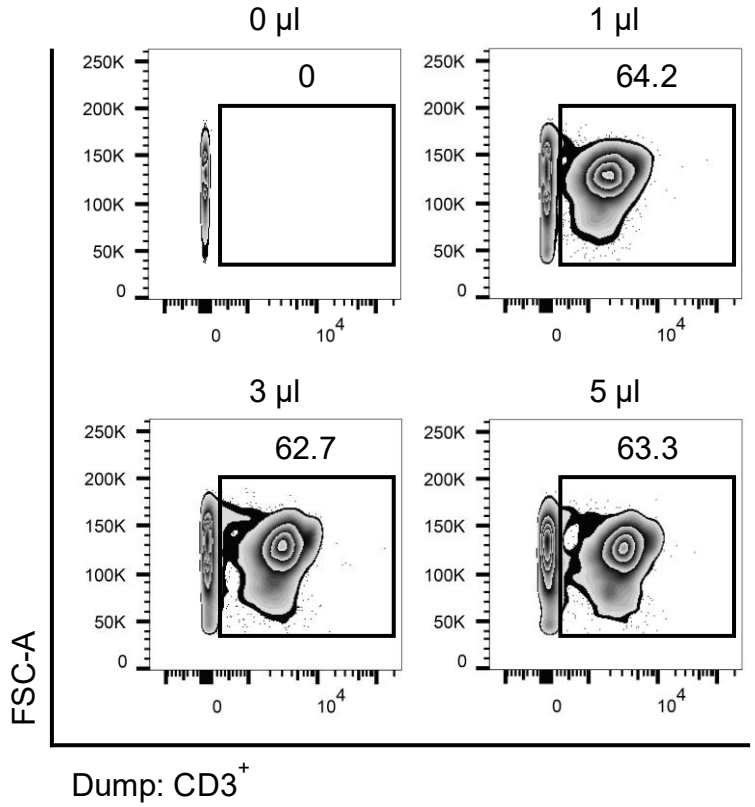


S.10: **Titration of fluorochrome-conjugated antibodies.** To perform flow cytometry analysis with an optimal amount of fluorochrome-conjugated antibodies (cf. following pages 131–135), crucial antibodies were titrated. To this end, $1 \cdot 10^6$ hPBMCs were stained in 100 µl FACS-buffer with indicated amounts of fluorochrome-conjugated antibodies (section 3.12, antibodies table 14) and analyzed using the BD LSRFortessa™. Data were analyzed using FlowJo and depicted in smooth zebra plots with outliers. Black squares indicate positive cells with their specific frequency.

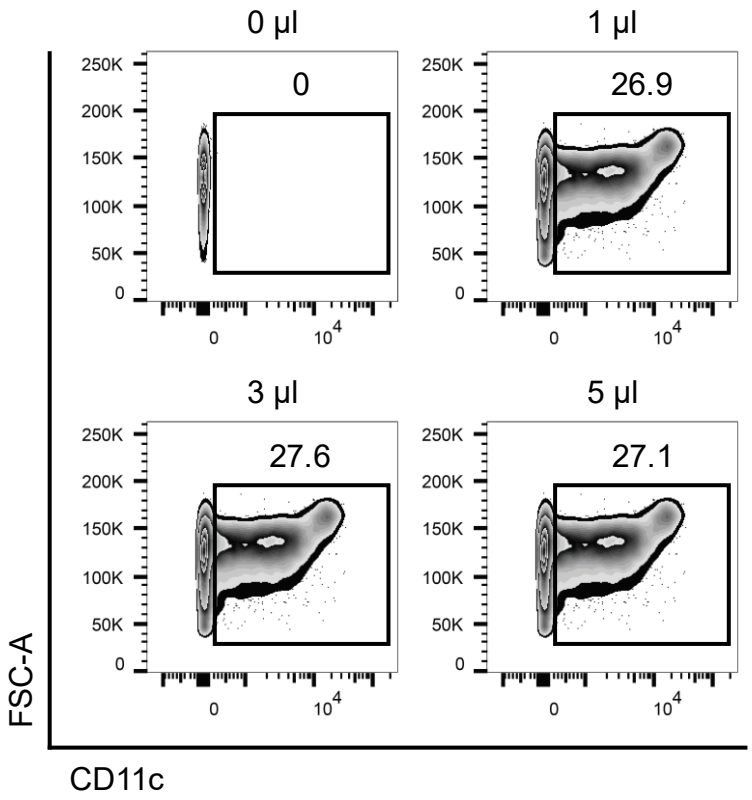


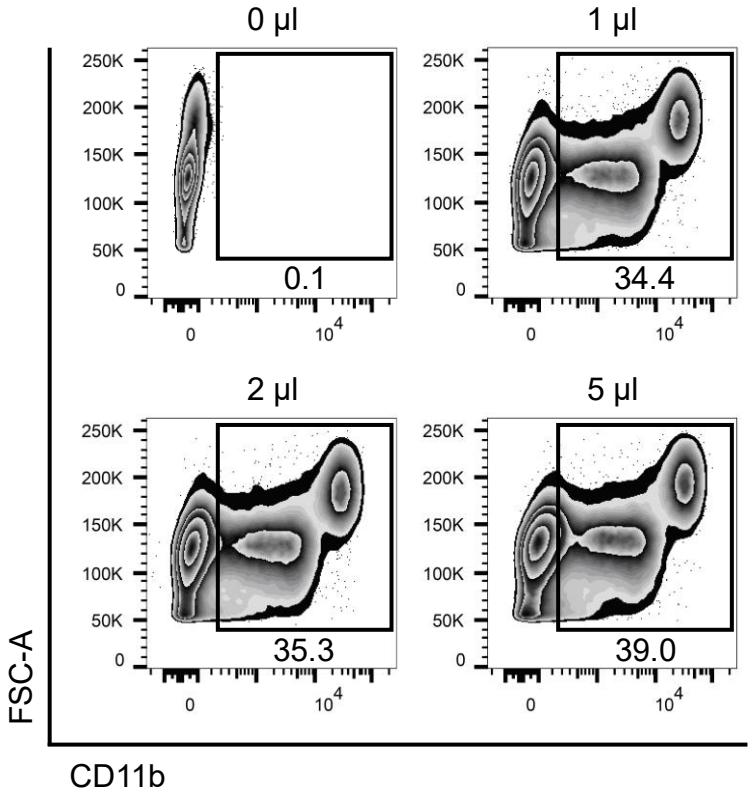


Figure legend depicted on page 131.

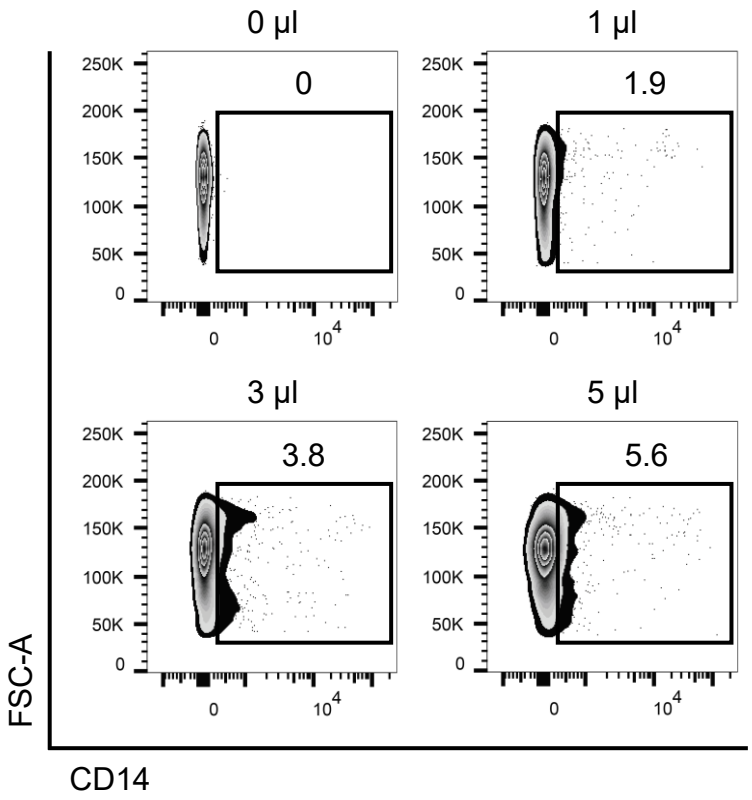


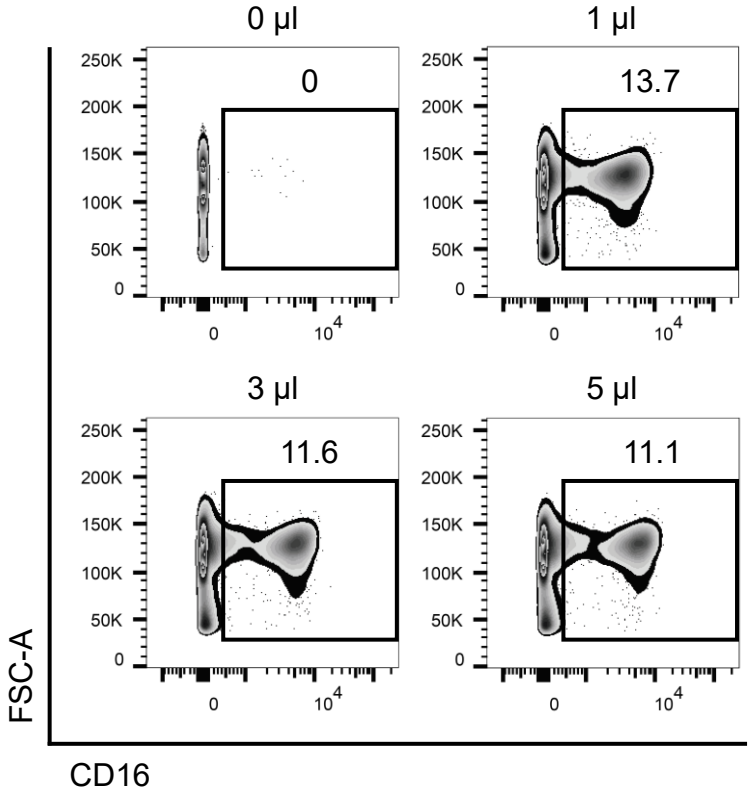


Figure legend depicted on page 131.

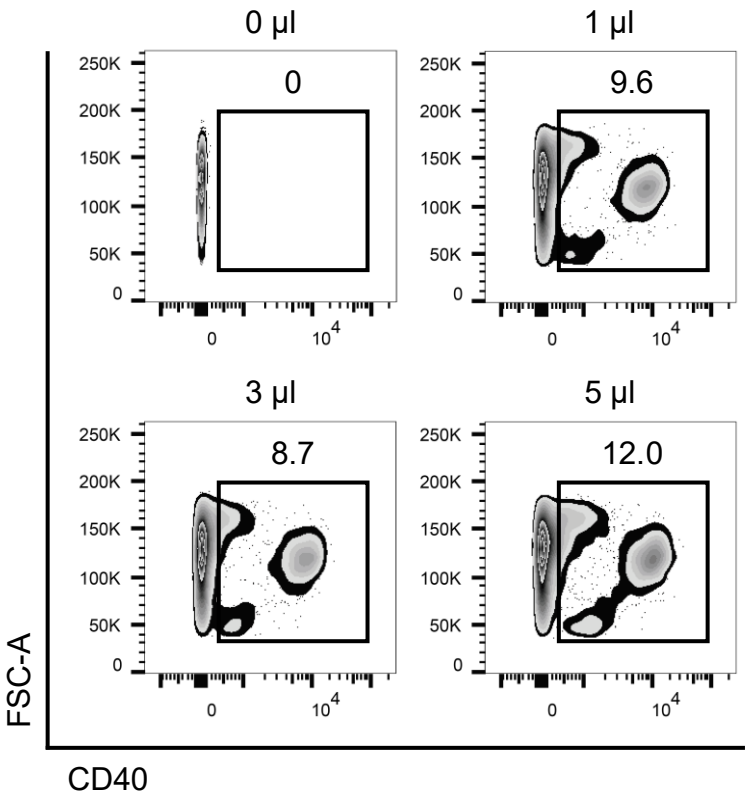


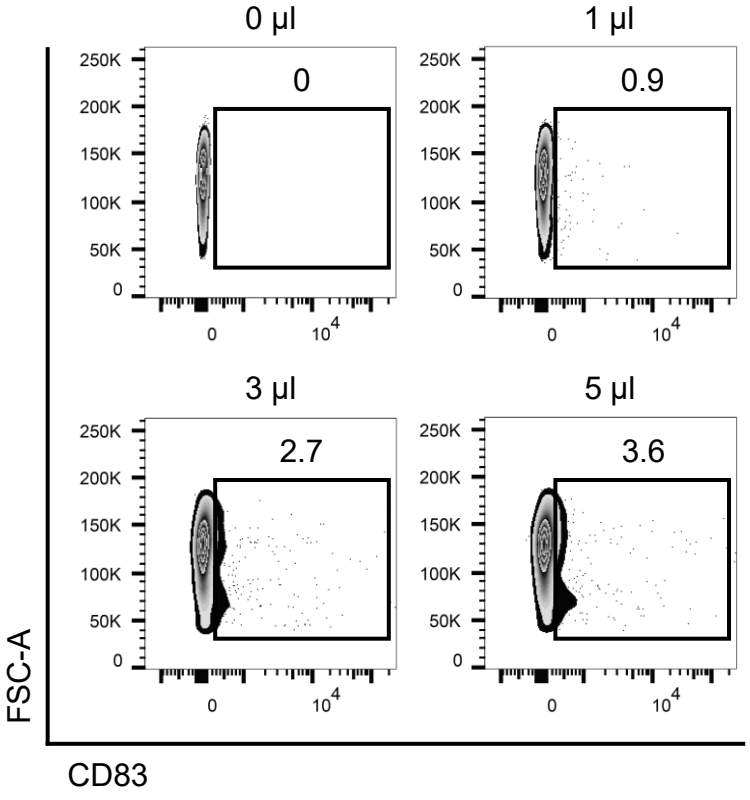


Figure legend depicted on page 131.

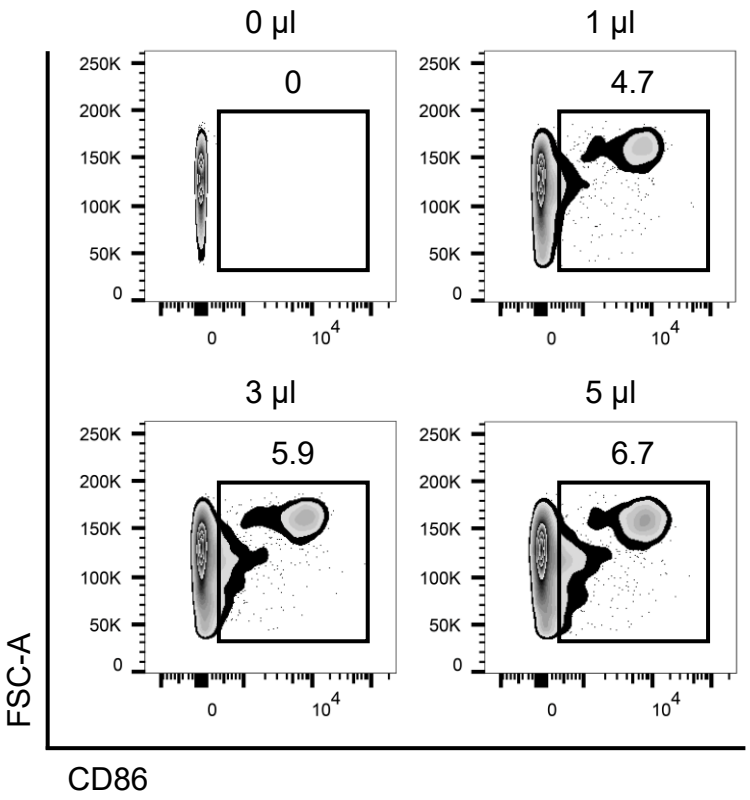


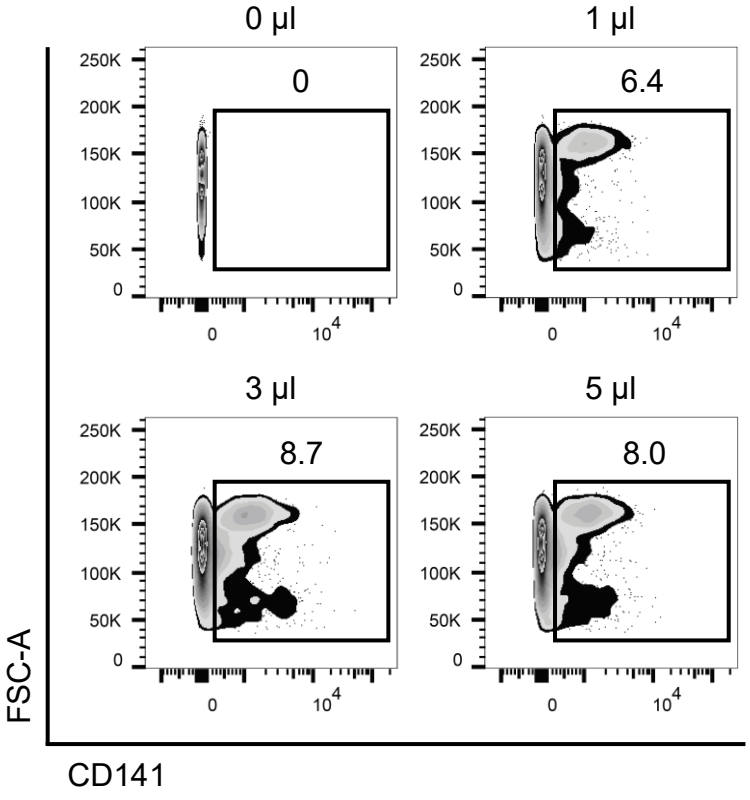


Figure legend depicted on page 131.

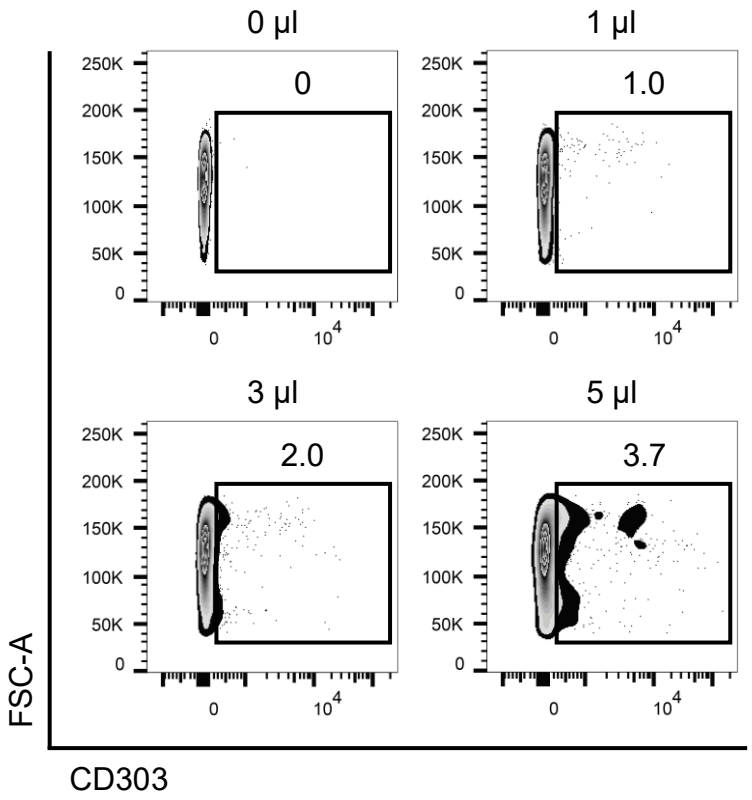


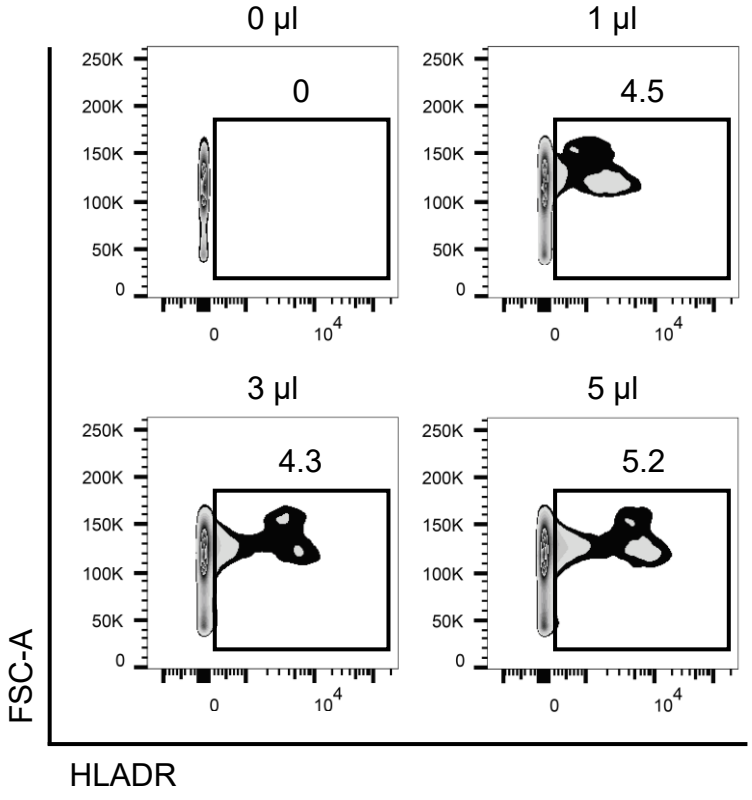


Figure legend depicted on page 131.

## 6.3 Activation of DC subsets upon VSV-EBOV and MVA-EBOV stimulation

To investigate the activation status of different DC subsets upon VSV-EBOV or MVA-EBOV stimulation (section 3.5), the expressions of CD40, CD83, and CD86 (S.11–14) were analyzed via flow cytometry (section 3.12). The gating strategy for all DC subsets: pDCs, $CD16^+$ DCs, $CD141^+$ DCs, and $CD1c^+CD11c^+$ DCs is shown in figure 12 (section 4.1.2).

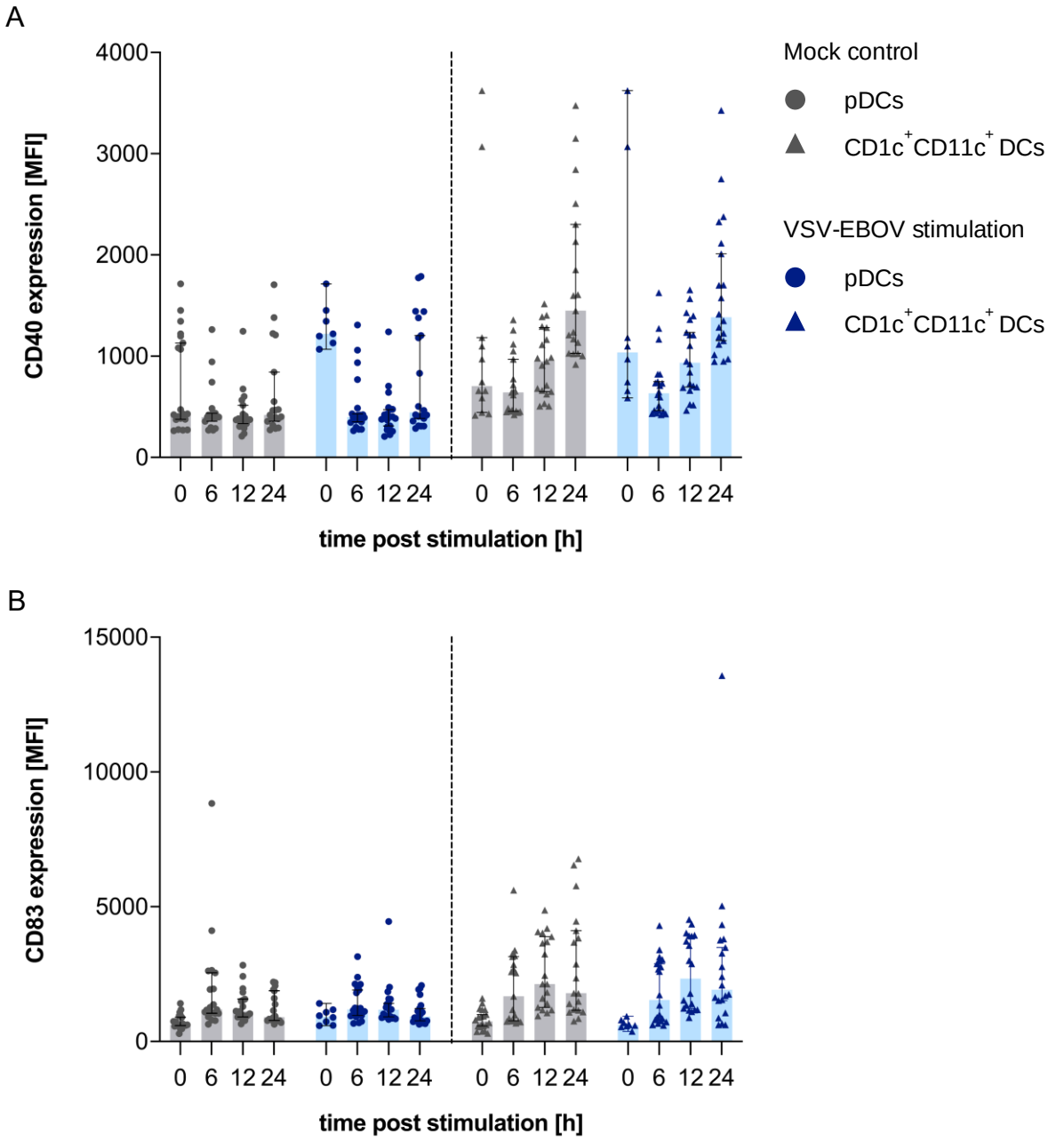


S.11: **Expression of activation markers on DCs upon stimulation using VSV-EBOV.** The expression of A) CD40 and B) CD83 on pDCs and $CD1c^+CD11c^+$ DCs were analyzed via flow cytometry and corresponding cell staining (section 3.12, antibodies table 14) upon *in vitro* stimulation of whole hPBMCs using VSV-EBOV (MOI 1). All samples were gated as described in figure 12. Besides stimulated (blue) also unstimulated samples (grey) were investigated based on the MFI of CD40 and CD83. Dots indicate pDCs and triangle $CD1c^+CD11c^+$ DCs. The maximum of each bar represents the median including error bars indicating the 95 % CI. No statistically significant differences in the expression of CD40 and CD83 were detected using the t-test based unpaired, nonparametric Mann-Whitney test. The p-values are indicated as follows: $p \leq 0.05$ *; $p \leq 0.01$ **; $p \leq 0.001$ ***; $p \leq 0.0001$ ****. Analyzed samples N=20 (section 2.2, table 3).

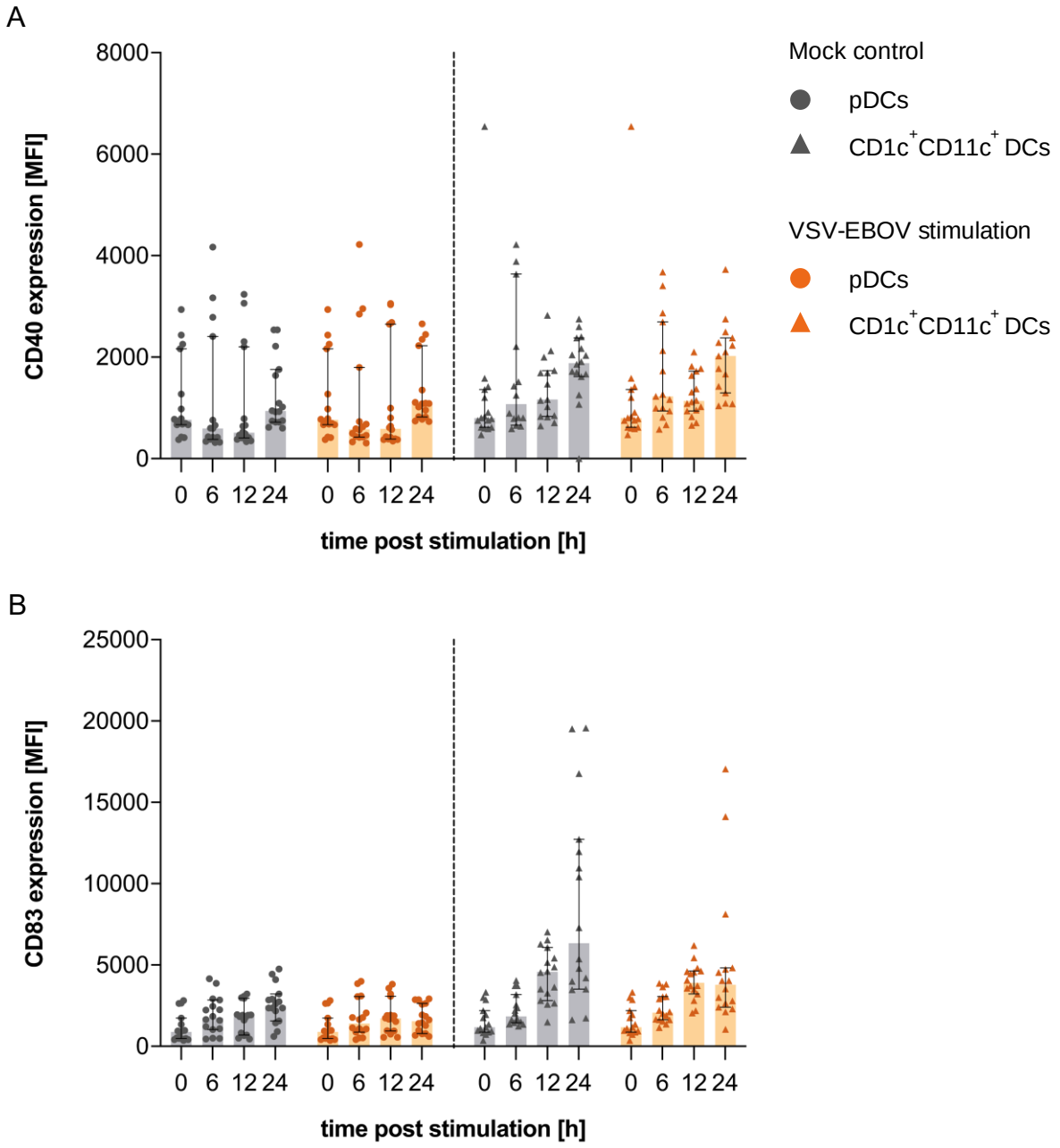


S.12: **Expression of CD40 and CD83 on DCs upon stimulation using MVA-EBOV.** The expression of A) CD40 and B) CD83 on pDCs and $CD1c^+CD11c^+$ DCs were analyzed by flow cytometry and corresponding cell staining (section 3.12, antibodies table 14) upon *in vitro* stimulation of whole hPBMCs using MVA-EBOV (MOI 1). All samples were gated as described in figure 12. Besides stimulated (orange) also unstimulated samples (grey) were investigated based on the MFI of CD40 and CD83. Dots indicate pDCs and triangle $CD1c^+CD11c^+$ DCs. The maximum of each bar represents the median including error bars indicating the 95 % CI. No statistically significant differences in the expression of CD40 and CD83 were detected using the t-test based unpaired, nonparametric Mann-Whitney test. The p-values are indicated as follows: $p \leq 0.05$ *; $p \leq 0.01$ **; $p \leq 0.001$ ***; $p \leq 0.0001$ ****. Analyzed samples N=16 (section 2.2, table 4).

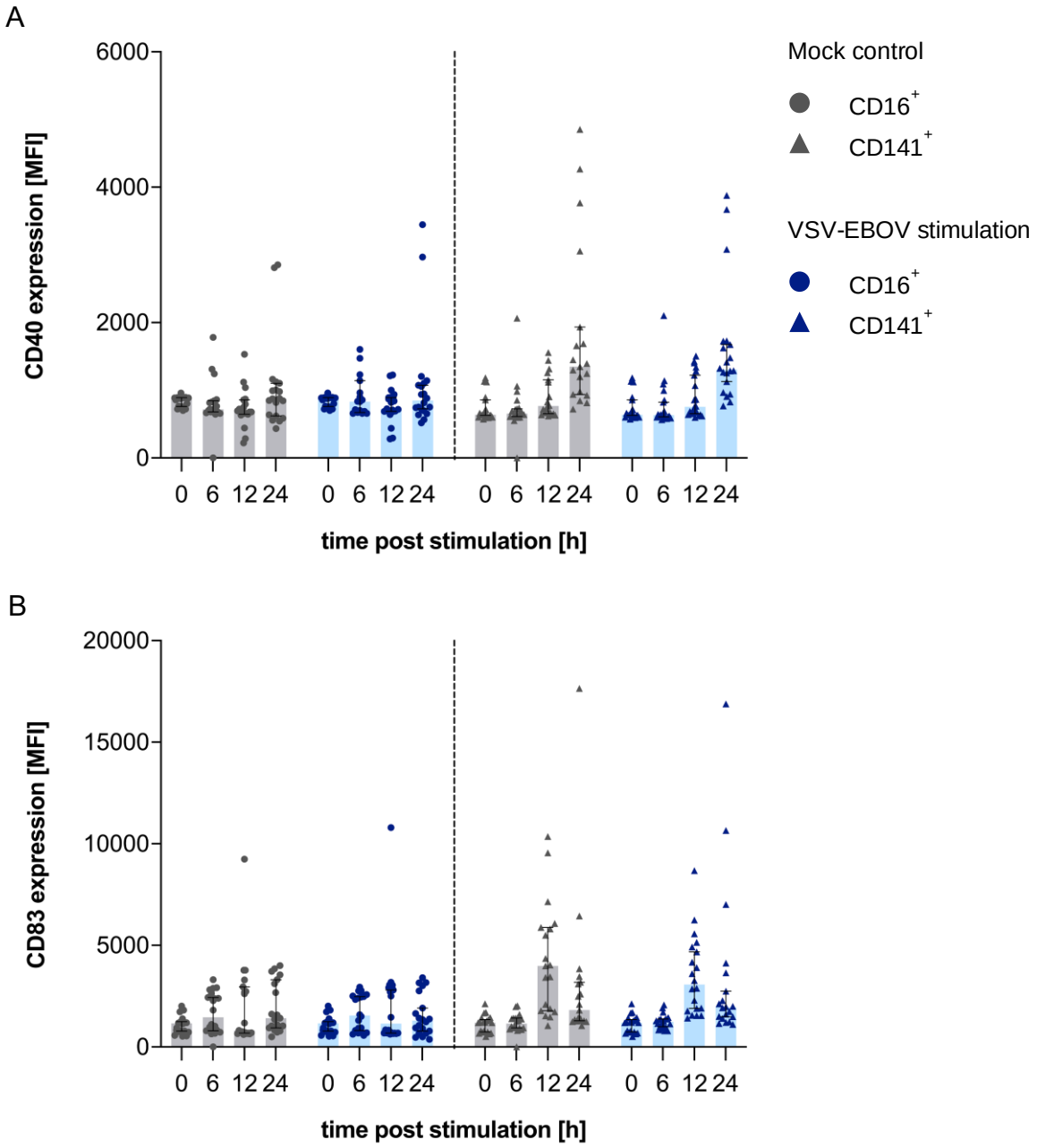


S.13: **Expression of activation markers on DCs upon stimulation using VSV-EBOV.** The expression of CD40 and CD83 on $CD16^+$ DCs and $CD141^+$ DCs were analyzed via flow cytometry and corresponding cell staining (section 3.12, antibodies table 14) upon *in vitro* stimulation of whole hPBMCs using VSV-EBOV (MOI 1). All samples were gated as described in figure 12. Besides stimulated (blue) also unstimulated samples (grey) were investigated based on the MFI of CD40 and CD83. Dots indicate $CD16^+$ DCs and triangle $CD141^+$ DCs. The maximum of each bar represents the median including error bars indicating the 95 % CI. No statistically significant differences in the expression of CD40 and CD83 were detected using the t-test based unpaired, nonparametric Mann-Whitney test. The p-values are indicated as follows: $p \leq 0.05$ *; $p \leq 0.01$ **; $p \leq 0.001$ ***; $p \leq 0.0001$ ****. Analyzed samples N=20 (section 2.2, table3).

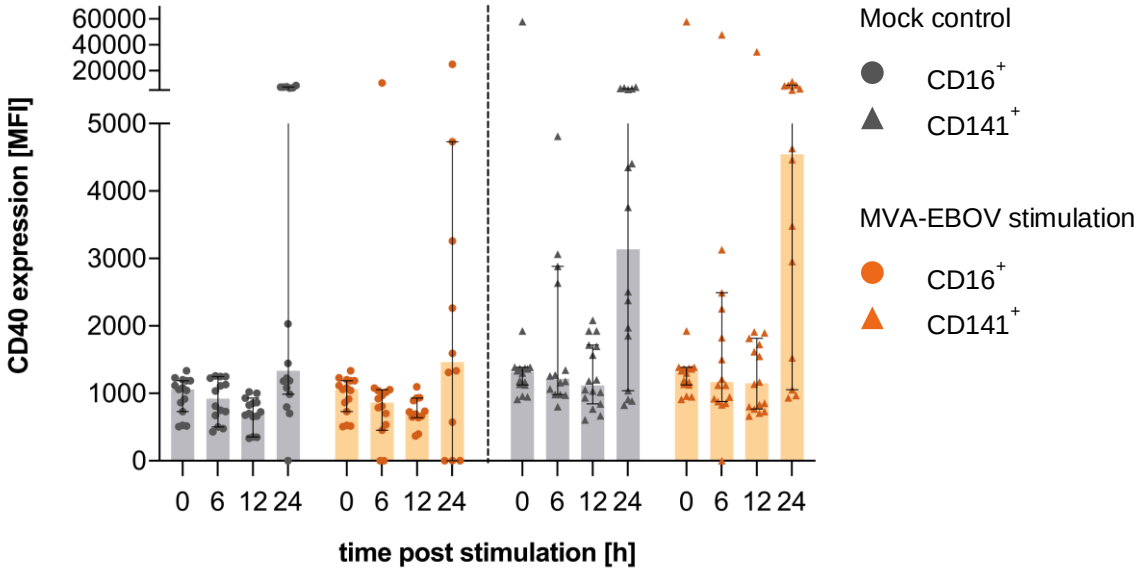


S.14: **Expression of CD40 on DCs upon stimulation using MVA-EBOV.** The expression of CD40 was analyzed via flow cytometry and corresponding cell staining (section 3.12, antibodies table 14) upon *in vitro* stimulation of whole hPBMCs using MVA-EBOV (MOI 1). All samples were gated as described in figure 12. Besides stimulated (orange) also unstimulated samples (grey) were investigated based on the MFI of CD40. Dots indicate $CD16^+$ DCs and triangle $CD141^+$ DCs. The maximum of each bar represents the median including error bars indicating the 95 % CI. No statistically significant differences in the expression of CD40 was detected using the t-test based unpaired, nonparametric Mann-Whitney test. The p-values are indicated as follows: $p \leq 0.05$ *; $p \leq 0.01$ **; $p \leq 0.001$ ***; $p \leq 0.0001$ ****. Analyzed samples N=16 (section 2.2, table 4).

## 6.4 Transcriptomic changes upon *in vitro* stimulation

### 6.4.1 Semi-qPCR of *IP-10* and *CLEC5A*

The expression of *IP-10* and *CLEC5A* was investigated via semi-qPCR (section 3.8.5). First, the relative expression of both genes to unstimulated 0 h was calculated with the ΔΔCt method ($2^{-\Delta\Delta Ct}$). This analysis revealed an induction of *IP-10* and *CLEC5A* over time peaking at 6 h post-stimulation (S.15).

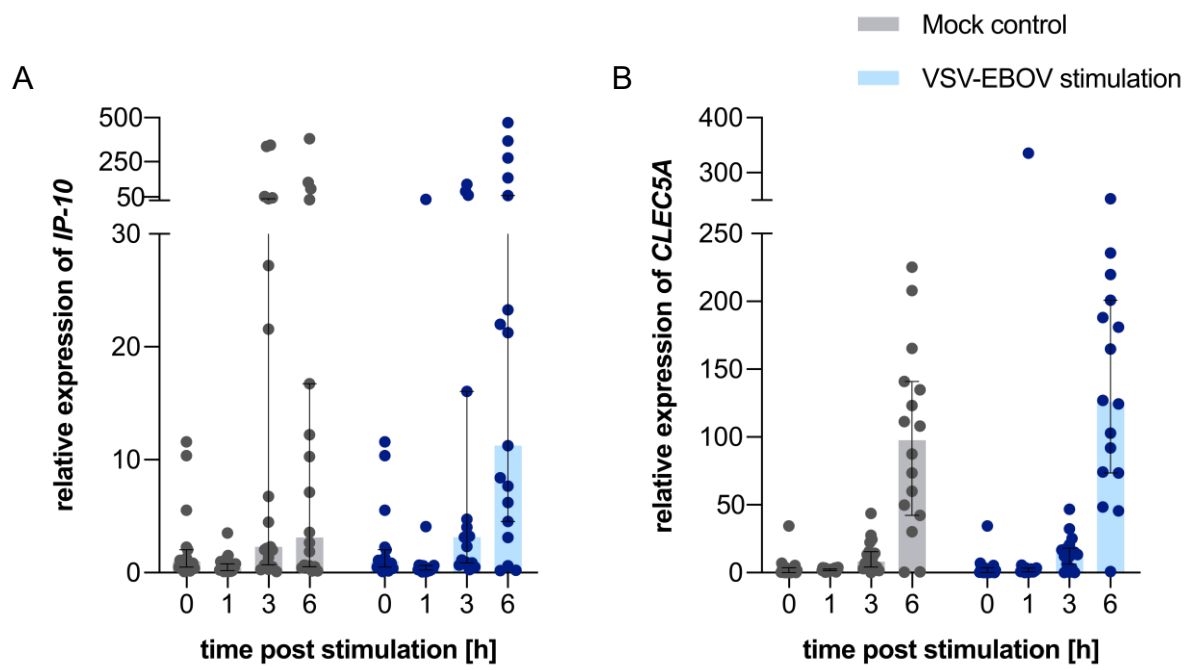


S.15: **Relative expression of *IP-10* and *CLEC5A* after VSV-EBOV *in vitro* stimulation.** Total RNA of 0 h, 1 h, 3 h, and 6 h was isolated upon *in vitro* stimulations using VSV-EBOV (MOI 1) and analyzed by semi-qPCR (section 3.8.5, primer sequence table 11). Besides stimulated (blue) also unstimulated samples (grey) were investigated at indicated time points. Each dot represents a different blood donor (N=20, section 2.2, table 3). The maximum of each bar shows the median including error bars indicating the 95 % CI. A) the relative expression of *IP-10* is shown. B) The relative expression of *CLEC5A* is depicted. Relative expressions were calculated with the ΔΔCt method (section 3.8.6).

### 6.4.2 RNA-Seq: hierarchical clustering heat maps

Total RNA of *in vitro* stimulated 6 h and unstimulated 0 h and 6 h was analyzed using RNA-Seq. Whole gene expression profiles upon *in vitro* stimulation using VSV-EBOV (S.16) or MVA-EBOV (S.17) depicted in hierarchical clustering heat maps were distinct between stimulations of both viral vector vaccines as wells as between their specific unstimulated counterparts.

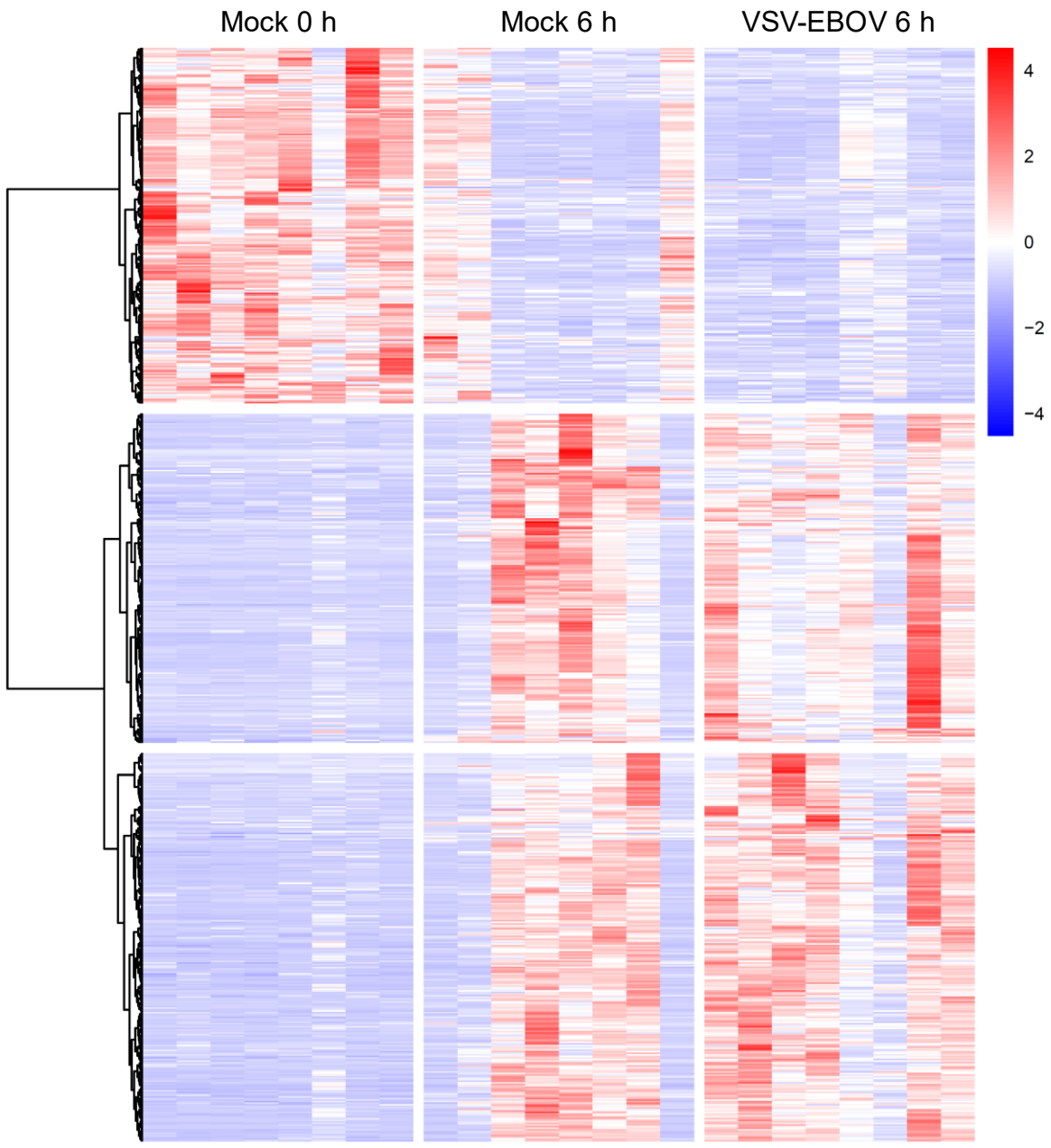


S.16: **Hierarchical clustering heat map of DEG upon VSV-EBOV stimulation.** Total RNA of 6 h *in vitro* VSV-EBOV−stimulated (MOI 1) and unstimulated samples (N=8, section 2.2, table 5) was analyzed via RNA-Seq (section 3.10). Genes which exhibited a log2 fold change ≤ -1.5 or ≥ 1.5 and an FDR < 0.01 were counted as DEG. Besides unstimulated 0 h and 6 h controls, also 6 h stimulated samples are depicted. Each condition is separated in further columns indicating different blood donors.

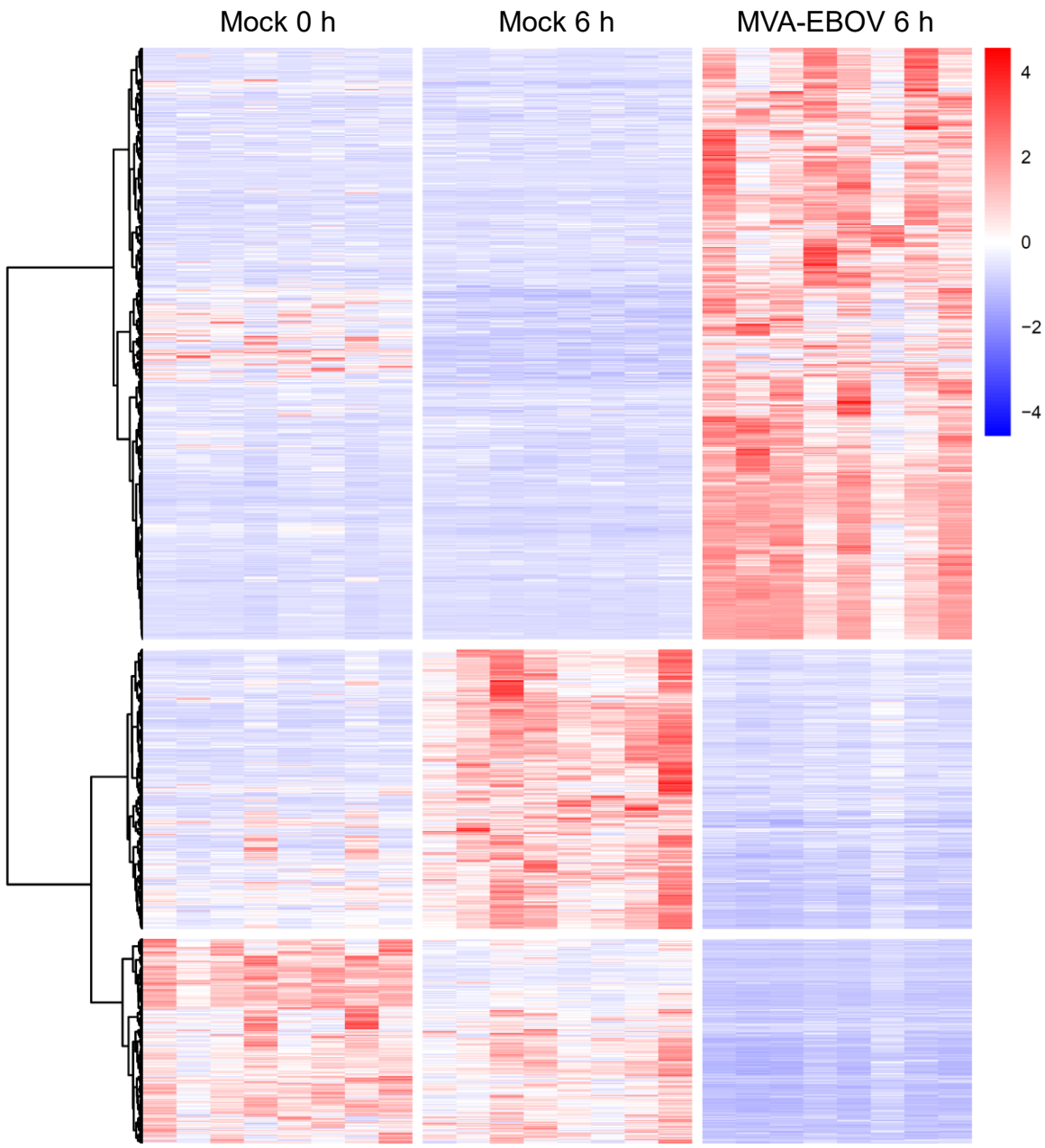


S.17: **Hierarchical clustering heat map of DEG upon MVA-EBOV stimulation.** Total RNA of 6 h *in vitro* MVA-EBOV−stimulated (MOI 1) and unstimulated samples (N=8, section 2.2, table 6) was analyzed via RNA-Seq (section 3.10). Genes which exhibited a log2 fold change ≤ -1.5 or ≥ 1.5 and an FDR < 0.01 were counted as DEG. Besides unstimulated 0 h and 6 h controls, also 6 h stimulated samples are depicted. Each condition is separated in further columns indicating different blood donors.

### 6.4.3 RNA-Seq: Pathways of 6 h unstimulated samples

Induced gene expression of 0 h and 6 h *in vitro* cultivated hPBMCswas investigated by RNA-Seq. The gene expression after 6 h was normalized to 0 h controls. All DEG were analyzed using ORA based on the reactome database. Here, no specific antiviral or pro-inflammatory pathway was detected in unstimulated 6 h samples of *in vitro* stimulations using VSV-EBOV or MVA-EBOV (S.18). Therefore, induced transcriptomic changes of single genes in unstimulated samples were not specific and were interpreted as background noise.

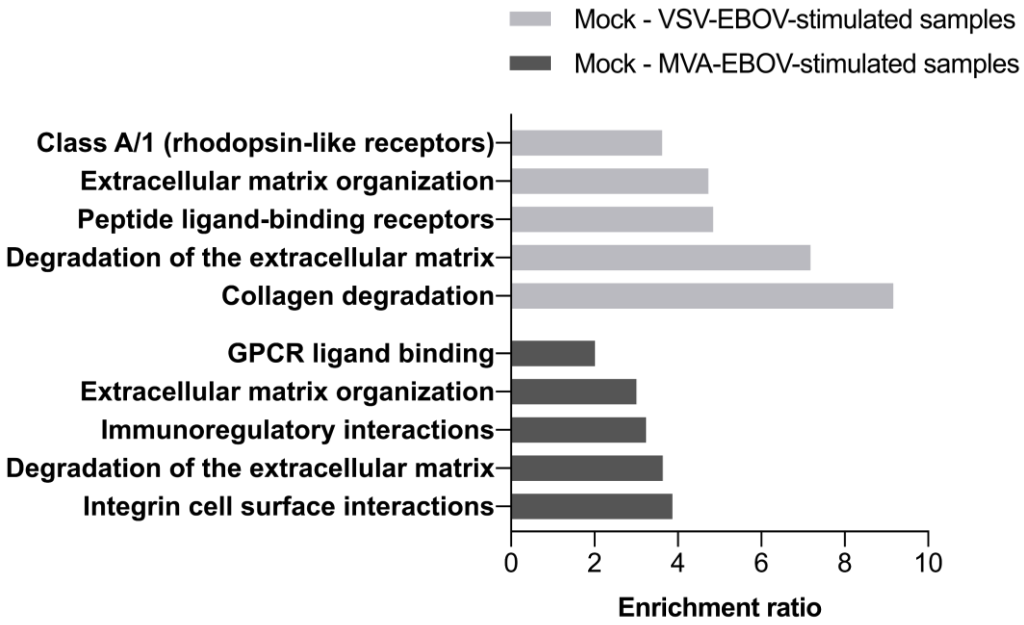


S.18: **ORA of DEG in unstimulated hPBMCs.** Total RNA of 0 h and 6 h unstimulated samples (N=8, section 2.2, table 5–6) was analyzed via RNA-Seq (section 3.10). Genes, which exhibited a log2 fold change ≤ -1.5 or ≥ 1.5 and an FDR < 0.01 compared to unstimulated 0 h controls, were counted as DEG. All genes of unstimulated samples belonging to VSV-EBOV stimulations are depicted in grey, whereas genes of unstimulated samples that belongs to MVA-EBOV stimulations are shown in black. Enrichment ratios were calculated with the web tool: webgestalt.org [228–231] using only the top 5 of pathways with an FDR ≤ 0.05.

### 6.4.4 RNA-Seq: Generally applicable gene-set enrichment

A GAGE based on KEGG revealed different induced pathways including different regulated genes post VSV-EBOV (S.19) and MVA-EBOV (S.20) stimulation.

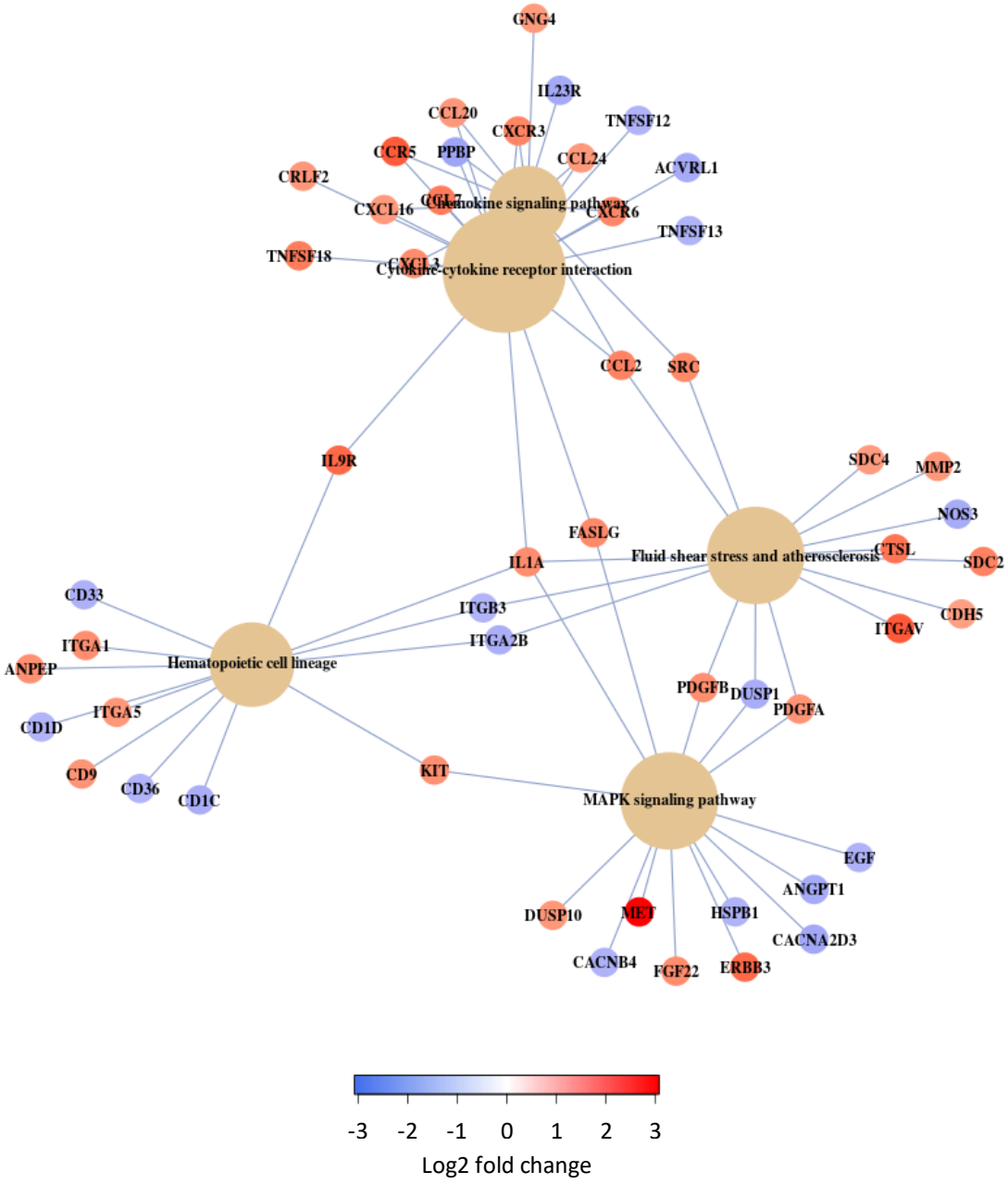


S.19: **GAGE of VSV-EBOV–stimulated hPBMCs.** Total RNA of 6 h *in vitro* VSV-EBOV–stimulated (MOI 1) and 0 h unstimulated samples (N=8, section 2.2, table 5) was analyzed via RNA-Seq (section 3.10). Genes, which exhibited a log2 fold change ≤ -1.5 or ≥ 1.5 and an FDR < 0.01 compared to unstimulated 0 h controls, were counted as DEG. Downregulated genes are depicted in bule, whereas upregulated genes are shown in red. Pathways (brown circles), which showed an FDR < 0.1, were counted as significantly regulated pathways. The GAGE analysis is based on KEGG.

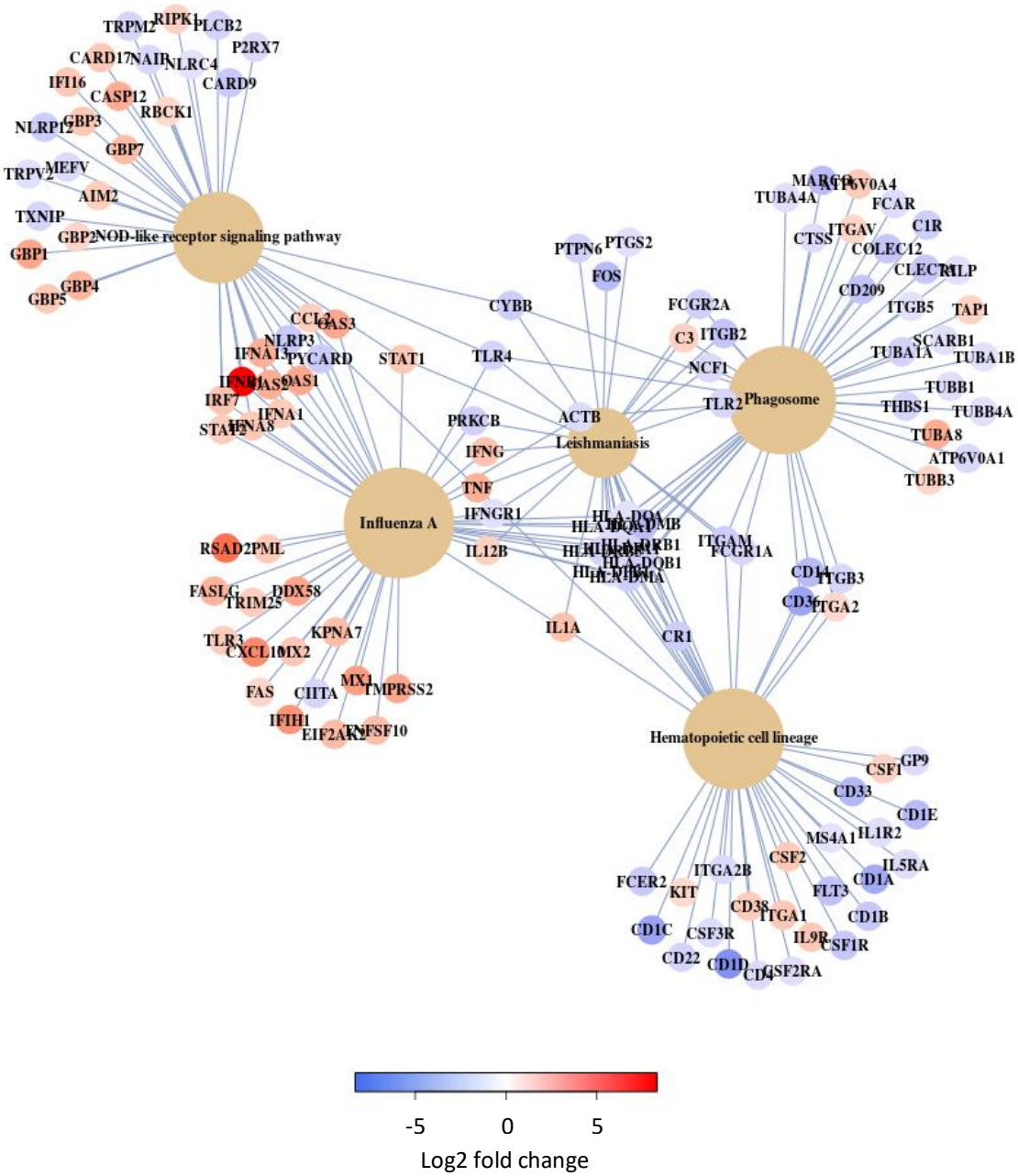


S.20: **GAGE of MVA-EBOV−stimulated hPBMCs.** Total RNA of 6 h *in vitro* MVA-EBOV−stimulated (MOI 1) and 0 h unstimulated samples (N=8, section 2.2, table 6) was analyzed via RNA-Seq (section 3.10). Genes, which exhibited a log2 fold change ≤ -1.5 or ≥ 1.5 and an FDR < 0.01 compared to unstimulated 0 h controls, were counted as DEG. Downregulated genes are depicted in bule, whereas upregulated genes are shown in red. Pathways (brown circles), which showed an FDR < 0.1, were counted as significantly regulated pathways. The GAGE analysis is based on KEGG.

### 6.4.5 Volcano plots of unstimulated samples

The gene expression of unstimulated 6 h was analyzed by RNA-Seq and normalized to unstimulated 0 h and depicted in volcano plots indicating their log2 fold changes and corresponding FDR (S.21–22). Besides unstimulated 6 h samples belonging to VSV-EBOV–stimulated samples (cf. section 4.2.2, figure 30), also unstimulated 6 h samples of MVA-EBOV stimulations (cf. section 4.2.2, figure 31) are depicted.

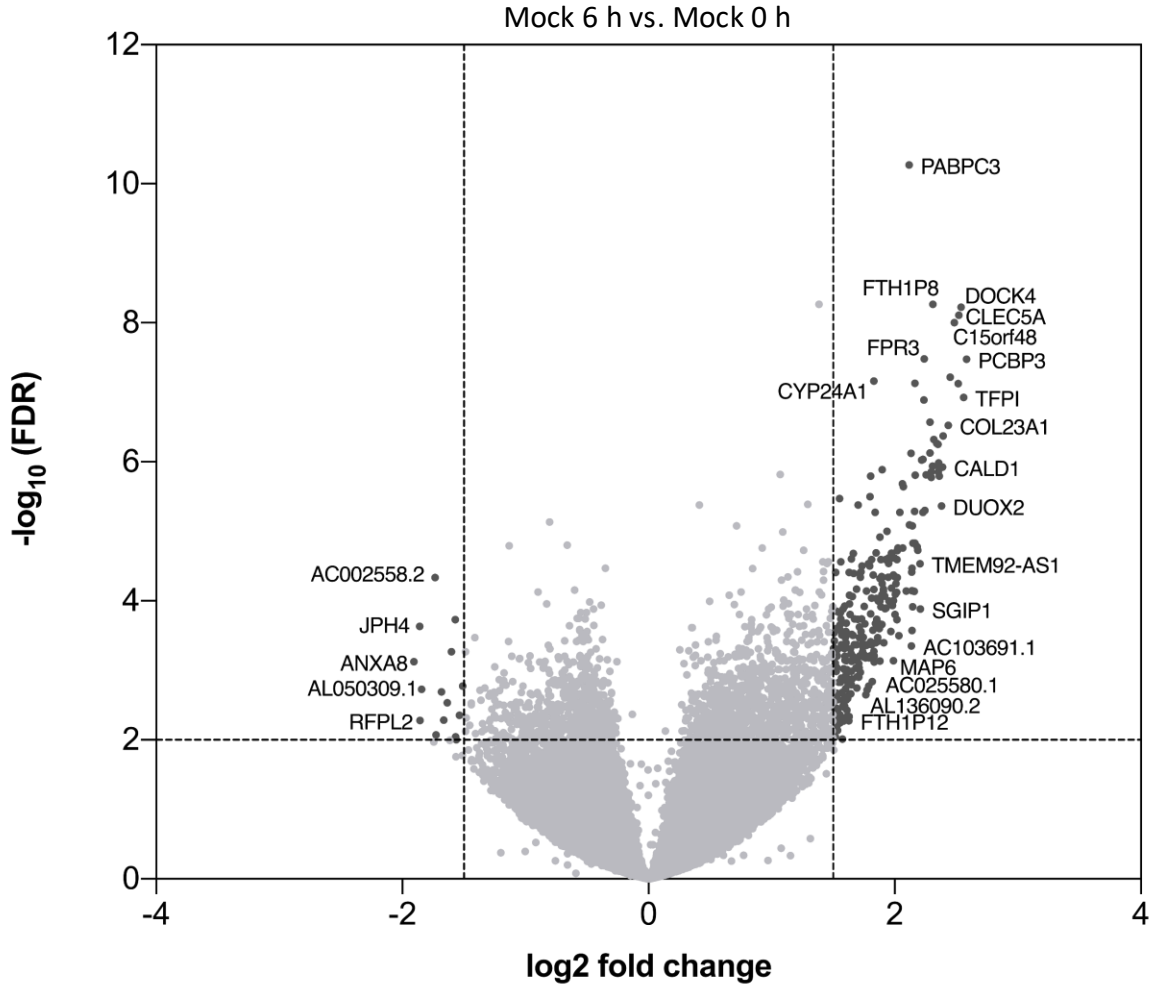


S.21: **Volcano plots of unstimulated hPBMCs that belongs to VSV-EBOV stimulations.** Total RNA of 0 h and 6 h unstimulated samples (N=8) was analyzed via RNA-Seq (section 3.10). Genes, which exhibited a log2 fold change ≤ -1.5 or ≥ 1.5 and an FDR < 0.01 compared to unstimulated 0 h controls, were counted as DEG. All genes of unstimulated samples that belongs to VSV-EBOV–stimulated once are depicted. Each dot indicates a different gene, where darker color represents DEG and lighter color not DEG as indicated also by the black dotted lines.

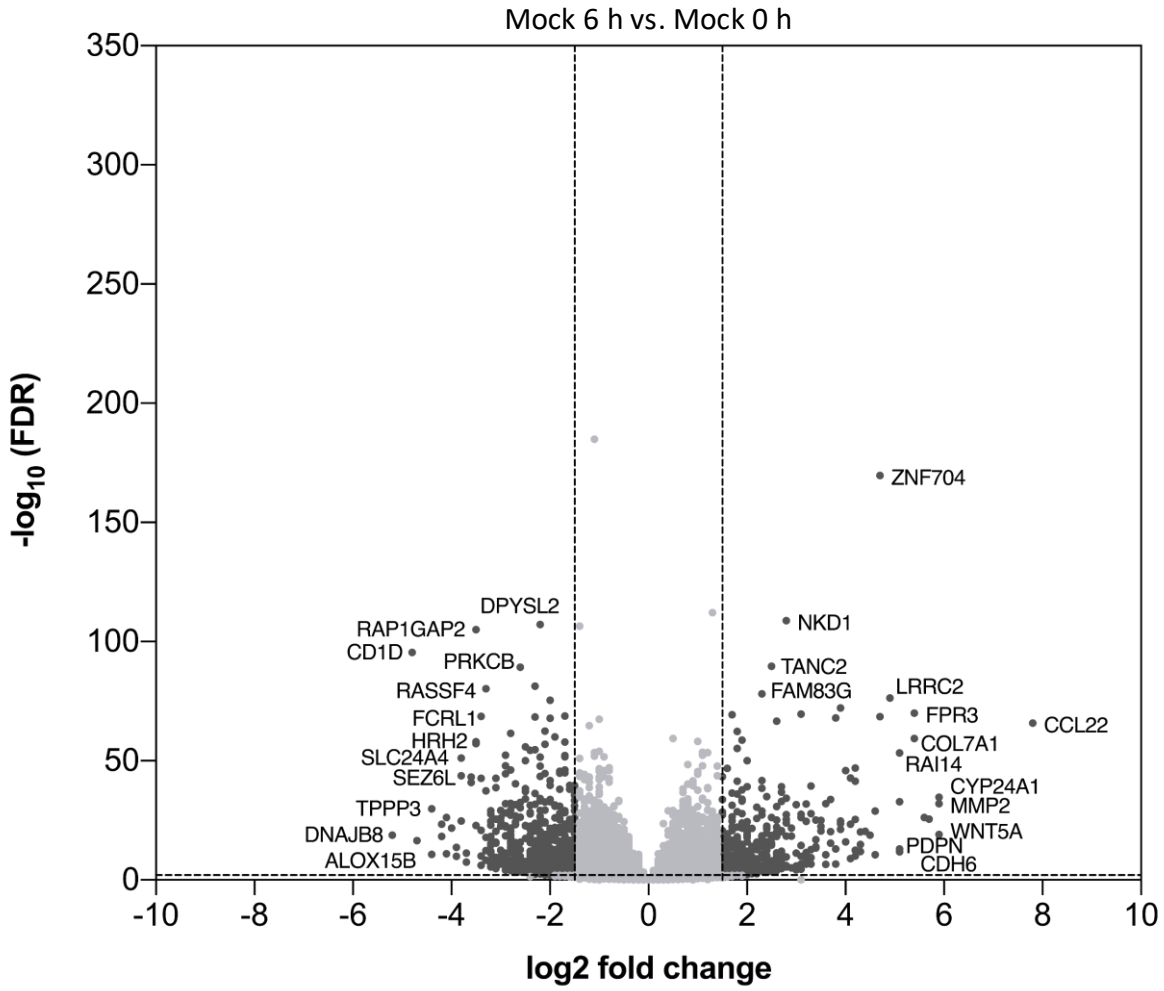


S.22: **Volcano plots of unstimulated hPBMCs that belongs to MVA-EBOV stimulations.** Total RNA of 0 h and 6 h unstimulated samples (N=8) was analyzed via RNA-Seq (section 3.10). Genes, which exhibited a log2 fold change ≤ -1.5 or ≥ 1.5 and an FDR < 0.01 compared to unstimulated 0 h controls, were counted as DEG. All genes of unstimulated samples that belongs to MVA-EBOV−stimulated once are shown. Each dot indicates a different gene, where darker color represents DEG and lighter color not DEG as indicated also by the black dotted lines.

# 7. References


1. Morse, S. S. Factors in the emergence of infectious diseases. *Emerg. Infect. Dis.* **1**, 7–15 (1995).
2. Nii-Trebi, N. I. Emerging and Neglected Infectious Diseases: Insights, Advances, and Challenges. *Biomed Res. Int.* **2017**, (2017).
3. Binder, S., Levitt, A. M., Sacks, J. J. & Hughes, J. M. Emerging infectious diseases: Public health issues for the 21st century. *Science* **284**, 1311–1313 (1999).
4. Morens, D. M., Folkers, G. K. & Fauci, A. S. The challenge of emerging and re-emerging infectious diseases. *Nature* **463**, 122 (2010).
5. Jones, K. E., Patel, N. G., Levy, M. A., Storeygard, A., Balk, D., Gittleman, J. L. & Daszak, P. Global trends in emerging infectious diseases. *Nature* **451**, 990–993 (2008).
6. World Health Organization (WHO). Origins of the 2014 Ebola epidemic. https://www.who.int/csr/disease/ebola/one-year-report/virus-origin/en/ (2015).
7. World Health Organization (WHO). Ebola outbreak 2014-2016. https://www.who.int/csr/disease/ebola/en/ (2016).
8. Coltart, C. E. M., Lindsey, B., Ghinai, I., Johnson, A. M. & Heymann, D. L. The Ebola outbreak, 2013–2016: Old lessons for new epidemics. *Philos. Trans. R. Soc. B Biol. Sci.* **372**, 1–24 (2017).
9. Kuhn, J. H. New filovirus disease classification and nomenclature. *Nat Rev. Microbiol.* **17**, 261–263 (2019).
10. Hoenen, T., Groseth, A., Falzarano, D. & Feldmann, H. Ebola virus: unravelling pathogenesis to combat a deadly disease. *Trends Mol. Med.* **12**, 206–215 (2006).
11. World Health Organization (WHO). Ebola virus disease - Key facts. https://www.who.int/news-room/fact-sheets/detail/ebola-virus-disease (2021).
12. Center for Disease Control and Prevention (CDC). 2014-2016 Ebola Outbreak in West Africa. https://www.cdc.gov/vhf/ebola/history/2014-2016-outbreak/index.html (2019).
13. World Health Organization (WHO). Prioritizing diseases for research and development in emergency contexts. https://www.who.int/activities/prioritizing-diseases-for-research-and-development-in-emergency-contexts (2020).

14. World Health Organization (WHO). Ebola in the Democratic Republic of the Congo. https://www.who.int/emergencies/diseases/ebola/drc-2019 (2021).
15. World Health Organization (WHO). Ebola virus disease – Democratic Republic of the Congo. https://www.who.int/csr/don/10-february-2021-ebola-drc/en/ (2021).
16. European Centre for Disease Prevention and Control (ECDC). Ebola virus disease outbreak in Guinea, 2021. https://www.ecdc.europa.eu/en/publications-data/ebola-virus-disease-outbreak-guinea-2021 (2021).
17. World Health Organization (WHO). Ebola virus disease – Guinea. https://www.who.int/csr/don/17-february-2021-ebola-gin/en/ (2021).
18. Kuhn, J. H., Amarasinghe, G. K., Basler, C. F., Bavari, S., Bukreyev, A., Chandran, K., Crozier, I., Dolnik, O., Dye, J. M., Formenty, P. B. H., *et al.* ICTV virus taxonomy profile: Filoviridae. *J. Gen. Virol.* **100**, 911–912 (2019).
19. Jacob, S. T., Crozier, I., Fischer, W. A., Hewlett, A., Kraft, C. S., Vega, M. A. de La, Soka, M. J., Wahl, V., Griffiths, A., Bollinger, L., *et al. Ebola virus disease*. *Nature Reviews Disease Primers* vol. 6 (Springer US, 2020).
20. Conlan, S., Serena, A., Towner, J. S., Sealy, T. K., Khristova, M. L., Quan, P., Lipkin, W. I., Downing, R., Tappero, J. W., Okware, S., *et al.* Newly Discovered Ebola Virus Associated with Hemorrhagic Fever Outbreak in Uganda. *PLOS Pathog.* **4**, 3–8 (2008).
21. International Committee on Taxonomy of Viruses & King, A. M. Family - Filoviridae. in *Virus Taxonomy* (eds. King, A. M. Q., Adams, M. J., Carstens, E. B. & Lefkowitz, E. J.) 665–671 (Elsevier, 2012). doi:10.1016/B978-0-12-384684-6.00055-0.
22. Report of an international commission. Ebola haemorrhagic fever in Zaire, 1976. *Bull. World Health Organ.* **56**, 271–293 (1978).
23. Centre for Disease Prevention and Control (CDC). History of Ebola Virus Disease. https://www.cdc.gov/vhf/ebola/history/summaries.html (2021).
24. Ezezika, O. & Keita, A. K. Outsmarting Ebola through stronger national health systems. *Sci. African* **7**, 18–20 (2020).
25. Skrip, L. A. & Galvani, A. P. Next Steps for Ebola Vaccination: Deployment in Non-Epidemic, High-Risk Settings. *PLoS Negl. Trop. Dis.* **10**, 1–6 (2016).
26. Vygen, S., Tiffany, A., Rull, M., Ventura, A., Wolz, A., Jambai, A. & Porten, K. Changes in health-seeking behavior did not result in increased all-cause mortality during the Ebola

outbreak in Western Area, Sierra Leone. *Am. J. Trop. Med. Hyg.* **95**, 897–901 (2016).

27. Sochas, L., Channon, A. A. & Nam, S. Counting indirect crisis-related deaths in the context of a low-resilience health system: The case of maternal and neonatal health during the Ebola epidemic in Sierra Leone. *Health Policy Plan.* **32**, iii32–iii39 (2017).
28. Wilhelm, J. A. & Helleringer, S. Utilization of non-Ebola health care services during Ebola outbreaks: A systematic review and meta-analysis. *J. Glob. Health* **9**, (2019).
29. Sun, X., Samba, T. T., Yao, J., Yin, W., Xiao, L., Liu, F., Liu, X., Zhou, J., Kou, Z., Fan, H., *et al.* Impact of the Ebola outbreak on routine immunization in western area, Sierra Leone - A field survey from an Ebola epidemic area. *BMC Public Health* **17**, 1–6 (2017).
30. Masresha, B. G., Luce, R., Weldegebriel, G., Katsande, R., Gasasira, A. & Mihigo, R. The impact of a prolonged ebola outbreak on measles elimination activities in Guinea, Liberia and Sierra Leone, 2014-2015. *Pan Afr. Med. J.* **35**, 8 (2020).
31. Zawilińska, B. & Kosz-Vnenchak, M. General introduction into the Ebola virus biology and disease. *Folia Med. Cracov.* **54**, 57–65 (2014).
32. Beniac, D. R., Lamboo, L. L. & Booth, T. F. Filovirus filament proteins. *Subcell. Biochem.* **88**, 73–94 (2018).
33. Cantoni, D. & Rossman, J. S. Ebolaviruses: New roles for old proteins. *PLoS Negl. Trop. Dis.* **12**, 1–17 (2018).
34. Carroll, S. A., Towner, J. S., Sealy, T. K., McMullan, L. K., Khristova, M. L., Burt, F. J., Swanepoel, R., Rollin, P. E. & Nichola, S. T. Molecular Evolution of Viruses of the Family Filoviridae Based on 97 Whole-Genome Sequences. *J. Virol.* **87**, 2608–2616 (2013).
35. Mahanty, S. & Bray, M. Pathogenesis of filoviral haemorrhagic fevers. *Lancet Infect. Dis.* **4**, 487–498 (2004).
36. Bwaka, M. A., Bonnet, M. J., Calain, P., Colebunders, R., De Ann, R., Guimard, Y., Katwiki, K. R., Kibadi, K., Kipasa, M. A., Kuvula, K. J., *et al.* Ebola hemorrhagic fever in Kikwit, Democratic Republic of the Congo: Clinical observations in 103 patients. *J. Infect. Dis.* **179**, 1–7 (1999).
37. Ksiazek, T. G., Rollin, P. E., Williams, A. J., Bressler, D. S., Martin, M. L., Swanepoel, R., Burt, F. J., Leman, P. A., Khan, A. S., Rowe, A. K., *et al.* Clinical Virology of Ebola Hemorrhagic Fever ( EHF ): Virus , Virus Antigen , and IgG and IgM Antibody Findings among EHF Patients in Kikwit , Democratic Republic of the Congo , 1995. *J. Infect. Dis.*

**179**, 177–187 (1999).

38. Towner, J. S., Rollin, P. E., Bausch, D. G., Sanchez, A., Crary, S. M., Vincent, M., Lee, W. F., Spiropoulou, C. F., Ksiazek, T. G., Lukwiya, M., *et al.* Rapid Diagnosis of Ebola Hemorrhagic Fever by Reverse Transcription-PCR in an Outbreak Setting and Assessment of Patient Viral Load as a Predictor of Outcome. *J. Virol.* **78**, 4330–4341 (2004).
39. Lee, J. E. & Saphire, E. O. Ebolavirus glycoprotein structure and mechanism of entry. *Future Virol.* **4**, 621–635 (2010).
40. Sullivan, N., Yang, Z.-Y. & Nabel, G. J. Ebola Virus Pathogenesis: Implications for Vaccines and Therapies. *J. Virol.* **77**, 9733–9737 (2003).
41. Manicassamy, B., Wang, J., Jiang, H. & Rong, L. Comprehensive Analysis of Ebola Virus GP1 in Viral Entry. *J. Virol.* **79**, 4793–4805 (2005).
42. Mulherkar, N., Raaben, M., de la Torre, J. C., Whelan, S. P. & Chandran, K. The Ebola virus glycoprotein mediates entry via a non-classical dynamin-dependent macropinocytic pathway. *Virology* **419**, 72–83 (2011).
43. Wang, Y., Li, J., Hu, Y., Liang, Q., Wei, M. & Zhu, F. Ebola vaccines in clinical trial: The promising candidates. *Hum. Vaccines Immunother.* **13**, 153–168 (2017).
44. Murphy, F. A. & Center for Disease Control and Prevention (CDC). Transmission electron microscopic image Ebola virus. https://phil.cdc.gov/Details.aspx?pid=1181 (1976).
45. Lüdtke, A., Ruibal, P., Wozniak, D. M., Pallasch, E., Wurr, S., Bockholt, S., Gómez-medina, S., Qiu, X., Kobinger, G. P., Rodríguez, E., *et al.* Ebola virus infection kinetics in chimeric mice reveal a key role of T cells as barriers for virus dissemination. *Sci. Rep.* **7**, 1–10 (2017).
46. Villinger, F., Rollin, P. E., Brar, S. S., Chikkala, N. F., Winter, J., Sundstrom, J. B., Zaki, S. R., Swanepoel, R., Ansari, A. A. & Peters, C. J. Markedly Elevated Levels of Interferon ( IFN ) - g , IFN- a , Interleukin ( IL ) -2 , IL- 10 , and Tumor Necrosis Factor- a Associated with Fatal Ebola Virus Infection. *J. Infect. Dis.* **179**, 188–191 (1999).
47. Hensley, L. E., Young, H. A., Jahrling, P. B. & Geisbert, T. W. Proinflammatory response during Ebola virus infection of primate models: Possible involvement of the tumor necrosis factor receptor superfamily. *Immunol. Lett.* **80**, 169–179 (2002).

48. Geisbert, T. W., Young, H. A., Jahrling, P. B., Davis, K. J., Larsen, T., Kagan, E. & Hensley, L. E. Pathogenesis of Ebola Hemorrhagic Fever in Primate Models Evidence that Hemorrhage Is Not a Direct Effect of virus-induced cytolysis of endothelial cells. *Am. J. Pathol.* **163**, 2371–2382 (2003).

49. Geisbert, T. W., Hensley, L. E., Larsen, T., Young, H. A., Reed, D. S., Geisbert, J. B., Scott, D. P., Kagan, E., Jahrling, P. B. & Davis, K. J. Pathogenesis of Ebola Hemorrhagic Fever in Cynomolgus Macaques Evidence that Dendritic Cells Are Early and Sustained Targets of Infection. *Am. J. Pathol.* **163**, 2347–2370 (2003).

50. Martinez, O., Johnson, J. C., Honko, A., Yen, B., Shabman, R. S., Hensley, L. E., Olinger, G. G. & Basler, C. F. Ebola Virus Exploits a Monocyte Differentiation Program To Promote Its Entry. *J. Virol.* **87**, 3801–3814 (2013).

51. Marcinkiewicz, J., Bryniarski, K. & Nazimek, K. Ebola haemorrhagic fever virus: pathogenesis, immune responses, potential prevention. *Folia Med. Cracov.* **54**, 39–48 (2014).

52. Ruibal, P., Oestereich, L., Lüdtke, A., Becker-ziaja, B., Wozniak, D. M., Kerber, R., Korva, M., Cabeza-cabrerizo, M., Bore, J. A., Koundouno, F. R., *et al.* Unique human immune signature of Ebola virus disease in Guinea. *Nature* **533**, 100–104 (2016).

53. Ansari, A. A. Clinical features and pathobiology of Ebolavirus infection. *J. Autoimmun.* **55**, 1–9 (2014).

54. Malvy, D., Mcelroy, A. K., Clerck, H. De, Günther, S. & Griensven, J. Van. Ebola virus disease. *Lancet* **393**, 936–948 (2019).

55. Murphy, K. & Weaver, C. Die angeborene Immunität. in *Janeway Immunologie* 47–87 (Springer Berlin Heidelberg, 2018). doi:https://doi.org/10.1007/978-3-662-56004-4.

56. Murphy, K. & Weaver, C. Die induzierten Reaktionen der angeborenen Immunität. in *Janeway Immunologie* 95–162 (Springer Berlin Heidelberg, 2018). doi:https://doi.org/10.1007/978-3-662-56004-4.

57. Murphy, K. & Weaver, C. Die T-Zell-vermittelte Immunität. in *Janeway Immunologie* 443–516 (Springer Berlin Heidelberg., 2018). doi:https://doi.org/10.1007/978-3-662-56004-4.

58. Murphy, K. & Weaver, C. Die humorale Immunantwort. in *Janeway Immunologie* (Springer Berlin Heidelberg, 2018). doi:https://doi.org/10.1007/978-3-662-56004-4.

59. Murphy, K. & Weaver, C. Die Dynamik der angeborenen und adaptiven Immunantwort. in *Janeway Immunologie* 614–629 (Springer Berlin Heidelberg, 2018). doi:https://doi.org/10.1007/978-3-662-56004-4.

60. Andre, F. E., Booy, R., Bock, H. L., Clemens, J., Datta, S. K., John, T. J., Lee, B. W., Lolekha, S., Peltola, H., Ruff, T. A., *et al.* Vaccination greatly reduces disease, disability, death and inequity worldwide. *Bull. World Health Organ.* **86**, 140–146 (2008).

61. Doherty, M., Buchy, P., Standaert, B., Giaquinto, C. & Prado-Cohrs, D. Vaccine impact: Benefits for human health. *Vaccine* **34**, 6707–6714 (2016).

62. Needham, J. *Science and Civilisation in China*. (Cambridge University Press, 2000, 2000).

63. Riedel, S. Edward Jenner and the History of Smallpox and Vaccination. *Baylor Univ. Med. Cent. Proc.* **18**, 21–25 (2005).

64. World Health Organization (WHO). Vaccines and diseases. https://www.who.int/immunization/diseases/en/ (2020).

65. Shukla, V. V. & Shah, R. C. Vaccinations in Primary Care. *Indian J. Pediatr.* **85**, 1118–1127 (2018).

66. World Health Organization (WHO). Vaccines & Diseases. https://www.who.int/teams/immunization-vaccines-and-biologicals/diseases (2020).

67. World Health Organization (WHO). Vaccines and immunization. https://www.who.int/health-topics/vaccines-and-immunization#tab=tab_1 (2020).

68. Center for Disease Control and Prevention (CDC). Measles, Mumps, and Rubella (MMR) Vaccination: What Everyone Should Know. https://www.cdc.gov/vaccines/vpd/mmr/public/index.html (2019).

69. World Health Organization (WHO). Poliomyelitis. https://www.who.int/en/news-room/fact-sheets/detail/poliomyelitis (2019).

70. Center for Disease Control and Prevention (CDC). Smallpox. https://www.cdc.gov/smallpox/prevention-treatment/index.html (2020).

71. World Health Organization (WHO). Smallpox - Symptoms. https://www.who.int/health-topics/smallpox#tab=tab_2 (2020).

72. Fenner, F., Henderson, D. A., Arita, I., Jezek, Z. & Ladnyi, I. D. Smallpox and its eradication. *J. Epidemiol. Community Heal.* **43**, 92–92 (1989).

73. Ehreth, J. The global value of vaccination. *Vaccine* **21**, 596–600 (2003).

74. Roush, S. W., Murphy, T. V. & Vaccine-Preventable Disease Table Working Group. Historical comparisons of morbidity and mortality for vaccine-preventable diseases in the United States. *J. Am. Med. Assoc.* **298**, 2155–2163 (2007).

75. Center for Disease Control and Prevention (CDC). Notifiable Diseases and Mortality Tables. MMWR Morb Mortal Wkly Rep. 61(52):ND-719–ND-32 (2013).

76. Slifka, M. K. & Amanna, I. How advances in immunology provide insight into improving vaccine efficacy. *Vaccine* **32**, 2948–2957 (2014).

77. Robinson, H. L. & Pertmer, T. M. DNA vaccines for viral infections: Basic studies and applications. *Adv. Virus Res.* **55**, 1–74 (2000).

78. Cui, Z. DNA Vaccine. *Adv. Genet.* **54**, 257–289 (2005).

79. Braciale, T. J., Morrison, L. A., Sweetser, M. T., Sambrook, J., Gething, M. -J & Braciale, V. L. Antigen Presentation Pathways to Class I and Class II MHC-Restricted T Lymphocytes. *Immunol. Rev.* **98**, 95–114 (1987).

80. Heath, W. R. & Carbone, F. R. Cross-presentation in viral immunity and self-tolerance. *Nat. Rev. immunlogy* **1**, 126–135 (2001).

81. Hewitt, E. W. The MHC class I antigen presentation pathway: strategies for viral immune evasion. *Immunology* **110**, 163–169 (2003).

82. Saalmüller, A. New understanding of immunological mechanisms. *Vet. Microbiol.* **117**, 32–38 (2006).

83. Choi, Y. & Chang, J. Viral vectors for vaccine applications. *Clin. Exp. Vaccine Res.* **2**, 97–105 (2013).

84. Henao-Restrepo, A. M., Camacho, A., Longini, I. M., Watson, C. H., Edmunds, W. J., Egger, M., Carroll, M. W., Dean, N. E., Diatta, I., Doumbia, M., *et al.* Efficacy and effectiveness of an rVSV-vectored vaccine in preventing Ebola virus disease: final results from the Guinea ring vaccination, open-label, cluster-randomised trial (Ebola Ça Suffit!). *Lancet* **389**, 505–518 (2017).

85. Regules, J. A., Beigel, J. H., Paolino, K. M., Voell, J., Castellano, A. R., Hu, Z., Muñoz, P., Moon, J. E., Ruck, R. C., Bennett, J. W., *et al.* A Recombinant Vesicular Stomatitis Virus Ebola Vaccine. *N. Engl. J. Med.* **376**, 330–341 (2017).

86. Dahlke, C., Kasonta, R., Lunemann, S., Krähling, V., Zinser, M. E., Biedenkopf, N.,

Fehling, S. K., Ly, M. L., Rechtien, A., Stubbe, H. C., *et al.* Dose-dependent T-cell Dynamics and Cytokine Cascade Following rVSV-ZEBOV Immunization. *EBioMedicine* **19**, 107–118 (2017).

87. Ewer, K. J., Lambe, T., Rollier, C. S., Spencer, A. J., Hill, A. V. S. & Dorrell, L. Viral vectors as vaccine platforms: From immunogenicity to impact. *Curr. Opin. Immunol.* **41**, 47–54 (2016).
88. Poetsch, J. H., Dahlke, C., Zinser, M. E., Kasonta, R., Lunemann, S., Rechtien, A., Ly, M. L., Stubbe, H. C., Krähling, V., Biedenkopf, N., *et al.* Detectable Vesicular Stomatitis Virus ( VSV )– Specific Humoral and Cellular Immune Responses Following VSV – Ebola Virus Vaccination in Humans. *J. Infect. Dis.* **219**, (2019).
89. Kutzler, M. A. & Weiner, D. B. DNA vaccines: ready for prime time? *Nat. Rev. Genet.* **9**, 776–788 (2008).
90. Ura, T., Okuda, K. & Shimada, M. Developments in viral vector-based vaccines. *Vaccines* **2**, 624–641 (2014).
91. Fischer, T., Spohn, M., Olearo, F., Zinser, M. E., Kasonta, R., Stubbe, H. C., Rechtien, A., Ly, M. L., Schmiedel, S., Lohse, A. W., *et al.* Dynamic changes of circulating miRNAs induced by the Ebola virus vaccine VSV-EBOV. *Vaccine* **36**, 7083–7094 (2018).
92. Rechtien, A., Richert, L., Lorenzo, H., Martrus, G., Hejblum, B., Dahlke, C., Kasonta, R., Zinser, M., Stubbe, H., Matschl, U., *et al.* Systems Vaccinology Identifies an Early Innate Immune Signature as a Correlate of Antibody Responses to the Ebola Vaccine rVSV-ZEBOV. *Cell Rep.* **20**, 2251–2261 (2017).
93. Menicucci, A. R., Jankeel, A., Feldmann, H., Marzi, A. & Messaoudi, I. Antiviral innate responses induced by VSV-EBOV vaccination contribute to rapid protection. *MBio* **10**, 1–14 (2019).
94. van Riel, D. & de Wit, E. Next-generation vaccine platforms for COVID-19. *Nat. Mater.* **19**, 810–812 (2020).
95. Gray, R. Creating vaccines drop by drop. https://www.ddw-online.com/creating-vaccines-drop-by-drop-1273-202008/ (2020).
96. Lambert, L. C. & Fauci, A. S. Influenza Vaccines for the Future. *N. Engl. J. Med.* **363**, 2036–2044 (2010).
97. Pollard, A. J. & Bijker, E. M. A guide to vaccinology: from basic principles to new

developments. *Nat. Rev. Immunol.* **21**, 83–100 (2021).

98. Gilbert, S. C. T-cell-inducing vaccines – what ' s the future. *Immunology* **135**, 19–26 (2011).
99. Henrique, J., Prince, R., Bizerra, R., Araújo, S., Ramos, L., Lina, D., Fabris, N., Andreata, R., Carlos, L. & Ferreira, D. S. Antibodies are not required to a protective immune response against dengue virus elicited in a mouse encephalitis model. *Virology* **487**, 41–49 (2016).
100. Raeven, R. H. M., Riet, E. van, Meiring, H. D., Metz, B. & Kersten, G. F. A. Systems vaccinology and big data in the vaccine development chain. *Immunology* **156**, 33–46 (2019).
101. Cortese, M., Sherman, A. C., Rouphael, N. G. & Pulendran, B. Systems Biological Analysis of Immune Response to Influenza Vaccination. *Cold Spring Harb. Perspect. Biol.* **a038596**, (2020).
102. Pulendran, B., Li, S. & Nakaya, H. I. Systems Vaccinology. *Immunity* **33**, 516–529 (2010).
103. Querec, T. D., Akondy, R. S., Lee, E. K., Cao, W., Nakaya, H. I., Teuwen, D., Pirani, A., Gernert, K., Deng, J., Marzolf, B., *et al.* Systems biology approach predicts immunogenicity of the yellow fever vaccine in humans. *Nat. Immunol.* **10**, 116–125 (2009).
104. Hoek, K. L., Samir, P., Howard, L. M., Niu, X., Prasad, N., Galassie, A., Liu, Q., Allos, T. M., Floyd, K. A., Guo, Y., *et al.* A Cell-Based Systems Biology Assessment of Human Blood to Monitor Immune Responses after Influenza Vaccination. *PLoS One* **10**, 1–24 (2015).
105. Nakaya, H. I., Clutterbuck, E., Kazmin, D., Wang, L., Cortese, M., Bosinger, S. E., Patel, N. B., Zak, D. E., Aderem, A., Dong, T., *et al.* Systems biology of immunity to MF59-adjuvanted versus nonadjuvanted trivalent seasonal influenza vaccines in early childhood. *Proc. Natl. Acad. Sci. U. S. A.* **113**, 1853–1858 (2016).
106. Donnell, K. O. & Marzi, A. The Ebola virus glycoprotein and its immune responses across multiple vaccine platforms. *Expert Rev. Vaccines* **19**, 267–277 (2020).
107. Geisbert, T. W., Pushko, P., Anderson, K., Smith, J., Davis, K. J. & Jahrling, P. B. Evaluation in nonhuman primates of vaccines against Ebola virus. *Emerg. Infect. Dis.* **8**, 503–507 (2002).

108. Martin, J. E., Sullivan, N. J., Enama, M. E., Gordon, I. J., Roederer, M., Koup, R. A., Bailer, R. T., Chakrabarti, B. K., Bailey, M. A., Gomez, P. L., *et al.* A DNA vaccine for Ebola virus is safe and immunogenic in a phase I clinical trial. *Clin. Vaccine Immunol.* **13**, 1267–1277 (2006).

109. Marzi, A., Robertson, S. J., Haddock, E., Feldmann, F., Hanley, P. W., Scott, D. P., Strong, J. E., Kobinger, G., Best, S. M. & Feldmann, H. VSV-EBOV rapidly protects macaques against infection with the 2014/15 Ebola virus outbreak strain. *Science* **349**, 739–742 (2015).

110. Warfield, K. L., Swenson, D. L., Olinger, G. G., Kalina, W. V., Aman, M. J. & Bavari, S. Ebola virus-like particle-based vaccine protects nonhuman primates against lethal Ebola virus challenge. *J. Infect. Dis.* **196**, S430–S437 (2007).

111. Liu, M. A. Immunologic basis of vaccine vectors. *Immunity* **33**, 504–515 (2010).

112. Kumar, A., Meldgaard, T. S. & Bertholet, S. Novel platforms for the development of a universal influenza vaccine. *Front. Immunol.* **9**, (2018).

113. Pardi, N., Hogan, M. J., Porter, F. W. & Weissman, D. mRNA vaccines-a new era in vaccinology. *Nat. Rev. Drug Discov.* **17**, 261–279 (2018).

114. Marzi, A., Halfmann, P., Hill-batorski, L., Feldmann, F., Lesley, W., Neumann, G., Feldmann, H. & Kawaoka, Y. An Ebola whole-virus vaccine is protective in nonhuman primates. *Science* **348**, 439–442 (2015).

115. Rao, M., Matyas, G. R., Grieder, F., Anderson, K., Jahrling, P. B. & Alving, C. R. Cytotoxic T lymphocytes to Ebola Zaire virus are induced in mice by immunization with liposomes containing lipid A. *Vaccine* **17**, 2991–2998 (1999).

116. Sarwar, U. N., Costner, P., Enama, M. E., Berkowitz, N., Hu, Z., Hendel, C. S., Sitar, S., Plummer, S., Mulangu, S., Bailer, R. T., *et al.* Safety and immunogenicity of DNA vaccines encoding ebolavirus and marburgvirus wild-type glycoproteins in a phase i clinical trial. *J. Infect. Dis.* **211**, 549–557 (2015).

117. Reynard, O., Mokhonov, V., Mokhonova, E., Leung, J., Page, A., Mateo, M., Pyankova, O., Georges-Courbot, M. C., Raoul, H., Khromykh, A. A., *et al.* Kunjin virus replicon-based vaccines expressing Ebola virus glycoprotein GP protect the guinea pig against lethal Ebola virus infection. *J. Infect. Dis.* **204**, 1060–1065 (2011).

118. Pyankov, O. V., Bodnev, S. A., Pyankova, O. G., Solodkyi, V. V., Pyankov, S. A., Setoh, Y.

X., Volchkova, V. A., Suhrbier, A., Volchkov, V. V., Agafonov, A. A., *et al.* A Kunjin Replicon Virus-like Particle Vaccine Provides Protection Against Ebola Virus Infection in Nonhuman Primates. *J. Infect. Dis.* **212**, S368–S371 (2015).

119. Zhu, F. C., Hou, L. H., Li, J. X., Wu, S. P., Liu, P., Zhang, G. R., Hu, Y. M., Meng, F. Y., Xu, J. J., Tang, R., *et al.* Safety and immunogenicity of a novel recombinant adenovirus type-5 vector-based Ebola vaccine in healthy adults in China: Preliminary report of a randomised, double-blind, placebo-controlled, phase 1 trial. *Lancet* **385**, 2272–2279 (2015).
120. De Santis, O., Audran, R., Pothin, E., Warpelin-Decrausaz, L., Vallotton, L., Wuerzner, G., Cochet, C., Estoppey, D., Steiner-Monard, V., Lonchampt, S., *et al.* Safety and immunogenicity of a chimpanzee adenovirus-vectored Ebola vaccine in healthy adults: A randomised, double-blind, placebo-controlled, dose-finding, phase 1/2a study. *Lancet Infect. Dis.* **16**, 311–320 (2016).
121. Ewer, K., Rampling, T., Venkatraman, N., Bowyer, G., Wright, D., Lambe, T., Imoukhuede, E. B., Payne, R., Fehling, S. K., Strecker, T., *et al.* A Monovalent Chimpanzee Adenovirus Ebola Vaccine Boosted with MVA. *N. Engl. J. Med.* **374**, 1635–1646 (2016).
122. Venkatraman, N., Ndiaye, B. P., Bowyer, G., Wade, D., Sridhar, S., Wright, D., Powlson, J., Ndiaye, I., Dièye, S., Thompson, C., *et al.* Safety and immunogenicity of a heterologous prime-boost ebola virus vaccine regimen in healthy adults in the United Kingdom and Senegal. *J. Infect. Dis.* **219**, 1187–1197 (2019).
123. University of Oxford. A Study to Assess Ebola Vaccines ChAd3-EBO-Z and Ad26.ZEBOV. ClinicalTrials.gov Identifier: NCT02495246 https://clinicaltrials.gov/ct2/show/study/NCT02495246 (2021).
124. Ledgerwood, J. E., Costner, P., Desai, N., Holman, L., Enama, M. E., Yamshchikov, G., Mulangu, S., Hu, Z., Andrews, C. A., Sheets, R. A., *et al.* A replication defective recombinant Ad5 vaccine expressing Ebola virus GP is safe and immunogenic in healthy adults. *Vaccine* **29**, 304–313 (2010).
125. National Institute of Allergy and Infectious Diseases (NIAID). Evaluating the Safety of and Immune Response to a Human Parainfluenza Virus Type 3 Ebola Virus Vaccine (HPIV3-EbovZ GP) in Healthy Adults. https://clinicaltrials.gov/ct2/show/NCT02564575

(2017).

126. European Medicines Agencies (EMA). Mvabea. https://www.ema.europa.eu/en/medicines/human/EPAR/mvabea (2020).
127. Paul-Ehrlich-Institut. Ebola Vaccines. https://www.pei.de/EN/medicinal-products/vaccines-human/ebola/ebola-node.html (2020).
128. Pushko, P., Bray, M., Ludwig, G. V., Parker, M., Schmaljohn, A., Sanchez, A., Jahrling, P. B. & Smith, J. F. Recombinant RNA replicons derived from attenuated Venezuelan equine encephalitis virus protect guinea pigs and mice from Ebola hemorrhagic fever virus. *Vaccine* **19**, 142–153 (2001).
129. U.S. Food & Drug Administration (FDA). First FDA-approved vaccine for the prevention of Ebola virus disease, marking a critical milestone in public health preparedness and response. https://www.fda.gov/news-events/press-announcements/first-fda-approved-vaccine-prevention-ebola-virus-disease-marking-critical-milestone-public-health (2019).
130. European Medicines Agencies (EMA). First vaccine to protect against Ebola. https://www.ema.europa.eu/en/news/first-vaccine-protect-against-ebola (2019).
131. Moss, B., Smith, G. L., Gerin, J. L. & Purcell, R. H. Live recombinant vaccinia virus protects chimpanzees against hepatitis B. *Nature* **311**, 67–69 (1984).
132. Gómez, C. E., Perdiguero, B., García-Arriaza, J. & Esteban, M. Clinical applications of attenuated MVA poxvirus strain. *Expert Rev. Vaccines* **12**, 1395–1416 (2013).
133. Volz, A. & Sutter, G. Modified Vaccinia Virus Ankara: History, Value in Basic Research, and Current Perspectives for Vaccine Development. *Adv. Virus Res.* **97**, 187–243 (2017).
134. Koch, T., Dahlke, C., Fathi, A., Kupke, A., Krähling, V., Okba, N. M. A. A., Halwe, S., Rohde, C., Eickmann, M., Volz, A., *et al.* Safety and immunogenicity of a modified vaccinia virus Ankara vector vaccine candidate for Middle East respiratory syndrome: an open-label, phase 1 trial. *Lancet Infect. Dis.* **20**, 827–838 (2020).
135. Ramezanpour, B., Haan, I., Osterhaus, A. & Claassen, E. Vector-based genetically modified vaccines: Exploiting Jenner's legacy. *Vaccine* **34**, 6436–6448 (2016).
136. Rauch, S., Jasny, E., Schmidt, K. E. & Petsch, B. New vaccine technologies to combat outbreak situations. *Front. Immunol.* **9**, 1963 (2018).
137. Garbutt, M., Liebscher, R., Wahl-Jensen, V., Jones, S., Möller, P., Wagner, R., Volchkov,

V., Klenk, H.-D., Feldmann, H. & Ströher, U. Expressing Glycoproteins of Filoviruses Vesicular Stomatitis Virus Vectors Properties of Replication-Competent. *J. Virol.* **78**, 5458–65 (2004).

138. Thiebaut, R., Snape, M. D., Goldstein, N., Robinson, C., Gaddah, A., Bockstal, V., Launay, O., Lelievre, J., Richert, L., Betard, C., *et al.* P0399 Safety and immunogenicity of 2-dose Ebola vaccine regimen with Ad26 . ZEBOV and MVA-BN-Filo in a phase II clinical trial in Europe (EBOVAC2). in *European Society of Clinical Microbiology and Infectious Diseases Live* 28–29 (2014).
139. Winslow, R. L., Milligan, I. D., Voysey, M., Luhn, K., Shukarev, G., Douoguih, M. & Snape, M. D. Immune Responses to Novel Adenovirus Type 26 and Modified Vaccinia Virus Ankara–Vectored Ebola Vaccines at 1 Year. *J. Am. Med. Assoc.* **317**, 1075–1077 (2017).
140. European Medicines Agencies (EMA). Ervebo. https://www.ema.europa.eu/en/medicines/human/EPAR/ervebo (2021).
141. Marzi, A., Reynolds, P., Mercado-hernandez, R., Callison, J., Feldmann, F., Rosenke, R., Thomas, T., Scott, D. P., Hanley, P. W., Haddock, E., *et al.* Single low-dose VSV-EBOV vaccination protects cynomolgus macaques from lethal Ebola challenge. *EBioMedicine* **49**, 223–231 (2019).
142. World Health Organization (WHO). Preliminary results on the efficacy of rVSV-ZEBOV-GP Ebola vaccine using the ring vaccination strategy in the control of an Ebola outbreak in the Democratic Republic of the Congo: an example of integration of research into epidemic response. *WHO - Rep.* (2019).
143. Mehta, A. & Baltimore, D. MicroRNAs as regulatory elements in immune system logic. *Nat. Rev. Immunol.* **16**, 279–294 (2016).
144. Lodish, H. F., Zhou, B., Liu, G. & Chen, C. Z. Micromanagement of the immune system by microRNAs. *Nat. Rev. Immunol.* **8**, 120–130 (2008).
145. Lindsay, M. A. microRNAs and the immune response. *Trends Immunol.* **29**, 343–351 (2008).
146. Tsitsiou, E. & Lindsay, M. A. microRNAs and the immune response. *Curr. Opin. Pharmacol.* **9**, 514–520 (2009).
147. Klein, S. L. Sex influences immune responses to viruses, and efficacy of prophylaxis and therapeutic treatments for viral diseases. *BioEssays* **34**, 1050–1059 (2012).

148. Flanagan, K. L., Fink, A. L., Plebanski, M. & Klein, S. L. Sex and gender differences in the outcomes of vaccination over the life course. *Annu. Rev. Cell Dev. Biol.* **33**, 577–599 (2017).

149. Hall, O. J., Nachbagauer, R., Vermillion, M. S., Fink, A. L., Phuong, V., Krammer, F. & Klein, S. L. Progesterone-Based Contraceptives Reduce Adaptive Immune Responses and Protection against Sequential Influenza A Virus Infections. *J. Virol.* **91**, 1–17 (2017).

150. Ingersoll, M. A. Sex differences shape the response to infectious diseases. *PLOS Pathog.* **13**, 6–11 (2017).

151. Vermillion, M. S., Ursin, R. L., Kuok, D. I. T., Vom Steeg, L. G., Wohlgemuth, N., Hall, O. J., Fink, A. L., Sasse, E., Nelson, A., Ndeh, R., *et al.* Production of amphiregulin and recovery from influenza is greater in males than females. *Biol. Sex Differ.* **9**, 1–12 (2018).

152. Klein, S. L. The effects of hormones on sex differences in infection: from genes to behavior. *Neurosci. Biobehav. Rev.* **24**, 627–638 (2000).

153. Roberts, C. W., Walker, W. & Alexander, J. Sex-Associated Hormones and Immunity to Protozoan Parasites. *Clin. Microbiol. Rev.* **14**, 476–488 (2001).

154. Vázquez-Martínez, E. R., García-Gómez, E., Camacho-Arroyo, I. & González-Pedrajo, B. Sexual dimorphism in bacterial infections. *Biol. Sex Differ.* **9**, 1–20 (2018).

155. McClelland, E. E. & Smith, J. M. Gender specific differences in the immune response to infection. *Arch. Immunol. Ther. Exp. (Warsz).* **59**, 203–213 (2011).

156. Kverneland, A. H., Streitz, M., Geissler, E., Hutchinson, J., Vogt, K., Boës, D., Niemann, N., Pedersen, A. E., Schlickeiser, S. & Sawitzki, B. Age and gender leucocytes variances and references values generated using the standardized ONE-Study protocol. *Cytom. Part A* **89**, 543–564 (2016).

157. Tollerud, D. J., Clark, J. W., Brown, L. M., Neuland, C. Y., Pankiw-Trost, L. K., Blattner, W. A. & Hoover, R. N. The influence of age, race, and gender on peripheral blood mononuclear-cell subsets in healthy nonsmokers. *J. Clin. Immunol.* **9**, 214–222 (1989).

158. Xia, H. J., Zhang, G. H., Wang, R. R. & Zheng, Y. T. The influence of age and sex on the cell counts of peripheral blood leukocyte subpopulations in Chinese rhesus macaques. *Cell. Mol. Immunol.* **6**, 433–440 (2009).

159. Keverne, E. B. Genomic Imprinting and the Evolution of Sex Differences in Mammalian

Reproductive Strategies. *Adv. Genet.* **59**, 217–243 (2007).

160. Fish, E. N. The X-files in immunity: sex-based differences predispose immune responses. *Nat. Rev. Immunol.* **8**, 737–744 (2008).
161. Markle, J. G. & Fish, E. N. SeXX matters in immunity. *Trends Immunol.* **35**, 97–104 (2014).
162. Vasanthakumar, A., Chisanga, D., Blume, J., Gloury, R., Britt, K., Henstridge, D. C., Zhan, Y., Torres, S. V., Liene, S., Collins, N., *et al.* Sex-specific adipose tissue imprinting of regulatory T cells. *Nature* **579**, 581–585 (2020).
163. World Health Organization (WHO) Ebola Response Team, J, A.-A., A, A., IM, B., A, C., CA, D., I, D., C, D., T, E., NM, F., *et al.* Ebola Virus Disease among Male and Female Persons in West Africa. *N. Engl. J. Med.* **374**, 96–98 (2016).
164. World Health Organization (WHO). Addressing sex and gender in epidemic-prone infectious diseases. 1–46 (2007).
165. Klein, S. L., Jedlicka, A. & Pekosz, A. The Xs and Y of immune responses to viral vaccines. *Lancet Infect. Dis.* **10**, 338–349 (2010).
166. Bouman, A., Heineman, M. J. & Faas, M. M. Sex hormones and the immune response in humans. *Hum. Reprod.* **11**, 411–423 (2005).
167. Mcdonnell, D. P. & Norris, J. D. Connections and Regulation of the Human Estrogen Receptor. *Science* **296**, 1642–1644 (2002).
168. Addo, M. M. & Altfeld, M. Sex-based differences in HIV type 1 pathogenesis. *J. Infect. Dis.* **209**, 86–92 (2014).
169. Griesbeck, M., Ziegler, S., Laffont, S., Smith, N., Chauveau, L., Tomezsko, P., Sharei, A., Kourjian, G., Porichis, F., Hart, M., *et al.* Sex Differences in Plasmacytoid Dendritic Cell Levels of IRF5 Drive Higher IFN- a Production in Women. *J. Immunol.* **195**, 5327–5336 (2015).
170. Berghöfer, B., Frommer, T., Haley, G., Bein, G., Hackstein, H., Frommer, T., Haley, G., Fink, L. & Bein, G. TLR7 Ligands Induce Higher IFN-α Production in Females. *J. Immunol.* **177**, 2088–2096 (2018).
171. Ziegler, S., Beisel, C., Sutter, K., Griesbeck, M., Hildebrandt, H., Hagen, S., Dittmer, U. & Altfeld, M. Human pDCs display sex-specific differences in type I interferon subtypes and interferon α/β receptor expression. *Eur. J. Immunol.* **47**, 251–256 (2017).

172. Bouman, A., Schipper, M., Heineman, M. J. & Faas, M. M. Gender difference in the non-specific and specific immune response in humans. *Am. J. Reprod. Immunol.* **52**, 19–26 (2004).

173. Posma, E., Moes, H., Heineman, M. J. & Faas, M. M. The effect of testosterone on cytokine production in the specific and non-specific immune response. *Am. J. Reprod. Immunol.* **52**, 237–243 (2004).

174. Vom Steeg, L. G., Vermillion, M. S., Hall, O. J., Alam, O., McFarland, R., Chen, H., Zirkin, B. & Klein, S. L. Age and testosterone mediate influenza pathogenesis in male mice. *Am. J. Physiol. - Lung Cell. Mol. Physiol.* **311**, L1234–L1244 (2016).

175. Libert, C., Dejager, L. & Pinheiro, I. The X chromosome in immune functions: When a chromosome makes the difference. *Nat. Rev. Immunol.* **10**, 594–604 (2010).

176. Wang, J., Syrett, C. M., Kramer, M. C., Basu, A., Atchison, M. L. & Anguera, M. C. Unusual maintenance of X chromosome inactivation predisposes female lymphocytes for increased expression from the inactive X. *Proc. Natl. Acad. Sci. U. S. A.* **113**, E2029–E2038 (2016).

177. Oghumu, S., Varikuti, S., Stock, J. C., Saljoughian, N., Terrazas, C. A., Satoskar, A. R., Terrazas, C. A. & Satoskar, A. R. Cutting Edge: CXCR3 Escapes X Chromosome Inactivation in T Cells during Infection: Potential Implications for Sex Differences in Immune Responses. *J. Immunol.* **203**, 789–794 (2019).

178. Meier, A., Chang, J. J., Chan, E. S., Pollard, R. B., Sidhu, H. K., Kulkarni, S., Wen, T. F., Lindsay, R. J., Orellana, L., Mildvan, D., *et al.* Sex differences in the Toll-like-receptor-mediated response of plasmacytoid dendritic cells to HIV-1. *Nat. Med.* **15**, 955–959 (2009).

179. Berletch, J. B., Yang, F., Xu, J., Carrel, L. & Disteche, C. M. Genes that escape from X inactivation. *Hum. Genet.* **130**, 237–245 (2011).

180. Hagen, S. H., Henseling, F., Hennesen, J., Savel, H., Delahaye, S., Richert, L., Ziegler, S. M. & Altfeld, M. Heterogeneous Escape from X Chromosome Inactivation Results in Sex Differences in Type I IFN Responses at the Single Human pDC Level. *Cell Rep.* **33**, (2020).

181. Ivashkiv, L. B. & Donlin, L. T. Regulation of type I interferon responses Lionel. *Nat. Rev. Immunol.* **14**, 1–7 (2014).

182. Klein, S. L., Passaretti, C., Anker, M., Olukoya, P. & Pekosz, A. The impact of sex, gender

and pregnancy on 2009 H1N1 disease. *Biol. Sex Differ.* **1**, 5 (2010).

183. Napravnik, S., Poole, C., Thomas, J. C. & Jr., J. J. E. Gender Differences in HIV RNA Levels: A Meta-Analysis of Published Studies. *J. Aquired Immune Defic. Syndr.* **1;31**, 11–19 (2002).
184. Wald, A. Herpes simplex virus type 2 transmission: risk factors and virus shedding. *Herpes* **11**, 130A–7A (2004).
185. Dickson, N., Righarts, A., Roode, T. Van, Paul, C., Taylor, J. & Cunningham, A. L. HSV-2 incidence by sex over four age periods to age 38 in a birth cohort. *Sex. Transm. Infect.* **90**, 243–245 (2014).
186. Wensing, B., Mochizuki, M. & De Boer, J. H. Clinical Characteristics of Herpes Simplex Virus Associated Anterior Uveitis. *Ocul. Immunol. Inflamm.* **26**, 333–337 (2018).
187. Chen., C. J., Yang, H.-I., Su, J., Jen, C.-L., You, S.-L., Lu, S.-N., Huang, G.-T., Iloeje, U. H. & REVEAL-HBV Study Group. Risk of hepatocellular carcinoma across a biological gradient of serum hepatitis B virus DNA level. *Rev. Francoph. des Lab.* **2006**, 17 (2006).
188. Tsay, P. K., Tai, D. I., Chen, Y. M., Yu, C. P., Wan, S. Y., Shen, Y. J. & Lin, D. Y. Impact of gender, viral transmission and aging in the prevalence of hepatitis b surface antigen. *Chang Gung Med. J.* **32**, 155–164 (2009).
189. Wang, S. H., Yeh, S. H., Lin, W. H., Wang, H. Y., Chen, D. S. & Chen, P. J. Identification of androgen response elements in the enhancer I of hepatitis B virus: A mechanism for sex disparity in chronic hepatitis B. *Hepatology* **50**, 1392–1402 (2009).
190. Di Martino, V., Lebray, P., Myers, R. P., Pannier, E., Paradis, V., Charlotte, F., Moussalli, J., Thabut, D., Buffet, C. & Poynard, T. Progression of liver fibrosis in women infected with hepatitis C: Long-term benefit of estrogen exposure. *Hepatology* **40**, 1426–1433 (2004).
191. Karlberg, J., Chong, D. S. Y. & Lai, W. Y. Y. Do Men Have a Higher Case Fatality Rate of Severe Acute Respiratory Syndrome than Women Do ? *Am. J. Epidemiol.* **159**, 229–231 (2004).
192. Leong, H.-N., Earnest, A., Lim, H.-H., Chin, C.-F., Tan, C. S., Puhaindran, M. E., Tan, A. C., Chen, M. I. & Leo, Y.-S. SARS in Singapore – Predictors of Disease Severity. *Ann. Acad. Med. Singapore* **35**, 326–331 (2006).
193. Alghamdi, I. G., Hussain, I. I., Almalki, S. S., Alghamdi, M. S., Alghamdi, M. M. & El-

Sheemy, M. A. The pattern of Middle East respiratory syndrome coronavirus in Saudi Arabia : a descriptive epidemiological analysis of data from the Saudi Ministry of Health. *Int. J. Gen. Med.* **20**, 417–423 (2014).

194. Jansen, A., Chiew, M., Konings, F., Lee, C.-K. & Ailan, L. Sex matters – a preliminary analysis of Middle East respiratory syndrome in the Republic of Korea, 2015. *West. Pacific Surveill. Response J.* **6**, 68–71 (2015).
195. Chen, N., Zhou, M., Dong, X., Qu, J., Gong, F., Han, Y., Qiu, Y., Wang, J., Liu, Y., Wei, Y., *et al.* Epidemiological and clinical characteristics of 99 cases of 2019 novel coronavirus pneumonia in Wuhan, China: a descriptive study. *Lancet* **395**, 507–513 (2020).
196. Yang, X., Yu, Y., Xu, J., Shu, H., Xia, J., Liu, H., Wu, Y., Zhang, L., Yu, Z., Fang, M., *et al.* Clinical course and outcomes of critically ill patients with SARS-CoV-2 pneumonia in Wuhan, China: a single-centered, retrospective, observational study. *Lancet Respir. Med.* **8**, 475–481 (2020).
197. Meng, Y., Wu, P., Lu, W., Liu, K., Ma, K., Huang, L., Cai, J., Zhang, H., Qin, Y., Sun, H., *et al.* Sex-specific clinical characteristics and prognosis of coronavirus disease-19 infection in Wuhan, China: A retrospective study of 168 severe patients. *PLoS Pathog.* **16**, 1–13 (2020).
198. Gebhard, C., Regitz-Zagrosek, V., Neuhauser, H. K., Morgan, R. & Klein, S. L. The impact of sex and gender on COVID-19 outcomes in Europe. *Biol. Sex Differ.* **11**, 1–13 (2020).
199. Lewin, S. Chapter 45: Gender Differences in Emerging Infectious Diseases. in *Principles of Gender-Specific Medicine* (ed. Marianne J. Legato) 497–515 (Academic Press, 2020) doi:10.1016/B978-0-12-374271-1.00045-9.
200. Bunders, M. J. & Altfeld, M. Implications of Sex Differences in Immunity for SARS-CoV-2 Pathogenesis and Design of Therapeutic Interventions. *Immunity* **53**, 487–495 (2020).
201. Takahashi, T., Ellingson, M. K., Wong, P., Israelow, B., Lucas, C., Klein, J., Silva, J., Mao, T., Oh, J. E., Tokuyama, M., *et al.* Sex differences in immune responses that underlie COVID-19 disease outcomes. *Nature* **588**, 315–320 (2020).
202. Nkangu, M. N., Olatunde, O. A. & Yaya, S. The perspective of gender on the Ebola virus using a risk management and population health framework : a scoping review. *Infect. Dis. Poverty* **6**, 1–9 (2017).
203. Ebola Outbreak Epidemiology Team. Outbreak of Ebola virus disease in the Democratic

Republic of the Congo , April – May , 2018 : an epidemiological study. *Lancet* **392**, 213–221 (2018).

204. Cook, I. I. F. Sexual dimorphism of humoral immunity with human vaccines. *Vaccine* **26**, 3551–3555 (2008).
205. Engler, R. J. M., Nelson, M. R., Klote, M. M., VanRaden, M. J., Huang, C.-Y., Cox, N. J., Klimov, A., Keitel, W. A., Nichol, K. L., Carr, W. W., *et al.* Half- vs Full-Dose Trivalent Inactivated Influenza Vaccine (2004-2005). *Arch. Intern. Med.* **168**, 2405–2415 (2008).
206. Klein, S. L. & Flanagan, K. L. Sex differences in immune responses. *Nat. Publ. Gr.* **16**, 626–638 (2016).
207. Zhang, X., Castelli, F. A., Zhu, X., Wu, M., Maillere, B. & BenMohamed, L. Gender-Dependent HLA-DR-Restricted Epitopes Identified from Herpes Simplex Virus Type 1 Glycoprotein D▽. *Clin. Vaccine Immunol.* **15**, 1436–1449 (2008).
208. Umlauf, B. J., Haralambieva, I. H., Ovsyannikova, I. G., Kennedy, R. B., Pankratz, V. S., Jacobson, R. M. & Poland, G. A. Associations Between Demographic Variables and Multiple Measles-Specific Innate and Cell-Mediated Immune Responses After Measles Vaccination. *Viral Immunol.* **25**, 29–36 (2012).
209. Furman, D., Hejblum, B. P., Simon, N., Jojic, V., Dekker, C. L., Thiébaut, R., Tibshirani, R. J. & Davis, M. M. Systems analysis of sex differences reveals an immunosuppressive role for testosterone in the response to influenza vaccination. *Proc. Natl. Acad. Sci. U. S. A.* **111**, 869–874 (2014).
210. Treanor, J., Keitel, W., Belshe, R., Campbell, J., Schiff, G., Zangwill, K., Wolff, M., Klimov, A., Levandowski, R. & Lambert, L. Evaluation of a single dose of half strength inactivated influenza vaccine in healthy adults. *Vaccine* **20**, 1099–1105 (2002).
211. Kramer, J. S., Durham, C., Schroeder, T. & Garrelts, J. C. Effectiveness of half-dose versus full-dose influenza vaccine in health care workers. *Am. J. Heal. Pharm.* **63**, 2111–2115 (2006).
212. Kennedy, R. B., Ovsyannikova, I. G., Pankratz, V. S., Vierkant, R. A., Jacobson, R. M., Ryane, M. A. K. & Polanda, G. A. Gender effects on humoral immune responses to smallpox vaccine. *Vaccine* **27**, 3319–3323 (2010).
213. Haralambieva, I. H., Ovsyannikova, I. G., Kennedy, R. B., Larrabee, B. R., Pankratz, V. S. & Poland, G. A. Race and Sex-Based Differences in Cytokine Immune Responses to

Smallpox Vaccine in Healthy Individuals. *Hum. Immunol.* **74**, 1263–1266 (2014).

214. Troy, J. D., Hill, H. R., Ewell, M. G. & Frey, S. E. Sex Difference in Immune Response to Vaccination: A Participant-Level Meta-Analysis of Randomized Trials of IMVAMUNE® Smallpox Vaccine. *Vaccine* **33**, 5425–5431 (2015).
215. Lindsey, N. P., Schroeder, B. A., Miller, E. R., Braun, M. M., Hinckley, A. F., Marano, N., Slade, B. A., Barnett, E. D., Brunette, G. W., Horan, K., *et al.* Adverse event reports following yellow fever vaccination. *Vaccine* **26**, 6077–6082 (2008).
216. Monath, T. P., Nichols, R., Archambault, W. T., Moore, L., Marchesani, R., Tian, J., Shope, R. E., Thomas, N., Schrader, R., Furby, D., *et al.* Comparative safety and immunogenicity of two yellow fever 17D vaccines (ARILVAX and YF-VAX) in a phase III multicenter, double-blind clinical trial. *Am. J. Trop. Med. Hyg.* **66**, 533–541 (2002).
217. Camacho, L. A. B., Freire, M. da S., Leal, M. da L. F., Aguiar, S. G. de, Nascimento, J. P. do, Iguchi, T., Lozana, J. de A., Farias, R. H. G. & Collaborative Group for the Study of Yellow Fever Vaccines. Immunogenicity of WHO-17D and Brazilian 17DD yellow fever vaccines: A randomized trial. *Rev. Saude Publica* **38**, 671–678 (2004).
218. Pfister, M., Kürsteiner, O., Hilfiker, H., Favre, D., Durrer, P., Ennaji, A., L'Age-Stehr, J., Kaufhold, A. & Herzog, C. Immunogenicity and safety of BERNA-YF compared with two other 17D yellow fever vaccines in a phase 3 clinical trial. *Am. J. Trop. Med. Hyg.* **72**, 339–346 (2005).
219. Roukens, A. H., Vossen, A. C., Bredenbeek, P. J., van Dissel, J. T. & Visser, L. G. Intradermally Administered Yellow Fever Vaccine at Reduced Dose Induces a Protective Immune Response: A Randomized Controlled Non-Inferiority Trial. *PLoS One* **3**, e1993 (2008).
220. Suder, E., Furuyama, W., Feldmann, H., Marzi, A. & de Wit, E. The vesicular stomatitis virus-based Ebola virus vaccine: From concept to clinical trials. *Hum. Vaccines Immunother.* **14**, 2107–2113 (2018).
221. Fathi, A., Addo, M. M. & Dahlke, C. Sex Differences in Immunity: Implications for the Development of Novel Vaccines Against Emerging Pathogens. *Front. Immunol.* **11**, 1–7 (2021).
222. Cheng, Y., Lin, Y., Chen, C., Tsai, T., Tsai, C., Wu, Y., Ou, Y., Chu, Y., Wang, J., Yu, C., *et al.* Activation of Nrf2 by the dengue virus causes an increase in CLEC5A , which

enhances TNF- α production by mononuclear phagocytes. *Nat. Publ. Gr.* **6**, 1–15 (2016).

223. Chahroudi, A., Chavan, R., Kozyr, N., Waller, E. K., Silvestri, G. & Feinberg, M. B. Vaccinia Virus Tropism for Primary Hematolymphoid Cells Is Determined by Restricted Expression of a Unique Virus Receptor. *J. Virol.* **79**, 10397–10407 (2006).
224. Meyer, H., Sutter, G. & Mayr, A. Mapping of deletions in the genome of the highly attenuated vaccinia virus MVA and their influence on virulence. *J. Gen. Virol.* **72**, 1031–1038 (1991).
225. Kremer, M., Volz, A., Kreijtz, J. H. C. M., Fux, R., Lehmann, M. H. & Sutter, G. Easy and Efficient Protocols for Working with Recombinant Vaccinia Virus MVA. *Methods Mol. Biol.* **890**, 59–92 (2012).
226. Lülf, A., Freudenstein, A., Marr, L., Sutter, G. & Volz, A. Non-plaque-forming virions of Modified Vaccinia virus Ankara express viral genes. *Virology* **499**, 322–330 (2016).
227. Hulsen, T., de Vlieg, J. & Alkema, W. BioVenn - A web application for the comparison and visualization of biological lists using area-proportional Venn diagrams. *BMC Genomics* **9**, 1–6 (2008).
228. Zhang, B., Kirov, S. & Snoddy, J. WebGestalt: An integrated system for exploring gene sets in various biological contexts. *Nucleic Acids Res.* **33**, 741–748 (2005).
229. Wang, J., Duncan, D., Shi, Z. & Zhang, B. WEB-based GEne SeT AnaLysis Toolkit (WebGestalt): update 2013. *Nucleic Acids Res.* **41**, W77–W83 (2013).
230. Wang, J., Vasaikar, S., Shi, Z., Greer, M. & Zhang, B. WebGestalt 2017: A more comprehensive, powerful, flexible and interactive gene set enrichment analysis toolkit. *Nucleic Acids Res.* **45**, W130–W137 (2017).
231. Liao, Y., Wang, J., Jaehnig, E. J., Shi, Z. & Zhang, B. WebGestalt 2019: gene set analysis toolkit with revamped UIs and APIs. *Nucleic Acids Res.* **47**, W199–W205 (2019).
232. Whelan, J. A., Russell, N. B. & Whelan, M. A. A method for the absolute quantification of cDNA using real-time PCR. *J. Immunol. Methods* **278**, 261–269 (2003).
233. Lee, C., Kim, J., Shin, S. G. & Hwang, S. Absolute and relative QPCR quantification of plasmid copy number in Escherichia coli. *J. Biotechnol.* **123**, 273–280 (2006).
234. ThermoFisher Scientific Inc. DNA and RNA Molecular Weights and Conversions. https://www.thermofisher.com/de/de/home/references/ambion-tech-support/rna-tools-and-calculators/dna-and-rna-molecular-weights-and-conversions.html (2021).

235. Le Bon, A. & Tough, D. F. Links between innate and adaptive immunity via type I interferon. *Curr. Opin. Immunol.* **14**, 432–436 (2002).

236. Pashine, A., Valiante, N. M. & Ulmer, J. B. Targeting the innate immune response with improved vaccine adjuvants. *Nat. Med.* **11**, 63–68 (2005).

237. Akira, S., Uematsu, S. & Takeuchi, O. Pathogen recognition and innate immunity. *Cell* **124**, 783–801 (2006).

238. Pulendran, B. & Ahmed, R. Translating Innate Immunity into Immunological Memory : Implications for Vaccine Development. *Cell* **124**, 849–863 (2006).

239. Steinman, R. M. Dendritic Cells In Vivo : A Key Target for a New Vaccine Science. *Immunity* **29**, 319–324 (2008).

240. Aoshi, T., Koyama, S., Kobiyama, K., Akira, S. & Ishii, K. J. Innate and adaptive immune responses to viral infection and vaccination. *Curr. Opin. Virol.* **1**, 226–232 (2011).

241. Zepp, F. Principles of Vaccination. in Vaccine Design (ed. Thomas, S.) vol. 1403 57–84 (Humana Press, New York, NY, 2016) https://doi.org/10.1007/978-1-4939-3387-7_3

242. Blok, B. A., Arts, R. J. W., van Crevel, R., Benn, C. S. & Netea, M. G. Trained innate immunity as underlying mechanism for the long-term, nonspecific effects of vaccines. *J. Leukoc. Biol.* **98**, 347–356 (2015).

243. Fensterl, V. & Sen, G. C. Interferons and viral infections. *BioFactors* **35**, 14–20 (2009).

244. Sokol, C. L. & Luster, A. D. The chemokine system in innate immunity. *Cold Spring Harb. Perspect. Biol.* **7**, 1–20 (2015).

245. Thieblemont, N., Weiss, L., Sadeghi, H. M., Estcourt, C. & Haeffner-Cavaillon, N. CD14low CD16high: a cytokine-producing monocyte subset which expands during human immunodeficiency virus infection. *Eur. J. Immunol.* **25**, 3418–3424 (1995).

246. Tisoncik, J. R., Korth, M. J., Simmons, C. P., Farrar, J., Martin, T. R. & Katze, M. G. Into the Eye of the Cytokine Storm. *Microbiol. Mol. Biol. Rev.* **76**, 16–32 (2012).

247. Aarreberg, L. D., Wilkins, C., Ramos, H. J., Green, R., Davis, M. A., Chow, K. & Gale, M. Interleukin-1β Signaling in Dendritic Cells Induces Antiviral Interferon Responses. *MBio* **9**, 1–14 (2018).

248. Pirhonen, J., Sareneva, T., Kurimoto, M., Julkunen, I. & Matikainen, S. Virus infection activates IL-1β and IL-18 production in human macrophages by a caspase-1-dependent pathway. *J. Immunol.* **162**, 7322–7329 (1999).

249. Liu, M. T., Armstrong, D., Hamilton, T. A. & Lane, T. E. Expression of Mig (Monokine Induced by Interferon-γ) Is Important in T Lymphocyte Recruitment and Host Defense Following Viral Infection of the Central Nervous System. *J. Immunol.* **166**, 1790–1795 (2001).

250. Monteiro, J. M., Harvey, C. & Trinchieri, G. Role of Interleukin-12 in Primary Influenza Virus Infection. *J. Virol.* **72**, 4825–4831 (1998).

251. Smiley, S. T. & Grusby, M. J. Interleukin 4. in *Encyclopedia of Immunology* (eds. Roitt, I. & Delves, P.) vol. 1 (Academic Press, 1998).

252. Jongbloed, S. L., Kassianos, A. J., McDonald, K. J., Clark, G. J., Ju, X., Angel, C. E., Chen, C. J. J., Dunbar, P. R., Wadley, R. B., Jeet, V., *et al.* Human CD141+ (BDCA-3)+ dendritic cells (DCs) represent a unique myeloid DC subset that cross-presents necrotic cell antigens. *J. Exp. Med.* **207**, 1247–1260 (2010).

253. Cesano, A. nCounter® PanCancer Immune Profiling Panel (NanoString Technologies, Inc., Seattle, WA). *J. Immunother. Cancer* **3**, 1–3 (2015).

254. GeneCards - The Human Gene Database. CLEC5A Gene (Protein Coding). https://www.genecards.org/cgi-bin/carddisp.pl?gene=CLEC5A (2021).

255. Liu, M., Guo, S., Hibbert, J. M., Jain, V., Singh, N., Wilson, N. O. & Stiles, J. K. CXCL10/IP-10 in infectious diseases pathogenesis and potential therapeutic implications. *Cytokine Growth Factor Rev.* **22**, 121–130 (2011).

256. Bonecchi, R., Bianchi, G., Bordignon, P. P., D'Ambrosio, D., Lang, R., Borsatti, A., Sozzani, S., Allavena, P., Gray, P. A., Mantovani, A., *et al.* Differential expression of chemokine receptors and chemotactic responsiveness of type 1 T helper cells (Th1s) and Th2s. *J. Exp. Med.* **187**, 129–134 (1998).

257. Khan, I. A., MacLean, J. A., Lee, F. S., Casciotti, L., DeHaan, E., Schwartzman, J. D. & Luster, A. D. IP-10 is critical for effector T cell trafficking and host survival in Toxoplasma gondii infection. *Immunity* **12**, 483–494 (2000).

258. Aksoy, M. O., Yang, Y., Ji, R., Reddy, P. J., Shahabuddin, S., Litvin, J., Rogers, T. J. & Kelsen, S. G. CXCR3 surface expression in human airway epithelial cells: Cell cycle dependence and effect on cell proliferation. *Am. J. Physiol. - Lung Cell. Mol. Physiol.* **290**, 909–918 (2006).

259. Shahabuddin, S., Ji, R., Wang, P., Brailoiu, E., Dun, N., Yang, Y., Aksoy, M. O. & Kelsen,

S. G. CXCR3 chemokine receptor-induced chemotaxis in human airway epithelial cells: Role of p38 MAPK and PI3K signaling pathways. *Am. J. Physiol. - Cell Physiol.* **291**, 34–39 (2006).

260. Liu, M., Guo, S. & Stiles, J. K. The emerging role of CXCL10 in cancer. *Oncol. Lett.* **2**, 583–589 (2011).
261. Cheung, R., Shen, F., Phillips, J. H., Mcgeachy, M. J., Cua, D. J., Heyworth, P. G. & Pierce, R. H. Activation of MDL-1 (CLEC5A) on immature myeloid cells triggers lethal shock in mice. *J. Clin. Invest.* **121**, 4446–4461 (2011).
262. Teng, O., Chen, S.-T., Hsu, T.-L., Sia, S. F., Cole, S., Valkenburg, S. A., Hsu, T.-Y., Zheng, J. T., Tu, W., Bruzzone, R., *et al.* CLEC5A-Mediated Enhancement of the Inflammatory Response in Myeloid Cells Contributes to Influenza Virus Pathogenicity In Vivo. *J. Virol.* **91**, 1–16 (2017).
263. Sung, P. S. & Hsieh, S. L. CLEC2 and CLEC5A: Pathogenic Host Factors in Acute Viral Infections. *Front. Immunol.* **10**, 1–9 (2019).
264. Takada, A., Robison, C., Goto, H., Sanchez, A., Murti, K. G., Whitt, M. A. & Kawaoka, Y. A system for functional analysis of Ebola virus glycoprotein. *Proc. Natl. Acad. Sci. U. S. A.* **94**, 14764–14769 (1997).
265. Mpanju, O. M., Towner, J. S., Dover, J. E., Nichol, S. T. & Wilson, C. A. Identification of two amino acid residues on Ebola virus glycoprotein 1 critical for cell entry. *Virus Res.* **121**, 205–214 (2006).
266. Barba-Spaeth, G., Longman, R. S., Albert, M. L. & Rice, C. M. Live attenuated yellow fever 17D infects human DCs and allows for presentation of endogenous and recombinant T cell epitopes. *J. Exp. Med.* **202**, 1179–1184 (2005).
267. Drillien, R., Spehner, D. & Hanau, D. Modified vaccinia virus Ankara induces moderate activation of human dendritic cells. *J. Gen. Virol.* **85**, 2167–2175 (2004).
268. Liu, L., Chavan, R. & Feinberg, M. B. Dendritic Cells are preferentially targeted among hematolymphocytes by Modified Vaccinia Virus Ankara and play a key role in the induction of virus-specific T cell responses in vivo. *BMC Immunol.* **9**, 1–14 (2008).
269. Higbee, R. G., Byers, A. M., Dhir, V., Drake, D., Fahlenkamp, H. G., Gangur, J., Kachurin, A., Kachurina, O., Leistritz, D., Ma, Y., *et al.* An immunologic model for rapid vaccine assessment - A clinical trial in a test tube. *Altern. to Lab. Anim.* **37**, 19–27 (2009).

270. Drake, D. R., Singh, I., Nguyen, M. N., Kachurin, A., Wittman, V., Parkhill, R., Kachurina, O., Moser, J. M., Burdin, N., Moreau, M., *et al.* In Vitro Biomimetic Model of the Human Immune System for Predictive Vaccine Assessments. *Disruptive Sci. Technol.* **1**, 28–40 (2012).

271. Dauner, A., Agrawal, P., Salvatico, J., Tapia, T., Dhir, V., Shaik, S. F., Drake, D. R. & Byers, A. M. The in vitro MIMIC® platform reflects age-associated changes in immunological responses after influenza vaccination. *Vaccine* **35**, 5487–5494 (2017).

272. Gaucher, D., Therrien, R., Kettaf, N., Angermann, B. R., Boucher, G., Filali-Mouhim, A., Moser, J. M., Mehta, R. S., Donald R. Drake, I., Castro, E., *et al.* Yellow fever vaccine induces integrated multilineage and polyfunctional immune responses. *J. Exp. Med.* **205**, 3119–3131 (2008).

273. Russell, W. M., Burch, R. l. & Hume, C. w. *Principles of Human Experimental Technique*. (Universities Federation for Animal Welfare (UFAW), 1992).

274. Hoonakker, M. E., Verhagen, L. M., Hendriksen, C. F. M., Els, C. A. C. M. Van, Vandebriel, R. J., Sloots, A. & Han, W. G. H. In vitro innate immune cell based models to assess whole cell Bordetella pertussis vaccine quality : A proof of principle. *Biologicals* **43**, 100–109 (2015).

275. Ming, M., Bernardo, L., Williams, K., Kolattukudy, P., Kapoor, N., Chan, L. G., Pagnon, A., Piras, F., Su, J., Gajewska, B., *et al.* An in vitro functional assay to measure the biological activity of TB vaccine candidate H4-IC31. *Vaccine* **37**, 2960–2966 (2019).

276. Salata, C., Calistri, A., Alvisi, G., Celestino, M., Parolin, C. & Palù, G. Ebola virus entry: From molecular characterization to drug discovery. *Viruses* **11**, 274 (2019).

277. Hendriksen, C. F. M. Replacement reduction and refinement alternatives to animal use in vaccine potency measurement. *Expert Rev. Vaccines* **8**, 313–322 (2009).

278. Wagar, L. E., Difazio, R. M. & Davis, M. M. Advanced model systems and tools for basic and translational human immunology. *Genome Med.* **10**, 1–14 (2018).

279. Bray, M. The role of the Type I interferon response in the resistance of mice to filovirus infection. *J. Virol.* **82**, 1365–1373 (2001).

280. Claire, M. C. S., Ragland, D. R., Bollinger, L. & Jahrling, P. B. Animal Models of Ebolavirus Infection. **67**, 253–262 (2017).

281. Querec, T., Bennouna, S., Alkan, S., Laouar, Y., Gorden, K., Flavell, R., Akira, S., Ahmed,

R. & Pulendran, B. Yellow fever vaccine YF-17D activates multiple dendritic cell subsets via TLR2, 7, 8, and 9 to stimulate polyvalent immunity. *J. Exp. Med.* **203**, 413–424 (2006).

282. Kumar, H., Kawai, T., Kato, H., Sato, S., Takahashi, K., Coban, C., Yamamoto, M., Uematsu, S., Ishii, K. J., Takeuchi, O., *et al.* Essential role of IPS-1 in innate immune responses against RNA viruses. *J. Exp. Med.* **203**, 1795–1803 (2006).
283. Wongthida, P., Jengarn, J., Narkpuk, J., Koonyosying, P., Srisutthisamphan, K., Wanitchang, A., Leaungwutiwong, P., Teeravechyan, S. & Jongkaewwattana, A. In Vitro and In Vivo Attenuation of Vesicular Stomatitis Virus (VSV) by Phosphoprotein Deletion. *PLoS One* **11**, 1–14 (2016).
284. Liu, J., Wyatt, L. S., Amara, R. R., Moss, B. & Robinson, H. L. Studies on in vitro expression and in vivo immunogenicity of a recombinant MVA HIV vaccine. *Vaccine* **24**, 3332–3339 (2006).
285. Altenburg, A. F., Sandt, C. E. Van De, Li, B. W. S., Macloughlin, R. J., Fouchier, R. A. M., Amerongen, G. Van, Volz, A., Hendriks, R. W., Swart, R. L. De, Sutter, G., *et al.* Modified Vaccinia Virus Ankara Preferentially Targets Antigen Presenting Cells In Vitro , Ex Vivo and In Vivo. *Sci. Rep.* **7**, 1–14 (2017).
286. Tomczyk, T., Wróbel, G., Chaber, R., Siemieniec, I., Piasecki, E., Krzystek-Korpacka, M. & Orzechowska, B. U. Immune Consequences of in vitro Infection of Human Peripheral Blood Leukocytes with Vesicular Stomatitis Virus. *J. Innate Immun.* **10**, 131–144 (2018).
287. Johnson, M. Fetal Bovine Serum. *MATER METHODS* **2**, (2012).
288. Oakey, R. Steroid Hormones : A Practical Approach. in *Biochemical Education* (eds. Green, B. & Leake, R. E.) vol. 16 213–214 (IRL Press, 1988).
289. Sigma-Aldrich Chemie GmbH Taufkrichen Germany. Charcoal, Dextran Coated. *Product Information Sheet* 1 https://www.sigmaaldrich.com/catalog/product/sigma/c6241?lang=en&region=CA&cm_sp=Insite-_-caSrpResults_srpRecs_srpModel_charcoal stripped-_-srpRecs3-2 (2020).
290. Climent, N., Guerra, S., García, F., Rovira, C., Miralles, L., Gómez, C. E., Piqué, N., Gil, C., Gatell, J. M., Esteban, M., *et al.* Dendritic cells exposed to MVA-based HIV-1 vaccine induce highly functional HIV-1-specific CD8+ T cell responses in HIV-1-infected

individuals. *PLoS One* **6**, (2011).

291. Gómez, C. E., Perdiguero, B., Jiménez, V., Filali-Mouhim, A., Ghneim, K., Haddad, E. K., Quakkerlaar, E. D., Delaloye, J., Harari, A., Roger, T., *et al.* Systems analysis of MVA-C induced immune response reveals its significance as a vaccine candidate against HIV/AIDS of clade C. *PLoS One* **7**, (2012).
292. Cong, Y., McArthur, M. A., Cohen, M., Jahrling, P. B., Janosko, K. B., Josleyn, N., Kang, K., Zhang, T. & Holbrook, M. R. Characterization of Yellow Fever Virus Infection of Human and Non-human Primate Antigen Presenting Cells and Their Interaction with CD4+T Cells. *PLoS Negl. Trop. Dis.* **10**, 1–25 (2016).
293. Jefford, M., Schnurr, M., Toy, T., Masterman, K., Shin, A., Beecroft, T., Tai, T. Y., Shortman, K., Shackleton, M., Davis, I. D., *et al.* Functional comparison of DCs generated in vivo with Flt3 ligand or in vitro from blood monocytes : differential regulation of function by specific classes of physiologic stimuli. *Blood* **102**, 1753–1763 (2003).
294. Helft, J., Böttcher, J., Chakravarty, P., Zelenay, S., Huotari, J., Schraml, B. U., Goubau, D. & Sousa, C. R. e. GM-CSF Mouse Bone Marrow Cultures Comprise a Heterogeneous Population of CD11c+ MHCII+ Macrophages and Dendritic Cells. *Immunity* **42**, 1197–1211 (2015).
295. Collin, M. & Bigley, V. Human dendritic cell subsets : an update. *Immunology* **154**, 3–20 (2018).
296. Menicucci, A. R., Sureshchandra, S., Marzi, A., Feldmann, H. & Messaoudi, I. Transcriptomic analysis reveals a previously unknown role for CD8+ T-cells in rVSV-EBOV mediated protection. *Sci. Rep.* **7**, 1–12 (2017).
297. Santoro, F., Donato, A., Lucchesi, S., Sorgi, S., Gerlini, A., Haks, M. C., Ottenhoff, T. H. M., Gonzalez-Dias, P., Nakaya, H. I., Huttner, A., *et al.* Human transcriptomic response to the VSV-vectored ebola vaccine. *Vaccines* **9**, 1–15 (2021).
298. Dufour, J. H., Dziejman, M., Liu, M. T., Leung, J. H., Lane, T. E. & Luster, A. D. IFN-γ-Inducible Protein 10 (IP-10; CXCL10)-Deficient Mice Reveal a Role for IP-10 in Effector T Cell Generation and Trafficking. *J. Immunol.* **168**, 3195–3204 (2002).
299. Mitchell, L. A., Henderson, A. J. & Dow, S. W. Suppression of Vaccine Immunity by Inflammatory Monocytes. *J. Immunol.* **189**, 5612–5621 (2012).

300. Sanchez, A., Trappier, S. G., Mahy, B. W. J., Peters, C. J. & Nichol, S. T. The virion glycoproteins of Ebola viruses are encoded in two reading frames and are expressed through transcriptional editing. *Proc. Natl. Acad. Sci. U. S. A.* **93**, 3602–3607 (1996).

301. Dolnik, O., Volchkova, V., Garten, W., Carbonnelle, C., Becker, S., Kahnt, J., Ströher, U., Klenk, H. D. & Volchkov, V. Ectodomain shedding of the glycoprotein GP of Ebola virus. *EMBO J.* **23**, 2175–2184 (2004).

302. Escudero-Pérez, B., Volchkova, V. A., Dolnik, O., Lawrence, P. & Volchkov, V. E. Shed GP of Ebola Virus Triggers Immune Activation and Increased Vascular Permeability. *PLoS Pathog.* **10**, (2014).

303. Okumura, A., Pitha, P. M., Yoshimura, A. & Harty, R. N. Interaction between Ebola Virus Glycoprotein and Host Toll-Like Receptor 4 Leads to Induction of Proinflammatory Cytokines and SOCS1. *J. Virol.* **84**, 27–33 (2010).

304. Lai, C. Y., Strange, D. P., Wong, T. A. S., Lehrer, A. T. & Verma, S. Ebola virus glycoprotein induces an innate immune response in vivo via TLR4. *Front. Microbiol.* **8**, 1–15 (2017).

305. Wagstaffe, H. R., Clutterbuck, E. A., Bockstal, V., Stoop, J. N., Luhn, K., Douoguih, M., Shukarev, G., Snape, M. D., Pollard, A. J., Riley, E. M., *et al.* Ebola virus glycoprotein stimulates IL-18-dependent natural killer cell responses. *J. Clin. Invest.* **130**, 3936–3946 (2020).

306. A Gould, T. S. Pathogenic flaviviruses. *Lancet* **371**, 500–509 (2008).

307. Tolle, M. A. Mosquito-borne Diseases. *Curr. Probl. Pediatr. Adolesc. Health Care* **39**, 97–140 (2009).

308. Nakaya, H. I., Wrammert, J., Lee, E. K., Racioppi, L., Marie-Kunze, S., Haining, W. N., Means, A. R., Kasturi, S. P., Khan, N., Li1, G.-M., *et al.* Systems Biology of Seasonal Influenza Vaccination in Humans. *Nat. Immunol.* **12**, 786–795 (2012).

309. Baggiolini, M. & Clark-Lewis, I. Interleukin-8, a chemotactic and inflammatory cytokine. *FEBS Lett.* **307**, 97–101 (1992).

310. Deshmane, S. L., Kremlev, S., Amini, S. & Sawaya, B. E. Monocyte chemoattractant protein-1 (MCP-1): An overview. *J. Interf. Cytokine Res.* **29**, 313–325 (2009).

311. Huttner, A., Combescure, C., Grillet, S., Haks, M. C., Quinten, E., Modoux, C., Agnandji, S. T., Brosnahan, J., Dayer, J.-A., Harandi, A. M., *et al.* A dose-dependent plasma signature of the safety and immunogenicity of the rVSV-Ebola vaccine in Europe and

Africa. *Sci. Transl. Med.* **9**, (2017).

312. Whelan, S. P. J. Vesicular Stomatitis Virus. in *Encyclopedia of Virology* (eds. Mahy, B. W. J. & Regenmortel, M. H. V. Van) 291–299 (Academic Press, 2008). doi:https://doi.org/10.1016/B978-012374410-4.00529-X.
313. Younan, P., Iampietro, M., Nishida, A., Ramanathan, P., Santos, R. I., Dutta, M., Lubaki, N. M., Koup, R. A., Katze, M. G. & Bukreyev, A. Ebola virus binding to Tim-1 on T lymphocytes induces a cytokine storm. *MBio* **8**, 1–20 (2017).
314. Farooq, F., Beck, K., Paolino, K. M., Phillips, R., Waters, N. C., Regules, J. A. & Bergmann-Leitner, E. S. Circulating follicular T helper cells and cytokine profile in humans following vaccination with the rVSV-ZEBOV Ebola vaccine. *Sci. Rep.* **6**, 1–9 (2016).
315. Jensen, S. & Thomsen, A. R. Sensing of RNA Viruses: a Review of Innate Immune Receptors Involved in Recognizing RNA Virus Invasion. *J. Virol.* **86**, 2900–2910 (2012).
316. Baize, S., Leroy, E. M., Georges-Courbot, M.-C., Capron, M., Lansoud-Soukate, J., Debré, P., Fisher-Hoch, S. P., McCormick, J. B. & Georges, A. J. Defective humoral responses and extensive intravascular apoptosis are associated with fatal outcome in Ebola virus-infected patients. *Nat. Med.* **5**, 423–426 (1999).
317. Leroy, E. M., Baize, S., Debre, P., Lansoud-Soukate, J. & Mavoungou, E. Early immune responses accompanying human asymptomatic Ebola infections. *Clin. Exp. Immunol.* **124**, 453–460 (2001).
318. Teigler, J. E., Phogat, S., Franchini, G., Hirsch, V. M., Michael, N. L. & Barouch, D. H. The Canarypox Virus Vector ALVAC Induces Distinct Cytokine Responses Compared to the Vaccinia Virus-Based Vectors MVA and NYVAC in Rhesus Monkeys. *J. Virol.* **88**, 1809–1814 (2014).
319. Mohanty, S., Joshi, S. R., Ueda, I., Wilson, J., Blevins, T. P., Siconol, B., Meng, H., Devine, L., Raddassi, K., Tsang, S., *et al.* Prolonged Proin fl ammatory Cytokine Production in Monocytes Modulated by Interleukin 10 After In fl uenza Vaccination in Older Adults. *J. Infect. Dis.* **211**, 1174–1184 (2015).
320. Lim, W., Ma, W., Gee, K., Aucoin, S., Nandan, D., Diaz-Mitoma, F., Kozlowski, M. & Kumar, A. This information is current as of February 16, 2021. *J. Immunol.* **168**, 1759–1769 (2002).
321. Duin, D. Van, Allore, H. G., Mohanty, S., Ginter, S., Newman, F. K., Belshe, R. B.,

Medzhitov, R. & Shaw, A. C. Prevaccine Determination of the Expression of Costimulatory B7 Molecules in Activated Monocytes Predicts Influenza Vaccine Responses in Young and Older Adults. *J. Infect. Dis.* **195**, 1590–1597 (2007).

322. Akbari, B. O., Panjwani, N., Garcia, S., Tascon, R., Lowrie, D. & Stockinger, B. DNA Vaccination : Transfection and Activation of Dendritic Cells as Key Events for Immunity. *J. Exp. Med.* **189**, 169–178 (1999).
323. Sparwasser, T., Koch, E., Vabulas, R. M., Heeg, K., Grayson, B., Ellwart, J. W. & Wagner, H. Bacterial DNA and immunostimulatory CpG oligonucleotides trigger maturation and activation of murine dendritic cells. *Eur. J. Immunol.* **28**, 2045–2054 (1998).
324. Harrison, S. C., Alberts, B., Ehrenfeld, E., Enquist, L., Fineberg, H., Mcknight, S. L., Moss, B., Donnell, M. O., Ploegh, H., Schmid, S. L., *et al.* Discovery of antivirals against smallpox. *Proc. Natl. Acad. Sci.* **101**, 11178–11192 (2004).
325. Apte-Sengupta, S., Sirohi, D. & Kuhn, R. J. Coupling of replication and assembly in flaviviruses. *Curr. Opin. Virol.* **9**, 134–142 (2014).
326. Gerold, G., Bruening, J., Weigel, B. & Pietschmann, T. Protein Interactions during the Flavivirus and Hepacivirus Life Cycle. *Mol. Cell. Proteomics* **16**, S75–S91 (2017).
327. Sutter, G. A vital gene for modified vaccinia virus Ankara replication in human cells. *Proc. Natl. Acad. Sci.* **117**, 6289–6291 (2020).
328. Grosjean, B. I., Caux, C., Bella, C., Berger, I., Wild, F., Banchereau, J. & Kaiserlian, D. Measles Virus Infects Human Dendritic Cells and Blocks Their Allostimulatory Properties for CD41 T Cells. *J. Exp. Med.* **186**, 801–812 (1997).
329. Grigoleit, U., Riegler, S., Einsele, H., Sampaio, K. L., Jahn, G., Hebart, H., Brossart, P., Frank, F. & Sinzger, C. Human cytomegalovirus induces a direct inhibitory effect on antigen presentation by monocyte-derived immature dendritic cells. *Br. J. Haematol.* **119**, 189–198 (2002).
330. Griffin, D. E. Measles virus-induced suppression of immune responses. *Immunol. Rev.* **236**, 176–189 (2010).
331. Reyes-rodriguez, A. L., Reuter, M. A. & Mcdonald, D. Dendritic Cells Enhance HIV Infection of Memory CD4+ T Cells in Human Lymphoid Tissues. *AIDS Res. Hum. Retroviruses* **32**, 203–210 (2016).
332. Nakaya, H. I., Hagan, T., Duraisingham, S. S., Lee, E. K., Kwissa, M., Rouphael, N., Frasca,

D., Gersten, M., Mehta, A. K., Gaujoux, R., *et al.* Systems Analysis of Immunity to Influenza Vaccination across Multiple Years and in Diverse Populations Reveals Shared Molecular Signatures. *Immunity* **43**, 1186–1198 (2015).

333. Caballero, I. S., Honko, A. N., Gire, S. K., Winnicki, S. M., Melé, M., Gerhardinger, C., Lin, A. E., Rinn, J. L., Sabeti, P. C., Hensley, L. E., *et al.* In vivo Ebola virus infection leads to a strong innate response in circulating immune cells. *BMC Genomics* **17**, 1–13 (2016).
334. Càrdenas, W. B., Loo, Y., Gale, M., Hartman, A. L., Kimberlin, C. R., Martı, L., Saphire, E. O. & Basler, C. F. Ebola Virus VP35 Protein Binds Double-Stranded RNA and Inhibits Alpha / Beta Interferon Production Induced by RIG-I Signaling. *J. Virol.* **80**, 5168–5178 (2006).
335. Reid, S. P., Leung, L. W., Hartman, A. L., Martinez, O., Shaw, M. L., Carbonnelle, C., Volchkov, V. E., Nichol, S. T. & Basler, C. F. Ebola Virus VP24 Binds Karyopherin alpha 1 and Blocks STAT1 Nuclear Accumulation. *J. Virol.* **80**, 5156–5167 (2006).
336. Jin, H., Yan, Z., Prabhakar, B. S., Feng, Z., Ma, Y., Verpooten, D., Ganesh, B. & He, B. The VP35 protein of Ebola virus impairs dendritic cell maturation induced by virus and lipopolysaccharide. *J. Gen. Virol.* **91**, 352–361 (2010).
337. Yen, B., Mulder, L. C. F., Martinez, O. & Basler, C. F. Molecular Basis for Ebolavirus VP35 Suppression of Human Dendritic Cell Maturation. *J. Virol.* **88**, 12500–12510 (2014).
338. Edwards, M. R., Liu, G., Mire, C. E., Sureshchandra, S., Luthra, P., Amarasinghe, G. K. & Basler, C. F. Differential regulation of interferon responses by Ebola and Marburg virus VP35 proteins. *Cell Rep.* **14**, 1632–1640 (2016).
339. Yen, B. C. & Basler, C. F. Effects of Filovirus Interferon Antagonists on Responses of Human Monocyte-Derived Dendritic Cells to RNA Virus Infection. *J. Virol.* **90**, 5108–5118 (2016).
340. Barrenas, F., Green, R. R., Thomas, M. J., Law, G. L., Proll, S. C., Engelmann, F., Messaoudi, I., Marzi, A., Feldmann, H. & Katze, M. G. Next-Generation sequencing reveals a controlled immune response to Zaire Ebola virus challenge in cynomolgus macaques immunized with vesicular stomatitis virus expressing Zaire Ebola virus glycoprotein (VSVΔG/EBOVgp). *Clin. Vaccine Immunol.* **22**, 354–356 (2015).
341. Waibler, Z., Anzaghe, M., Ludwig, H., Akira, S., Weiss, S., Sutter, G. & Kalinke, U. Modified Vaccinia Virus Ankara Induces Toll-Like Receptor-Independent Type I

Interferon Responses. *J. Virol.* **81**, 12102–12110 (2007).

342. Dai, P., Wang, W., Cao, H., Avogadri, F., Dai, L., Drexler, I., Joyce, J. A., Li, X., Chen, Z., Merghoub, T., *et al.* Modified Vaccinia Virus Ankara Triggers Type I IFN Production in Murine Conventional Dendritic Cells via a cGAS / STING-Mediated Cytosolic DNA-Sensing Pathway. *PLOS Pathog.* **10**, 1003989 (2014).
343. Scherer, C. A., Magness, C. L., Steiger, K. V., Poitinger, N. D., Caputo, C. M., Miner, D. G., Winokur, P. L., Klinzman, D., McKee, J., Pilar, C., *et al.* Distinct Gene Expression Profiles in Peripheral BloodMononuclear Cells from Patients Infected with Vaccinia Virus,Yellow Fever 17D Virus, or Upper Respiratory Infections RunningTitle: PBMC Expression Response to Viral Agents. *Vaccine* **25**, 6458–6473 (2007).
344. Li, S., Rouphael, N., Duraisingham, S., Romero-steiner, S., Presnell, S., Davis, C., Schmidt, D. S., Johnson, S. E., Milton, A., Rajam, G., *et al.* Molecular signatures of antibody responses derived from a systems biology study of five human vaccines. *Nat. Immunol.* **15**, 195–204 (2014).
345. Garbutt, M., Liebscher, R., Wahl-Jensen, V., Jones, S., Möller, P., Wagner, R., Volchkov, V., Klenk, H.-D., Feldmann, H. & Ströher, U. Properties of Replication-Competent Vesicular Stomatitis Virus Vectors Expressing Glycoproteins of Filoviruses and Arenaviruses. *J. Virol.* **78**, 5458–5465 (2004).
346. Connor, J. H. & Lyles, D. S. Vesicular Stomatitis Virus Infection Alters the eIF4F Translation Initiation Complex and Causes Dephosphorylation of the eIF4E Binding Protein 4E-BP1. *J. Virol.* **76**, 10177–10187 (2002).
347. Dunn, E. F. & Connor, J. H. Dominant Inhibition of Akt/Protein Kinase B Signaling by the Matrix Protein of a Negative-Strand RNA Virus. *J. Virol.* **85**, 422–431 (2011).
348. Walsh, D. & Mohr, I. Viral subversion of the host protein synthesis machinery. *Nat. Rev. Microbiol.* **9**, 860–875 (2011).
349. Neidermyer, W. J. & Whelan, S. P. J. Global analysis of polysome-associated mRNA in vesicular stomatitis virus infected cells. *PLoS Pathog.* **15**, 1–27 (2019).
350. Kuroda, M., Halfmann, P. J., Hill-batorski, L., Ozawa, M., Lopes, T. J. S., Neumann, G., Schoggins, J. W., Rice, C. M. & Kawaoka, Y. Identification of interferon-stimulated genes that attenuate Ebola virus infection. *Nat. Commun.* **11**, 1–14 (2020).
351. Rogers, K. J. & Maury, W. The role of mononuclear phagocytes in Ebola virus infection.

*J. Leukoc. Biol.* **104**, 717–727 (2018).

352. Mesman, A. W., Zijlstra-Willems, E. M., Kaptein, T. M., Swart, R. L. de, Davis, M. E., Ludlow, M., Duprex, W. P., Gack, M. U., Gringhuis, S. I. & GeijtenbeeK, T. B. H. Measles virus suppresses RIG-I-like receptor activation in dendritic cells via DC-SIGN-mediated inhibition of PP1 phosphatases. *Cell Host Microbe* **16**, 31–42 (2014).
353. Azamor, T., da Silva, A. M. V., Melgaço, J. G., Dos Santos, A. P., Xavier-Carvalho, C., Alvarado-Arnez, L. E., Batista-Silva, L. R., de Souza Matos, D. C., Bayma, C., Missailidis, S., *et al.* Activation of an Effective Immune Response after Yellow Fever Vaccination Is Associated with the Genetic Background and Early Response of IFN-γ and CLEC5A. *Viruses* **13**, 1–12 (2021).
354. Syrett, C. M., Sindhava, V., Sierra, I., Dubin, A. H., Atchison, M. & Anguera, M. C. Diversity of Epigenetic Features of the Inactive X-Chromosome in NK Cells , Dendritic Cells , and Macrophages. *Front. Immunol.* **9**, (2019).
355. European Medicines Agencies (EMA). EMA recommends COVID-19 Vaccine AstraZeneca for authorisation in the EU. https://www.ema.europa.eu/en/news/ema-recommends-covid-19-vaccine-astrazeneca-authorisation-eu (2021).
356. U.S. Food & Drug Administration (FDA). Janssen COVID-19 Vaccine. https://www.fda.gov/emergency-preparedness-and-response/coronavirus-disease-2019-covid-19/janssen-covid-19-vaccine#additional (2021).
357. Universitätsklinikum Hamburg-Eppendorf. Erste Daten des Corona-Impfstoffes zeigen gute Verträglichkeit, aber schwache Immunreaktion. https://www.uke.de/allgemein/presse/pressemitteilungen/detailseite_102920.html (2021).
358. Stanberry, L. R., Spruance, S. L., Cunningham, A. L., Bernstein, D. I., Mindel, A., Sacks, S., Tyring, S., Aoki, F. Y., Slaoui, M., Denis, M., *et al.* Glycoprotein-D–Adjuvant Vaccine to Prevent Genital Herpes. *N. Engl. J. Med.* **347**, 1652–1661 (2002).
359. Schroeder, M., Schaumburg, B., Müller, Z., Parplys, A., Jarczak, D., Kloetgen, A., Schneider, B., Peschka, M., Stoll, F., Bai, T., *et al.* Sex hormone and metabolic dysregulations are associated with critical illness in male Covid-19 patients. *medRxiv* **20073817**, 1–32 (2020).
360. Vasson, M. P., Farges, M. C., Goncalves-Mendes, N., Talvas, J., Ribalta, J., Winklhofer-

Roob, B., Rock, E. & Rossary, A. Does aging affect the immune status? A comparative analysis in 300 healthy volunteers from France, Austria and Spain. *Immun. Ageing* **10**, 1–11 (2013).

361. Márquez, E. J., Chung, C. han, Marches, R., Rossi, R. J., Nehar-Belaid, D., Eroglu, A., Mellert, D. J., Kuchel, G. A., Banchereau, J. & Ucar, D. Sexual-dimorphism in human immune system aging. *Nat. Commun.* **11**, (2020).